ABSTRACT

WANG, YONGXIN. Robustness of Hydrophobic and Oleophobic Fabrics. (Under the direction of Drs. Stephen Michielsen and Hoon Joo Lee).

A hydrophobic and oleophobic surface can be defined as a surface with an apparent contact angle higher than 90° both for water and oil. Robustness is used to describe the property of a hydrophobic and oleophobic rough surface to resist the penetration by a liquid under a pressure. The robust pressure of a rough surface is the most common expression of robustness. The robust pressure depends on the surface tension and Laplace pressure of the liquid, and the surface energy and the structure of the rough surface.

Robustness can be measured and modeled by pushing a droplet into a hydrophobic and oleophobic surface with another surface. Since a capillary bridge forms between the two surfaces, capillary forces, capillary profiles and wetting behavior of liquid bridges between two surfaces are reviewed. In the initial phase of this research, a robustometer was constructed and its characteristics were determined using flat smooth substrates. Then, the capillary profiles of liquid bridges were modeled for symmetric/asymmetric and bi-concave/bi-convex shapes, where gravity was negligible. Good agreement was found between theoretical and experimental profiles of the liquid bridges. When an external force was applied to a droplet, both the Laplace pressure and profile of the liquid would change, which was manifest in the spread and penetration of the drop on the rough surface. The capillary forces for liquid bridges between smooth film substrates were also modeled, and excellent agreement was found between the experimental results and theoretical analysis. With the effective action area

known, robust pressure was expressed as robust force per unit area. In addition, for a liquid under an applied force, the Laplace pressure can also be obtained.

In order to study the robustness of parallel monofilaments and fabrics against liquids under pressures, they were tested with the robustometer by compressing a drop on their surface with a polytetrafluoroethylene film. The robust pressures were obtained from the robust forces and action areas, which were compared among different fabrics and liquids. From the capillary force analysis, the Laplace pressure was calculated for each pair of substrates with a liquid. In addition, guidance will be provided to avoid or reduce chemical warfare agent (CWA) hazards adhered to the hydrophobic and oleophobic fabrics, during the interaction between the wipe and liquids.

Robustness of Hydrophobic and Oleophobic Fabrics

by
Yongxin Wang

A dissertation submitted to the Graduate Faculty of
North Carolina State University
in fulfillment of the
requirements for the degree of
Doctor of Philosophy

Fiber and Polymer Science

Raleigh, North Carolina

2013

APPROVED BY:

_____	_____
Dr. Stephen Michielsen (Co-Chair of Advisory Committee)	Dr. Hoon Joo Lee (Co-Chair of Advisory Committee)
_____	_____
Dr. Melissa A. Pasquinelli	Dr. Tushar K. Ghosh
_____	
Dr. Orlando J. Rojas	

BIOGRAPHY

Yongxin Wang received her Bachelor of Science degree in Educational Technology (Media-Making and Communication) in the College of Humanities at Donghua University in fall 2008. Then Yongxin Wang transferred to the College of Textiles and obtained her Master degree in Textile Materials and Product Design in the College of Textiles at Donghua University in Fall, 2010. She came to North Carolina State University and enrolled in the Fiber and Polymer Science Doctoral program in August 2010.

ACKNOWLEDGMENTS

I would like to express my sincere gratitude to my advisers, Drs. Stephen Michielsen and Hoon Joo Lee, who offered the best opportunity and allowed me to pursue my Ph. D. degree in their research group. They have been guiding me to do research, helping me get through difficult times, encouraging me and supporting me through my graduate years. Without their guidance and encouragement, this dissertation would not have been possible.

I would also like to thank Drs. Melissa Pasquinelli, Tushar Ghosh, and Orlando Rojas for being on my committee and helping me with my final defense. Their invaluable suggestions and guidance paved the way for this project. Special thanks to Dr. Melissa Pasquinelli for helping me understand and solve problems and leading me to the right directions.

I wish to express my sincere thank you to Prof. Nancy Powell for giving precious suggestions about my dissertation and presentations. I appreciated her expectations of me and faith in me throughout the entire process. Many sincere thanks go to Drs. Marian McCord and Bhupender Gupta for their kind help during my study.

I would like to show my gratitude to Chuck Mooney for helping me with the SEM, Birgit Andersen for training me with FTIR, Judy Elson and Jeffrey Krauss for allowing me to use various instruments in their lab. I wish to thank Hai Bui and Dzung Nguyen for helping me build up the robustometer and prepare samples in the machine shop. I also thank Tri Vu for offering technical support.

I wish to acknowledge my former team members, Archana Mohan, Priscilla Tan, Jinlin Zhang, Rahul Saraf, Sarah Hoit, and Dr. Jinmei Du, who have been training me to work in

the lab, sharing their understanding and experience about research with me, and offering support and giving help to me in the early stage of this project. I also thank my present research coworkers, Xiaohang Sun, Guoqing Li, Jihye Lim, Jing Chen, Lun Lou, Wenwen Zhang, Wei Du and Yue Zhu, for the stimulating discussions and suggestions about this project. Guoqing Li deserves a special “thank you” for assisting me with experiments and preparations of samples.

In addition, I would like to thank Kun Fu for offering help and support at various stages of this work. I thank Renbo Cao for helping me prepare defense presentation, and Easa Khan, Gang Fang and Juan Lin for helping me work on the Visual Basic program. I also thank to Yidan Zhu, Edmir Silva, Ganesh Narayanan, Maqbool Hussain for their kind help.

Last but not the least, I wish to express my deepest love and gratitude to my beloved family for their support and understanding all the time.

TABLE OF CONTENTS

LIST OF SCHEMES

LIST OF FIGURES

LIST OF TABLES

LIST OF SYMBOLS

Symbol	Designatum	Unit
$\Delta\theta_H$	Contact angle hysteresis	degrees (°)
A	Surface area	m^2
V	Liquid volume	m^3
N	Number of molecules	*unitless*
T	Temperature	°C or °K
γ_{LV}	Liquid-vapor surface tension	J/m^2 or N/m
ΔP	Laplace pressure	Pa
P_{in}	Pressure inside a droplet	Pa
P_{out}	Pressure outside a droplet	Pa
R_1	Principal radii of a surface	m
R_2	Principal radii of a surface	m
H	Mean surface curvature	m^{-1}
θ_e	Young's contact angle	degrees (°)
γ_{SV}	Solid-vapor surface tension ($\approx \gamma_S$)	J/m^2 or N/m
γ_{SL}	Solid-liquid surface tension ($\approx \gamma_L$)	J/m^2 or N/m
α	Roll-off angle	degrees (°)
θ_A	Advancing contact angle	degrees (°)
θ_R	Receding contact angle	degrees (°)
$\Delta\theta_H$	Contact angle hysteresis	degrees (°)

m	Mass of the drop	kg
g	Gravitational acceleration	m/s^2
α	Roll-off angle	degrees (°)
l	Length of drop on a tilting surface	m
θ_i	Intrinsic contact angle	degrees (°)
θ_a	Apparent contact angle	degrees (°)
${W_{SL}}^a$	Work of adhesion for solid-liquid interaction	J/m^2 or N/m
β	Constant (= 0.0001247)	$(m^2/mJ)^2$
γ^d	Surface tension caused by London-van der Waals forces	J/m^2 or N/m
γ^p	Surface tension caused by permanent dipoles	J/m^2 or N/m
γ^{ind}	Surface tension caused by induced dipoles	J/m^2 or N/m
γ^H	Surface tension caused by hydrogen bonds	J/m^2 or N/m
γ^m	Surface tension caused by metallic interaction	J/m^2 or N/m
${\theta_r}^W$	Apparent contact angle of a Wenzel state	degrees (°)
r	Surface roughness (≥ 1)	*unitless*
${\theta_r}^{CB}$	Apparent contact angle of a Cassie-Baxter state	degrees (°)
f_1	True contact area between liquid and solid divided by the projected area	*unitless*
f_2	Area of the droplet in contact with the vapor divided by the projected area	*unitless*
θ_1	Equilibrium contact angle between liquid and solid	degrees (°)
${\theta_r}^*$	Apparent contact angle on a rough surface	degrees (°)
r_f	Roughness of a wetted area	*unitless*

f	Fraction of the projected area below the wetted solid surface	*unitless*
R	Radius of a fiber or monofilament or a spherical bead	m
D	Half edge-to-edge distance between adjacent fibers or monofilaments	m
A_{LV}	Liquid-vapor contact area	m^2
A_{SV}	Solid-vapor contact area	m^2
A_{SL}	Solid-liquid contact area	m^2
β	Encompassing or embracing contact angle	degrees (°)
c	Constant	*unitless*
h_f	Height of a flock fiber	m
F_{cap}	Capillary force	N
φ	Contact angle of a liquid bridge on a surface	degrees (°)
φ_1	Contact angle of a liquid bridge on surface Ⅰ	degrees (°)
φ_2	Contact angle of a liquid bridge on surface Ⅱ	degrees (°)
h	Height of a liquid bridge between two flat surfaces, or smallest distance between a spherical bead and a flat substrate	m
H_s	Largest distance between a spherical bead and a flat substrate	m
R_{11}	Principal radius at a point on the liquid-vapor interface of a liquid bridge	m
R_{12}	Principal radius at another point on the liquid-vapor interface of a liquid bridge	m
R_D	Radius of the liquid-solid contact area	m
ρ	Liquid density	Kg/m^3
l_{cap}	Capillary length	m

ε	Angle between z-axis and a line perpendicular to the tangent line of a liquid bridge	degrees (°)
W	Half length of the hat of microhoodoo shape	m
P_H	Robust pressure	J/m^2 or Pa
$\delta\theta$	Sagging angle	degrees (°)
$\delta\theta_a$	Sagging angle	degrees (°)
$\delta\theta_b$	Sagging angle	degrees (°)
L	Solid-liquid contact line length	m
Wp	Work has been done through the composite interface by the pressure	J
$Ecomp$	Change in interfacial energy of the interface	J
h_d	Depth of the liquid-vapor interface penetrating into the surface structure	m
λ	Distance of the centers of two adjacent protuberances	m
θ	Contact angle between fiber and meniscus of a liquid	degrees (°)
f_s	Area fraction of the liquid-vapor interface occluded by the texture	*unitless*
r_f	Roughness of the wetted area	*unitless*
$\bar{b}$	Mean length between centers of two adjacent fibers	m
$\bar{b}_b$	Mean length of overlapping fibers	m
R_{sag}	Radius of meniscus	m
κ	Curvature of the meniscus	m^{-1}
κ_{max}	Maximum curvature of the meniscus	m^{-1}
D^*	Spacing ratio	*unitless*
P^*	Dimensionless robust pressure	*unitless*

x_1	X coordinate of a point on the liquid-vapor interface	m
x_2	X coordinate of another point on the liquid-vapor interface	m
B	Bond number	*unitless*
P_1	Atmospheric pressure	Pa
P_2	Pressure inside the liquid	Pa
F	Force applied by the substrate	N
P_A	Applied pressure	Pa
R_{D1}	Radius of liquid-solid contact area	m
R_{D2}	Radius of liquid-solid contact area	m
$\Delta P'$	Laplace pressure including gravity effect	Pa
P_{hydro}	Hydrostatic pressure	Pa
z	Height of a liquid for hydrostatic pressure tests	m
D'	Half distance between two liquid-vapor-solid interfacial contact points	m
ψ	Central angle	degrees (°)
ψ_c	Central angle at point C	degrees (°)
$\delta\varphi$	Supplementary angle to apparent contact angle	degrees (°)
n	Number of gaps spanned by the liquid	*unitless*

CHAPTER 1. INTRODUCTION

A hydrophobic surface is defined as a surface with an apparent contact angle (CA) greater than 90°.[1] Likewise, an oleophobic surface can be defined for oil.[2–4] There are two criteria to prepare a hydrophobic or oleophobic surface: low surface energy[5,6] and proper surface roughness.[7–9] On a smooth surface, the wetting behavior of a liquid is described by Young[10] with the Young's equation; on a rough surface, the wetting behavior can be described with the Cassie-Baxter[11] (CB) and Wenzel[12] models, depending on whether the liquid will completely wet (Wenzel) or partially wet the surface (CB). On the two surfaces, the wetting behavior of a liquid will be affected by the Laplace pressure[13,14] and surface tensions[14,15] of both liquid and solid.

The apparent CA is used to define a hydrophobic and oleophobic rough surface in most studies. However, they cannot completely represent the hydrophobicity and oleophobicity of a surface, since the resistance of the surface to a liquid under pressures cannot be revealed. Robustness of a rough surface, such as a fabric, is defined as the capability of the surface to retain its inherent structure against the interactions with liquid droplets under certain pressures. Robust pressure is used to describe the robustness of a rough surface,[1,16] and a robustometer has been designed and constructed to measure it.

The objective of the project is to design hydrophobic and oleophobic fabrics with high robustness when exposed to various liquids. To complete this objective, several steps are re-

quired. First, the mechanisms of forming a solid-liquid-vapor composite within the structure of hydrophobic and oleophobic fabrics will be studied. It provides information for developing hydrophobic and oleophobic fabrics from hydrophilic and oleophilic fabrics with CB model. Then, the meta-stable CB state will be introduced to describe the wetting behavior of a liquid in an unstable condition, which can be applied to study the liquid resistance of fabrics. Moreover, robustness of a fabric will be characterized with the robust pressure by performing robust tests with the robustometer. The influencing factors of a fabric will also be investigated. This will contribute to reducing or avoiding chemical warfare agent (CWA) hazards, which is also helpful for protection and decontamination of fabrics. Challenges include: (1) an instrument needs to be constructed to quantify the robustness; (2) appropriate surface modifications of fabrics are required to develop hydrophobic and oleophobic fabrics; (3) wetting behavior of a liquid on a hydrophobic and oleophobic fabric should be determined when spreading on and penetrating into the fabric; and (4) robustness of parallel monofilaments and fabrics with different geometrical structures should be tested and compared with each other to investigate the effects of textile structures.

CHAPTER 2. LITERATURE REVIEW

2.1 Introduction

Hydrophobic surfaces exist broadly in nature, such as a Lotus leaf and a duck's feather. They have excellent water-repellency due to their unique rough surfaces with hierarchical structures. Since there is a wide range of applications for hydrophobic materials, industry and researches have shown great interest in studying the mechanism and technologies of the hydrophobicity and oleophobicity of surfaces. Generally, when a water drop is deposited on a surface, if the CA is larger than 90°, it is said to be a hydrophobic surface; if the water is replaced by oil and the CA is still larger than 90°, it is known as a oleophobic surface. Otherwise, when the CA is less than 90°, the surface is regarded as hydrophilic for water, or oleophilic for oil.

Surfaces with superhydrophobicity and superoleophobicity have also attracted much attention for the broad applications, such as roofs, outdoor furniture and military uniforms. A superhydrophobic (SH) and superoleophobic (SO) surface can be defined as a surface for which water or a suitable oil has an apparent CA larger than 150° and a low roll-off angle or low contact angle hysteresis (CAH).[17] The hydrophobicity and oleophobicity can be achieved by increasing the surface roughness or decreasing the surface tension.[18,19] In general, micro scale roughness works for water, but nano scale roughness may be necessary to repel oil from the surface. The technologies for producing hydrophobic and oleophobic surfaces include plasma treatment, carbon nanotubes, photolithography, coating nano-particles and so on. In

particular, fluorochemicals are used extensively for research and military applications. The main goal is to satisfy the two criteria, high roughness and low surface tension.

The wetting behavior of a liquid will be affected by the surface tension and Laplace pressure, especially for a small drop. When the volume is larger, gravity will also influence its behavior. The CA and CAH of a liquid on a surface directly reflect the hydrophobicity and oleophobicity of a surface, and they will be discussed. Moreover, the wetting behavior of a liquid on smooth surfaces and rough surfaces vary. Even for surfaces with the same roughness, the wetting behavior may exhibit dramatic changes for different liquids. Wenzel and Cassie-Baxter (CB) cases are good examples.

In addition to the wetting behavior, the CAs and CA hystereses only reflect the static superhydrophobicity and superoleophobicity of a surface. Other characteristics, such as robustness, cannot be revealed, but they are important additional features of a hydrophobic and oleophobic surface. Robustness refers the capability of a rough surface to resist liquid from penetrating into its structure, and high robustness implies that the surface has large resistance to a liquid. This characteristic can be evaluated by the robustness of a hydrophobic and oleophobic surface from its physical and chemical structures.[20]

Robustness is a criterion to evaluate the resistance to penetration of a hydrophobic and oleophobic surface. Robust pressure or breakthrough pressure can be used to describe the robustness of a surface, which refers to the minimum pressure to push a liquid into and penetrate

through the surface.[1] Wetting behavior of a liquid on a rough surface include Cassie-Baxter (CB) and Wenzel states.[11,20–24] In Wenzel model, the surface is entirely wet by the liquid, while in CB model, a composite structure of a mixture of solid, liquid and vapor will be formed. For a droplet on a surface, the transformation and barrier between CB and Wenzel states could be illustrated by robustness of the surface, by forming meta-stable CB states.[25–30] Gibbs surface free energy of a system can also be applied to predict the final state of a liquid on a rough surface, since the liquid will move to the global minimum energy to achieve thermodynamic equilibrium.[21,30–32]

To assess the robustness and obtain the robust pressure of rough surfaces, the wetting behavior of the liquid between two surfaces has been reviewed. The robust pressure equals the robust force divided by the area. Usually, a capillary bridge will be formed between the surfaces. The robust force of a capillary bridge,[33–35] influenced by the surface tensions and Laplace pressure, will also be reviewed as well as the profiles of the liquid bridges.[36,37]

Robustness of a surface will comprehensively reveal its resistance to penetration and inherent hydrophobicity and oleophobicity, in conjunction with the CAs. The wetting behavior of liquid between two substrates under pressure indirectly reflects the hydrophobicity and oleophobicity of a rough surface, depending on whether the liquid mainly spreads on or penetrates into the surface. Therefore, resistance of the hydrophobic and oleophobic protective surfaces from penetration by liquids could be evaluated through robustness and meta-stable wetting behavior. In addition, robust pressure can be used to study the hydrophobic and oleo-

phobic property of a surface when a drop with a small volume is applied, while the hydrostatic pressure does not have a significant effect. Once the mechanism of robustness of a liquid on a rough surface has been systematically understood, structural parameters of the surface influencing robustness can be designed and optimized. Therefore, the potential superhydrophobicity and superoleophobicity of a surface will be dramatically improved, and meanwhile, the robustness of a hydrophobic and oleophobic surface with a fixed structure can also be predicted.

In this review, the background will be introduced first, including the surface tension and Laplace pressure, CA and CAH, and the definitions of hydrophobic and oleophobic surfaces. The wetting behaviors of liquids on both smooth and rough surfaces and on different textile structures will also be reviewed for preparation of the wetting behavior of a liquid between two surfaces. Bio-mimicry technologies are used to develop hydrophobic and oleophobic surfaces and prepare samples for robustness. Robust pressure is used to describe and evaluate the robustness. Three approaches will be discussed to obtain the robust pressure, including capillary bridge, force balance and energy conservation. These methods can be applied to investigate the robustness of homogeneous rough surface and hydrophobic and oleophobic fabrics.

2.2 Hydrophobic and oleophobic surfaces with their wetting behaviors

In this chapter, a hydrophobic and oleophobic surface is defined from the apparent CA[7,38] and the related concepts are reviewed, such as surface tension and Laplace pressure. Moreo-

ver, the wetting behavior of a liquid varies on surfaces made of different materials or with different morphologies, such as surfaces with different roughness. Finally, the preferable wetting behaviors for hydrophobic and oleophobic surfaces will be discussed, as well as the bio-mimicry technologies.

2.2.1 Surface tension and Laplace pressure

Surface tension

The phenomenon that a droplet maintains its own shape, such as bubbles and soap film, is due to the effect of surface tension or surface energy. Surface tension is generally caused by the attraction force between liquid molecules, and it can be explained by intermolecular force analysis or creation of a new interface.[14,15]

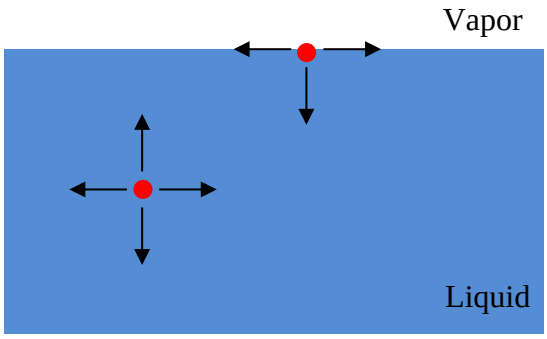

Figure 1. Attractive intermolecular force in a liquid.

Figure 1 shows the attractive forces of the molecules both in the liquid and on the liquid-vapor interface. In the liquid, the molecule experiences forces from all directions; at the inter-

face, the attractive force of the molecule in the direction perpendicular to the interface and departing from liquid is missing, if the very weak attractive force caused by the vapor phase is ignored. The imbalances give rise to an increase in the surface free energy. The surface free energy per unit area is defined as surface energy, which is expressed as:[14]

$$\gamma_{LV} = \frac{dG}{dA}\Big|_{V,N,T} \tag{1}$$

where G is Gibbs free energy of a surface, A is surface area and γ_{LV} is liquid-vapor surface tension. The liquid volume is V and number of molecules is N at temperature T. The unit of surface energy is J/m^2, and it is often reported as force per unit length, N/m.

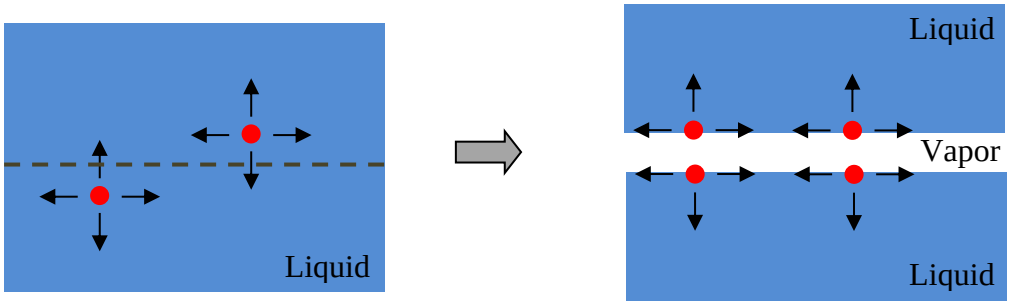

Figure 2. Creation of a new interface.

Figure 2 shows the creation of interfaces by separating a liquid of infinite volume. The dotted line displays the dividing line. Equal forces with opposite directions are applied to pull the liquid apart and create a new interface. Again, the force analysis for molecules inside the liquid and on the interface varies due to the missing of intermolecular bonds. Therefore, the surface tension can be defined in the same way as Equation (1). Surface tension generally quan-

tifies the effects of intermolecular bonds in a material when a new interface forms, and it is valid both for liquid and solid materials.

Laplace pressure

The other important term is the Laplace pressure, which is defined as the pressure difference between the inside and the outside of a droplet, caused by the surface tension of the interface between liquid and the other media.[13,14] It is related to the geometric shape of an interface, and expressed as,

$$\Delta P = P_{in} - P_{out} = \gamma\left(\frac{1}{R_1} + \frac{1}{R_2}\right) \tag{2}$$

where ΔP is Laplace pressure, P_{in} and P_{out} are the pressures inside and outside the droplet respectively, γ refers to the interfacial energy, and R_1 and R_2 refer to the two principal radii of curvature for a specific surface.

Principal radii refer to the maximum and minimum radii of a regular surface at each point, which can be defined from the two planes normal to the existing surface in the principal directions. The surface normal planes at a point are perpendicular to each other in the principal directions, and they are both perpendicular to the existing surface tangent plane at this point. As shown in Figure 3, R_1 and R_2 are the two principal radii of curvature at point *A* on the surface, which is marked as a shadowed area. A pair of mutually orthogonal dashed lines are drawn to obtain the principal radii in X and Y direction, respectively. For a droplet in a spherical cap shape sitting on a surface, $R_1 = R_2$ and the Laplace pressure becomes $2\gamma/R_1$ or

$2\gamma/R_2$. If a droplet is in thermodynamic equilibrium, the Laplace pressure is the same throughout the entire liquid-vapor interface. If the Laplace pressure is not constant within the liquid, the liquid shape will change until the pressures become uniform.

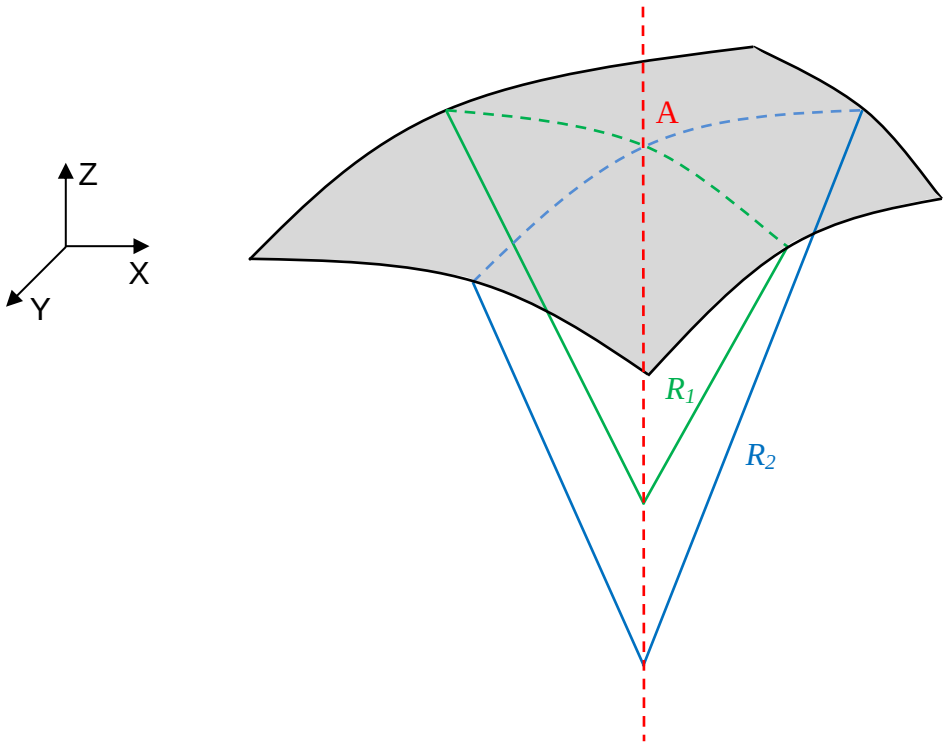

Figure 3. Principal radii of a surface.

For a surface of revolution by rotating $z = z(x)$ surrounding z axis, the Laplace pressure can also be obtained from mean surface curvature (H) by using the principal radii, and its relationship with Laplace pressure is:[34,39]

$$\Delta P = \gamma \cdot 2H = \gamma \left[\frac{1}{z(1+(\frac{dz}{dx})^2)^{1/2}} - \frac{\frac{d}{dx}\frac{dz}{dx}}{(1+(\frac{dz}{dx})^2)^{3/2}} \right] \quad (3)$$

2.2.2 Hydrophobic and oleophobic surfaces

Contact angle, roll-off angle and contact angle hysteresis

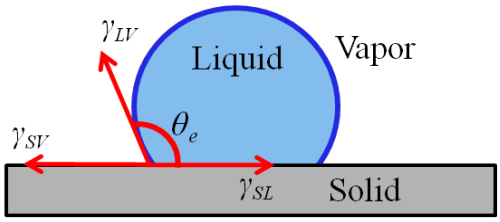

Figure 4. A droplet on a smooth surface.

When a liquid drop is placed on a smooth flat surface, it takes a spherical shape as shown in Figure 4. The CA in Figure 4 is defined as the included angle between the tangent line of spherical drop at a liquid-vapor-solid interfacial point and the solid substrate when the surface is perfectly smooth. It can be used to describe the phobicity or philicity of a surface. Details can be found in section 2.2.2. By balancing the surface forces on a drop, Young derived what is now called Young's equation:

$$\cos\theta_e = \frac{\gamma_{SV} - \gamma_{SL}}{\gamma_{LV}} \quad (4)$$

where θ_e is Young's CA. γ_{SV} , γ_{LV} *and* γ_{SL} refer to the solid-vapor, liquid-vapor and solid-liquid interfacial energies, respectively.

The roll-off angle has also been used to illustrate the hydrophobic and oleophobic property of a surface. The roll-off angle refers to the minimum angle that a surface must be tilted to make the liquid roll off due to its own weight. As shown in Figure 5, α is the roll-off angle. Experiments show that the roll-off angle is highly related to the volume of liquid. For the same kind of surface and liquid, a larger volume leads to a lower roll-off angle and a smaller volume results in larger a roll-off angle.[40,41]

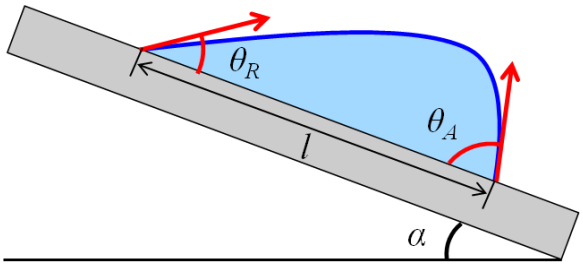

Figure 5. Tilting plate method. θ_A is the advancing CA, while θ_R is the receding CA. α is the roll-off angle.

In addition to CA and roll-off angle, the contact angle hysteresis (CAH) has also been applied to describe the hydrophobicity and oleophobicity of a surface. CAH is defined as the difference between the advancing and receding CAs.[7,42] There are two methods to measure the CAH as shown in Figure 5 and Figure 6. The first way to obtain the CAH is tilting plate

method in Figure 5. The CAs at the two ends of the liquid-vapor-solid interfacial points are measured just before the liquid begins to roll off. By using the equation $\Delta\theta_H = (\theta_A - \theta_R)$, the CAH is obtained. The relationship between roll-off angle and advancing and receding CAs is expressed as:[40]

$$mg \sin \alpha / l = \gamma_{LV} (\cos \theta_R - \cos \theta_A) \quad (5)$$

where m is the mass of the drop, g is gravitational acceleration, α is the roll-off angle, l is the length of the drop on a tilting surface and it equals to the width of the drop since the liquid could be considered circular in plane, γ_{LV} is liquid-vapor interfacial energy, θ_R is receding CA and θ_A is advancing CA.

For a liquid with fixed volume, ($cos\theta_R$ - $cos\theta_A$) can be obtained from its roll-off angle. However, the CAH cannot be obtained except by measuring the angles in the image of droplet shown in Figure 5.The other method is to inject and remove the liquid as shown in Figure 6. When a liquid is injected into a droplet, the liquid-vapor-solid interface of the drop will move away from the droplet center. The CA just before the edge of the liquid begins to move is known as advancing CA (θ_A). Likewise, when a liquid is removed from the droplet, the edge of the drop will move toward the droplet center and the CA just before the three phase interface moves is regarded as receding CA (θ_R). Therefore, the CAH can be obtained by either method. A lower CAH indicates that a surface can shed off the liquid more easily, and vice versa.

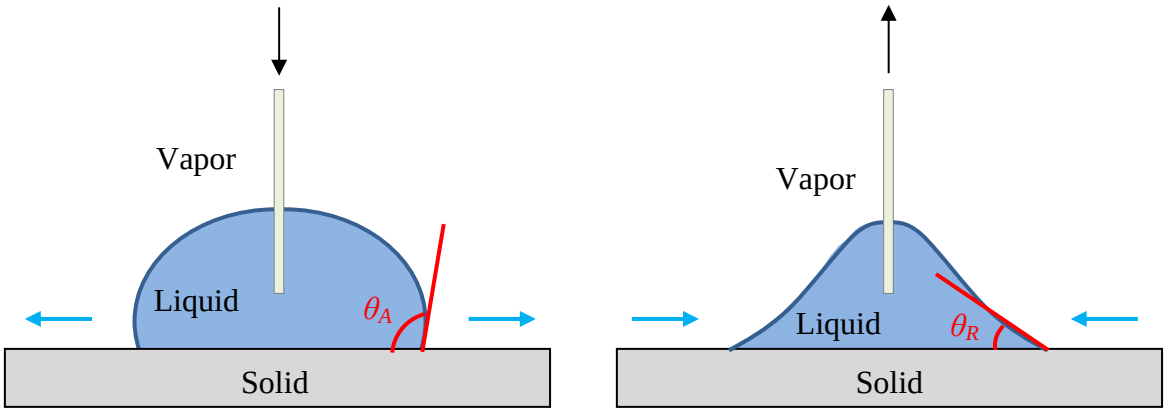

Figure 6. Inject and remove liquid method. (a) Inject liquid into a droplet; (b) remove liquid from a droplet. θ_A is the advancing CA, while θ_R is the receding CA.

Hydrophobicity and superhydrophobicity

Hydrophobic surfaces exist broadly in nature, such as a Lotus leaf[43–45], a Lady's mantle leaf[9,46,47] and a duck's feather[11,48]. They share the same characteristics, high roughness and high CAs for water. Young's CAs on smooth surfaces can reflect the wetting behavior of a liquid on a specific surface, as shown in Figure 7. When Young's CA for water is larger than 0° and smaller than 90°, the surface is said to be hydrophilic; when CA for water is larger than 90°, the surface is said to be hydrophobic. If the CA equals 0°, the surface is completely wet, while the surface is non-wetting when CA equals 180°.

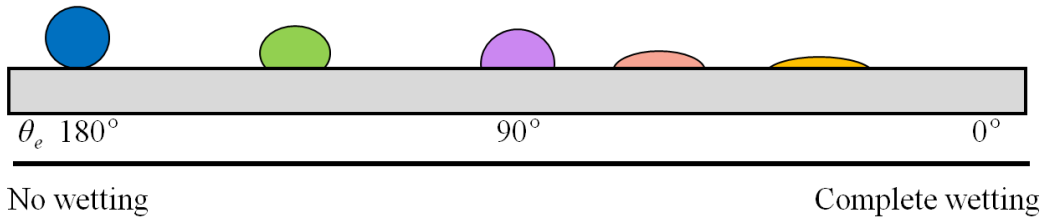

Figure 7. Different Young's CAs for various liquids on a smooth surface.

However, Young's CA is an ideal CA since perfectly smooth surfaces do not exist in real life. Smooth surfaces exhibit roughness in micro or nano scales when magnified. So, for a rough surface, the intrinsic and apparent CAs are used, as shown in Figure 8.

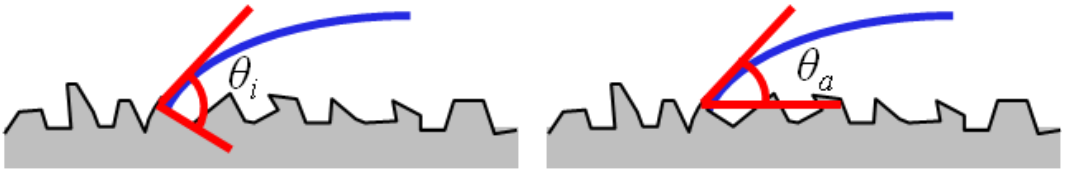

Figure 8. A droplet on a rough surface. θ_i is the intrinsic CA, while θ_a is the apparent CA.[41]

The figure shows the CAs at one of the solid-liquid-vapor interfacial points. The local intrinsic CA (θ_i) refers to the equilibrium CA when a droplet is deposited on a smooth surface with the same material, while the apparent CA (θ_a) refers to the CA that would be measured if the roughness is not taken into consideration.

A hydrophobic or SH surface is defined from the apparent CA and roll-off angle or CAH.[9,38,41,49,50] Hydrophobic surface has an apparent CA larger than 90°, while for a SH sur-

face the apparent CA is larger than 150°, both with low CAH. In this case, CAH is more accurate than roll-off angle, since a surface is not necessary hydrophobic with CA larger than 90° and smaller roll-off angle for a larger liquid.

To achieve a SH surface, a proper roughness is critical. Figure 9 shows the scanning electron microscope (SEM) photos for Lady's mantle leaf and duck's feather. Both of them have micro scale roughness, which contribute to their superhydrophobicity and the mechanism will be discussed in *Section 2.2.3 Wetting behavior of liquids*. To increase the hydrophobic and oleophobic property of a surface, such as for oil to survival, roughness in nano-scale might be necessary or surface energy needs to be decreased significantly.

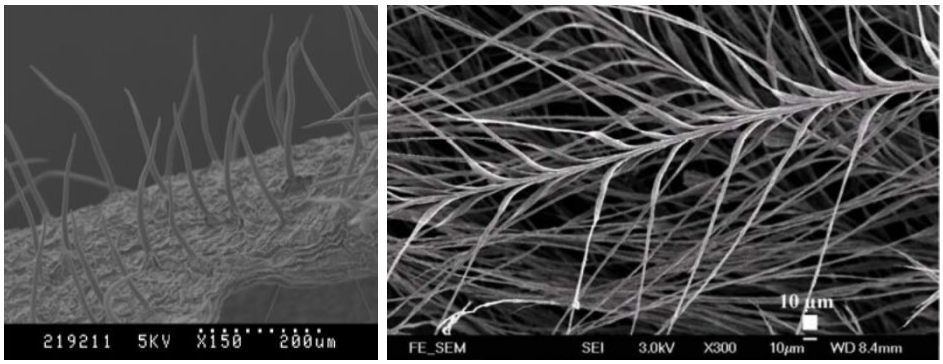

(a) (b)

Figure 9. SEM of surface structures. (a) Lady's mantle leaf,[46] (b) duck's feather.[48]

Oleophobicity and superoleophobicity

Similar to hydrophobicity and superhydrophobicity, an oleophobic or SO surface refers to a surface with apparent CA larger than 90° or 150° for oils, such as glycerol (γ = 64 mN/m) or

ethylene glycol (γ = 47.7 mN/m). There is no agreed-on value for the CAH. Compared with water (γ = 72.8 mN/m), oils have much lower surface tensions, which make it more difficult to achieve the oleophobicity or superoleophobicity of a surface, such as dodecane (γ = 25 mN/m). SO surfaces do not exist in nature, but they can be designed with appropriate roughened texture in conjunction with chemical composition.[51] When a water drop is deposited on a SH surface, it stays on the top surface and a liquid-vapor-solid composite forms; when an oil drop is deposited on a surface, a meta-stable state might occur. The oily liquid may move from a CB state to a Wenzel state gradually.

A water or oily liquid can survive on either hydrophobic/oleophobic or hydrophilic/oleophobic surfaces with the appropriate roughness. Robustness is used to study a liquid on a surface only when a liquid-vapor-solid composite is formed (CB state), which is less meaningful for a completely wet surface (Wenzel state).

2.2.3 Wetting behavior of liquids

Wetting behavior on smooth surfaces

Wetting behavior of a liquid on a flat smooth surface can be illustrated by Figure 4 and Equation (4). To obtain the CA from Young's equation, when the adsorption at the solid-vapor and liquid-vapor interface is neglected, which implies $\gamma_{SV} \approx \gamma_S$ and $\gamma_{LV} \approx \gamma_L$, Young's equation can be rewritten as:[5]

$$\cos\theta_e = \frac{\gamma_S - \gamma_{SL}}{\gamma_L} \tag{6}$$

where θ_e exceeds 20° for a low-energy surface.

The Dupré equation indicates that the reversible work of adhesion for solid-liquid interaction equals to the negative of the surface free energy of adhension:[5]

$$W_{SL}{}^{a} = \gamma_S + \gamma_L - \gamma_{SL} \tag{7}$$

where $W_{SL}{}^{a}$ refers to the work of adhesion for solid-liquid interaction.[5]

Combining Equations (6) and (7) gives the Young-Dupré equation below:[5]

$$W_{SL}{}^{a} = \gamma_L(1+\cos\theta_e) \tag{8}$$

A method for γ_{LV} is proposed by Fowkes et al[41,52,53]. The solid-liquid interfacial energy is given:

$$\gamma_{SL} = \left(\sqrt{\gamma_S} - \sqrt{\gamma_L}\right)^2 \tag{9}$$

The thermodynamic work can be calculated as follows:

$$W_{SL}{}^{a} = 2\sqrt{\gamma_S \cdot \gamma_L} \tag{10}$$

Combing Equations (9) and (10), Equation (7) can also be derived. The surface tension of a liquid or solid can be obtained:[5]

$$\gamma = \gamma^d + \gamma^p + \gamma^{ind} + \gamma^H + \gamma^m + \ldots \tag{11}$$

where *d, p, ind, H* and *m* refer to London-van der Waals forces, permanent dipoles, induced dipoles, hydrogen bonds and metallic interaction, respectively. All of the components or dominant components can be substituted into the equations above to achieve related variables.

Also, from Equations (7) and (8), (γ_S - γ_{SL}) can be obtained from CA measurements. Therefore, when γ_{SL} is known, γ_S can be evaluated. γ_{SL} can be described as a function of γ_S and γ_L as below:[5]

$$\gamma_{SL} = \gamma_L + \gamma_S - 2\sqrt{\gamma_L \gamma_S}\, e^{-\beta(\gamma_L - \gamma_S)^2} \tag{12}$$

where β =*0.0001247*$(\mathrm{m}^2/\mathrm{mJ})^2$. It is determined by a series of experiments with a number of liquids on different surfaces. This is applicable only when γ_{SL} and γ_{SV} are very close or for similar type molecules following the geometric mean combining rule.

Wetting behavior on rough surfaces

The wetting behavior of a sessile drop on a smooth surface can be described by Young's equation[5,10] and Laplace pressure,[54] which have already been discussed in *Sections 2.2.1* Surface tension and Laplace pressure and *2.2.2* Hydrophobic and oleophobic surfaces. As shown in Figure 10, when a droplet is deposited on a rough surface and is in thermodynamic equilibrium, two scenarios can occur, either the surface will be completely wet or partially wet.

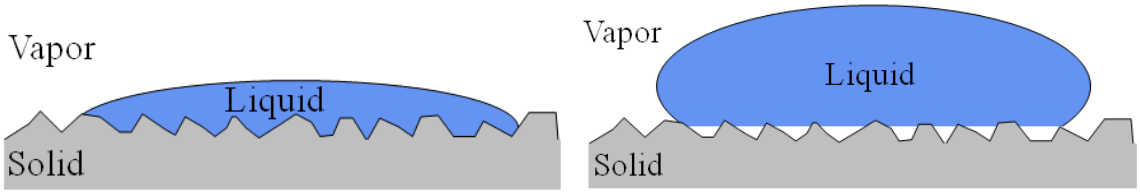

(a) (b)

Figure 10. Wetting behaviors of liquids on rough surfaces. (a) Wenzel model, and (b) Cassie-Baxter (CB) model.[11,12,23]

In first case in Figure 10(a), the droplet fully wets the rough surface and this case is called the Wenzel state. The apparent CA of the Wenzel state is defined as θ_r^W, which is directly affected by the surface roughness *r*:

$$\cos\theta_r^{\,W} = r\cos\theta_e \tag{13}$$

r refers to the real area of a rough surface divided by the projected area, and is no smaller than 1. Roughness will increase the original phobic or philic property of a surface, which means that the surface will be more hydrophobic/oleophobic or hydrophilic/oleophilic as the roughness increases, compared with the smooth surface made from the same material.

In the second situation shown in Figure 10(b), the liquid is unable to displace the air gaps trapped and sits on a mixture of air spaces and peaks of the rough material. This is the Cassie-Baxter (CB) state where the apparent CA, θ_r^{CB} is affected by f_1 and f_2. f_1 is the true contact area between the droplet and the solid divided by the projected area, while f_2 is the area of the droplet in contact with the vapor divided by the projected area. It is expressed as:

$$\cos\theta_r^{\,CB} = f_1\cos\theta_1 - f_2 \tag{14}$$

where θ_1 refers to the equilibrium CA between liquid and solid.

Marmur[20] studied the "competition" between CB and Wenzel states and rewrote the equation as:

$$\cos\theta_r^* = r_f f \cos\theta_e + f - 1 \tag{15}$$

where θ_r^* refers to the apparent CA for a rough surface, r_f is roughness of wetted area, f is the fraction of the projected area below the wetted solid surface.

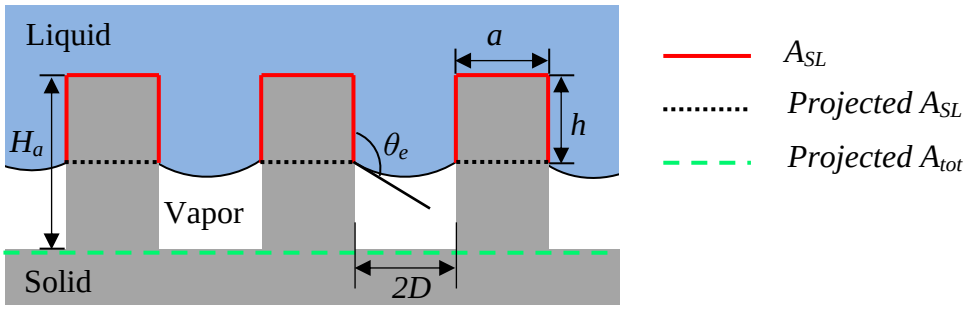

Figure 11. A Liquid on a rough surface in CB state and the parameters.

The parameters mentioned above can be explained with Figure 11, which shows a liquid sitting on a rough surface in CB state. Young's CA (θ_e) is depicted in the figure. A_{SL} refers to the solid-liquid contact area, *Projected* A_{SL} refers to the projected area of solid-liquid actual contact area, and *Projected* A_{tot} refers to the total projected area of the rough surface. The total roughness r, f_1, r_f and f in one unit cell are calculated below. The following equation for f_2 is only valid when the liquid-vapor interface is flat or the sagging is very small,

$$r = \frac{a + 2D + 2H}{a + 2D} \tag{16}$$

$$f_1 = \frac{a + 2h}{a + 2D} \tag{17}$$

$$r_f = \frac{a + 2h}{a} \tag{18}$$

$$f = \frac{a}{a + 2D} \tag{19}$$

$$f_2 = 1 - f = \frac{2D}{a + 2D} \tag{20}$$

Equation (15) describes both homogeneous (Wenzel) and heterogeneous (CB) wetting behaviors, which is essential to design a SH and SO surface. In addition to the Wenzel and CB states, there is a third of kind wetting behavior for a drop sitting on a rough surface, the meta-stable state. It is defined as an unstable state, which will be transformed to a CB or Wenzel model, depending on the local and global minimum Gibbs surface free energy.[22,27,30,31] Gibbs free energy of a surface refers to the thermodynamics potential of a system at a constant temperature and pressure. It can be calculated as, $G = \gamma_{LV} A_{LV} + \gamma_{SV} A_{SV} + \gamma_{SL} A_{SL}$. In the expression, G is the free energy of a surface; $A_{LV,} A_{SV}$ and A_{SL} refer to the contact areas of liquid-vapor, solid-vapor, and solid-liquid, respectively. Between CB and Wenzel states of a system, there might be an energy barrier and a series of meta-stable states may occur during the transition between the two states. The meta-stable state is very important for the study of robustness of a rough surface.

2.2.4 Wetting behavior and textile structures

Fiber structure

In addition to wetting on flat surfaces, the wetting behavior of liquids on fibers with different geometries have also been widely studied[55–60]. The most simple wetting behavior for a single fiber is capillary action shown in Figure 12.[61] For a hydrophilic or oleophilic fiber in Figure 12(a), the liquid adsorbs on the solid surface and forms a CA smaller than 90°; for a hydrophobic or oleophobic fiber in Figure 12(b), the liquid is repelled from the solid surface and forms a CA larger than 90°.[56]

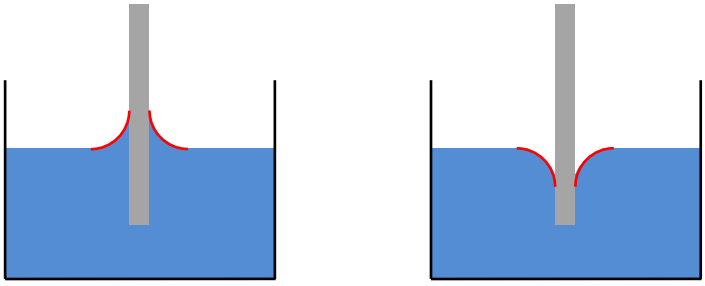

Figure 12. Capillary action of a single fiber in a tank. (a) a hydrophilic or oleophilic fiber, and (b) a hydrophobic or oleophobic fiber.

The bell-shape of liquid on a cylindrical fiber body has been studied with elliptic integrals[55] under the condition that the pressure through the entire liquid-vapor interface is the same. In the same manner, Du et al extended the liquid shapes to those both on the top part and at the bottom section of a fiber.[59,60] In addition to the wetting behavior of liquids on cylindrical fibers, the behavior of small droplets on conical fibers were also discussed.[57,58]

Then, Hoit[62] researched the liquid behavior on parallel nylon and modified nylon monofilaments. As shown in Figure 13, a liquid sits on parallel monofilaments while the sagging is simplified. When it is in CB state,[19]

$$\cos\theta_r^{CB} = \frac{R(\pi-\theta_e)}{R+D}\cos\theta_e + \frac{R}{R+D}\sin\theta_e - 1 \tag{21}$$

When it is in Wenzel state,[62]

$$\cos\theta_r^{W} = \frac{\pi R + R + D}{R+D}\cos\theta_e \tag{22}$$

and reasonable agreement was found between experimental and predicted results for the apparent CAs. The liquid behavior between fibers are often used to simulate the wetting characteristics and to study the robustness of nonwoven fabrics.[33–36,39,63–66]

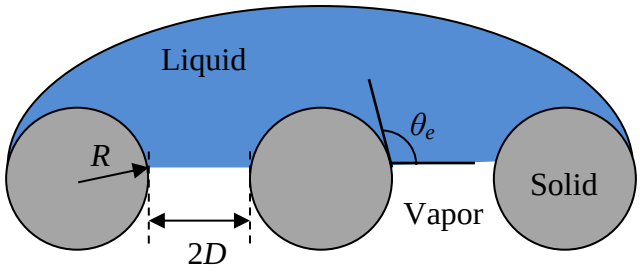

Figure 13. A liquid on parallel monofilaments.

Yarn structure

Yarns include twisted staple yarns and untwisted parallel multifilament. There are very few studies of the wetting behavior of staple yarns due to their complex structures. Parallel fila-

ments can be assumed to be rigid cylinders, the wetting behavior has been studied for multi-filaments shown as follows:[67,68]

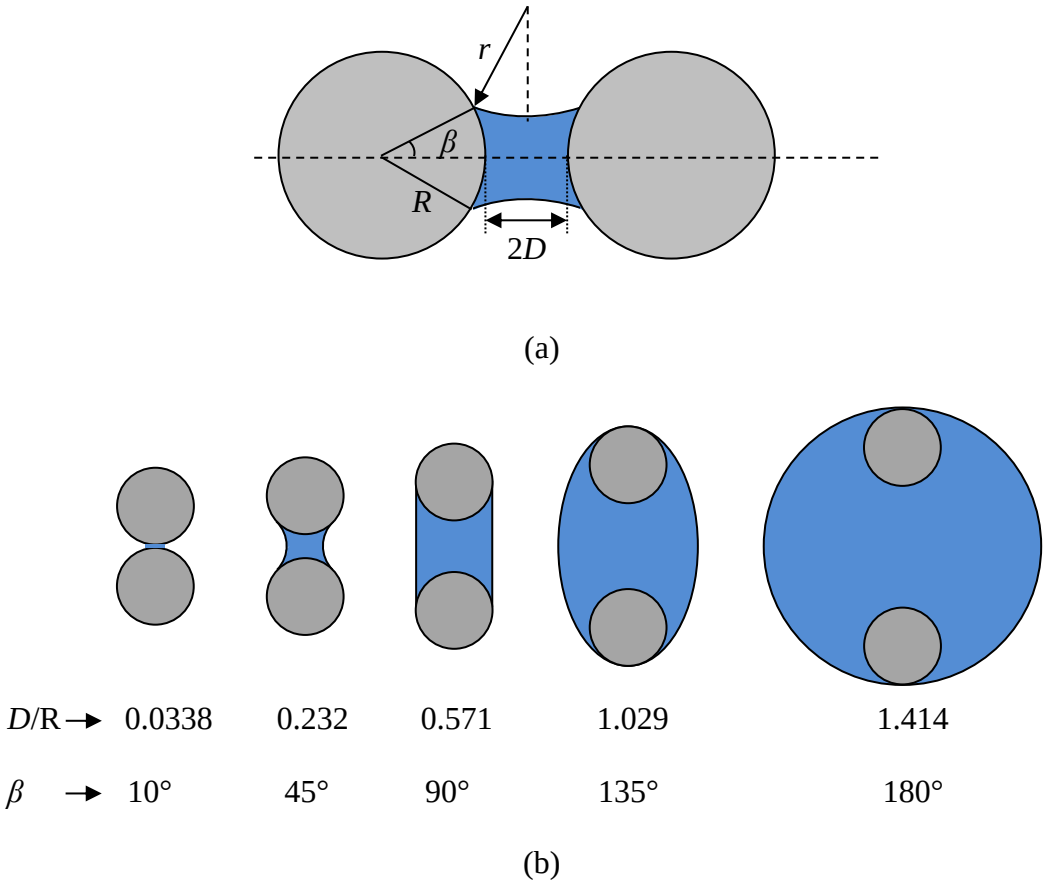

Figure 14. Cross-section of a liquid between two cylinders, (a) parameters explanation, (b) cross-section of a liquid between two cylinders when Young's CA is 0°.[62]

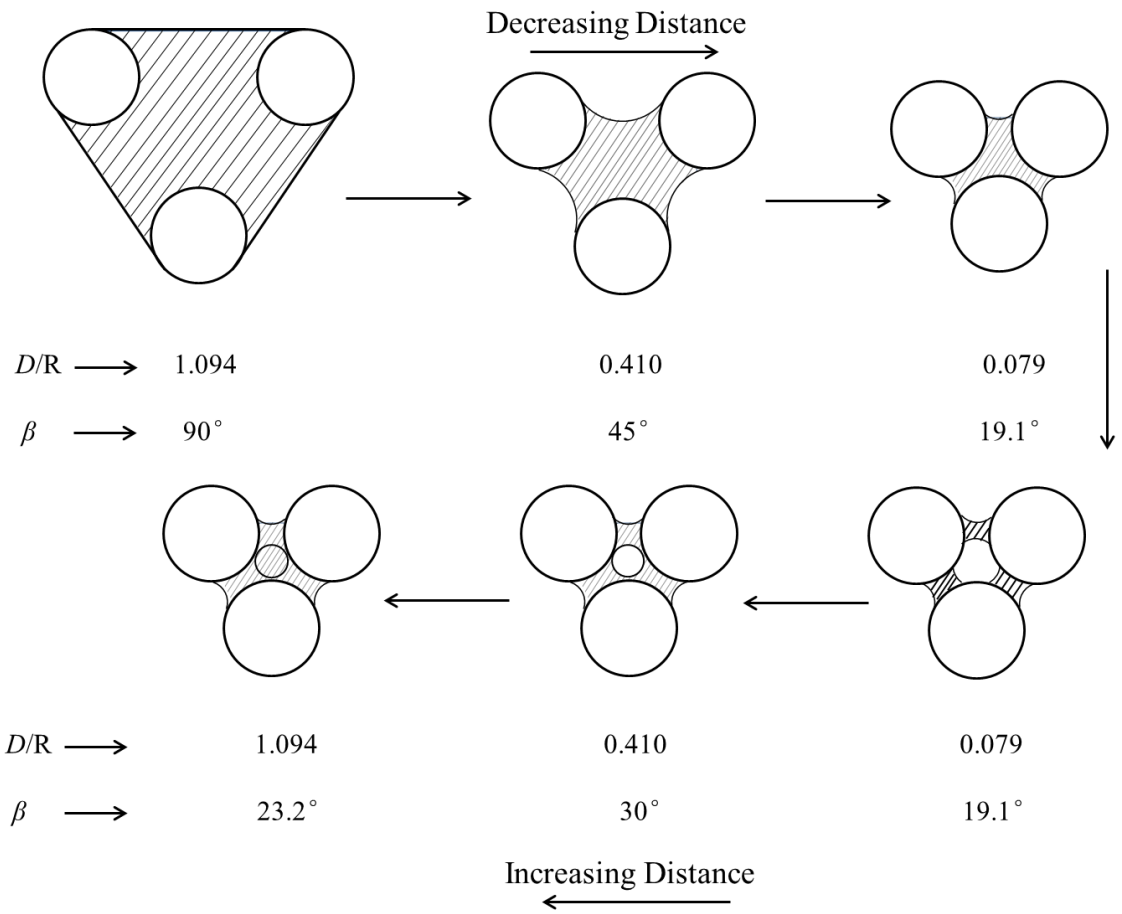

Figure 15. Cross-section of a liquid between three cylinders when Young's CA is 0°.[62]

In Figure 14 and Figure 15, both wetting behaviors of two and three cylinders are shown. When the separation distance and encompassing CA are changed, the cross-sections for wetting will also change. In Figure 15, there is a critical separation *D/R*= 0.079. A hole forms when the separation is decreased to less than 0.079, and a higher encompassing angle needs to be reached to eliminate the hole. These properties provide evidence to design yarns with desired wetting behaviors.

Fabric structure

The appropriate fabric structure to produce hydrophobic and oleophobic surface includes nonwoven, woven and flock fabrics.[9,19,69] Nonwoven fabric has relatively random structure, which can be simplified to model the apparent CA in CB state as described by Equation (23). However, the random structure of nonwoven fabric is made of fibers with different radii and different fiber spaces. Therefore, the average number of each parameter is more accurate. Both multifilament yarns and monofilament plain woven fabric can be used to make hydrophobic and oleophobic surfaces. As an example, a monofilament woven fabric is shown in Figure 16. A liquid-vapor-solid composite forms when a droplet is deposited on its surface. The predicated apparent CA is:[69]

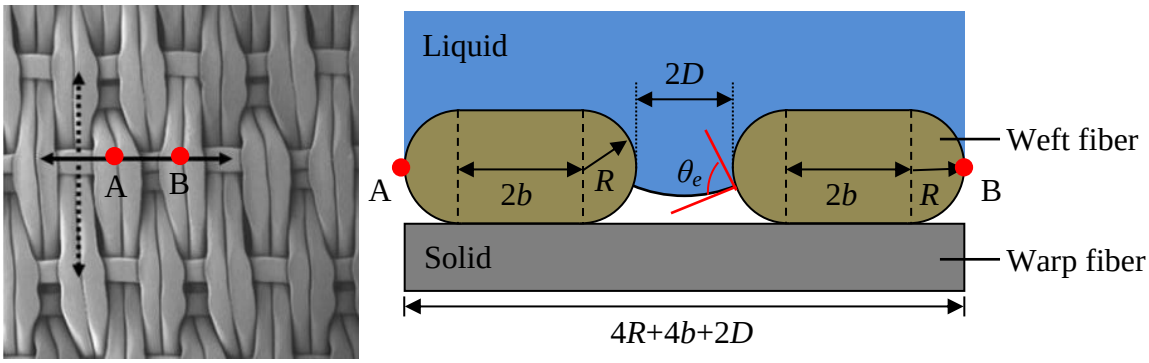

(a) (b)

Figure 16. A monofilament made into a plain woven fabric. (a) Monofilament woven, solid line is warp direction while dotted line is weft direction, (b) cross-section view.[69]

$$\cos\theta_r^{CB} = \frac{b + R(\pi - \theta_e)}{b + R + 0.5D}\cos\theta_e + \frac{b + R\sin(\pi - \theta_e)}{b + R + 0.5D} - 1 \qquad (23)$$

where θ_e is the Young's CA. Similarly, for a flock fabric,

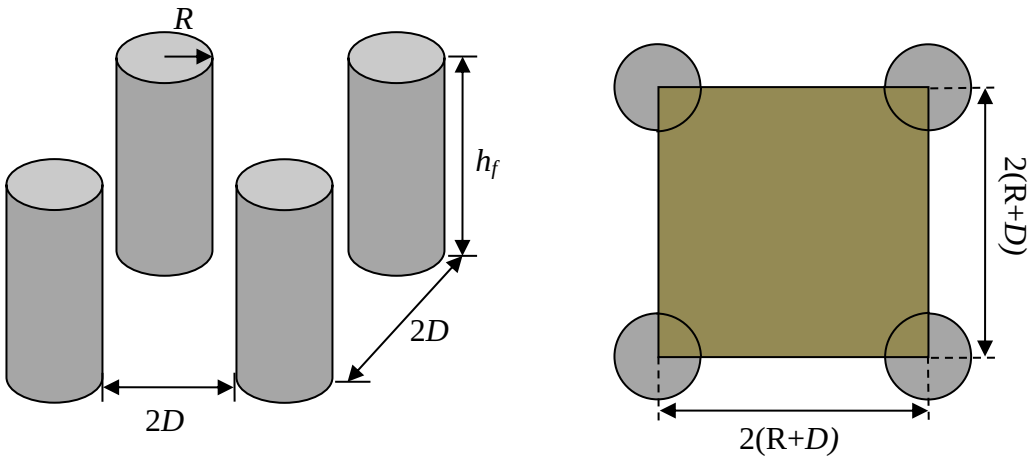

Figure 17. A flocked fabric (a) side view, and (b) top view.[9]

The predicted apparent CA is:

$$\cos\theta_r^{CB} = \frac{\pi R^2}{(2R+2D)^2}(\cos\theta_e + 1) - 1 \qquad (24)$$

All the fabrics with different structures need chemical treatment to decrease the surface tension; the roughness can also be designed by adjusting the construction.

2.2.5 Chemical modification

The concept of hydrophobicity such as Lotus leaf and duck's feather is that the structures of these surfaces are highly rough on a small scale. It indicates that roughness will be helpful to increase the hydrophobicity and oleophobicity of a surface, and that agrees with the discus-

sion for the wetting behavior of liquids. Another criterion is the surface energy of the solid surface. When the surface energy of the solid is lower, the surface is more hydrophobic or oleophobic. For example, polytetrafluoroethylene (PTFE) (γ_{LV} = 18.5 mN/m) has higher hydrophobicity than that of nylon (γ_{LV} = 47 mN/m).

To make a hydrophobic and oleophobic surface, bio-mimicry technologies have been used to increase the roughness and decrease the surface tension of a rough surface. Bhushan et al[43,70] mimic the hierarchical roughness of Lotus leaves, by replication of a micro patterned surface using the recrystallization of tubular waxes. Nano structure is made from the three-dimensional wax casting. This technology produces surfaces with good superhydrophobicity (160°-170°) and low CAH (2°-5°). SH surfaces can also be made by coating carbon nanotubes (CNT) with polybenzoxazine coatings on glass or metal substrates, which experiments show are durable and robust.[71] Similarly, perfluoropolyether oligomer based organic-inorganic hybrid material can be coated on glass substrates through a sol-gel process, and the modified surfaces display strong hydrophobic and oleophobic characteristics.[72]

Gao and McCarthy[73] researched the effects of organosilane on hydrophobicity, and produced a perfectly hydrophobic surface called "Lichao's surface" as shown in Scheme 1. They studied the reaction of silicon wafer with $MeSiCl_3$, and found that "vertical polymerization" of $MeSiCl_3$ might be promoted into a covalent toluene-swollen 3D network. The methylsilicone network on the surface dramatically increases the CA and decrease CAH for water (θ_A/θ_R = 180°/180°). Later they[38] reported a commercial lubricant, oligomeric tetrafluoroethylene

(OTFE), which is a mixture of "trifluoromethy-terminated tetrafluoroethylene oligomers of molecular weight 700-4000 with a higher vapor pressure" according to company information. OTFE can form a monolithic film when compressed between two flat surfaces. It exhibits perfect hydrophobicity with nearly 180° CA and θ_A/θ_R = 180°/180° for water, and very good lyophobicity showing θ_A/θ_R = (>175°)/(>175°) for oils with surface tension larger than 49 mN/m. They also reported that the OTFE surface has lower CAH for oils compared with Lichao's surface. In addition, Gao and McCarthy[74] proposed the wetting behavior of a polymer surface changes considerately when topography varied from studies of polyethylene (PE) and polytetrafluoroethylene (PTFE) which were heated while in contact with anodized aluminum membranes.

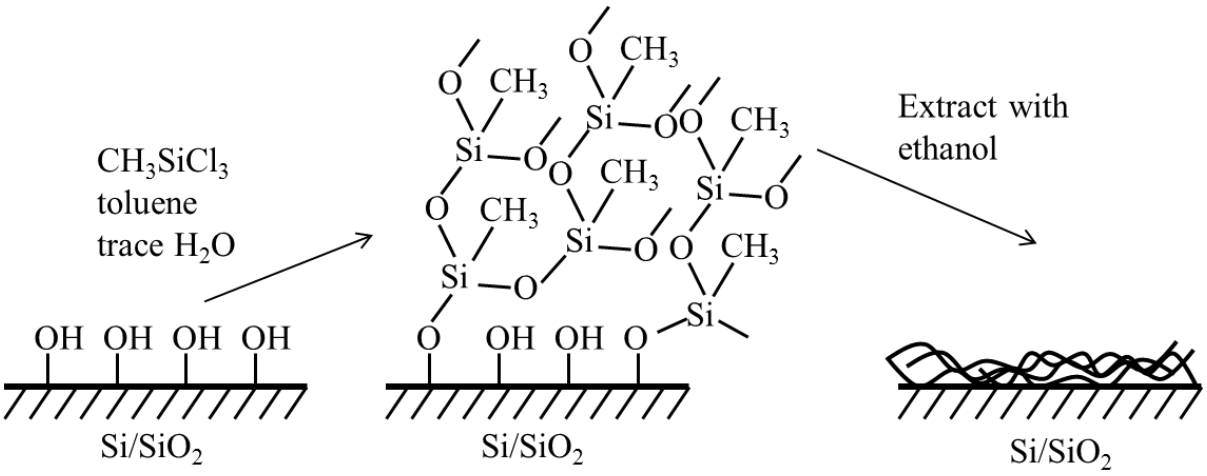

Scheme 1. Formation of methylsilicone network on silicon wafer.[73]

Lee et al[9,18,19,75] made woven, nonwoven and flock fabrics with nylon, nyco (the ratio of nylon and cotton is 50:50) and other materials, and grafted fluoro chemicals, such as fluorosilane, onto the surfaces to obtain the superhydrophobicity and superoleophobicity. The mechanism is to decrease the surface tension by converting the (-OH) groups into carbon-fluoride groups as shown in Scheme 2. (-XH) group can be (-OH), (-COOH) and ($-NH_2$) in the scheme. As the chemical structure of the surfaces is changed, the roughness of these surfaces will also vary. The combination of these effects lead to the superhydrophobicity and superoleophobicity, which are the two criteria for SH and SO surfaces.

In addition, an intelligent SH surface can be fabricated from ZnO nanorod arrays, where the adhesion between water and the surface is reversible by applying UV illumination to decrease the hydrophobicity or heat treatment to gain the hydrophobicity back.[76] Plasma treatment can do the polymerization or coat low-surface tension chemicals on a surface to achieve phobicity.[77–83] Other methods, such as electro spinning[84], chemical vapor deposition[17] and others could also be used.[2–4,85–87]

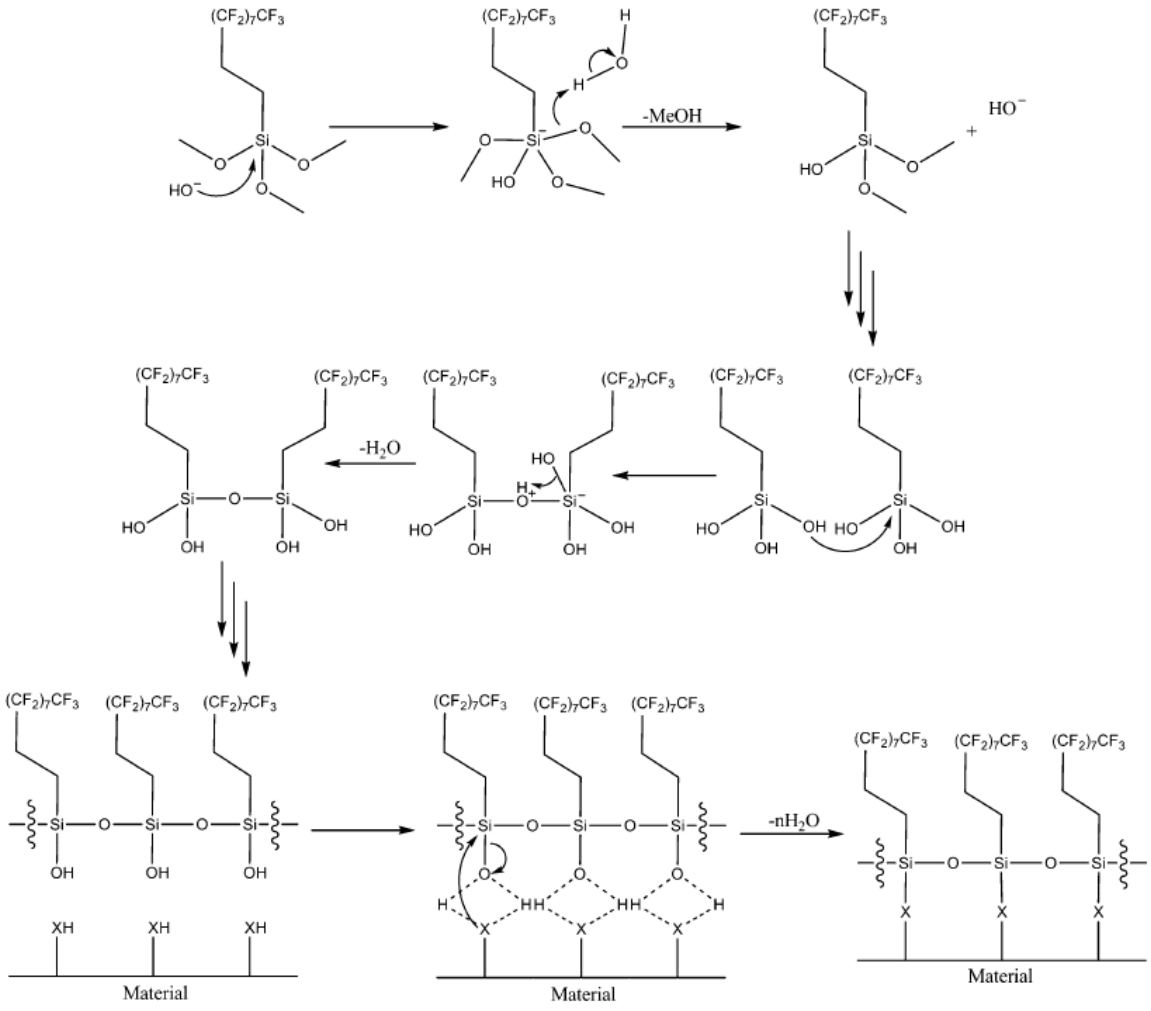

Scheme 2. Mechanism of modification of surfaces with fluorosilane.[2]

2.3 Robustness of hydrophobic and oleophobic surfaces

Even though SH and SO surfaces have been studied for decades, robustness of a rough surface is still a new research field, which has drawn considerable attention in recent years. In this section, wetting behavior of a liquid between two smooth substrates or a capillary bridge is reviewed as preparation for study of rough surfaces. Theoretical modeling for the robust

pressure of two parallel monofilaments is discussed, and Gibbs free energy of the surface is also used to evaluate the robustness of a uniform rough surface qualitatively. Finally, robust pressures for nonwoven fabric and electrospun mat have been briefly reviewed.

2.3.1 Robustness and robust pressure

Robustness is used to describe the minimum pressure required to push a sagging liquid-vapor interface to touch the bottom of a rough surface or to achieve a Wenzel state, as shown in Figure 18. The minimum pressure is defined as robust pressure, which can be caused by external force or even its own weight.[88] Once the liquid penetrates through the texture and reaches the bottom, the surface will be completely wet and the surface is not robust to this liquid; if the liquid stays in meta-stable CB state, the surface is robust to this liquid. Robustness can only be defined based on the properties of a liquid and a rough surface. It is only valid for rough and hydrophobic or oleophobic surfaces since there will be no sagging of liquid-vapor interface on a smooth or hydrophilic or oleophilic surface.

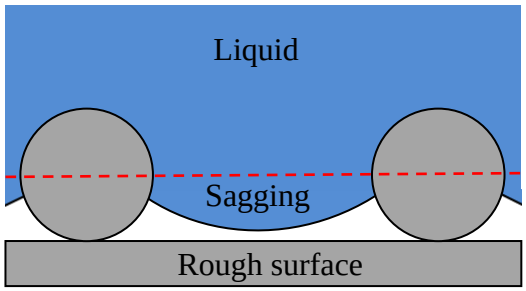

Figure 18. Liquid sagging on a rough surface.

To represent robustness, the dimensionless robust height and robust angle were used to predict the robust pressure or breakthrough pressure.[1] The robust pressure is the external pressure required to force the liquid-vapor interface to move, and transit from a liquid-vapor interface to a fully wet solid-liquid interface. The robust pressure due to the external force is different from the hydrostatic pressure which causes the penetration of a liquid under gravity. The SI unit of robust pressure is N/m^2 or Pa, which can be experimentally obtained from robust force per unit area.

Currently, there is no commercial instrument to measure the robust pressure, but many researchers have developed their own equipment to measure robust force. The general approach is to push a liquid on a rough surface with a desired material.[33,34,39]

2.3.2 Robustness and capillary bridges

Robustness and capillary forces

For a robustness test, a droplet needs to be squeezed on a rough surface by introducing another surface, thus a capillary bridge forms between them. The external force applied by pushing the second surface leads to changing shapes of the liquid bridge; the force due to curvature changes of the liquid is called the capillary force. The capillary force can be positive or negative, depending on the properties of liquid and solid surfaces. If the liquid tends to draw two surfaces together, the capillary force is negative and at least one of the two surfaces is hydrophilic or oleophilic to the liquid; if the liquid tends to push two surfaces apart, the capillary force is positive and at least one of the two surfaces is hydrophobic or oleopho-

bic to the liquid. Therefore, the capillary force is an adhesive force in the first case, while it refers to the robust force when a rough surface is used in the second case.

The robust force of a hydrophobic and oleophobic rough surface can be measured via the capillary bridges by compressing a water or oil droplet into hydrophobic and oleophobic rough surface. Likewise, the anti-adhesive property of the fabric can also be determined by drawing the liquid out of the fabric. The anti-adhesive force describes the preference of a surface to keep itself clean, and weak adhesive force shows better anti-adhesive properties. Vagharchakia et al,[39] inspired by the Johnson, Kendall and Roberts (JKR) test, developed a quantitative test to characterize the very weak adhesive surfaces through the formation and breakage of capillary bridges. As mentioned before, robustness does not have a realistic meaning when smooth or hydrophilic or oleophilic surfaces are applied. However, due to the complex structure of a rough surface and the simultaneous spreading and penetration behaviors of the liquid under pressure, smooth surfaces could be a better choice to understand the wetting behavior of droplets between two surfaces in the beginning. Most of the studies about capillary bridges are for smooth surfaces. It will be very helpful in the study of the robust pressure on a rough surface.

The wetting behavior of a sessile drop on a smooth surface or a liquid bridge between two surfaces can both be described by Young's equation[89] and Laplace pressure[54], but an applied external force will be considered for a capillary bridge. In earlier studies, capillary bridges are roughly divided into three types based on the geometrical shapes of the substrates, includ-

ing liquid bridges between spherical-spherical surfaces[33,90–93], spherical-flat surfaces[37,39,94] and flat-flat surfaces.[34,64,95]

McFarlane and Tabor[96] presented the capillary force of a liquid contacting with a sphere and a flat surface. The spherical bead and substrate should be made from the same material, so surface tensions of the solid surfaces and solid-liquid-vapor CAs are the same. When the influence of humidity in the atmosphere is neglected, the capillary force was described as:

$$F_{cap} = 4\pi R\gamma_{LV}\cos\varphi \tag{25}$$

where F_{cap} is capillary force, R is radius of the spherical bead, φ is the CA between liquid and solid (either the spherical bead or the flat surface), and γ_{LV} is liquid-vapor interfacial energy.

This equation applies only when the thickness of the liquid film is very thin (below 1000 Å) and the contact angels are very small. Later, O'Brien and Hermann[97] improved the equation as:

$$F_{cap} = 2\pi R\gamma_{LV}(\cos\phi_1 + \cos\phi_2) \tag{26}$$

where F_{cap} is capillary force, R is radius of a spherical bead, and φ_1 and φ_2 are the CAs between liquid and the spherical bead or the flat surface as shown in Figure 19.

This expression can be used for dissimilar solid materials. When $\varphi_1 = \varphi_2$, Equation (26) will become Equation (25). However, the equations only describe the capillary forces due to Laplace pressure, and the force caused by surface tension is not given. Equation (26) shows the

capillary force with the reduced and simplified Laplace pressure component. This expression applies for small volumes of liquids and small β.

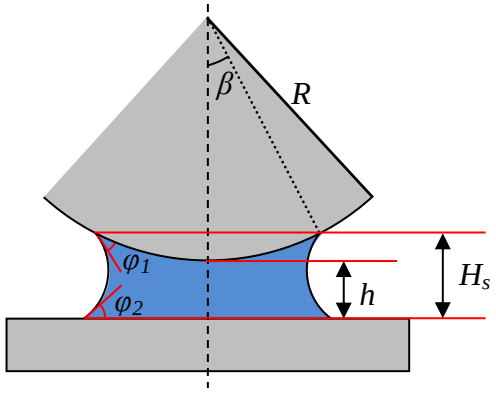

Figure 19. Liquid bridge between a spherical bead and a flat surface with separation *h*.

The force expressions for the capillary bridges with a fixed volume between a sphere and a plate surface were later adopted and improved by Rabinovich et al[33], and the effects of surface tension term were added as follows:

$$F_{cap} = \frac{H_s - h}{H_s} \cdot 4\pi R\gamma_{LV} \cdot \cos\varphi + 2\pi\gamma_{lv} R \cdot \sin\alpha \sin(\varphi + \alpha) \qquad (27)$$

where β is "embracing angle", h and H_s are the smallest and largest distance between the spherical bead wetted by liquid and the flat substrate as shown in Figure 19.

Rabinovich et al[33] derived the capillary force, Laplace pressure and volume mathematical expressions for the capillary bridge between a sphere and a flat surface, with the assumption that the profile of the bridge is part of a circle in one dimension. Then, they extended the

force expressions to liquid bridges between two spheres with a fixed liquid volume and similar results were obtained (not shown). Several groups have made a circular approximation for the profiles, which simplifies the curvature, but it does not meet the condition that the pressures through the entire liquid-vapor interface must be the same. As shown in Figure 20, from the definition of principal radii, for a liquid bridge between two surfaces, if the profile of liquid-vapor interface is assumed to be an arc from a circle with radius R_2 in one dimension, the other principal radius at point *A* or point *B* would be R_{11} or R_{12} respectively. Obviously, R_{11} or R_{12} are not equal, but the Laplace pressure requires them to be equal since they share the same R_2. Therefore, a circular approximation might work for small droplets but it is not valid in general.

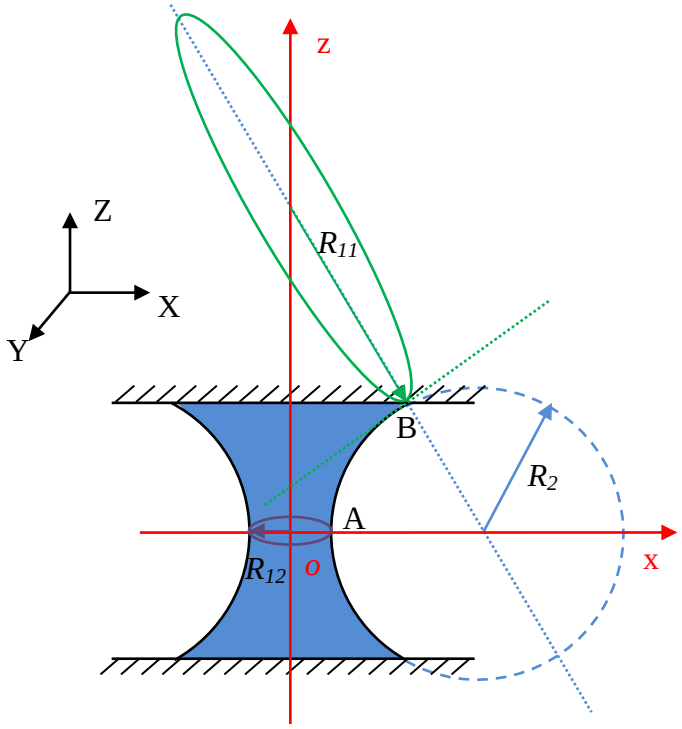

Figure 20. Schematic diagram for a liquid bridge between identical parallel substrates.

The earliest study for liquid bridges between two spheres goes back to Fisher et al,[97,98] who first presented the behavior of a capillary bridge between ideal soil particles and how to get the capillary force quantitatively. Mason and Clark[90] also proposed numerical methods for the capillary force between two identical spheres as well as the relationships between capillary force and Laplace pressure. Their capillary force expression for identical spheres is:

$$F_{cap} = \pi R^2 \sin^2 \beta \cdot \Delta P + 2\pi R \sin \beta \cdot \gamma_{LV} \tag{28}$$

where F_{cap} is capillary force, R is radius of a spherical bead, and β is "embracing angle" as shown in Figure 21. γ_{LV} is liquid-vapor interfacial energy and ΔP is Laplace pressure.

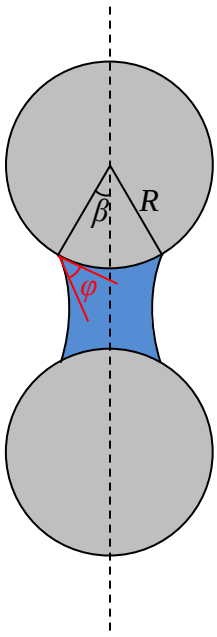

Figure 21. A capillary bridge between two identical spheres.

The capillary force for a liquid bridge between two spheres is composed of two parts, due to Laplace pressure and surface tension, respectively. The total capillary force is the sum of the partial forces in vertical direction. This equation is valid for a thin liquid film between two spheres, but the CA φ was not included, which implies that it is incorrect even for small volume liquid with this approach.

Orr and Scriven,[37] Knospe and Nezamoddini[63], and De Souza et al[34,64] generated the force analysis of a liquid bridge between parallel substrates as shown in Figure 22. The expression is quite similar to that of liquid bridges between two identical spheres, but the CA is brought in:

$$F_{cap} = \pi R_D{}^2 \cdot \Delta P + 2\pi R_D \cdot \gamma_{LV} \sin\varphi \tag{29}$$

where R_D is the radius of the wetting area of liquid and solid interface, and φ is the CA between a liquid and a solid.

This capillary force is also divided into two parts: a surface tension force ($2\pi R_D \gamma_{LV} sin\varphi$) which resides in the meniscus and a capillary pressure force ($\pi R_D{}^2 \Delta P$) which is transmitted by the liquid based on the Young-Laplace equation. The expression of capillary force by Orr and Scriven[37] is obtained from equilibrium force analysis of the solid-liquid interface of the capillary bridge and the bottom substrate, and it can be applied to flat smooth surfaces.

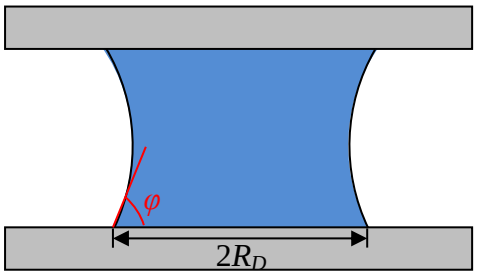

Figure 22. A liquid bridge between two parallel smooth surfaces.

De Souza et al[34] presented the numerical and analytical calculations of the capillary forces of liquid bridges between chemically different substrates based on the curvature of the capillary bridge, and revealed that the capillary force and the rupture separation decreases as the asymmetry in CAs is increased with the sum of the CAs fixed. Gao and McCarthy et al[64] also employed this capillary force expression when they were researching the effect of CAH on the measurement of capillary forces. Butt[35] studied the influence of roughness and heterogeneity on the capillary force with an asperity distribution function. The capillary force was expressed as a function of integrated height distribution, with the assumption that the liquid menisci stay parallel to the apparent surface and the projected length of the rough surface is much larger than the depth of the rough structure. The capillary force between rough spheres was calculated with this approach but there were no experimental results shown. This force analysis will contribute to evaluating the robustness and anti-adhesive properties of SH and SO surfaces.

Robustness and capillary profiles

Capillary force of a liquid bridge with a hydrophobic and oleophobic rough surface is the robust force, which can help obtain the robust pressure or robustness of the rough surface for known contact area. To maintain the uniformity of the applied external pressure, parallel substrates are often used both for theoretical modeling and in experimental design. In Equation (29), all the parameters are easy to obtain except the Laplace pressure. From the definition of Laplace pressure, it can be calculated from two principle radii of any point on the liquid-vapor interface or the liquid-vapor profile of a liquid bridge. Therefore, capillary profiles of liquid bridges are reviewed. The mean surface curvature and Laplace pressure have been applied to derive the profile of a liquid bridge between a sphere and a flat surface.

Vagharchakian et al[39] explored the curvature of the liquid between a glass sphere and a liquid bath from the surface curvature method and concluded that the velocity, viscosity, and the volume of the drop can strongly affect the changing shape of the liquid. As shown in Figure 23, they used Mathematica to simulate the profile of the liquid numerically, with the equation below:

$$\frac{Z}{l_{cap}} = \frac{\ddot{X}}{(1+\dot{X}^2)^{3/2}} - \frac{1}{r(1+\dot{X}^2)^{1/2}} \tag{30}$$

where $\ddot{X} = d^2X/dZ^2$ and $\dot{X} = dX/dZ$. The boundary conditions are $X(0) \rightarrow \infty$ at the liquid tank, while $\dot{X}(z_0) = \tan^{-1}(\beta+\varphi)$ at the glass surface with φ as the CA between glass and liquid and $\beta = \sin^{-1}(X/R)$. $l_{cap} = (\gamma_{LV}/\rho g)^{1/2}$, where γ_{LV} is liquid-vapor interfacial energy, ρ is liquid density and g is gravitational acceleration.

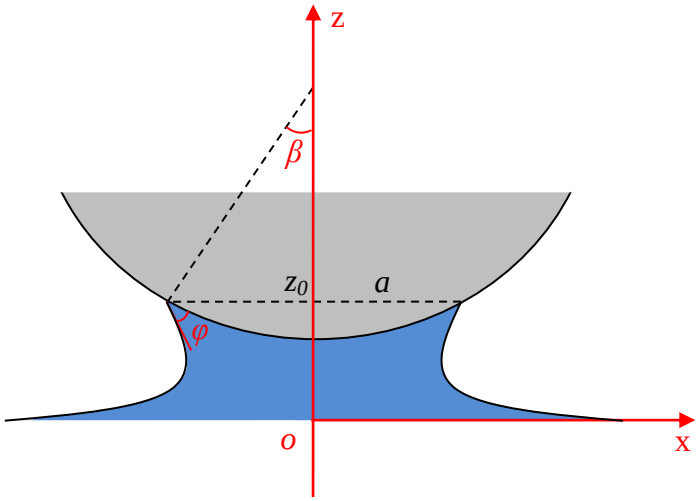

Figure 23. A liquid bridge between a glass sphere and a liquid bath, and the parameters.[39]

With the minimum energy approach, the *Z* value for each X can be found with other parameters fixed in the numerical simulation. They reported that the simulated profiles are fully consistent with their experimental results.

Orr and Scriven[37] also explained the curvature of liquid between a sphere and a flat surface but more systematically and comprehensively. The curvatures of liquids were predicted with different parameters, such as the CAs between liquid and substrates, the mean surface curvature and the surface tension. As shown in Figure 24, the curvature could be obtained from the expressions:[37]

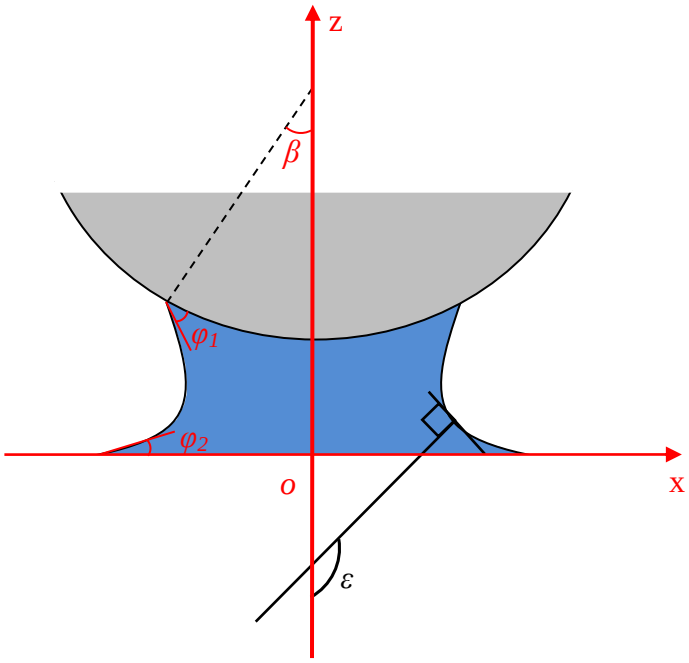

Figure 24. A liquid bridge between a sphere and a flat substrate, and the parameters.[37]

$$X = -\frac{1}{2H}\left[(-\sin\varepsilon) \pm \sqrt{(-\sin\varepsilon)^2 + c}\right] \tag{31}$$

$$Z = \frac{1}{2HR}\int_{-\sin(\pi-\varphi_2)}^{-\sin\varepsilon} \left(\frac{(-\sin\varepsilon)d(-\sin\varepsilon)}{\sqrt{1-(-\sin\varepsilon)^2}} \cdot \frac{(-\sin\varepsilon) \pm \sqrt{(-\sin\varepsilon)^2 + c}}{\pm\sqrt{(-\sin\varepsilon)^2 + c}}\right) \tag{32}$$

$$c = 4H^2R^2\sin^2\beta - 4HR\sin\alpha\sin(\varphi_1 + \beta) \tag{33}$$

where H is the mean surface curvature of the liquid-vapor interface, R is the radius of the sphere, φ_1 is the CA between liquid and the spherical bead, φ_2 is the CA between liquid and the flat surface, c is a constant shown in Equation (33).

The mathematical solutions theoretically explained the curvatures of shape of liquid bridges between sphere and flat surfaces, which can be part of the nodoid, catenoid, unduloid and

cylinder segments. However, no experimental profiles were reported, and there is no method proposed to obtain the mean surface curvature *H* in this analytical solution.

To get the mean surface curvature, Laplace pressure and profiles or capillary force of a liquid bridge between two substrates, similar assumptions were made as capillary force. The liquid-vapor interface was assumed to be an arc, and for the circular approximation of the bridge profile, De Souza et al[34] studied the capillary forces as shown in the following equations and Figure 25:

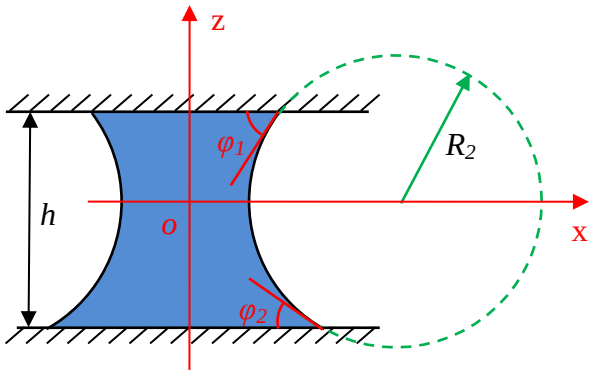

Figure 25. Schematic of a circular meniscus of a liquid bridge between two parallel substrates.[34]

$$R_2 = \frac{h}{(\cos\varphi_1 + \cos\varphi_2)} \tag{34}$$

$$F = \frac{\gamma_{LV} V(\cos\varphi_1 + \cos\varphi_2)}{h^2} + O(h^{-1/2}) \tag{35}$$

where R_2 is the radius of the circular approximated profile, h is the separation distance between two substrates, φ_1 and φ_2 are CAs for liquid with top and bottom substrates respectively, V is the volume of the liquid, and $O(D^{-1/2})$ is scaled surface tension term in the capillary force, which will be very small when D is close to zero.

In this case, the profile of liquid bridge is simplified to be an arc, which is determined by the center point and radius of the circle. This approximation only fits for small volume of liquid, and the reason has also been explained in Figure 20. Another more accurate method is given by Honschoten[36] as shown in Figure 26. When the liquid volume is larger, the profile of the liquid bridge needs to be derived from the mean surface curvature and Laplace pressure.[55,58–60] The second principal curvature radius R_2 is in the plane of the figure, while the first principal curvature R_1 is in the plane perpendicular to the figure plane. They are given by,[36] $ds = -R_2 d\theta$ and $\xi = R_1 \cos\theta$. Then from the definition of Laplace pressure:[36]

$$-\frac{d\theta}{ds} + \frac{\cos\theta}{\xi} = \frac{\Delta P}{\gamma} \tag{36}$$

The designated boundary conditions are two points on the surface, x_1 and x_2 with $\theta = \pi$ and $\theta = 0$, which do not always exist on the profile of liquid bridges. Then, based on the normalized coordinates $x = \xi/r_\kappa$, $z = \zeta/r_\kappa$ and $1/r_\kappa = 1/R_1 + 1/R_2$,[36]

$$\frac{dz}{dx} = \frac{x^2 - x_1 x_2}{\sqrt{-x^4 + (2x_1 x_2)x^2 - (x_1 x_2)^2}} \tag{37}$$

The solution can be expressed by elliptic integrals, with the transformations $1/m^2 = b/(b-a)$ and $\sin^2\varphi = (b-x^2)/(b-a)$, where $a = (x_1x_2+2)+2(x_1x_2+1)^{(1/2)}$ and $b = (x_1x_2+2)-2(x_1x_2+1)^{(1/2)}$:

$$z = \pm\left(\frac{x_1 x_2}{\sqrt{b}} F(m,\phi) - \sqrt{b} E(m,\phi)\right) \tag{38}$$

where $F(m,\varphi) = \int_0^{\phi} \frac{d\psi}{\sqrt{1-m^2\sin^2\psi}}$, and $E(m,\varphi) = \int_0^{\phi} \sqrt{1-m^2\sin^2\psi}\, d\psi$.

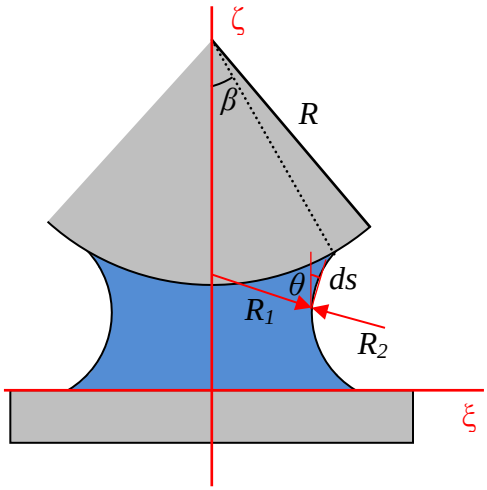

Figure 26. Profile of a liquid bridge between a spherical probe and a flat surface.[36]

Therefore, the Laplace pressure can be obtained from Equation (4).[34,36,93] When the Laplace pressure equation is substituted back into Equation (29), the capillary force can be obtained. The profile study can also test the theoretical modeling by matching experimental and modeling curvatures. The wetting behavior of a liquid bridge between substrates will help to study the robustness of rough surfaces.

In addtion, De Boer et al[99] and Alexandrou et al[66] studied the breakup of a liquid bridge and the work required to rupture the bridge between a sphere and a flat surface. They presented the work of rupture in two limiting thermodynamic cases, constant volume and constant pressure. They found that the constant pressure method offers a lower limit of the work, since liquid takes heat from surroundings and evaporates, and this reduced the work of adhesion; constant volume approach provides an upper limit, and the work of adhesion is equal to the surface energy created when the evaporation of liquid is ignored. Also, a simple equation was given to fit the work of rupture of pendular bridges for the two cases.

Fortes[95] studied the liquid bridges between two identical parallel plates and divided them into two configurations, *r* bridge and θ bridge, depending on whether the edge of the liquid touches the circumference of the plate, as shown in Figure 27. The capillary force and its relation to the Helmholtz energy of the system were researched. It was found that, when the radius of liquid-vapor contact area is much larger than the separation distance between substrates, the capillary force increases with separation distance in *r* bridges but decreases in θ bridges with a proportion to d^{-2}. He also discussed the stability of various configurations for the same separation of plates at a given volume, and considered the possibility of transitions between *r* and θ bridges.

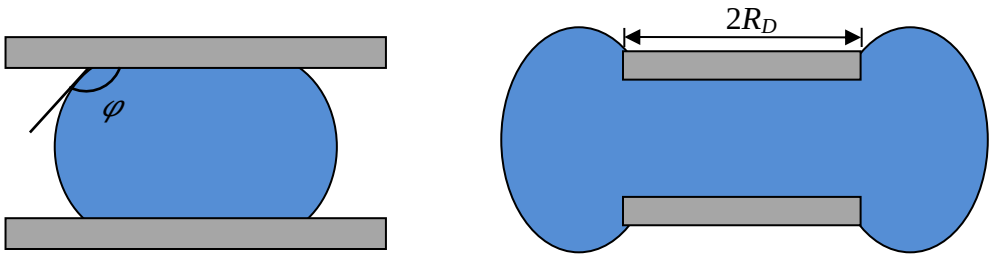

(a) (b)

Figure 27. Configurations of liquid bridges between identical substrates. (a) θ bridges, where φ is the CA between liquid and substrate, (b) r bridges, where R_D is the radius of substrate.

Mazzoneet al[100] and Adams et al[93] researched the effect of gravity on the profile of a liquid bridge between two spheres, and concluded that gravity has a significant effect on the characteristics of the liquid bridge when the Bond number is of the order unity and larger. The liquid bridge profile will distort, the attractive force will become smaller and rupture of the bridge will occur at a smaller separation distance. The Bond number is used to measure the importance of surface tension force compared to body force which usually refers to gravity. A high Bond number indicates that the effect of gravity is significant compared to surface tension effect; a low Bond number implies that the surface tension is dominant compared to the effect the gravity. Mathematica or Surface Evolver have also been used in previous studies to simulate the curvature of the liquid bridge based on simplifying assumptions that do not always satisfy the physical requirements.[36,39]

The capillary profile between smooth surfaces can be introduced to analyze the liquid bridges between smooth-rough or rough-rough surfaces. The concepts of the Laplace pressure and

mean surface curvature for a liquid bridge are quite similar, so it will provide useful information for robustness study when rough surfaces are applied.

2.3.3 Robustness of homogeneous rough surfaces

Robustness for uniform rough surfaces has been modeled by Tuteja et al,[1,16,101] who proposed the potential of robust omniphobic surfaces. A meta-stable system forms when a liquid sits on a rough surface under a certain pressure. They discussed the transition between Wenzel and meta-stable CB states using the sagging height, and a method to obtain the breakthrough pressure or robust pressure was derived. The geometric structure of their rough surfaces includes an electrospun surface and a microhoodoo surface, as shown in Figure 28.

Figure 28(a) shows the liquid-vapor interface between two fibers. The texture parameters *R* and *D* for the rough surface are also shown, where *R* is the radius of the fiber, and *2D* is distance between the edges of two fibers. In Figure 28(b), the microhoodoo surfaces with a small pore-depth is shown, where *W* is a horizontal feature, half length of the hat of the microhoodoo shape in the structure. Based on the force balance, Tuteja et al[1,16,101] defined and derived the robust parameters, which refers to the pressure when the sagging height reaches the pore length and the bottom of the substrate will be completely wet. The pressure across the interface can be balanced by the liquid-vapor surface tension when the gravity is ignored, which is:

$$P_H = \frac{\gamma_{LV} \cdot (Contact\ Line\ Length) \cdot \sin \delta\theta}{(Area)} \tag{39}$$

where P_H is the robust pressure and $\delta\theta$ is sagging angle for the fiber geometry.

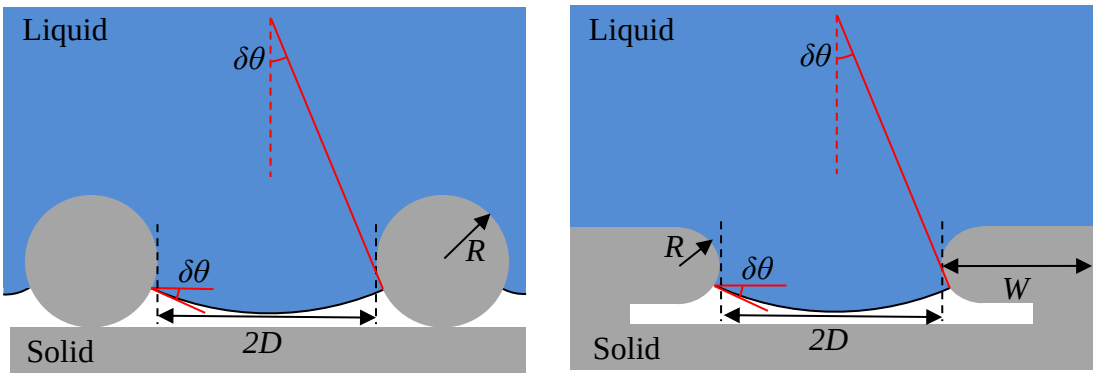

(a) (b)

Figure 28. Schematic illustrations for design parameters for a robust composite interface. (a) electrospun surface, (b) microhoodoo surface.[1]

For structures shown in Figure 28(a) and (b), the robust pressure expressions are

$$P_{HA} = \frac{\gamma_{LV} \cdot 2L \cdot \sin \delta\theta_a}{2D \cdot L} \qquad P_{HB} = \frac{\gamma_{LV} \cdot 2W \cdot \sin \delta\theta_b}{((W+D)^2 - W^2)} \tag{40}$$

where L is the solid-liquid contact line length, $2D$ is the edge-to-edge distance of protuberances in the rough surface, W is half length of the microhoodoo hat, $\delta\theta_a$ *and* $\delta\theta_b$ are sagging angles, and γ_{LV} is the liquid-vapor interfacial energy. Therefore, for electrospun and microhoodoo structure, the robust pressure can be obtained. This method fits for a droplet when gravity is negligible and the profile of liquid-vapor interface is an arc.

In addition, Gibbs free energy of the surface can be applied to evaluate the robustness of a SH and SO rough surface qualitatively and quantitatively.[1,102,103] Im et al[102,103] reported one surface with inverse-trapezoidal microstructure, which shows excellent superhydrophobicity with an automatic transition from Wenzel state to CB state in energy analysis. In the transition, an energy barrier does not always exist. The wetting behavior and effects of design parameters were analyzed and the surface was verified to be qualitatively robust. Gibbs surface free energy method has also been used by Tuteja et al[1] to analyze the pressure. When a composite interface has been pushed by the internal pressure within a liquid, the work which has been done through the composite interface by the pressure (W_p), should be equal to the change in interfacial energy of the interface (E_{comp}), expressed as $\delta W_p = dE_{com}$.[20] Then, the robust pressure was derived as:

$$P_H = \frac{-\gamma_{LV}}{1-r_f}\left(\frac{d(r_f f)}{dr_f}\frac{dr_f}{dh_d}\cos\theta_e + \frac{dr_f}{dh_d}\right) \tag{41}$$

where h_d is the depth of the liquid-vapor interface penetrating into the surface structure, r_f is roughness of wetted area, f is the fraction of the projected area below the wetted solid surface, θ_e is Young's CA, and γ_{LV} is the liquid-vapor interfacial energy.

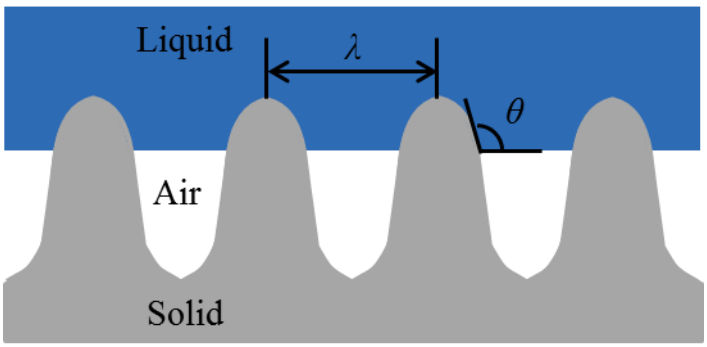

Figure 29. A schematic illustration of a composite interface and the parameters.[104]

For a rough surface with the structure shown in Figure 29,[104]

$$P_H = \frac{2\gamma_{LV}(\cos\theta - \cos\theta_e)}{(1-\phi_s)\lambda\sin\theta} \tag{42}$$

where λ is the distance of the centers of the two adjacent protuberances, θ is the CA shown in Figure 29, f_s is the area fraction of the liquid-air interface occluded by the texture and r_f is the roughness of the wetted area. Therefore, the robust pressure for a SH and SO rough surface with uniform structure can be obtained using both force balance and surface free energy method.

2.3.4 Robustness of hydrophobic and oleophobic fabrics

Robustness of SH and SO woven fabric has been studied by Mohan Krishnan[105], who first applied the word "robustness" to fabric. Her methodology is to find a way to measure the pressure required to push a liquid through a SH and SO fabric, since hydrostatic pressure has an insignificant effect when small droplets are applied. Also, the self-cleaning properties

were discussed when a droplet dewets the surface of the fabric after it has been pushed into the fabric structure.

In addition, Rawal[106] recently presented the effects of design parameters on obtaining higher CAs and robustness for an electrospun nonwoven mat. For irregular spaced fibers, a dimensionless pressure was proposed to determine the robustness of the fabric. As shown in Figure 30:

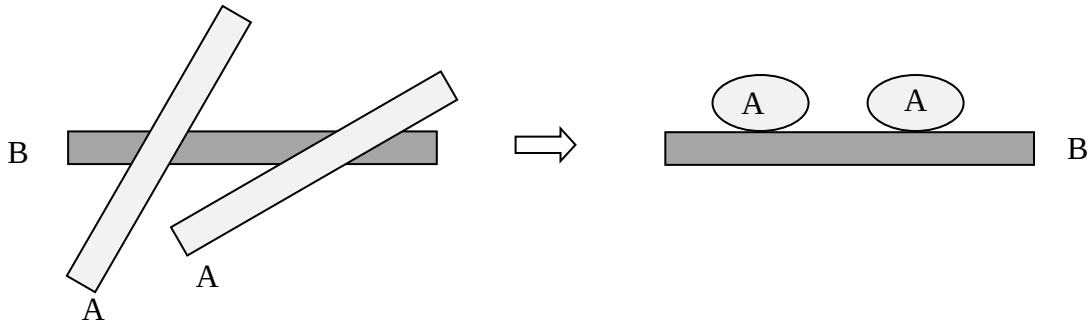

Figure 30. Simplification of electrospun mat.[106]

The electrospun fibers are randomly distributed, and to simplify the structure, the statistical variables are used for the structural parameters. Both top view and cross-section are shown in Figure 30. Three basic segments are needed to model the robust pressure, including the mean length between the centers of two adjacent fibers ($\bar{b}$), the mean length of overlapping fibers ($\bar{b}_b$) and the mean free fiber length (2*D*), as shown in Figure 31.

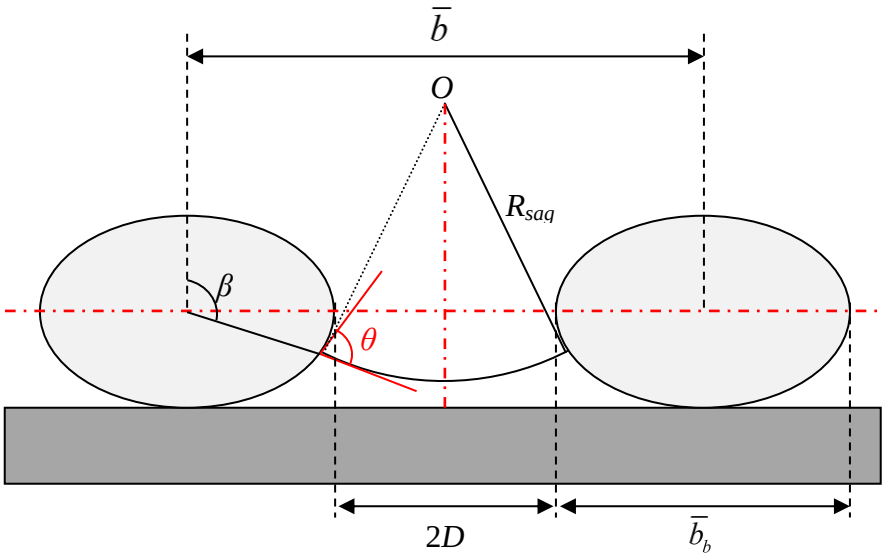

Figure 31. Schematic illustration of the sagging of liquid-vapor interface.[106]

The approach is to obtain the maximum pressure when the meniscus or the liquid-vapor interface has a maximum possible curvature before it touches the bottom substrate. From the geometric relationships between the parameters in Figure 31:[106]

$$\kappa = \frac{1}{R_{sag}} = \frac{2\sin(\beta+\theta)}{\bar{b}_b \sin\beta - \bar{b}} \tag{43}$$

where θ is the angle between the fiber and the meniscus of the liquid at the liquid-vapor-solid interfacial point, β is the position of the meniscus contact line on each fiber, R_{sag} is the radius of meniscus, and κ is the curvature of the meniscus.

When the liquid-vapor interface has the maximum curvature, $d\kappa/d\alpha = 0$, and κ_{max} is obtained,

$$\kappa_{\max} = \frac{2}{\bar{b}_b}\left[\frac{1}{\cos\theta + \sqrt{(D^*)^2 - \sin^2\theta}}\right] \tag{44}$$

where $D^* = \bar{b} / \bar{b}_b$, which refers to the spacing ratio.

Therefore, the Laplace pressure is achieved as below:

$$\Delta P = 2\gamma_{LV}[\sin(\theta + \alpha - \pi)]\kappa_{\max} \tag{45}$$

Finally the Laplace pressure was normalized as a dimensionless pressure:

$$P^* = \frac{4}{\pi D^*}\left[\frac{\sqrt{(D^*)^2 - \sin^2\theta}}{\cos\theta + \sqrt{(D^*)^2 - \sin^2\theta}}\right] \tag{46}$$

The final equation is expressed with the electrospun structural parameters, the spacing ratio $D^*$and equilibrium CA θ. From the equation, the robust pressure will increase significantly when the equilibrium CA increases or the spacing ratio decreases. In addition, the pressure would also increase by reducing the fiber diameter to nano scale. This method can be applied to solve the robust pressure for fabrics with random structures or monofilaments, such as nonwoven, but it has not been verified experimentally.

2.4 Summary

Hydrophobic/oleophobic and hydrophilic/oleophilic surfaces have been discussed as well as the surface tension and Laplace pressure, which have significant influence on liquid wetting behaviors. Both CA and CAH are used to define a SH and SO surface. Roll-off angle is not used since it is related to the mass of a liquid drop, which cannot accurately illustrate the hydrophobicity and oleophobicity of a surface. Wetting behaviors of liquids on both smooth (Young's equation) and rough surfaces (Wenzel and CB states) are compared. Also, the approaches to make hydrophobic and oleophobic surfaces have been studied briefly.

Robustness of a rough hydrophobic and oleophobic surface has been reviewed, which can be used to study the meta-stable wetting behavior of a liquid-on-surface system, and the transition between CB and Wenzel states by crossing the energy barrier. In order to obtain the robust force and robust pressure for a hydrophobic and oleophobic rough surface, capillary forces and profiles of liquid bridges between smooth surfaces were discussed and good preparations were done for the rough surface study. The expressions of robust pressure for simple structures were modeled both from force balance analysis and energy conservation methods. But only theoretical work has been done and there are no experimental results. Similarly, robust pressure is modeled for parallel monofilaments and electrospun mat.

The robust pressure for a rough surface can help to overcome the limits of hydrostatic pressure, since the effect of surface tension for an extremely small droplet is dominant, larger than the gravitational force. Through robustness, the dynamic liquid-repellency and self-cleaning properties of a rough surface could be evaluated. In summary, the robustness will contribute to obtaining a better understanding of the potential hydrophobicity and oleophobicity of fabrics.

CHAPTER 3. EXPERIMENTS

3.1 Materials

Three liquids have been used in the experiments: deionized water (surface tension γ = 72.8 mN/m, from NCSU), Kaydol (surface tension γ = 31 mN/m, from CBM group of North Carolina, INC) and dodecane (surface tension γ = 25 mN/m, from Sigma-Aldrich, St. Louis, MO). Substrates to test the robustness of SH and SO fabrics include PTFE films (from SmallParts LLC, Seattle, WA), glass slides (Corning INC., New York, NY), 1H,1H,2H,2H-perfluorodecyltrimethoxysilane (FS, Gelest INC., Morrisville, PA) treated glass slides, FS treated parallel nylon monofilaments, FS treated bridal veil nylon woven fabric, FS treated nylon woven fabric made of multifilament yarns, FS treated nylon nonwoven fabric and FS treated flame-retardant (FR) nonwoven fabric, which is composed of FR rayon and meta-aramid in the weight ratio of 4:1.

In addition, isopropyl alcohol (VWR, West Chester, PA), ammonium hydroxide (Sigma-Aldrich, St. Louis, MO) and FS have been used to perform surface modification to glass slides, monofilaments, and fabrics.

3.2 Preparation for low-surface tension surfaces

Before any treatment, the glass slides and textiles were ultrasonicly cleaned with Sonicwise SW-146H by immersing them in isopropyl alcohol for 30 minutes at room temperature. Then they were treated according to the following procedures.

3.2.1 Surface modification of nylon monofilaments and nylon fabric

The treated nylon woven and nonwoven fabrics were made by first immersing them in isopropyl alcohol to pre-wet them; then, the wetted fabrics were padded to remove excess isopropyl alcohol; after that, solutions of FS, isopropyl alcohol and ammonium hydroxide were dropped onto the nylon woven and nonwoven fabric mentioned above. The weight ratio for fabric, FS, isopropyl alcohol and ammonium hydroxide was 100: 10: 500: 5; after allowing the reaction to proceed for 2 hours, the nylon fabrics were removed from the solution, padded again and allowed to cure in an oven at 150°C for 2 minutes; finally, they were washed with isopropyl alcohol and dried in an oven at 120°C for 2 minutes. The chemical reaction of rayon with the FS after hydrolysis in basic conditions is described in Scheme 1. The treated nylon monofilaments were made with the same methods but without padding, and the properties of the surfaces both for fabric and monofilaments should be quite similar since they share the same chemical structure.

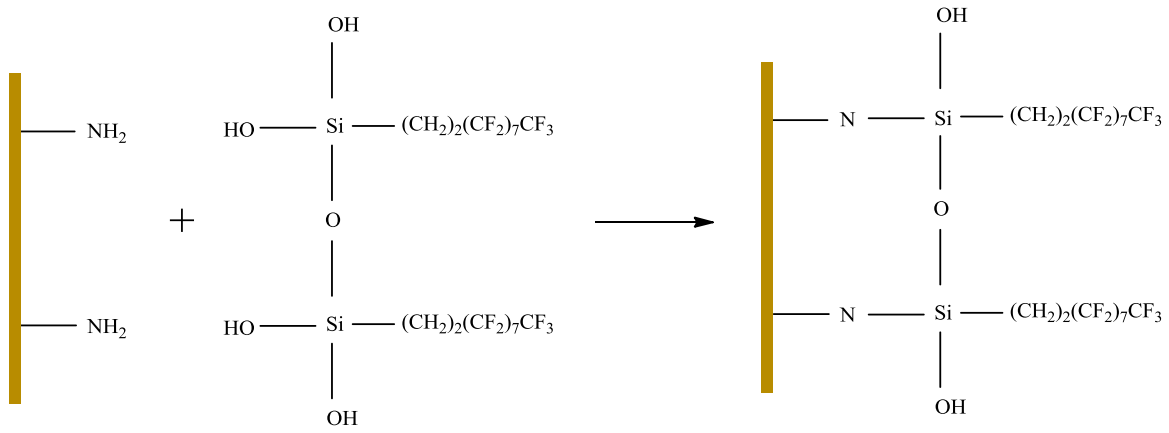

Scheme 3. Mechanism of chemical reactions of nylon and FS after hydrolysis in basic conditions.

3.2.2 Surface modification of glass slides

Similar to nylon nonwoven fabric, glass slides can also be treated by condensation of FS on their surface. The glass slides are soaked in isopropyl alcohol and treated with a solution of FS, isopropyl alcohol and ammonium hydroxide for 2 hours. The (Si-OH) groups on the surface of glass slides will react with FS and be converted into carbon-fluoride (-CF_2- CF_3) groups shown in Scheme 3.

3.3 Construction of robustometer

An instrument, a “robustometer”, was used to test the robustness of the SH and SO fabrics. There are several components in this instrument, and the equipment picture and schematic diagram are shown in Figure 32. Two substrates are needed in one experiment: one substrate is placed on the testing platform of the analytical balance (bottom substrate); and the other substrate (top substrate) is attached to a bent arm connected to a motor. The electronic con-

trol box (Compumotor, Parker Hannifin Corp., Rohnert Park, CA) moves the bent arm and the top substrate up and down. The analytical balance (Mettler Toledo AE 163, Mettler Instrument Corp., Highstown, NJ) measures the changing force of the liquid when the droplet is being compressed or stretched. A Canon EOS camera (Canon USA, INC., New York, NY) captures the changing shape of the droplet. A computer collects both the changing force from the analytical balance and the distance moved by the bent arm controlled by the motor drive through a Visual Basic (VB) program implanted in Microsoft Office Excel sheet.

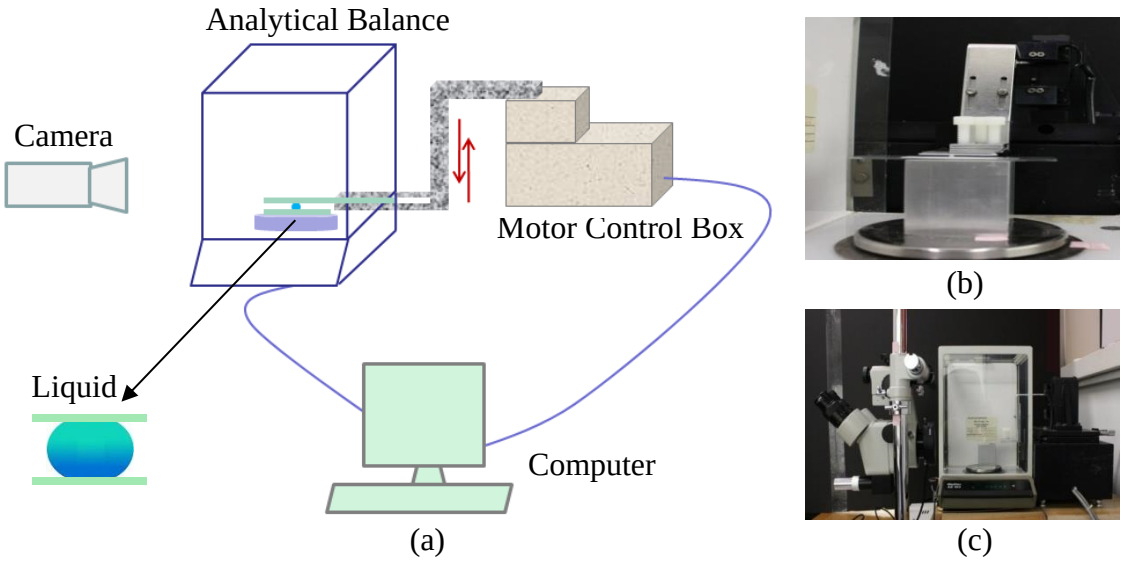

Figure 32. Robustometer. (a) Schematic diagram; (b) photograph of front view; and (c) photograph of side view.

When conducting experiments, as the separation distance decreases and increases, a capillary bridge will be formed, compressed, and stretched until it ruptures. It is defined as one com-

pression and tension cycle. A schematic presentation is shown in Figure 33. Since the computer will collect the data both from the balance and the motor drive, a force-separation distance curve can be obtained. For one combination of liquid, substrates and motor velocity, at least three cycles were conducted when performing experiments.

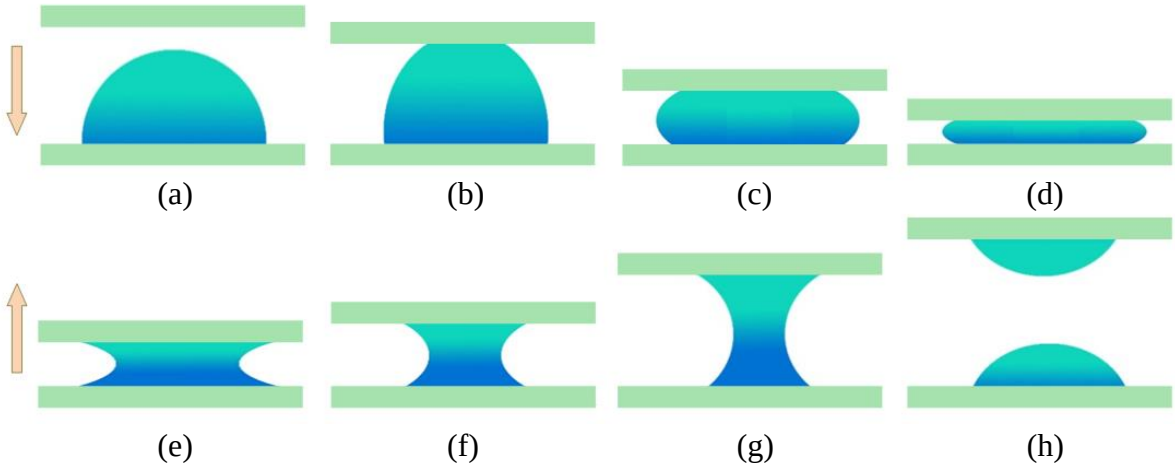

Figure 33. Schematic presentation of the experiment. (a) A droplet is deposited on the fixed bottom substrate; (b) top substrate moves toward the bottom substrate with certain velocity and a capillary bridge forms when it touches the droplet; (c) the droplet is being squeezed; and (d) the droplet spreads and penetrates into substrates. (a)-(d) are in the compression process. (e) The top substrate moves in the reverse direction; (f) the droplet is being stretched; (g) a narrow "waist" of the capillary bridge is shown just before break; and (h) the capillary bridge breaks with partial residual volume on both substrates. (e)-(h) are in the tension process.

3.4 Characterization

3.4.1 Scanning electron microscopy

The FS treated nylon fabrics were observed with a scanning electron microscope (SEM, JEOL, 6400F, Tokyo) operated at 10 kV and magnifications from × 50. RevolutionTM (4pi Analysis, v1.60b24) were used for image analysis of the SEM images.

3.4.2 Contact angles

The apparent contact angles of liquids drops on the surfaces of the nylon fabrics were measured with a lab-designed goniometer at room temperature (RT) and 65% relative humidity (RH). The volume of the deposited droplets was 10 µL. The range of contact angles was obtained from measurements taken at a minimum of three separate locations. The images of liquid droplets on the prepared surface were taken using a digital camera (Canon, EOS EF-S-18-55IS, Lake Success, NY) that has an optical microscopic focusing lenses (Meiji Techno, EMZ-13TR, Saitama).

CHAPTER 4. RESULTS AND DISCUSSION

4.1 Capillary profiles and Laplace pressure

For the capillary bridges between two surfaces, the profile is modeled and only two points are needed for the Laplace pressure when the effect of gravity is negligible. Once the relationship between Laplace pressure and robust pressure is known, the robustness of a structure can be evaluated, which greatly simplifies the problem. The profile of a capillary bridge between two surfaces can be obtained from the combination of Laplace pressure and mean surface curvature expressions.[34,36,39]

Figure 34 shows a schematic diagram of a concave capillary bridge between two identical parallel substrates, and the XOZ coordinate system. The liquid bridge is assumed to be in thermodynamic equilibrium and gravitational forces are assumed to be insignificant. Although several recent papers provide approximate solutions to this problem, it was first solved analytically in 1841 by Delaunay.[107] In Figure 34, the bridge is both X-axis and Z-axis symmetric since the two substrates are identical. This means that the profile of the bridge can be determined using only one quadrant. A and B are points on the profile of the liquid bridges, where A is located on the X-axis at the narrowest location of a concave bridge such that its X coordinate is smaller than any other point on the profile, while B is located at the solid-liquid-vapor phase intersection point with the largest X coordinate at the widest point on the concave liquid bridge. (For a convex bridge, A is located on the X-axis at the widest point on the bridge and B is located at the solid-liquid-vapor phase intersection point with the smallest

X coordinate.) The CA between the liquid bridge and the flat substrate at point B is defined as φ. A tangent line and a corresponding normal line can be drawn at point B, as shown in Figure 34 as the dash-dot lines. Two tangent circles with their centers lying on the normal line can be constructed with their curvatures matching the curvatures of the liquid surface at point B. The dashed tangent circle is in the XZ plane, with radius R_2. Likewise, the solid circle lies in the plane normal to the plane of the paper and tangent to the liquid surface at point B with radius R_1 and tilt angle ε between R_1 and the positive Z direction. For other points along the BA curve, the angle ε varies, since it is the angle between the normal of curve at each point and the z-axis. At position B, ε equals $(\pi - \varphi)$.

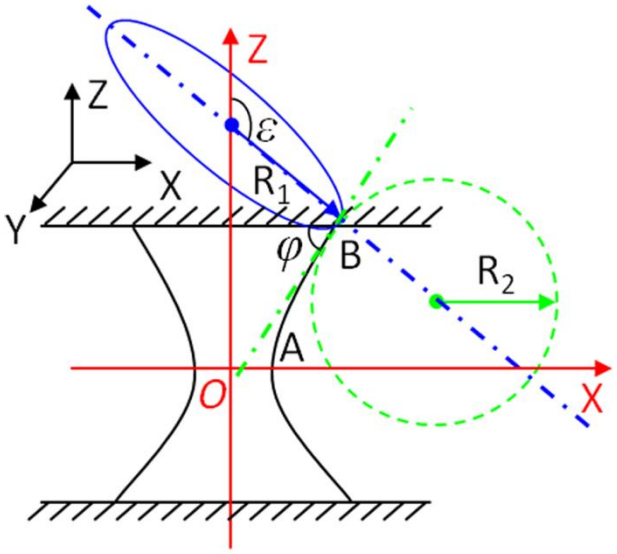

Figure 34. Schematic diagram for a liquid bridge between identical parallel substrates and definition of symbols.

Since the liquid bridge is in thermodynamic equilibrium, the Laplace pressure is the same at every point on the liquid-vapor surface. From the definitions of Laplace pressure, $\Delta P = \gamma_{LV}$ $(1/R_1 + 1/R_2)$, and mean surface curvature, $H = 0.5$ $(1/R_1 + 1/R_2)$, where R_1 and R_2 are the principal radii of the liquid bridge curvature at any point on the liquid-vapor surface and γ_{LV} is liquid-vapor interfacial energy, it is obtained:[35,37,39]

$$2H = \frac{\frac{dz}{dx}}{x\left[1+\left(\frac{dz}{dx}\right)^2\right]^{1/2}} + \frac{\frac{d}{dx}\left(\frac{dz}{dx}\right)}{\left[1+\left(\frac{dz}{dx}\right)^2\right]^{3/2}} \tag{47}$$

To simplify Equation (47), it is defined that $u = -\sin\varepsilon$, which gives,

$$\frac{dz}{dx} = -\tan\varepsilon = \frac{-\sin\varepsilon}{\cos\varepsilon} = -\frac{u}{\sqrt{1-u^2}} > 0 \tag{48}$$

where $\varepsilon \in [\frac{\pi}{2}, \pi - \varphi]$ For a bridge of the shape shown in Figure 34, $1/R_1 = -u/x > 0$ while .

$1/R_2 = -du/dx < 0$. Therefore, $2H = -u/x - du/dx$ and

$$x = \frac{-u \pm \sqrt{u^2 - 4Hc}}{2H} \tag{49}$$

From the boundary conditions:

$$\begin{aligned} &\text{At point A: } x = x_1, u = -\sin(\frac{\pi}{2}) = -1 \\ &\text{At point B: } x = x_2, u = -\sin(\pi - \varphi) = -\sin\varphi \end{aligned} \tag{50}$$

both c and H can be obtained.

Following Delaunay's approach, an analytical solution has been re-derived, which is shown below followed by experimental verification. For any point on the liquid-air interface shown in Figure 34, x is:

$$x = \frac{\sin\varepsilon \pm \sqrt{(\sin\varepsilon)^2 + C}}{2H} \tag{51}$$

when $\varepsilon \in [\frac{\pi}{2}, \pi - \varphi]$. At point A, $C_A = -4H(x_1 - Hx_1^2)$; at point B, $C_B = -4H(sin\varphi \cdot x_2 - Hx_2^2)$. Since C is just an integration constant, $C_A = C_B = C$.

Then H becomes:

$$H = \frac{x_1 - x_2 \cdot \sin\varphi}{x_1^2 - x_2^2} \tag{52}$$

Furthermore, $dz/du = dz/dx \times dx/du$. Therefore, z is given by:

$$\begin{aligned} z &= \frac{1}{2H}\int_{\pi/2}^{\varepsilon} \sin\varepsilon \cdot \left[-1 \pm \frac{\sin\varepsilon}{\sqrt{(\sin\varepsilon)^2 + C}}\right] d\varepsilon \\ &= \frac{1}{2H}\left\{\cos\varepsilon \pm \sqrt{C}\cdot\left[E(\sin\varepsilon, k) - F(\sin\varepsilon, k)\right]\right\}\Big|_{\pi/2}^{\varepsilon} \end{aligned} \tag{53}$$

where $k = (-1/C)^{1/2}$; F and E are the elliptical integrals of the first and second kinds. Then the final expression for the profile of a liquid bridge is simply the locus of points (x, z) where x and z are given by Equations (52) and (53), respectively. This solution is valid when the effect of gravity is insignificant and can be ignored. Mazzone et al[100] showed that gravity can be ignored when the ratio of Bond number to dimensionless surface curvature is much less than one. In the following experiments, the maximum Bond number was 0.33 for 5 μL do-decane, but it increases as the volume increases. Thus, in the experiments reported below

with a volume smaller than 5 μL, the effect of gravity on the capillary bridge shape is small. Finally, the Laplace pressure is:

$$\Delta P = 2\gamma_{LV} \cdot \frac{x_1 - \sin\varphi \cdot x_2}{x_1^{\,2} - x_2^{\,2}} \tag{54}$$

Therefore, for a capillary bridge, once the coordinates at points A and B are obtained as well as the advancing or receding CA at point B, the profile of the bridge and Laplace pressure can be obtained. This solution is suitable for the bi-concave shape of the liquid bridge shown in Figure 34, however, the analytical solution also fits the bi-convex shape of a bridge by choosing the correct signs for x and z in Equations (51) and (53). Below the experiments have been performed to verify the predicted capillary bridge profiles.

Capillary Profiles with Glass-Glass Substrates

Effect of Surface Tensions of Liquids

From theoretical analysis, only three parameters are needed to obtain the curvature of a capillary bridge from Equations (51) and (53), x_1, x_2, and φ, or, equivalently, C, H and φ. In other words, when the x-coordinates of points A and B and the advancing or receding CAs between liquid and substrate at point B are obtained as depicted in Figure 34, the profile for the liquid bridge can be calculated. In Equations (51) and (53), the +/– signs of the square root terms need to be chosen for x and z. For bi-concave shapes of liquid bridges as shown in Figure 35, the sign of the radical in x is chosen to be negative and the sign of the radical in z is chosen to be positive.

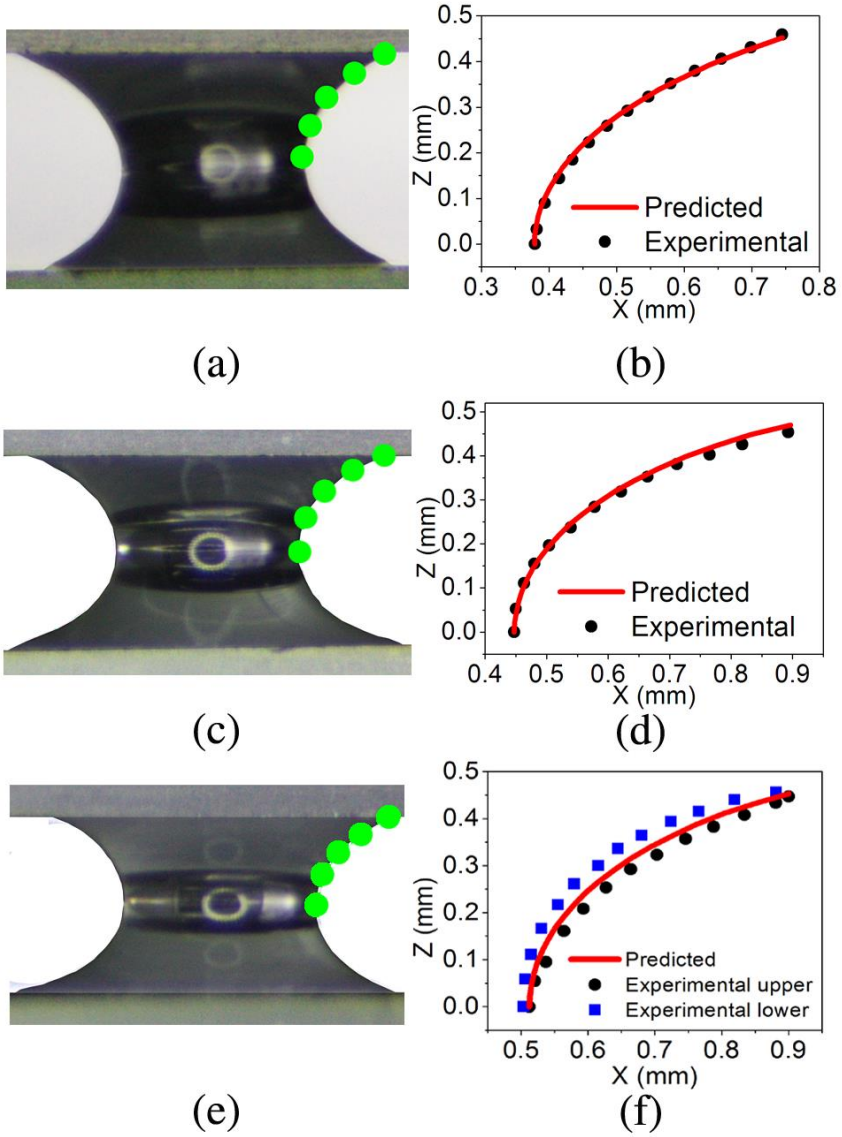

Figure 35. Images of profiles of water, Kaydol and dodecane bridges with volume $V = 1$ μL between two identical glass substrates. (a), (c) and (e) display the entire profiles of water, Kaydol and dodecane capillary bridges between glass substrates; and (b), (d) and (f) are comparisons between predicted and experimental profiles of the capillary bridges of the upper right quadrant from (a), (c) and (e), respectively. Symbols are the experimentally measured points while the solid curves are the predicted profiles.

The experimental profile was obtained directly from the captured photographs with the help of Adobe Photoshop (Adobe Photoshop CS5, Adobe Systems Inc.), and the results were

compared with the modeling predictions. Figure 35 shows profiles of liquid bridges with different surface tensions and Bond numbers (water, γ_{LV} = 72.8 mN/m, B = 0.052; Kaydol, γ_{LV} = 31 mN/m, B = 0.108; dodecane, γ_{LV} = 25 mN/m, B = 0.113; where the radius of the 1 μL liquid when in spherical shape was used as characteristic length), but for the same volume and the same separation distance or height. From these experiments, the general shapes of the bridges are very similar, but the contact angles between liquid and substrate are different as expected for these different liquids. In addition, the width of the narrowest part or "neck" of the liquid bridge, which is caused by the surface tensions of the liquids and Laplace pressures, are different for the different liquids. The agreement between the measured and predicted profiles is excellent for water. The minor offset in the Kaydol profile and slightly larger offset in the dodecane profile may be caused by gravity. The error should be largest for dodecane since it has the lowest surface tension and thus the highest Bond number, 0.113. Figure 35(f) shows both the upper and lower quadrant of the experimental profile, while the average receding contact angle for upper right and lower right quadrants was used in the predicted curve. The predicted curve lies between the lower experimental profile and the upper experimental profile. This is exactly what would be expected for gravitational forces distorting the profile. The offset could also be caused by small errors in the advancing or receding CA between liquid and the substrate, and to small shifts of the co-ordinates of the boundary points due to the blurry edge of the curvatures from the photo. In either case, the maximum error in the value of x at a given value of z is less than 5%. The error for Kaydol is much less, which indicates that gravity has only a minor effect on the profile shape of 1 μL drops for all three liquids. Due to the bi-axial symmetry of liquid bridges, each quadrant pro-

file reveals all the properties of the entire bridge, such as the separation distance or height between two substrates and the volume of the liquid. The comparisons of these parameters are shown in Table 1 along with the errors between predicted and experimental results, which are 1 – 4%. In these experiments, it is difficult to deliver exactly 1 μL due to the precision of syringe, the surface tension of the liquid and experimental error. Thus the experimental volume in Table 1 is obtained by integration of the volume contained within the profile from the captured picture. As one can see, the analytical solution of the profile fits the experimentally determined profile for symmetric capillary bridges even for different surface tension liquids.

Table 1. Comparisons of height (h) and volume (V = 1 μL) for different liquid bridges between predicted and experimental results for glass-glass flat substrates.

	Water	Kaydol	Dodecane
Receding CA (°)	26.0	17.4	20.0
Predicted h (mm)	0.90	0.94	0.91
Experimental h (mm)	0.92	0.91	0.89
h Error (%)	1.4	3.2	1.2
Predicted V (μL)	0.71	1.02	1.13
Experimental V (μL)	0.74	0.99	1.18
V Error (%)	3.7	3.2	3.9

Effect of Liquid Volume

In addition to the surface tension, the volume of the liquid will also affect the curvature of capillary bridges. To explore the volume effect, three volumes of Kaydol are used, 1, 2 and 5 μL. To avoid the blurry edges of the profile from the picture, thresholds have been applied to the original pictures in Adobe Photoshop, as shown in Figure 36(a). The bright area refers to the droplet, while the dark region refers to the background.

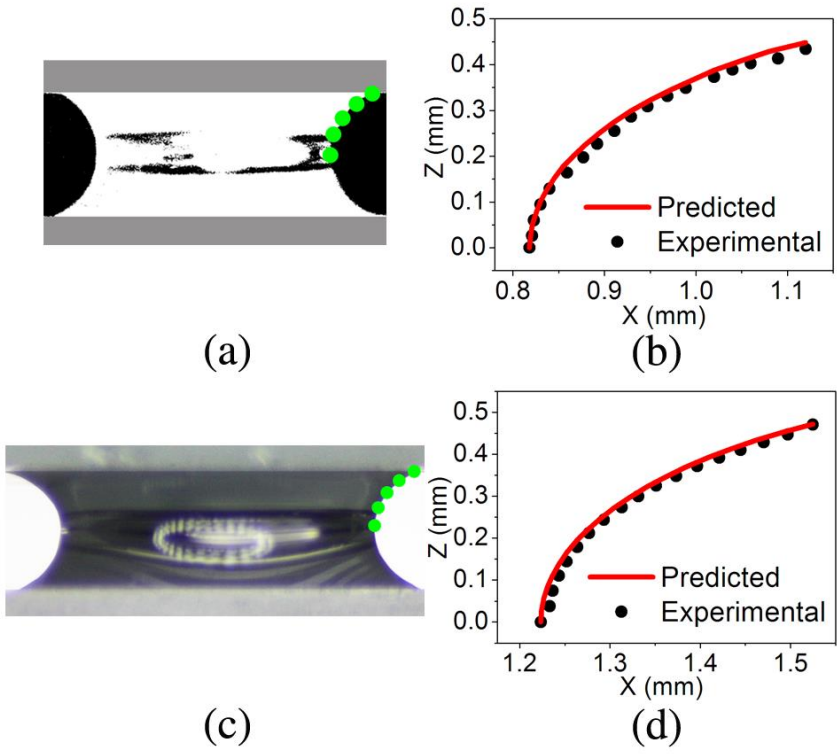

Figure 36. Images of profiles of Kaydol bridges with volume V = 2 and V = 5 μL between two identical glass substrates. (a) and (c) show the entire profiles of Kaydol bridges between glass substrates; (b) and (d) are comparisons between predicted and experimental profiles of the capillary bridges of the upper right quadrant from (a) and (c). Symbols are the experimentally measured points while the solid curves are the predicted profiles.

Comparing Figure 35(c) and (d) (V = 1 μL) with Figure 36, at similar separation distances or heights as shown in Table 2, the profiles are different since the 1 μL Kaydol drop will be stretched more than for larger volumes such as 5 μL Kaydol. Therefore, at a constant separation, the width of the "neck" of liquid bridge will increase as the volume increases, and the observed advancing or receding CAs also change. Table 2 shows the comparisons of parameters for different volumes of Kaydol bridges between predicted and experimental results. Although the receding contact angles for 2 and 5 μL are nearly the same, the receding CA for 1 μL is much smaller; it is not known what causes this discrepancy. Nevertheless, Table 2 and Figures 3 and 4 demonstrate that predicted profiles are in good agreement with the experimental profiles for different volumes. However, as before, gravity has a small effect (< 1%) on the profile of these larger drops.

Table 2. Comparisons of parameters for different volumes of Kaydol bridges between predicted and experimental results for glass-glass substrates.

Volume (μL)	1	2	5
Receding CA (°)	17.4	27.7	28.0
Predicted h (mm)	0.94	0.90	0.94
Experimental h (mm)	0.91	0.87	0.94
h Error (%)	3.2	3.2	0.2
Predicted V (μL)	1.02	2.33	5.12
Experimental V (μL)	0.99	2.27	5.17
V Error (%)	3.2	2.4	1.0

Capillary Profiles with PTFE-PTFE Substrates

Due to the high surface tension of glass substrates, the receding CAs for all three liquids are smaller than 90°, which leads to a bi-concave shape for the capillary bridge. PTFE film has a low surface tension, which results in a bi-convex shape of a capillary bridge for water during the compression process.

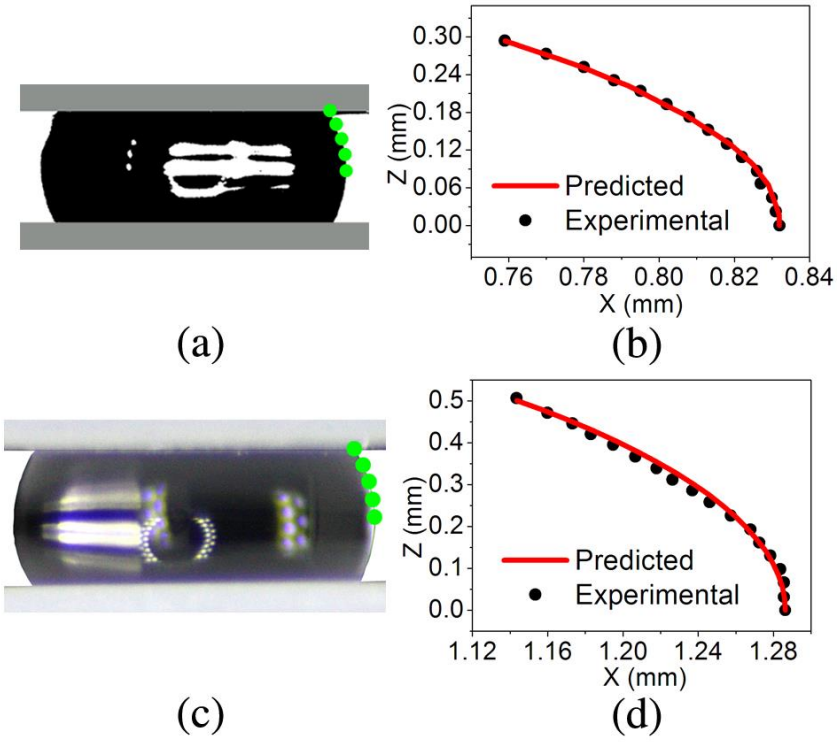

Figure 37. Images of profiles of water bridges with volume V = 1 and V = 5 μL between two identical PTFE substrates. (a) and (c) display entire profiles of water bridges between PTFE substrates; (b) and (d) are comparisons between predicted and experimental profiles of the capillary bridge of the upper right quadrant from (a) and (c). Symbols are the experimentally measured points while the solid curves are the predicted profiles.

Again, thresholding was used to highlight the edge of liquid bridge profiles, as shown in Figure 37. The analytical solution still results in good agreement with experiment provided the +/- signs for the radical in Equation (53) for x is chosen to be positive and the sign for the radical in Equation (55) for z is changed to negative. Figure 37 shows the bi-convex shapes of water bridges for 1 and 5 μL liquid between PTFE-PTFE substrates. The CAs between liquid and substrate are both larger than 90^o, and the profiles are different for the different volumes. At similar plate spacing, larger volumes lead to wider waists of the liquid bridge. The results show that the analytical solution from Equations (51) and (53) still fits the experimental profiles very well as shown in Table 3 and Figure 37.

Table 3. Comparisons of parameters for different volumes of water bridges between predicted and experimental results for PTFE-PTFE substrates.

Volume (μL)	1	5
Advancing CA (°)	118	122
Predicted *h* (mm)	0.59	1.00
Experimental *h* (mm)	0.59	1.01
h Error (%)	0.2	1.0
Predicted *V* (μL)	0.60	2.42
Experimental *V* (μL)	0.60	2.44
V Error (%)	0.3	0.6

Capillary Profiles with Glass-FS treated Glass Substrates

Effect of Surface Tensions of Liquids

When a capillary bridge forms between identical substrates, it is symmetric, while different substrates will lead to asymmetric capillary bridges. An asymmetric bridge can be separated into two regions as shown in Figure 38, the upper half of a symmetric bridge and the lower half of a different symmetric bridge. This changes the problem of asymmetric shape into two simple problems dealing only with symmetric shapes. The key point is to find the "neck" or "waist" point on the profile of an asymmetric bridge on a two dimensional plane. From the geometrical relationship, it will not be difficult to find the boundary point in a picture.

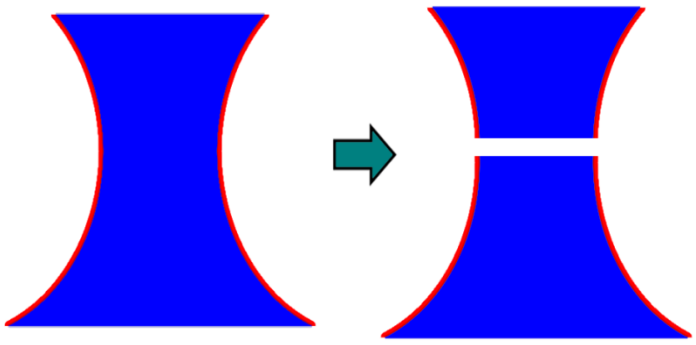

Figure 38. Schematic diagram for an asymmetric liquid bridge between different parallel substrates. The profile can be separated into a combination of two different symmetric half bridges.

Figure 39 shows the image of profile of an asymmetric water bridge with volume $V = 5$ μL between glass (top) and FS treated glass (bottom) substrates. Obviously, the CAs between liquid and top substrates and between liquid and bottom substrates are different as shown in

Table 4. To address this situation and to evaluate the validity of this analytical solution, both sides (right and left) as well as the top and bottom of the capillary bridge have been simulated as shown in the figure and table. Figure 39(b) shows that there is excellent agreement between predicted and experimental profiles both for the left and right sides of the liquid bridge. Table 4 quantitatively shows that the errors are very small, which indirectly emphasizes the validity of the modeling method. Similar results were obtained for asymmetric bridges of Kaydol and dodecane (not shown).

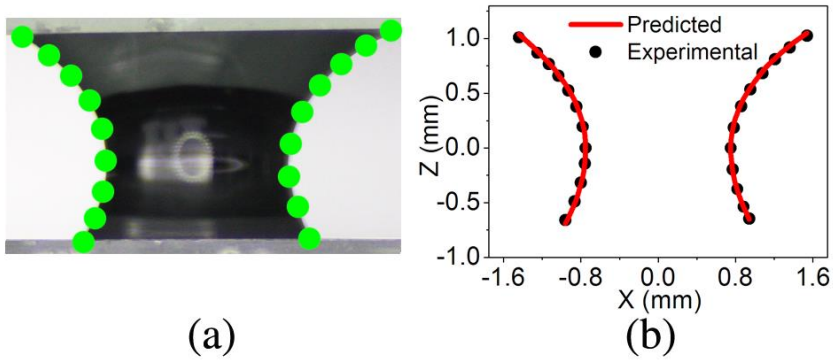

Figure 39. Image of profile of a water bridge with volume $V = 5$ μL between glass (top) and FS treated glass (bottom) substrates. (a) Entire profiles of a water bridge between substrates; (b) comparisons between predicted and experimental profiles of the capillary bridge for both sides from (a). Symbols are the experimentally measured points while the solid curves are the predicted profiles.

Table 4. Comparisons of parameters for different parts of an asymmetric water liquid bridges V = 5 μL between predicted and experimental results for glass (top) and FS treated glass (bottom) substrates.

	UL†	UR†	LL†	LR†
Receding CA (°)	36.0	31.4	59.6	60.0
Predicted h (mm)	1.04	1.05	0.69	0.65
Experimental h (mm)	1.01	1.03	0.66	0.65
h Error (%)	3.0	2.3	4.7	0.7
Predicted V (μL)	3.26	3.49	1.47	1.37
Experimental V (μL)	3.15	3.41	1.40	1.36
V Error (%)	3.4	2.2	5.0	0.8

†Note: UL refers to the upper left; UR to the upper right; LL to lower left; LR to the lower right quadrants.

Effect of Volumes of Liquids

Good agreement was also obtained between the predicted and measured profiles when the volume of the liquid was changed for asymmetric bridges (not shown), just as it was in the case of symmetric bridges.

Capillary Profiles with Film-Fabric and Fabric- Fabric Substrates

From Equations (51) and (53), the predicted profiles of liquid bridges between smooth surfaces match with the experimental results both for the same and different smooth substrates. However, in many applications, one or both substrates may be rough, e.g. a fabric. It is hypothesized that, if the droplet's dimensions are much larger than the roughness scale of the substrate, the same model for shape of the drop profile should apply provided that the apparent contact angle is used. The wetting behavior of a liquid on a rough surface can be de-

scribed with the CB and Wenzel models, depending on whether the liquid will completely wet (Wenzel) or partially wet the surface (CB). The wetting behavior of a liquid bridge between rough substrates are similar to that of a sessile drop, which will be affected by the Laplace pressure and surface tensions[15] of both liquid and substrates. Due to the compression and tension of the liquid, the wetting behavior on the rough fabric will change within CB and Wenzel states, which is closely related to the hydrophobicity or oleophobicity of the fabric. To test this hypothesis, two rough fabric substrates have also been tested, including both bi-concave and bi-convex shapes of the liquid bridges. Figure 40(a) shows the images of profiles of a water bridge with volume V = 2 μL between glass and FS treated FR fabric, and Figure 40(c) shows the images of profiles of a Kaydol bridge between PTFE and FS treated FR fabric substrates. The figure displays the receding CAs since the two substrates are stretching the liquid. It is clear that there is good agreement between the predicted and experimental curves. Thus this model can be extended to the liquid bridges formed between rough surfaces, where the angle is chosen to be the apparent CA. As a second test of the hypothesis, experiments have been conducted by testing the liquid bridges V = 2 μL between PTFE and FS treated nylon fabric substrates, as shown in Figure 41. Both receding (Figure 41(a)) and advancing (Figure 41(c)) CAs are used. Even though the shapes of the bridges are very different, there is excellent agreement between the predicted and experimental profiles.

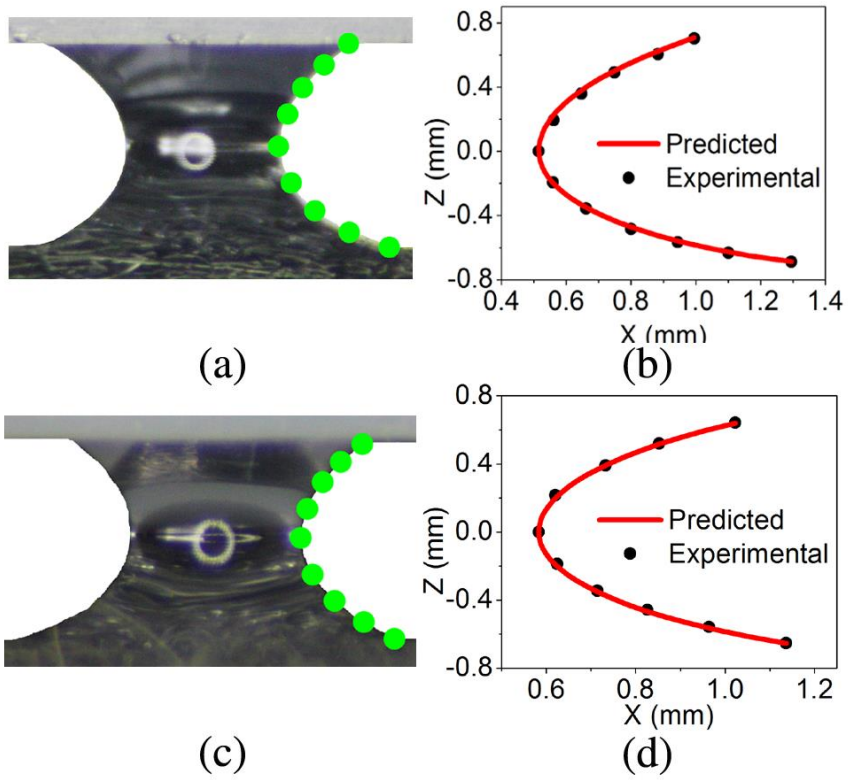

Figure 40. Images of profiles of (a) water bridge between glass and FS treated FR fabric and (c) Kaydol bridge between PTFE and FR fabric substrates. Both drop volumes $V = 2$ μL; (a) and (c) show the profiles of the right side of the liquid bridges (b) and (d) are comparisons between predicted and experimental profiles of the capillary bridges of the right part from (a) and (c). Symbols are the experimentally measured points while the solid curves are the predicted profiles.

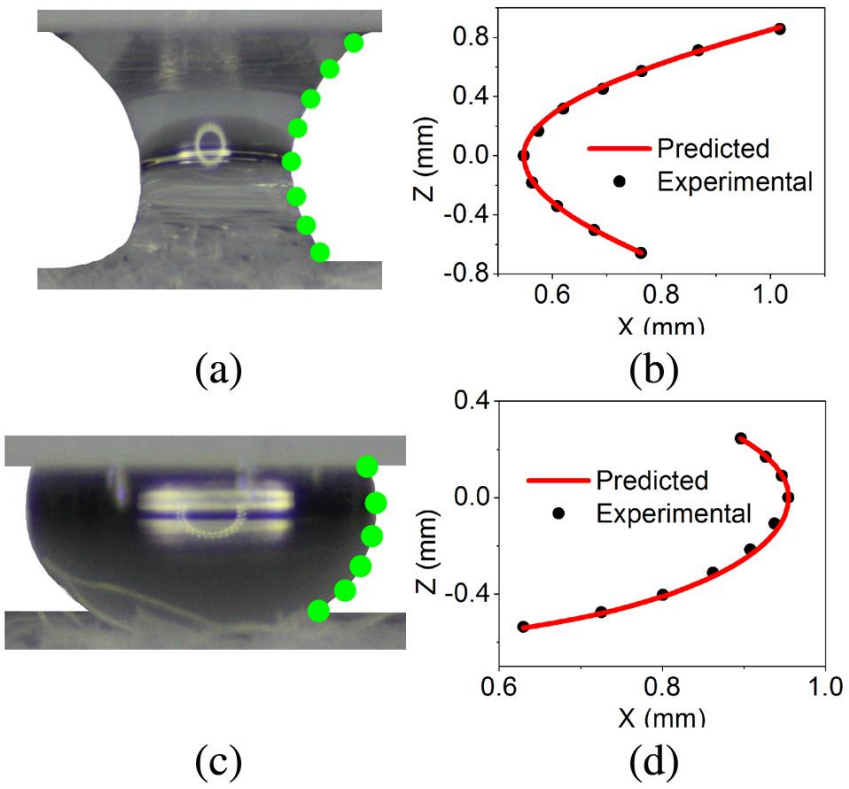

Figure 41. Images of profiles of (a) Kaydol and (c) water bridges with volume $V = 2$ μL between PTFE-(TCMS-FS) treated nylon fabric substrates. (a) and (c) show the profiles of the right side of the liquid bridges; (b) and (d) are comparisons between predicted and experimental profiles of the capillary bridges of the right part from (a) and (c). Symbols are the experimentally measured points while the solid curves are the predicted profiles.

To further verify this method, the profile liquid bridges have been studied between two rough surfaces. As shown in Figure 42, water and dodecane bridges formed between FS treated FR and FS treated nylon fabrics, and the advancing CA was used for water tested under a compression cycle, while the receding CA was employed for dodecane tested under a tensile cycle. For these asymmetric bridges, the predicted curve agrees with the experimental results very well (Figure 42 (b) and (d)) both for bi-concave and bi-convex shapes when the apparent CAs were used. Thus the model fits both the asymmetric bi-concave and bi-convex pro-

files of liquid bridges for both smooth and rough substrates. Therefore, the study of capillary bridges can be applied to the field of textiles, such as measurement of advancing and receding CAs of liquids on fabrics and evaluation or comparison of the hydrophobicity or oleophobicity of fabrics.[108]

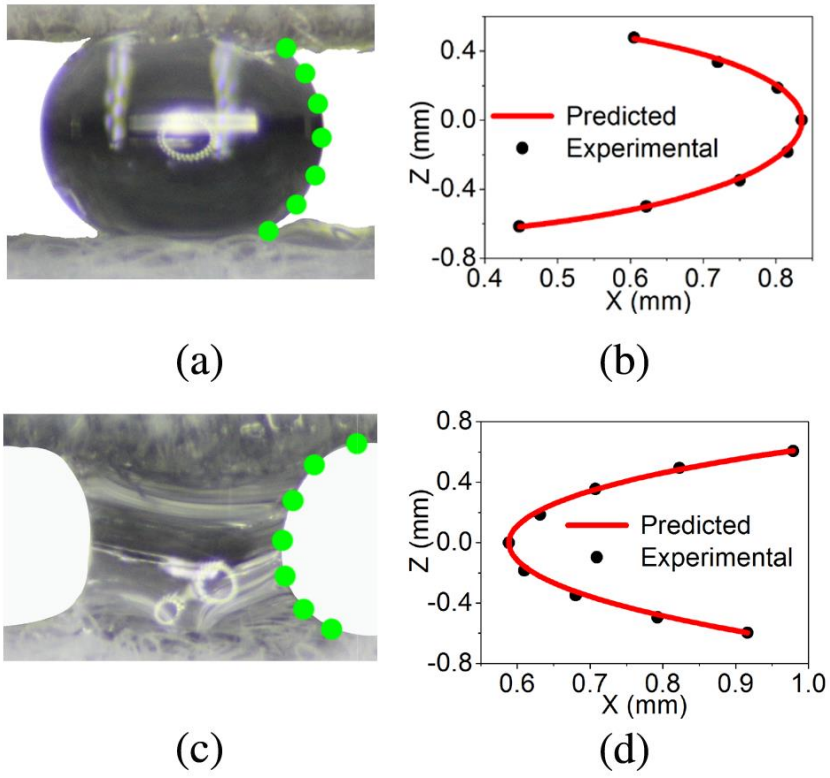

Figure 42. Images of profiles of (a) water and (b) dodecane bridges with volume $V = 2$ μL between FS treated FR and nylon fabric substrates. (a) and (c) show the profiles of the right side of the liquid bridges; (b) and (d) are comparisons between predicted and experimental profiles of the capillary bridges of the right part from (a) and (c). Symbols are the experimentally measured points while the solid curves are the predicted profiles.

In Figure 34, φ is defined as the advancing or receding CAs between a liquid and a substrate as the liquid spreads or retracts from the surface, respectively. They will be influenced by the properties of the substrate and liquid, Laplace pressure and external force. The profile model is very sensitive and minor changes in the advancing or receding CAs can lead to large changes in C and H in Equations (51) and (53).

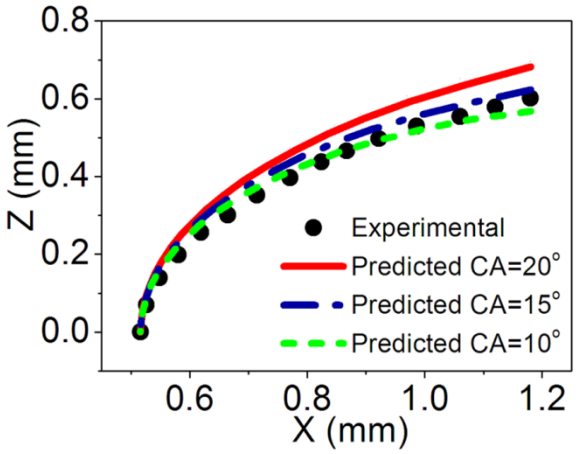

Figure 43. Effect of CAs on the profiles of a 2 μL water capillary bridge between two glass substrates with various CAs. Symbols are the experimentally measured points while the solid, dash-dot, and dotted curves are the predicted profiles.

As shown in Figure 43, the CA plays an important role in determining the accurate shape of the capillary bridge. From the predicted curves, as CA increases from 10° to 20°, the height of the liquid bridge increases by approximately 0.1 mm (or 15%). Therefore, the accuracy of CA is critical to obtain an exact profile of the liquid bridges. For a bi-axial symmetric liquid bridge, the average CA from four sides (upper left, upper right, lower left and lower right)

can be used; for an asymmetric liquid bridge, the average CA for top section and for the bottom section can be employed separately.

The experiments described above all include a "neck" or a "waist" on the profile of capillary bridges, which yields a distinct inflection point and makes the problem easier to solve. However, not all profiles include obvious inflection points, so a more general analytical solution is provided below for the case when the "neck" or "waist" is beyond the substrates. As shown in Figure 44, a coordinate system can be defined along the bottom substrate and the profile is symmetric to z-axis in two dimensions.

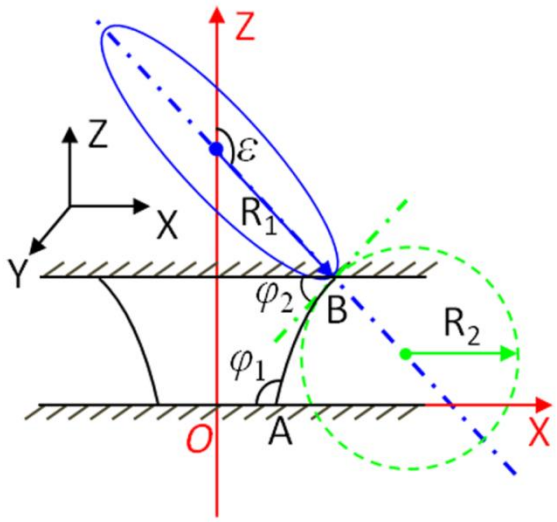

Figure 44. Capillary bridges without "neck" or "waist" inflection points between different parallel substrates.

The boundary conditions can be found from points A and B, and the general format for mean surface curvature *H* will be obtained as shown in equations (55) and (56).

$$\begin{aligned}&\text{At point A: } x = x_1, u = -\sin(\pi - \varphi_1) = -\sin\varphi_1, c = \sin\varphi_1 \cdot x_1 - Hx_1^{\,2}\\&\text{At point B: } x = x_2, u = -\sin(\pi - \varphi_2) = -\sin\varphi_2, c = \sin\varphi_2 \cdot x_2 - Hx_2^{\,2}\end{aligned} \tag{55}$$

Once again, the two *c*'s values must be the same, so *H* can be obtained:

$$H = \frac{\sin\varphi_1 \cdot x_1 - \sin\varphi_2 \cdot x_2}{x_1^{\,2} - x_2^{\,2}} \tag{56}$$

Then, Equations (55) and (56) are substituted into Equations (51) and (53) where $\varepsilon \in [\varphi_1, \pi - \varphi_2]$. Then, a more general analytical solution is obtained. Likewise, any two points, (x_1, z_1) and (x_2, z_2) can be chosen for the boundary conditions in Equation (55) with the appropriate choice of φ_1 and φ_2. For the best precision, x_1 and x_2 should be chosen to maximize $|(x_1^{\,2} - x_2^{\,2})|$, which acts as a denominator in Equation (56). Profiles of capillary bridges between parallel substrates can be used both for symmetric/asymmetric, bi-concave/bi-convex shapes bridges, when the effect of gravity is ignored.

In summary, profiles of the capillary bridges between parallel substrates were modeled for both bi-concave and bi-convex symmetric bridges and extended to asymmetric bridges for the case where the effect of gravity could be ignored. Different substrates (smooth and rough) and different liquids (surface tension and volume) were employed to form capillary bridges and the profiles of these bridges were simulated and the theoretical results were experimentally verified. Especially, the study of capillary bridges was introduced to the field of textiles by forming liquid bridges on fabrics, which acted as rough surfaces. The wetting be-

haviors of liquids on fabrics changed when the drops were stretched and compressed, which can be used to measure the advancing and receding CAs of the liquid on a fabric and evaluate the hydrophobicity or oleophobicity of a fabric. Good agreement was found between the predicted and the experimentally measured profiles of the liquid bridges. Finally, the analytical solution was extended to a more general format since a "neck" or "waist" does not exist in all liquid bridges. With this approach, the profiles of any kind of liquid bridge between parallel smooth or rough plates can be obtained as well as the Laplace pressure. Since the relations between robust pressure and Laplace pressure cannot be determined from the profile of a liquid bridge, the capillary force is studied in next section and it will help to determine this relation.

4.2 Capillary forces of a liquid between smooth surfaces

The Laplace pressure and Young's CA equation are introduced to solve the capillary force of the water or oil capillary bridge. Figure 45(a) shows a single droplet sitting on a perfectly flat surface. There are three phases, liquid, vapor and solid. The CA is Young's CA, which can be obtained from Young's equation.

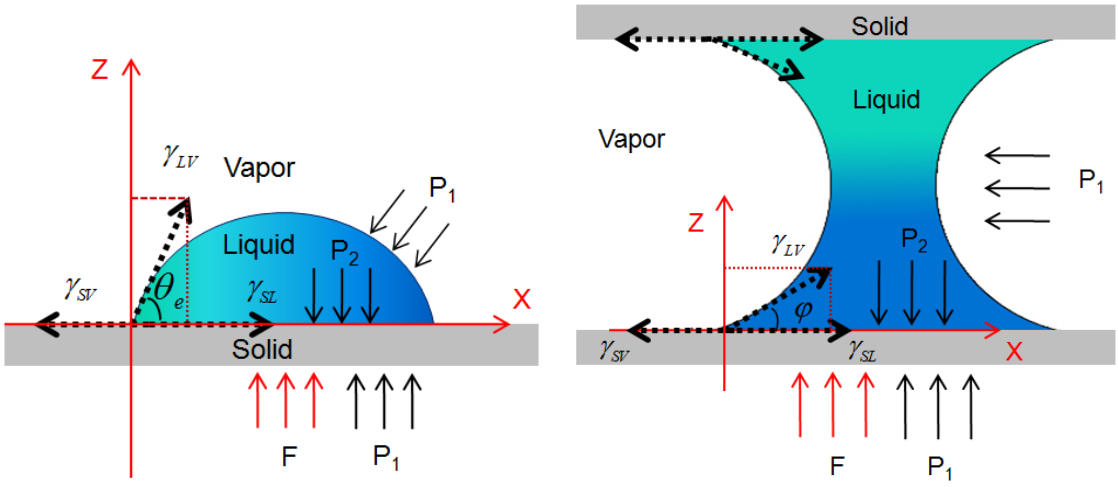

(a) (b)

Figure 45. Illustration of liquid states. (a) A droplet sitting on a smooth flat substrate; and (b) a capillary bridge formed between two flat substrates.

From Figure 45(a), X and Z are coordinates of the system. The droplet is in thermodynamic equilibrium state, so the external forces add to zero in each direction as follows:

Horizontal direction X-axis:

$$\gamma_{LV}\cos\theta_e + \gamma_{SL} - \gamma_{SV} = 0 \tag{57}$$

Perpendicular direction Z-axis:

$$2\pi R_D \gamma_{LV}\sin\theta_e + \pi R_D{}^2(P_1 - P_2) + F = 0 \tag{58}$$

$$\Delta P = P_2 - P_1 = \gamma_{LV}\left(\frac{1}{R_1} + \frac{1}{R_2}\right) \tag{59}$$

where γ_{SV}, γ_{LV}, γ_{SL} are solid-vapor, liquid-vapor and solid-liquid interfacial energy respectively, θ_e is Young's CA, φ is the advancing or receding CA between liquid and solid in a capillary bridge, R_D is the radius of the wetting area on the solid surface, P_1 is atmospheric pres-

sure, P_2 is the pressure inside the liquid, ΔP is Laplace pressure, R_1 and R_2 are the principal radii of curvature of the droplet, and F is the force applied by the substrate.

Equation (57) is Young's equation at a single point of the perimeter; the comprehensive force on the perimeter of the solid-liquid-vapor interfacial line is given by multiplying Equation (57) by $2\pi R_D$. In the perpendicular direction, all forces must sum to zero since it is in thermodynamic equilibrium. This method can be extended to the force analysis for the capillary bridge and F is the force which can be measured in the experiments as show in Figure 45(b). The capillary bridge is also in equilibrium state and similar descriptions will be obtained with Equation (57), where θ_e needs to be changed to φ. In the perpendicular direction, Z-axis, when gravity is ignored:[37]

$$2\pi R_D \gamma_{LV} \sin\varphi + \pi R_D{}^2 (P_1 - P_2) + F = 0 \tag{60}$$

$$F = F_{Laplace} + F_{tension} = \pi R_D{}^2 \gamma_{LV} \left(\frac{1}{R_1} + \frac{1}{R_2}\right) - 2\pi R_D \gamma_{LV} \sin\varphi \tag{61}$$

In Equation (60), When $F > 0$, it is a repulsive force; when $F < 0$, it is an attractive force. It shows that the expression of the force applied by the bottom substrate consists of two parts, the force arising from surface tension and the force from the Laplace pressure. The force-separation distance curves from the profile can be calculated and compared with experimental results as shown in Figure 46.

The force-separation distance curve in the push process is displayed in Figure 46(a). The force begins at zero, then there is a sharp decrease due to the formation of the capillary

bridge, and the magnitude of the force becomes larger gradually until the separation distance between substrates is zero. In Figure 46(b), the force-separation distance curve in the pull process is shown. The curve from the profile is also quite similar to the experimental curve except that there is a slight difference of the separation when the capillary bridge breaks. The curves from the profile are in good agreement with the experimental result. Therefore, the force caused by the liquid can be computed based on the images, and the capillary profile method has been verified again.

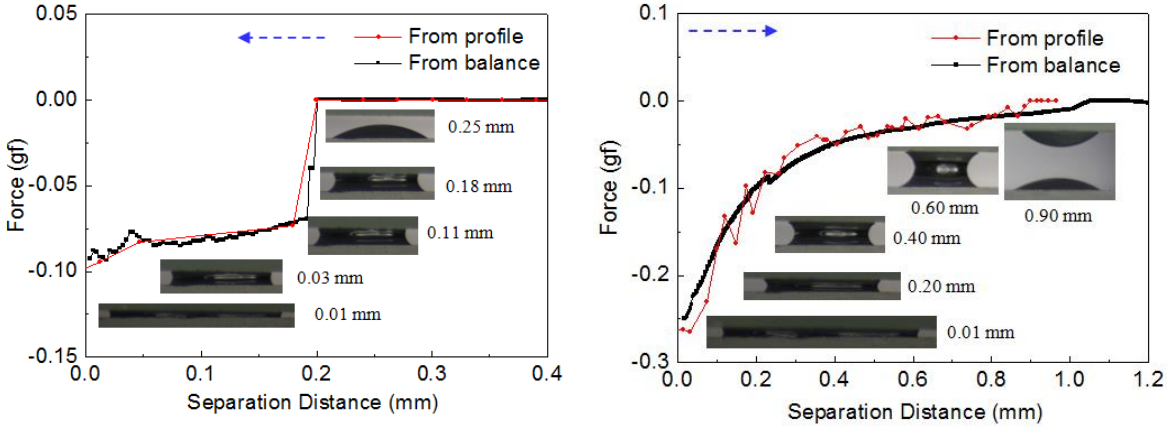

(a) (b)

Figure 46. Comparisons of the force-separation curves both from the profile and from the balance. (a) Force-separation distance curves in the push process; and (b) force-separation distance curves in the pull process.

Meanwhile, Equation (61) is verified, which relates the measured force to the Laplace pressure. In Figure 45(b), as a force is applied to the top solid surface gradually, the force at a

specific separation distance can be measured and the applied pressure will be equal to the force divided by the contact area, which is:

$$P_A = F / (\pi R_D^{\,2}) = \Delta P - 2\gamma_{LV} \sin\varphi / R_D \tag{62}$$

where P_A refers to the applied pressure, and ΔP refers to the Laplace pressure at this moment.

When the bottom substrate is changed into a hydrophobic and oleophobic fabric, and force is exerted on the top substrate until the liquid penetrates through the fabric, the applied pressure can be obtained, which is just the robust pressure. The Laplace pressure is obtained from its relationship with the applied pressure. In addition, for any liquid bridge between two substrates, the forces applied by the top and bottom surfaces must be the same according to the force interactions when the effect of gravity is negligible. For example, in Figure 45, the force applied by the two substrates are $F_1 = \pi x_1^{\,2}\Delta P - 2\pi x_1 \cdot \gamma_{LV} \cdot \sin\varphi_1$, and $F_2 = \pi x_2^{\,2}\Delta P - 2\pi x_2 \cdot \gamma_{LV} \cdot \sin\varphi_2$, where R_{D1} and R_{D2} refer to the radii of liquid-solid contact areas, φ_1 and φ_2 refer to the advancing or receding contact angles, and ΔP refers to the Laplace pressure. Since $F_1 = F_2$, it is found that:

$$\Delta P = \frac{2\gamma_{LV}(x_1 \sin\varphi_1 - x_2 \sin\varphi_2)}{(x_1^{\,2} - x_2^{\,2})} \tag{63}$$

this is exactly the same equation derived from the profile method. Thus all Equations (61-63) are applicable for the robust and Laplace pressures. If the capillary force is known and there is more than one rough surface for the liquid bridge, Equation (61) is preferred; if the capillary force is unknown or both substrates are smooth surfaces, Equation (63) is preferred.

In both Equations (58) and (61), gravity has been ignored. For a small drop with a small Bond number, it is negligible; for a larger drop or a drop with a large bond number, gravity will affect the shape of a liquid and the Laplace pressure will be different. At the bottom of the liquid bridge, it is:

$$\Delta P' = \rho g h + \gamma_{LV}(\frac{1}{R_1} + \frac{1}{R_2}) \tag{64}$$

Where ρ is the density of the liquid, g is gravitational acceleration, h is the height of liquid parallel to the direction of gravity at the test point, γ_{LV} is the liquid-vapor surface tension, R_1 and R_2 are the two principal radii. By substituting it back to Equations (61-63), both the Laplace pressure and the robust pressure of a rough surface can be obtained.

4.3 Hydrostatic and oleostatic pressure of hydrophobic and oleophobic fabrics

Hydrostatic or oleostatic pressure is different from the robust pressure, which refers to the pressure exerted by the fluid due to the force of gravity when it is in equilibrium. For this test, the contact area between liquid and fabric is restricted, and the liquid pressure can be changed by adding liquid into a tube due to the increase of liquid level. Robust pressure refers to the minimum pressure to push a liquid through a fabric, where the pressure can be caused by external forces or gravity, or the combination of them. In our study, the volume of liquid is finite (< = 20 μL), and the pressure will cause the liquid to both spread and penetrate into the fabric. The hydrostatic or oleostatic pressure is the upper limit of the robust pressure in vertical direction if the volume of the liquid is sufficient. Both hydrostatic or oleostatic and robust pressures are used to evaluate the liquid resistance of a fabric, which depends on prop-

erties of fibers (types of fibers, fiber structure), yarns (types of yarns, yarn structure), fabrics (fabric construction, surface modification). According to the AATCC test method 127-2003, the resistance of a fabric to water under hydrostatic pressure can be measured. It is applicable to different types of hydrophobic samples, such as the fabrics after chemical modification or plasma treatment. However, Hydrostatic Pressure/Head Tester can only test the resistance of a fabric to one liquid, which is water. This is not able to reveal the resistance of a sample to oil which is defined as oleostatic pressure, especially for an oleophobic fabric. Therefore, a simple instrument was designed in our lab, where the hydrostatic and oleostatic pressures can be tested with more than one liquid for our samples. The sketch is shown below.

In Figure 47, the buret (capacity, 50 mL) is used to drain the liquid into a glass tube, which allows good control of the liquid amount and the flow rate controlled by a stopcock. The flow rates for water and dodecane are measured the same, which is $4.87*10^{-7}$ m^3/s, and it is $2.24*10^{-8}$ m^3/s for Kaydol due to its high viscosity (DI water, η = 0.997 mPa*s; Kaydol, η = 203 mPa*s; and dodecane η = 1.344 mPa*s). Along with the buret is a glass tube (length, 1.22 m; diameter, 0.027 m). A small piece of fabric (diameter, 0.055 m) is placed at the bottom of the glass tube, where the edge of the fabric has been held by an elastic rubber band. One surface of the fabric faces up to the liquid, while the other surface faces down to the ground. Both the buret and the glass tube are fixed with an iron support, where they are set perpendicular to the ground. When experiment starts, the buret is filled with liquid and stopcock is open. The liquid flows down from the buret to the glass tube along the wall of the tube to reduce the liquid impact, until it reaches the fabric and begins to accumulate. The liq-

uid is allowed to flow into the glass tube until three points of leakage appear on the lower surface of the fabric, the stopcock was then closed. The height (z) of the liquid from the fabric to the liquid level is measured to calculate the hydrostatic or oleostatic pressure as follows:

$$P_{static} = \rho g z \tag{65}$$

where P_{static} refers to the hydrostatic or oleostatic pressure (Pa), ρ refers to the density of the liquid (kg/m^3), g refers to gravitational acceleration (m/s^2), and z refers to the height of the liquid.

The experiments were conducted at room temperature, 22ºC, and relative humidity 65%. Three fabrics were tested, including the single layer of nylon woven fabric made of monofilaments, nylon woven fabrics made of multifilament yarns, and nylon nonwoven fabrics. The fabric structures are shown in Figure 48. The structure of the single layer of nylon woven fabrics with monofilaments (thickness, 0.16 mm; monofilament diameter, 67.00-71.00 μm; edge-to-edge distance between warp yarns, 208.00-268.00 μm; edge-to-edge distance between weft yarns, 104.00-188.80 μm) is not stable due to the large space between adjacent monofilaments, especially under tension. Thus the uniformity of this loose structure is poor. This fabric acts as a low-robustness fabric, and the hydrostatic or oleostatic pressure was expected to be less than that of the other fabrics for the same liquid. The structure of the nylon woven fabrics made of multifilament yarns (thickness, 0.10 mm; diameter of warp yarn, 276.00-338.00 μm; diameter of weft yarn, 156.00-194.00; edge-to-edge distance between warp yarns, 54.70-97.70 μm; edge-to-edge distance between weft yarns, 33.70-49.00 μm) is

extremely stable, and this fabric acts as a high-robustness fabric. The feature of the structure of nonwoven fabric (thickness, 0.5 mm; fiber diameter, 16.48-17.55 μm; edge-to-edge space, 46.57-114.60 μm) is lack of uniformity as shown in Figure 48(c). Pores of different sizes exist unevenly on both front and back sides.

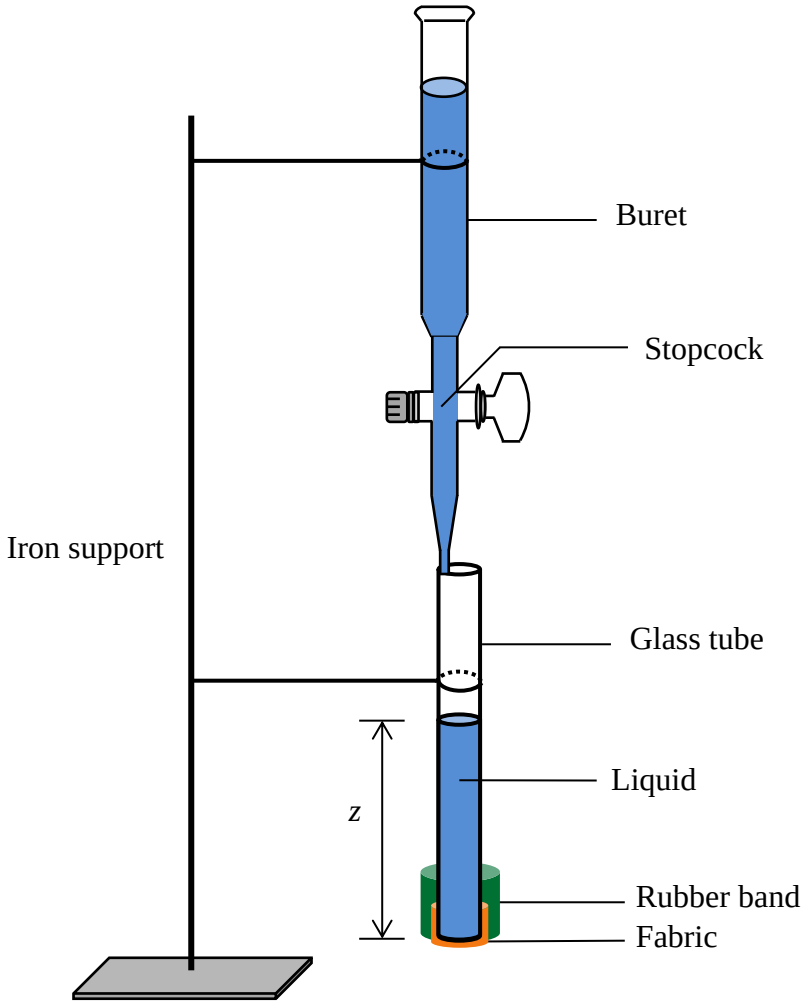

Figure 47. An instrument to measure the hydrostatic or oleostatic pressure of a hydrophobic and oleophobic fabric with a liquid.

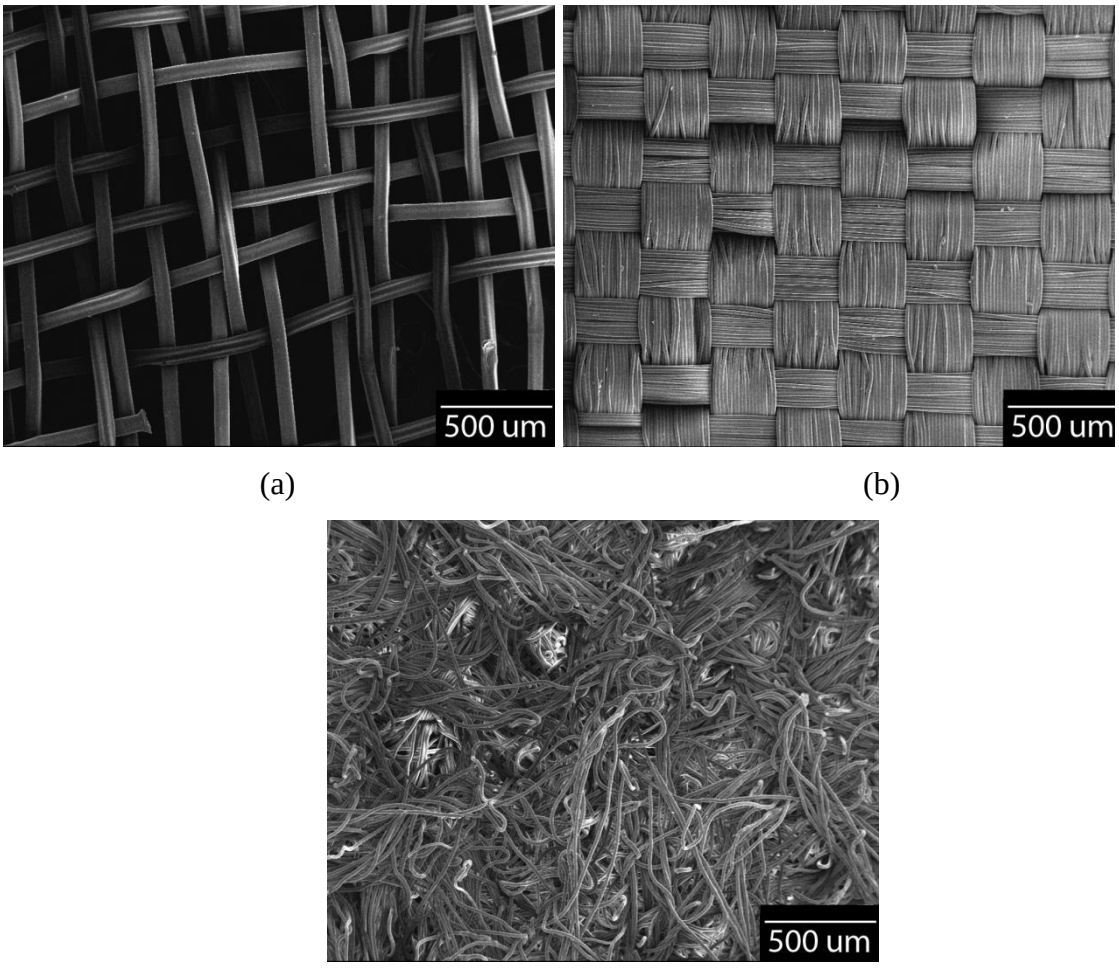

(a) (b)

(c)

Figure 48. Images of fabrics. (a) Single layer of woven fabric with monofilaments; (b) single layer of woven fabrics with multifilament yarns; and (c) multiple layers of nonwoven fabrics.

Figure 49 and Table 5 show the hydrostatic and oleostatic pressures of three fabrics for different liquids. For each fabric, the hydrostatic or oleostatic pressure increases as the surface tension of the liquid increases, which indicates the resistance of a fabric is higher to high surface tension liquid and lower to low surface tension liquid. This agrees with the equilibrium contact angle of a liquid on the same fabric. Comparing all fabrics in Figure 48, the single layer of woven fabric with monofilaments has the largest space between monofilaments,

which leads to the lowest hydrostatic or oleostatic pressure for each liquid since the liquid penetrates through the fabric from the area with the largest voids. Although the nonwoven fabric is thicker than the single layer of woven fabrics with multifilament yarns, the space between adjacent fibers is larger. This results in a lower hydrostatic or oleostatic pressure compared with the nonwoven fabric. The spaces between yarns or fibers of these fabrics could be revealed not only from Figure 48, but also from the air permeability. According to the ASTM D737-04 (reapproved 2012) Standard Test Method for Air Permeability of Textile Fabrics, the air flow passes through a fabric with a known area (circular area 5.07 cm^2 or 38.32 cm^2) perpendicularly, which can be adjusted to obtain a prescribed air pressure differential between the two fabric surfaces (125 Pa). From the rate of air flow, the air permeability of a fabric is determined, where the unit is $cm^3/s/cm^2$. The air permeability is 705.90 $cm^3/s/cm^2$ for woven fabric made from monofilaments, 75.95 $cm^3/s/cm^2$ for nonwoven fabric, and 7.02 $cm^3/s/cm^2$ for woven fabric made from multi-monofilament. Higher air permeability means more porosity of a fabric, and the test result agrees with that of the hydrostatic or oleostatic pressure experiments. For all the liquids, the smaller spaces between fibers or yarns or monofilaments in a structure, the higher liquid resistance of the fabric. For all the fabrics, the lower surface tensions of a liquid, the smaller liquid resistance of a fabric. Thus, with the same liquid, the resistance of all fabrics can be compared; with the same fabric, the surface tensions of liquids can be compared from the hydrostatic or oleostatic pressures.

Table 5. Hydrostatic and oleostatic pressures of fabrics for different liquids.

	Woven (Pa)		Nonwoven (Pa)
	Monofilament	Multifilament Yarn	
Water	791.42 ± 9.77	2198.39 ± 48.85	1664.26 ± 29.31
Kaydol	133.28 ± 16.66	952.40 ± 41.65	497.02 ± 24.99
Dodecane	11.03 ± 11.03	588.00 ± 7.35	44.10 ± 29.40

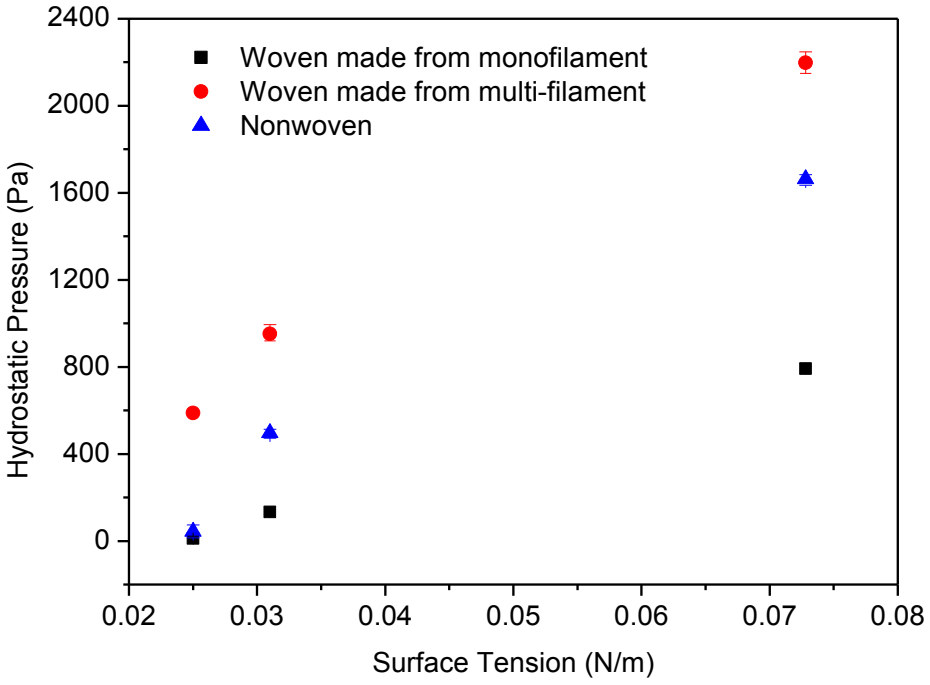

Figure 49. Hydrostatic and oleostatic pressures of fabrics for different liquids.

The partial pressure of the robust pressure in vertical direction equals the hydrostatic or oleostatic pressure of a fabric to a liquid if the volume of the liquid is sufficient, but the robust

pressure is larger than the hydrostatic or oleostatic pressure if the volume is limited, especially when the liquid mainly spreads on the surface and only wets the upper part of the fabric. To investigate the spread and penetration behavior of a liquid on a rough surface, the parallel monofilament arrays with low robustness were studied first.

4.4 Robustness of parallel monofilaments

The capillary forces and profiles of liquid bridges between smooth surfaces have been discussed, which will be applied to the capillary bridges when hydrophobic and oleophobic parallel monofilaments are used as substrates.

Unidirectional monofilament arrays were made and found to have low robustness. During a robustness test, at the moment when the water or oily liquids just wet the structure and touch the bottom line of monofilaments, the robust pressure can be measured. Robust pressure for parallel cylindrical monofilaments was proposed by Tuteja et al[1,16,101] to model the robustness of electrospun fibers when infinite volume of a liquid was applied as shown in Figure 28. In experiments, as the liquid is being pushed on the structure, the liquid-vapor-solid interfacial contact points move downwards as the sagging height reaches h_2 in Figure 50. It is not clear what the distance between the two three-phase interfacial points is before the liquid-vapor interface touches the bottom of the substrate, but the distance is defined as $2D'$ when the interface just wets the bottom of the substrate. Only when the liquid-vapor interface touches the monofilament at the points on the line which connects the centers of the two monofilaments, the space between the two interfacial points is $2D$, which is also the mini-

mum distance in this structure. In Tuteja et al[15]'s derivations, assumptions were made that $2D = 2D'$ and $\theta_e = \psi$ in Figure 28, where ψ refers to the central angle between a vertical line through a fiber center and the line which connects the fiber center and a solid-liquid-vapor interfacial point on this fiber. If the assumptions were eliminated, the robust pressure is re-derived as below, where ψ has been differentiated from θ_e and D has been differentiated from D'. Also, h_2 can be derived either from the wetting of the cylindrical fibers or from curvature of the liquid-vapor interface, which is $h_2 = R(1 - \cos\psi) = D'^2 / (2 \cdot R_{sag})$. With $D' = D + R(1 - \sin\psi)$, it will be found that $R_{sag} = D'^2 / (2 \cdot R \cdot (1 - \cos\psi))$ and $P_H' = 2 \cdot R \cdot \gamma_{LV}(1 - \cos\psi) / (D + R(1 - \sin\psi))^2$. From these equations and the figure below, P_H refers to the robust pressure, R refers to the radius of a single monofilament, $2D$ refers to the edge-to-edge fiber distance, $2D'$ refers to the distance between two liquid-vapor-solid interfacial contact points, γ_{LV} refers to the liquid-vapor interfacial energy, θ_e refers to the equilibrium contact angle, $\delta\theta$ refers to the sagging angle, and ψ refers to the central angle between a vertical line through a fiber center and the line which connects the fiber center and a solid-liquid-vapor interfacial point on this fiber. Also, the relationship between all three angles is $\psi = \theta_e - \delta\theta$.

Comparing P_H' with Tuteja et al's result $P_H = 2 \cdot R \cdot \gamma_{LV}(1 - \cos\theta_e) / D^2$, the differences are notable in the Robust pressure-Central Angle curves shown in Figure 51, where an example is given as a water drop is deposited on parallel monofilaments with the surface tension of 72.8 mN/m. The relationship between robust pressures (P_H and P_H') and central angle (ψ) or Young CA (θ_e) is shown in Figure 51, where the monofilament diameter ($2R$) is 0.58 mm and the space between adjacent fibers vary from $2D = R$ to $2D = 8R$. The derived equations are

valid when $2D < l_{cap}$, where l_{cap} refers to the capillary length of a liquid ($l_{cap} = (\gamma_{LV}/\rho g)^{1/2}$, where ρ is density of the liquid and g is gravity acceleration). There should be an offset ($\delta\theta$) between the two series of curves, but it has been removed to facilitate comparisons. For parallel fibers or monofilaments with the same radius and space, P_H increases as the central angle increases, while P_H' increases from 0 to a critical central angle ψ_c where $d(P_H') / d\psi = 0$ and continues to be the same as the central angle increases to 180°. For parallel monofilaments with the same radius but different spaces in Figure 51, both P_H and P_H' decrease as the space between monofilaments increases, and meanwhile the difference between P_H and P_H' varies at different central angles. Especially, when the space ($2D = 8R = 2.32$ mm) is close to the capillary length of the liquid ($l_{cap} = 2.73$ mm for water), the pressure decreases significantly to around 0 and there are no obvious differences between P_H and P_H'. When the radii of fibers are the same, the critical central angles ψ_c increase as the space between monofilaments increases. Therefore, the pressure required to push a liquid on parallel monofilaments and to change it from a Cassie-Baxter state to a Wenzel state mainly depends on the central contact angle (ψ), the radius (R) of a monofilament and space ($2D$) between the adjacent monofilaments, if other parameters do not change, such as γ_{LV}.

The robust pressure varies as the location of liquid-vapor interface between monofilaments changes. There are three cases exhibited in Figure 52: the interface is above (point *A*), at (point *B*), and below (point *C*) the center-to-center line of the two fibers. In Tuteja et al's derivations, the largest pressure required is to push liquid-vapor-solid interfacial points to reach

or exceed point B where the distance is smallest between the two fibers, since the robust pressure is $2R{\cdot}\gamma_{LV}(1-\cos\theta_e)/D^2$. However, when the assumptions ($2D = 2D'$ and $\theta_e = \psi$) were eliminated, the pressure can be obtained from $2R{\cdot}\gamma_{LV}(1-\cos\psi)/(D + R(1-\sin\psi))^2$, where ψ refers to the central angle at that point. The robust pressure reaches its maximum when $d(P_H')/d\psi = 0$ and ψ_c is always larger than 90°. Therefore, the robust pressure for this structure increases from 0 to $2R{\cdot}\gamma_{LV}(1-\cos\psi_c)/(D + R(1-\sin\psi_c))^2$ as ψ increases from 0 to ψ_c; then, although ψ continues to increase up to 180°, the robust pressure for this structure will continue to be the same. The two models share the same robust pressure when $\psi = 0$ and $\psi = 90°$ with the assumption that $\delta\theta$ is zero. Experiments showed that when a liquid with limited volume was deposited on parallel monofilaments (as shown in Figure 60), $\delta\theta$ could reach 36° under pressure and 32° when there is no external pressure. Thus, the derived model should more closely represent the real robust pressure since there are fewer approximations.

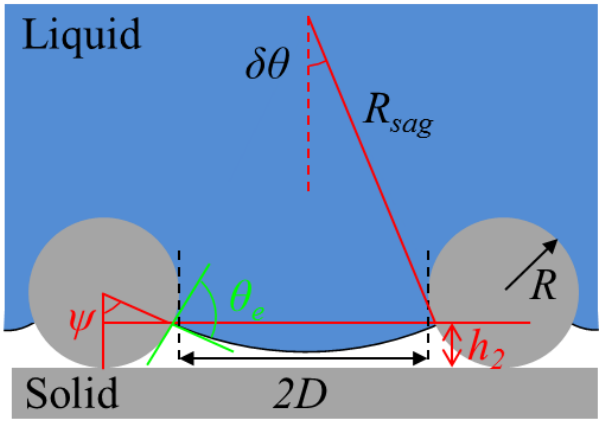

Figure 50. Schematic illustrations for design parameters for a robust composite interface made of parallel monofilaments.

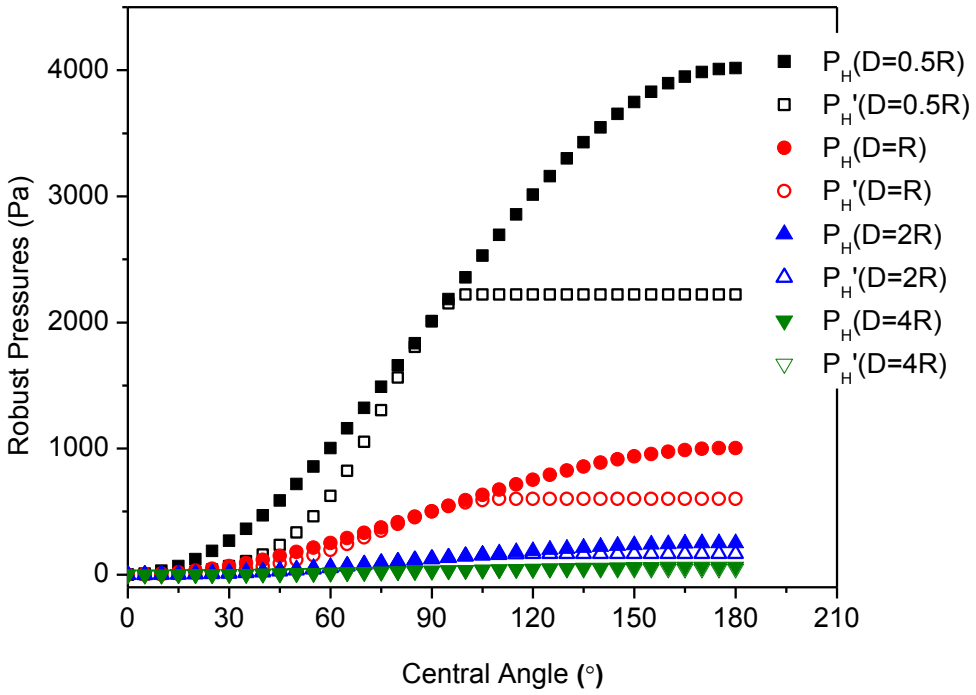

Figure 51. Comparisons of robust pressures for parallel monofilaments when the space between monofilaments changes.

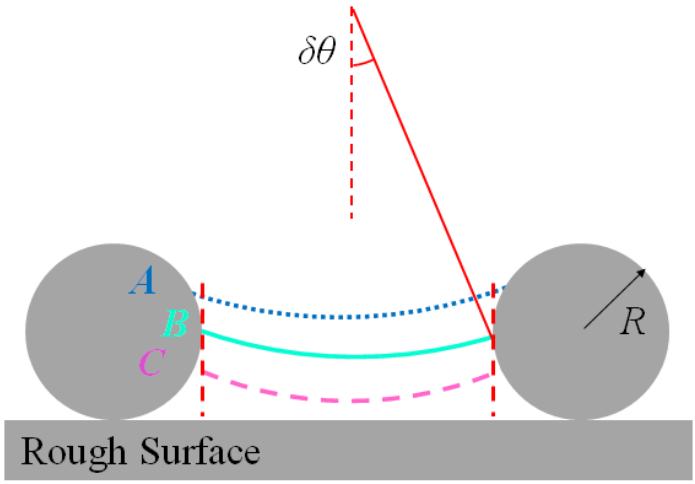

Figure 52. Liquid-Vapor interfaces of parallel monofilaments.

The robust pressure increases as the ratio of *D/R* decreases if the radius of a fiber does not change. For a particular monofilament with a fixed diameter, increasing the robustness requires a small separation distance between monofilaments, while increasing the CAs requires large spaces between them.[20] Hence there is a balance for the edge-to-edge fiber distance between the robustness and the static CA. In addition, the fiber distance must be compared with the capillary length for a liquid, in order to determine whether the surface tension or the gravitational force is dominant. For this method, two conditions must be satisfied: the fiber distance is smaller than the capillary length; the sag of the liquid-vapor interface is assumed to be an arc.

The derivations above are only for infinite volumes of liquids, which provide guidance but cannot be applied to the small drops with finite volumes. For small liquids, the robust pressure of parallel monofilaments was measured using different spaces and liquids with different volumes, which can be obtained from the capillary force method. Since the PTFE film is a flat substrate, with the robust test, Equation (58) can be used to model the capillary force and be compared with experimental results.

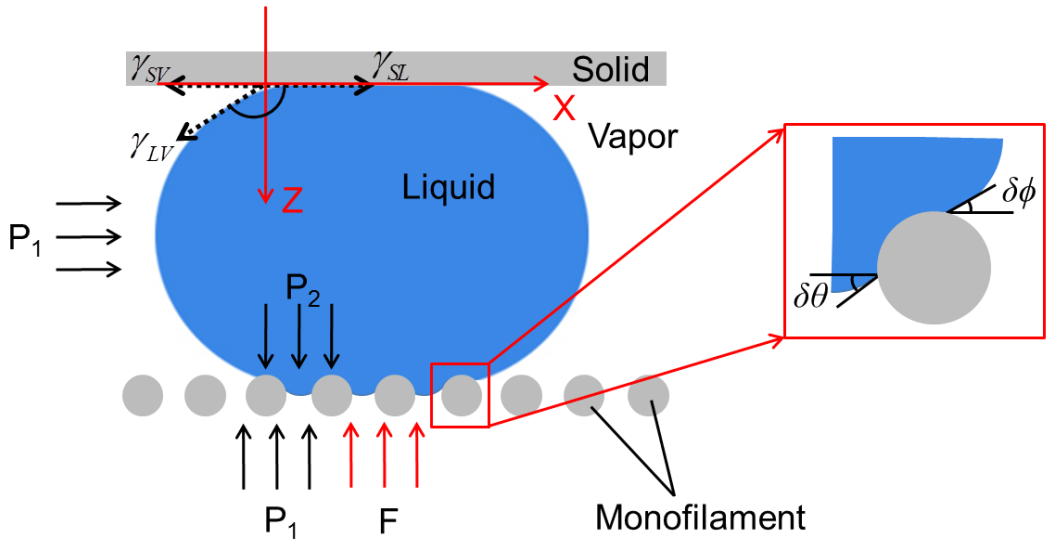

Figure 53. A liquid bridge forms between a solid smooth surface and parallel monofilaments.

In Figure 53, a liquid bridge forms between a solid smooth surface and parallel monofilaments, where P_1 and P_2 refer to the atmospheric and liquid internal pressures, F refers the force applied to the liquid, $\delta\theta$ refers to the sagging angle, $\delta\varphi$ and the apparent CA of the monofilaments are supplementary angles since they add up to 180°, and γ_{LV}, γ_{SV} and γ_{SL} refer to the interfacial energies between liquid and vapor, between solid and vapor, and between solid and liquid phases, respectively. The force (F) applied to the liquids can be obtained either from the top substrate or from the bottom monofilaments, and they must be equal due to the force interactions if gravity is negligible. For the top substrate, the exerted force is a combination of tension force and Laplace force according to Equation (58). The condition is that the contact area between the liquid and the top substrate is in a circular shape with a radius R_D, and experimental results show that the contact area is close to a circle as the liquid wets the structure since the ratio of the largest (along the fiber) to the smallest (perpendicular

to the fiber) span distance by the drop is between 1.02 and 1.04 for a liquid with the volume no more than 20 μL. For the bottom monofilaments, the force is:

$$F = 2nL\gamma_{LV}\sin\delta\theta - 2L\gamma_{LV}\sin\delta\phi + 2nD'L\times\Delta P \tag{66}$$

where F refers to the applied force, n refers to the number of gaps spanned by the liquid, L refers to the length of monofilament wet by the liquid, γ_{LV} refers to the liquid-vapor interfacial energy, $\delta\theta$ refers to the sagging angle, $\delta\varphi$ refers to the supplementary angle of the apparent CA of the monofilaments, and ΔP refers to the Laplace pressure, which equals (P_2 - P_1). When the liquid has been compressed, the liquid-vapor interface moves downwards into the structure and spans onto more monofilaments as well. There are still the Laplace and surface tension forces, but the force due to surface tension has been split to two parts, between gaps and at the edges. When there are only two parallel monofilaments (n = 1), the force will be:

$$F = 2L\gamma_{LV}(\sin\delta\theta - \sin\delta\phi) + 2D'L\times\Delta P \tag{67}$$

Therefore, the Laplace pressure can be obtained from the force equations if other parameters are known. The robust pressure is just the applied force per unit area. If gravity is counted, an extra pressure due to gravity (ρgh) can be added to the Laplace pressure. However, Equations (66) and (67) are valid only when the liquid-solid contact is a straight line along the fiber from the side view shown in Figure 54(a) rather than a distorted curve in Figure 54(b), since in this case, L cannot be used to describe the whole liquid-solid contact length.

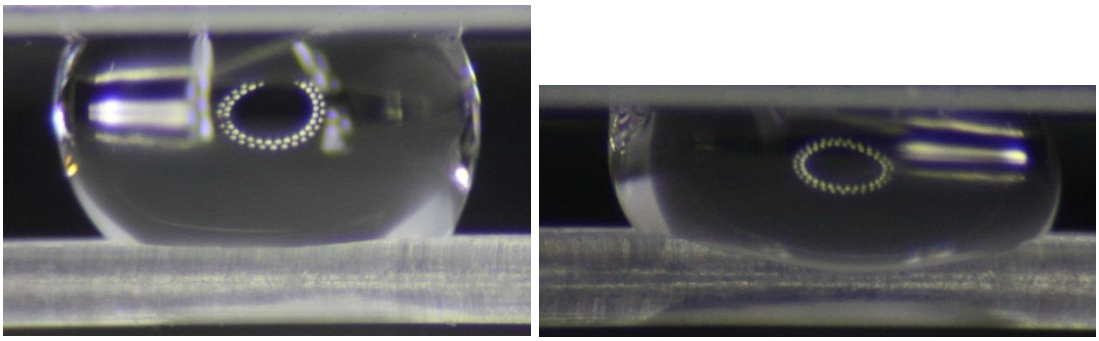

Figure 54. A water bridge between a PTFE film and two parallel monofilaments where the diameter is 0.58 mm, the space is 0.7 mm and the liquid volume is 10 μL.

Meanwhile, for the profile of the liquid-vapor interface above the monofilaments, it is under the assumption that the liquid-vapor interface is a surface of revolution by rotating $z = f(x)$ surrounding z axis, which does not fit this structure since the liquid wets the monofilaments non-uniformly along the radius and length directions.

Robustness of parallel monofilaments was measured when a liquid was being squeezed between a film and the monofilaments as shown in Figure 55. When a droplet is deposited on monofilaments, a PTFE film is used to push the liquid. At the moment the liquid-vapor interface contacts with the bottom line of the monofilaments, the applied pressure represents the robustness of this structure, which is also called "robust pressure". There are two pieces of liquid-vapor interface: one is between the gaps formed by monofilaments where the Laplace pressure is denoted as ΔP_1, and the other one is between the PTFE film and the monofilaments where the Laplace pressure is denoted as ΔP_2. If the gravity is negligible, the Laplace pressure through the entire liquid-vapor interface must be the same when it is in equilibrium

and the shape will not change, which implies $\Delta P_1 = \Delta P_2$. Thus both the Laplace pressure and robust pressure can be obtained from the capillary force analysis.

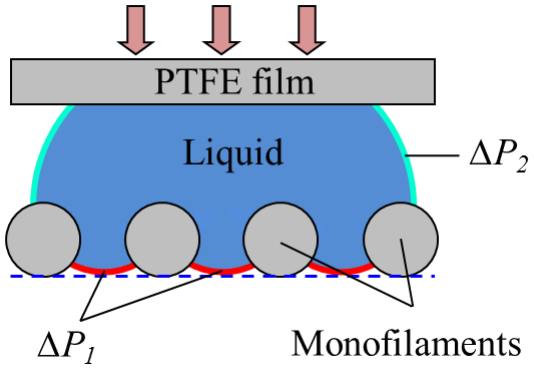

Figure 55. A capillary bridge between a PTFE film and the parallel monofilaments showing the point where the applied pressure equals to the robustness pressure.

An assumption is made that all experiments will be conducted under the same conditions, i.e. at 65% relative humidity and a temperature of 25°C . It is also assumed that the liquid is pure, that an exact volume of liquid can be deposited, that no evaporation of the liquid occurs, and that there are no air currents during the tests. In addition, the monofilaments are assumed to be completely straight and uniform, the surfaces are perfectly smooth, they do not change shape when interacting with the liquid, there is no absorption of liquid, and moisture regain does not change. Parallel nylon monofilaments (diameters, 0.58 mm) with different spaces and DI water with different volumes were used for the test; for each kind of nylon monofilament, different fiber spaces were constructed and to conduct the experiments. For each condition, the experiments were repeated at least three times.

A PTFE film acts as the top substrate to push the liquid on the FS treated parallel monofilaments rather than any other surface, which is because to the best of our knowledge, PTFE film is the most hydrophobic and least oleophilic smooth surface. When being squeezed, the liquid is expected to spread and penetrate into the space between parallel monofilaments rather than being transferred onto the top substrate. For example, if water is being squeezed by glass or aluminum, the drop will wet the top substrate and may not go into the spaces between monofilaments, since the FS treated monofilaments are too hydrophobic and oleophobic compared with the glass or aluminum. Meanwhile, the hydrophobicity and oleophobicity between PTFE and FS treated nylon film are very close, which is reflected from the CAs in Figure 56**.** The equilibrium CAs on PTFE film are 110° for water, 45° for Kaydol, and 30° for dodecane, respectively, while they are 111° for water, 78° for Kaydol, and 64° for dodecane on FS treated nylon film. This shows that the liquid will not spread on PTFE film spontaneously and thus it is appropriate to be used to squeeze the liquid on the FS treated monofilaments.

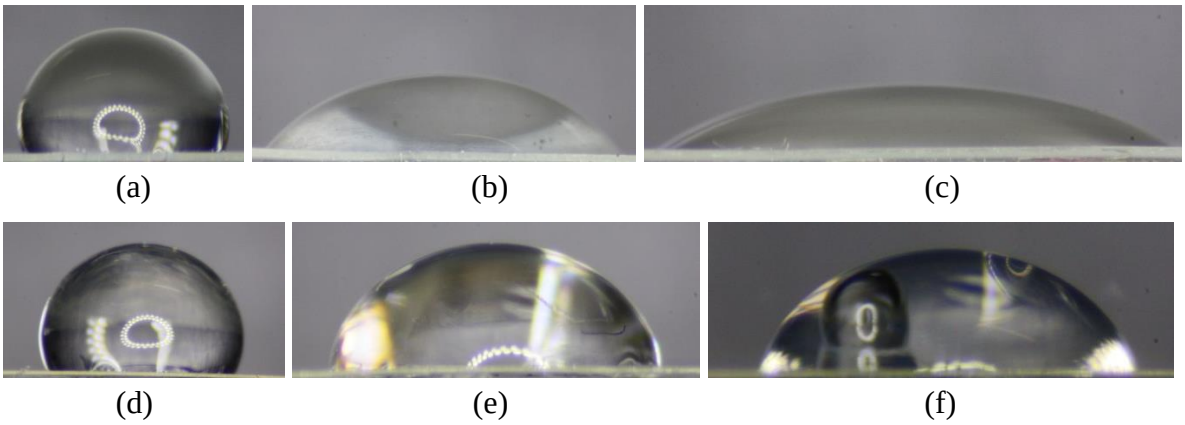

Figure 56. Equilibrium CAs of liquids on smooth surfaces. (a)-(c) refer to water, Kaydol and dodecane on PTFE films, where the CAs are 110°, 45°, and 30°, respectively; and (d)-(f) refer to water, Kaydol and dodecane on FS treated nylon films, where the CAs are 111°, 78°, and 64°, respectively. The volume of each liquid is 10 μL.

In addition, the surface topography of nylon films before and after the FS treatment is shown in Figure 57. Before the treatment, the nylon surface is very smooth; after the treatment, it is found that the surface is still relatively smooth even though the roughness has increased slightly, which can only be seen from the SEM image with the magnification of 2000x. Since the roughness is extremely small, it is negligible during the robust tests. Figure 58 shows the different wetting behaviors of sessile drops on two parallel nylon monofilaments before and after FS treatments in both from one side view. The diameter of the monofilament is 0.58 mm, and the space between the two monofilaments is 0.60 mm. Obviously, the equilibrium CAs are different for the initial and treated monofilaments (72° ± 2° and 111°± 2°). Most importantly, it is a Wenzel state in Figure 58(a) and (b), while it is in a Cassie-Baxter sate in Figure 58(c) and (d). Therefore, for this structure, the initial nylon monofilament is hydrophilic and not robust to water, while the monofilaments after treatment are hydrophobic and the robustness can be tested by pushing on the liquid.

(a) (b)

Figure 57. Surface topography of nylon films. (a) Before FS treatment, and (b) after FS treatment.

Three different liquids have been used for robust tests of fabrics, including water, Kaydol and dodecane. For all liquids, the Bond numbers ($Bo = \rho g L_2/\gamma_{LV}$, *Bo* refers to the Bond number, ρ refers to the density of liquids, *g* refers to the gravitational acceleration, *L* refers to the characteristic length, and γ_{LV} refers to the liquid-vapos interfacial energy) are shown in Table 6, which compares the importance of surface tension and gravitational forces. A high Bond number (close to or larger than 1) indicates that the gravitational force is dominant; a low Bond number (much smaller than 1) indicates that the surface tension force is dominant. The density and the radius squared of a liquid have a positive correlation to the Bond number, but surface tension has a negative correlation. Thus, for the same liquid, the gravitational force increases as the volume of liquids increases; for different liquids with the same volume, the gravitational force changes corresponding with the ratio of density to surface tension of a liquid. From Table 6, gravitational force changes in a larger range, especially for Kaydol and

dodeecane, and the effect will be added for robust modeling. Three liquids were used for robustness of the fabric, but only water was tested for parallel monofilaments, since Kaydol and dodecane penetrated through the structure immediately after being deposited and the wetting behavior is similar to that in Figure 58(a). In other words, the structure is not robust to the low surface tension liquids.

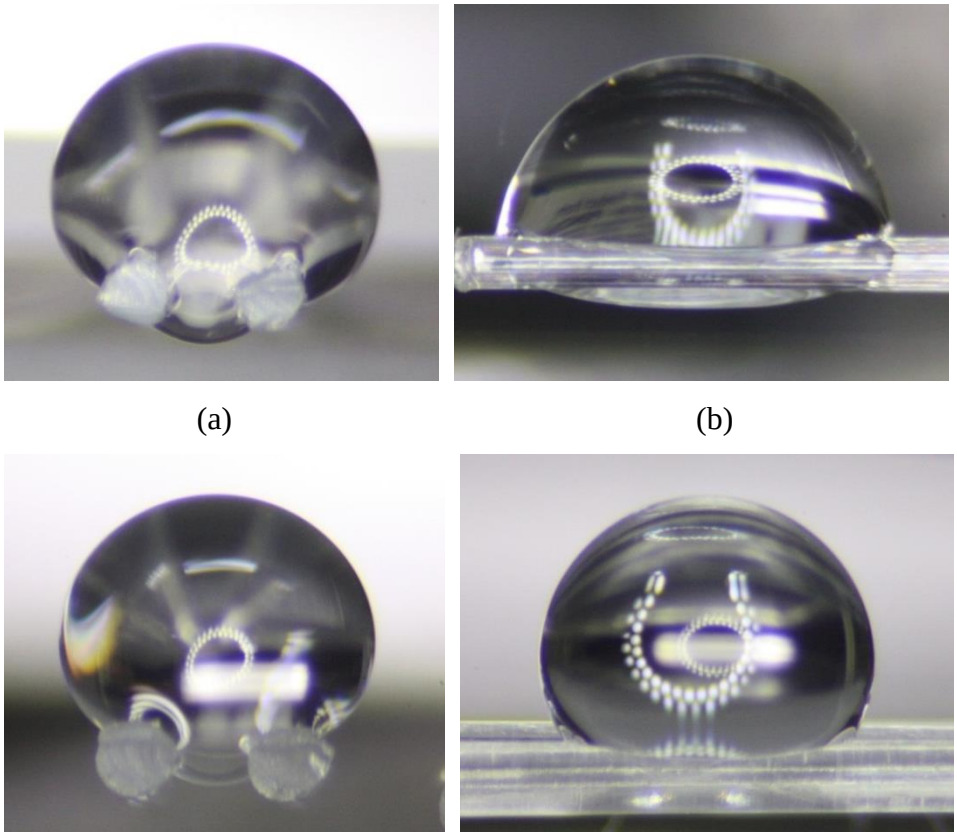

(a) (b)

(c) (d)

Figure 58. Views of sessile drops on parallel nylon monofilaments. (a) Front view, and (b) side view of nylon before treatment; (c) front view, and (d) side view of nylon after treatment. The volume of the liquid is 10 μL.

Table 6. Bond numbers of liquids with different volumes.

Volume (μL)	2	5	10	20
Water	0.08	0.15	0.24	0.38
Kaydol	0.16	0.3	0.48	0.76
Dodecane	0.18	0.33	0.53	0.83

Before tests, the robustometer was calibrated first by measuring the force-separation distance curves. As shown in Figure 59, when there is no liquid between two substrates, the magnitude of the measured force (solid curve) increases unexpectedly as the separation distance decreases from 3.5 mm to 1 mm. Since both PTFE film and nylon are good insulators, it was hypothesized that static charges existed on their surfaces. Subsequently, this hypothesis was proved by reducing the static charges with the Zerostat Antistatic gun and comparing the force-separation distance curves obtained before and after the static charges were reduced with the Zerostat Antistatic gun. It is observed that the force changes in a very small range after the static charges has been reduced, which is excellent for the robust tests of the hydrophobic and oleophobic fabrics. Therefore, when a liquid is deposited on the monofilaments, the change of force is only due to the deformation of the liquid. This calibration will be conducted if any component (top or bottom substrate, distance between substrates, and liquid) has been changed.

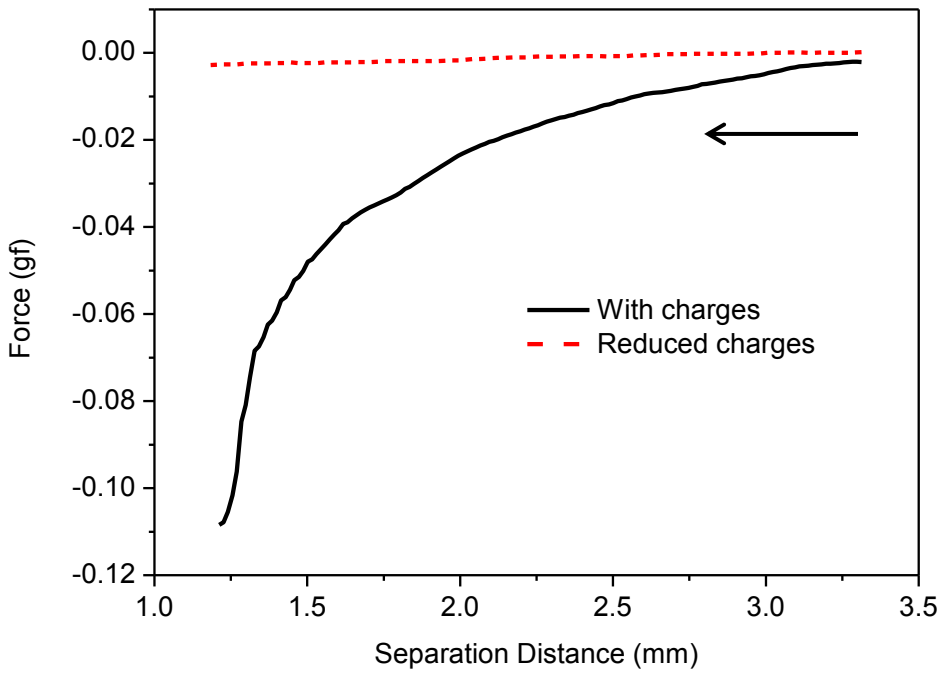

Figure 59. Force-separation distance curves for calibration, where top and bottom substrates are PTFE film and parallel monofilaments.

Effect of Water Volume

On Two Monofilaments

Two FS treated parallel nylon monofilaments were made for these tests, where the diameter of the monofilament was 0.58 mm and the space between them was 0.2 mm. Four different volumes were selected, including 2, 5, 10 and 20 μL. However, none of the liquid went through the gap between monofilaments but wrapped around the side of a monofilament to wet the structure when it was squeezed. The force-separation distance curves vary dramatically. Due to the different scales, they are shown separately in Figure 60. The force increases as the separation distance gets smaller for 2, 5 and 10 μL water, and it changes from zero to positive; there was also a sharp decrease for 20 μL force curve due to contact between the

PTFE film and water, and then the force increased in a short distance and decreased again as the liquid was squeezed. The force for 20 μL curve was always negative. The capillary force can be affected by the advancing or receding contact angles, the Laplace pressure, liquid volume, and liquid-vapor surface tension. For the parallel monofilaments, the liquid is distributed unevenly on the surface when being pushed, which results in non-uniform advancing contact angles on the monofilaments and relatively stable angles on PTFE films.

Figure 60. Force-separation distance curves, where top and bottom substrates are PTFE film and parallel monofilaments. The liquid is water, and the volumes are (a) 2 and 5 μL, where the images are for 5 μL water, (b) 10 μL, and (c) 20 μL.

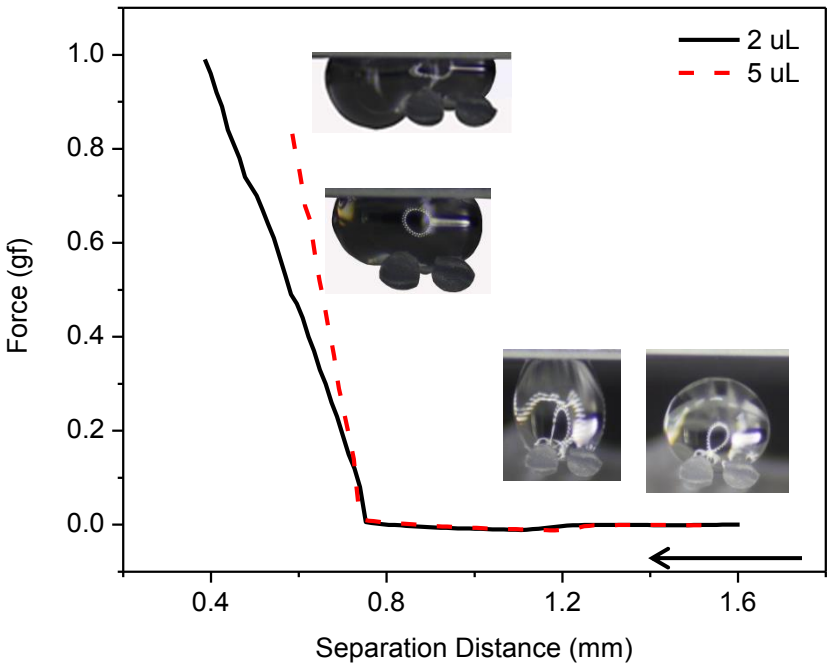
2 uL
5 uL
1.0
0.8
0.6
0.4
0.2
0.0
Force (gf)
0.4
0.8
1.2
1.6
Separation Distance (mm)

(a)

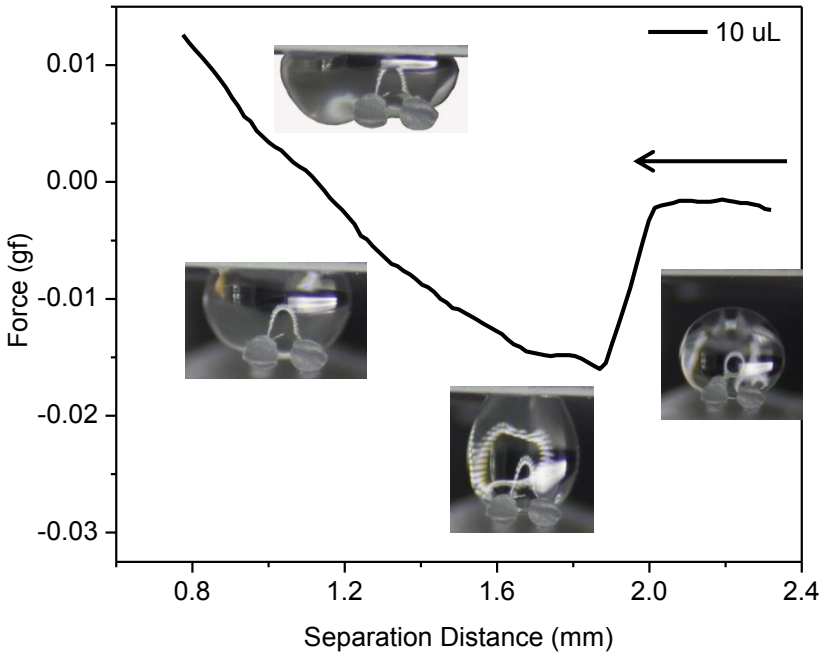
10 uL
0.01
0.00
-0.01
-0.02
-0.03
Force (gf)
0.8
1.2
1.6
2.0
2.4
Separation Distance (mm)

(b)

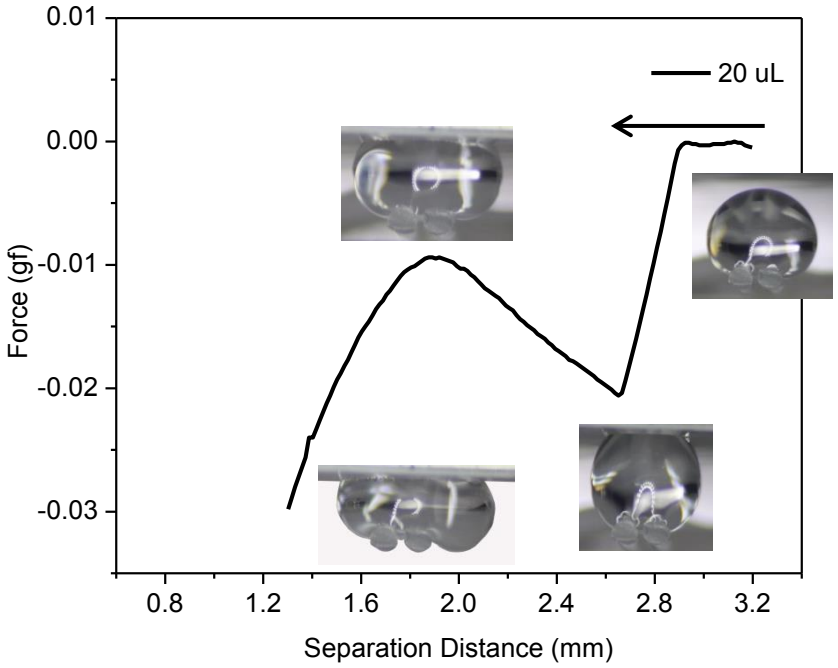

(c)

The average advancing contact angles on PTFE films are 113° ± 2° for the 2, 5 and 10 μL water at the minimum separation distance; as the liquid just penetrates through the structure, the advancing contact angles on PTFE film vary widely for 20 μL water even after the experiments had been repeated several times, which are 102° ± 2° from the left side and 120°± 2° from the right side. However, the equilibrium contact angle of water on PTFE film is 110°± 2°.

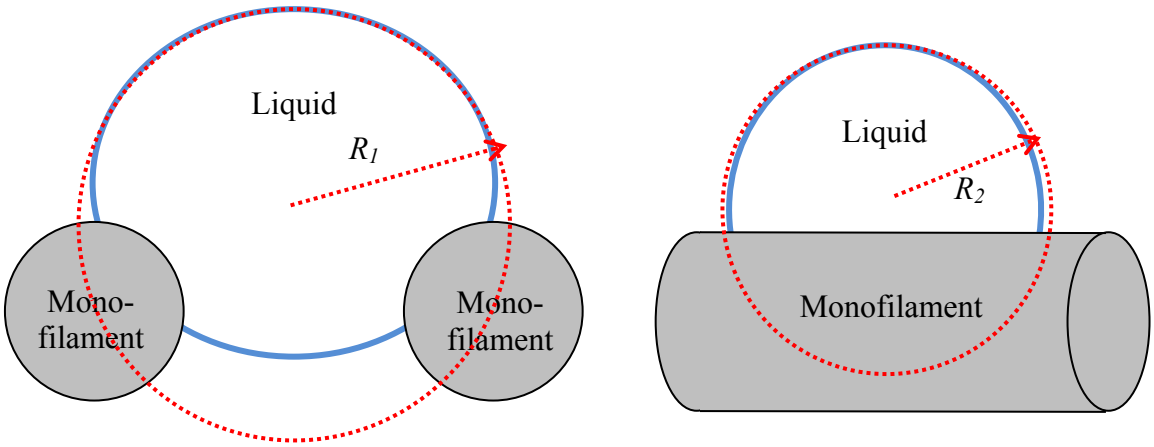

Figure 61. Front and side views of a liquid on two parallel monofilaments.

The initial Laplace pressures are large for small drops and small for large drops, since the principal radii for a particular point on the liquid-vapor interface increases as the volume gets larger as shown in Figure 61. The Laplace pressure changes as the liquid changes shapes when being squeezed. Increase of the Laplace pressure leads to a positive force if other parameters are kept the same, while decrease of the Laplace pressure results in a negative force. When the liquid volume increases, there is a higher possibility for the liquid to surround the monofilaments and go through the structure with the same applied force, especially when gravity has an effect. Therefore, the force required to push the liquid through the structure decreases as the volume gets larger.

At the minimum separation distance or height for each liquid, the height, contact area, pressure due to gravity, the Laplace pressure, and the applied pressure are compared in Table 7. The pressure due to gravity is calculated based on the separation distance between monofilaments and PTFE film, and the diameter of the monofilaments. The applied pressure is ob-

tained by dividing the applied force by the contact area between liquid and the PTFE film, and the Laplace pressure is calculated from its relationship with the applied pressure. As the liquid volume increases, the separation distance and contact area increases as well as the pressure due to gravity when the liquid just wets the structure, but the Laplace pressure and applied pressure decrease. The Laplace pressure for 20 μL is cannot be calculated, since the advancing contact angles vary at different liquid-vapor-solid contact points and the force equation cannot be applied. For all liquids, the robust pressure will be the combination of the applied pressure and the pressure due to gravity, which are larger than the sum of them since the liquid did not penetrate through the structure from spaces between monofilaments and it cannot be measured due to the high robustness. The actual Laplace pressure has a gradient, which increases from top of the liquid to the bottom. From this experiment, it is found that the liquid prefers to flow to a large gap between PTFE film and monofilaments, rather than to penetrate through the small gap between two monofilaments, as force is applied. This behavior also appeared when the substrate changed to hydrophobic and oleophobic monofilaments with at least two or more gaps.

Table 7. Comparisons of separation distances or heights, contact areas, pressures due to gravity, the Laplace pressures and the applied pressures of liquid bridges with different water volumes at the minimum heights (h_{min}).

Volume (μL)	2	5	10	20
Height (mm)	0.33±0.02	0.58±0.08	0.78±0.07	1.24±0.13
Contact Area (mm^2)	3.31±0.12	4.92±0.07	5.91±0.23	7.93±0.16
Pressure due to gravity (Pa)	8.92±0.20	11.37±0.78	13.33±0.79	17.83±1.27
Laplace Pressure (Pa)	3470±130	1820±69	110±5	N/C
Applied Pressure (Pa)	3340±120	1710±65	21±8	-37±2

†Note: N/C indicates that the value cannot be calculated.

On Multiple Monofilaments

On multiple monofilaments, there are different spaces between adjacent monofilaments. As an external force is pushed on the drop, the liquid spans onto more monofilaments after being deposited, and finally penetrates through gaps between monofilaments or from the gaps between the monofilaments and PTFE film. The liquids with the volumes of 2 and 5 μL behave similarly when being squeezed, spreading from two to three monofilaments and flowing through the structure from a large gap as shown in Figure 62(a). At the minimum separation distance, for 2 and 5 μL liquids, the Laplace pressures are 183 and 137 Pa, and the applied pressures are 57 and 50 Pa, respectively.

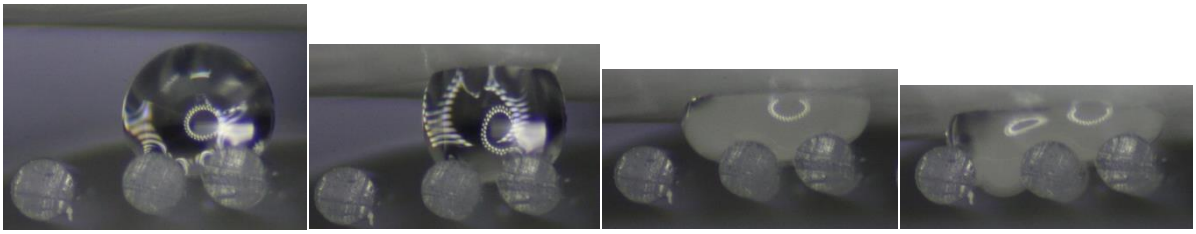

(a)

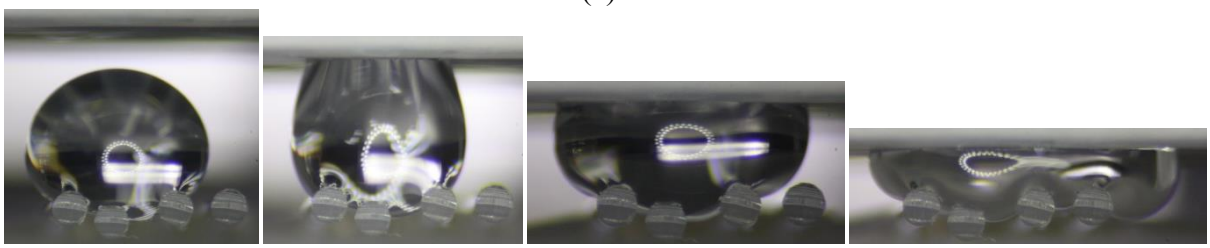

(b)

Figure 62. Images of liquid bridges as being squeezed between PTFE film and parallel multiple monofilaments. (a) the liquid volume is 5μL, and (b) the liquid volume is 20 μL.

The liquid with a volume of 10 and 20 μL behave similarly to the liquids on two monofilaments by wrapping around the side of the monofilaments and wetting the structure. At the same time, it spreads onto more monofilaments. The liquid in Figure 62(b) behaves in this way because the structure made of monofilaments is too robust, even when the liquid has been compressed very hard. The Laplace pressures are 117 and 98 Pa, and the applied pressures are 46 and 39 Pa, respectively. In general, as the liquid volume increases, both Laplace pressure and robust pressure at the minimum height decrease, which agrees with the result of robustness of two parallel monofilaments. However, since the liquids wet different local structures, it might be inappropriate to compare the pressures (liquids with 2 and 5 μL spread onto three monofilaments after being deposited on two monofilaments, and penetrates through the structure from the larger gap; the liquid with a volume of 10 μL spreads on three

monofilaments after being deposited on two monofilaments; the 20 μL liquid spreads on four monofilaments after being deposited on three monofilaments).

For all four liquids, they spread onto more monofilaments and penetrated through parallel monofilaments from large gaps as they were being squeezed. For the parallel monofilaments with the same diameters, the robust pressure is smaller for a large edge-to-edge distance between two monofilaments and it is larger for smaller distance. This is valid both for liquids with infinite and finite volumes. For a liquid with infinite volume, the liquid is restricted in horizontal direction and goes through the structure in vertical direction, when the hydrostatic or oleostatic pressure reaches the minimum robust pressure between adjacent monofilaments where the gap is largest. For a liquid with finite volume, as a pressure is applied to a liquid on parallel monofilaments, although the liquid changes shapes both in vertical and horizontal directions, the partial pressure in vertical direction has to reach the minimum robust pressure to penetrate through the monofilaments. To further study the effects of spaces between monofilaments, a liquid with the same volume were tested on two parallel monofilaments in the next section.

Effect of Spaces between Monofilaments

The two parallel monofilaments with a diameter of 0.58 mm were used to do the tests, and there were three different spaces ($2D$) between them, 0.2 mm, 0.6 mm and 0.8 mm. A water liquid with a volume of 10 μL was deposited on three different structures made of parallel monofilaments and tested with the robustometer. When $2D$ = 0.8 mm, experiments showed

that water drop just wets the two parallel monofilaments, where the behavior is similar to Figure 58(a). Thus this structure is not robust to water and it does not need to be tested by compressing with PTFE film. For the other two structures ($2D$ = 0.2 mm and $2D$ = 0.6 mm), the force-separation distance curves are shown in Figure 63. The applied forces share the same trend, starting from zero, decreasing sharply due to the formation of a liquid bridge and increasing gradually until the liquid goes through the structure, as the separation distance decreases. For the structure with a space $2D$ = 0.2 mm, the liquid stays on the upper portion of the monofilaments even when it is being pushed by the PTFE film. It shows that the liquid prefers to spread on rather than to penetrate into the structure and this behavior will not change when the applied force has been increased.

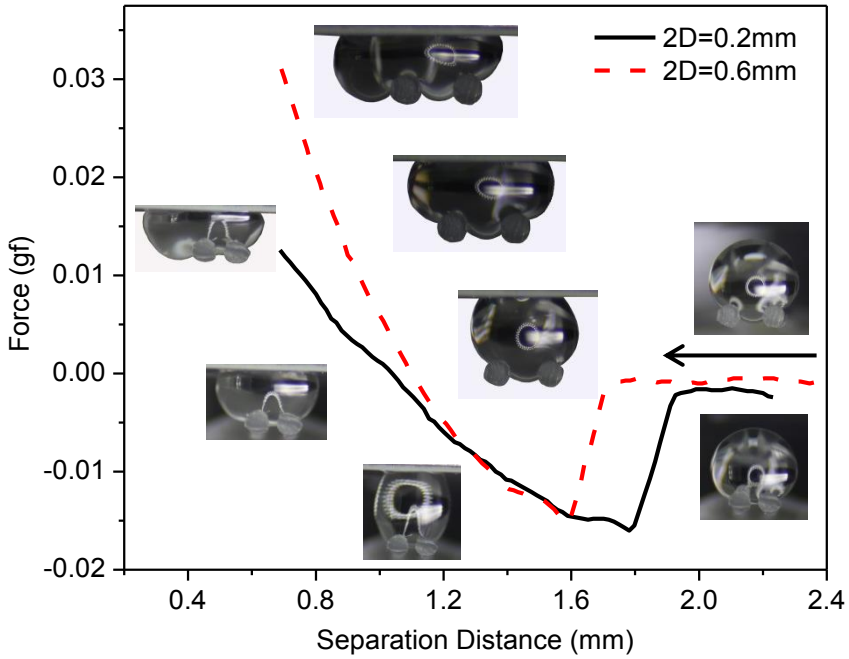

Figure 63. Force-separation distance curves, where top and bottom substrates are PTFE film and parallel monofilaments. The liquid is water with a volume of 10 μL.

As the space becomes 0.6 mm, the liquid wets middle lower portion of the monofilaments after it has been deposited; under pressure, the liquid first moves vertically along the monofilament and wets the structure. At this moment, the separation distance is 0.93 mm and the applied force is 0.0106 gf. If the force continues, the liquid then spreads around one of the monofilaments and touches the bottom line of the structure from the side, where the separation distance is 0.69 mm and the applied pressure is 0.0315 gf. This behavior implies that even if the applied pressure reaches the robust pressure of the structure, the liquid still prefers to spread on the surface. Comparing the three structures, before the liquids have been squeezed, they wet more and more parts of the monofilaments vertically as the spaces increase. Especially for the structure ($2D$ = 0.8 mm), the liquid wets the structure completely

without any external pressure. For the other two structures ($2D$ = 0.2 and 0.6 mm), the Laplace pressures are 115 and 103 Pa, and the applied pressures are 21 and 15 Pa, respectively. If the liquid has been compressed to the height 0.69 mm for the structure ($2D$ = 0.6 mm), the Laplace pressures and the applied pressures will be 132 and 45 Pa. The hypothesis that robust pressure is smaller for monofilaments with larger space is made under the condition that the liquid penetrates through the structure from the gaps between monofilaments. If the liquid behave as shown in the figure, the results might be different, since the space between PTFE film and the monofilament at the sides cannot be compared with that between adjacent monofilaments, due to their different physical shapes. This is also a difference between liquids with infinite and finite volumes. In addition, if there are more parallel monofilaments with the same spacings, the liquid could only spread on and never penetrate through the structures even if the separation distance between PTFE film and monofilaments is zero, which could happen on hydrophobic fabrics.

4.5 Robustness of single layer of woven fabric with monofilaments

The same assumptions as was made for parallel monofilaments are made for woven fabric made of monofilaments. In addition, all fabrics are assumed: 1) to have uniform structures; 2) to retain their shape when interacting with the liquids; and 3) to not absorb any liquid during the tests.

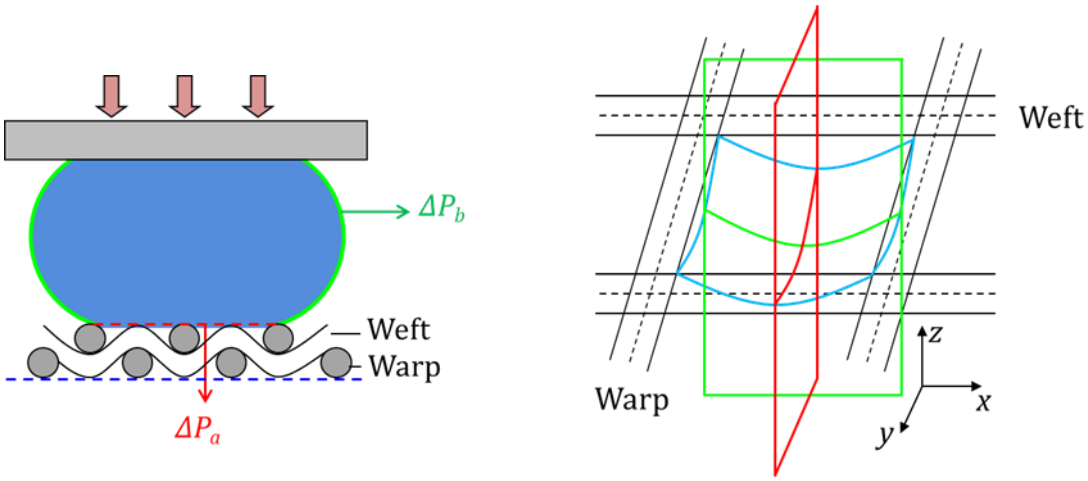

(a) (b)

Figure 64. Wetting behavior of a liquid between a smooth surface and a woven fabric. (a) Capillary bridges; and (b) the liquid behavior on one unit of the fabric.

Figure 64(a) shows a capillary bridge between a PTFE surface and a hydrophobic and oleophobic fabric. When the warp and weft filament density are nearly the same and the dimension of the filaments is much smaller than that of the liquid, the profile of liquid-vapor interface may be regarded as a surface of revolution by rotating $z = f(x)$ around the z-axis. From the profile of liquid bridge analysis, the Laplace pressure through the liquid-vapor interface will be obtained and denoted as ΔP_b. Meanwhile, the liquid stays on the surface of the fabric in CB state, which indicates that the air gaps exist in the structure of the fabric. With the assumption that the liquid bridge is in thermodynamic equilibrium, the Laplace pressures through the entire liquid-vapor interface must be the same. Then, it will be found that $\Delta P_a = \Delta P_b$. The Laplace pressure derived from the profile of a liquid bridge is directly related the robust pressure at the moment the wetting behavior of a liquid on a fabric converts from a CB state to a Wenzel state. From Sections *4.1 Capillary profiles and Laplace pressure* and

4.2 Capillary forces of a liquid between smooth surfaces, the robust pressure will be obtained as well as the Laplace pressure. The basic principles for capillary profiles and capillary forces are the same. Theoretically, the Laplace pressure $\Delta P = \gamma_{LV} (1/R_1 + 1/R_2)$ will be obtained from the sag of liquid-vapor interface or the two principal radii in warp R_1 and weft R_2 directions as shown in Figure 64(b), and the robust pressure equals the applied pressure at the moment where the sag touches the bottom of the fabric. However, the two principal radii are difficult to define especially for an extremely small drop (< < 2 μL) sitting on a high density fabric. Therefore, in our experiments, the capillary force method has been selected to calculate the Laplace pressure and robust pressure.

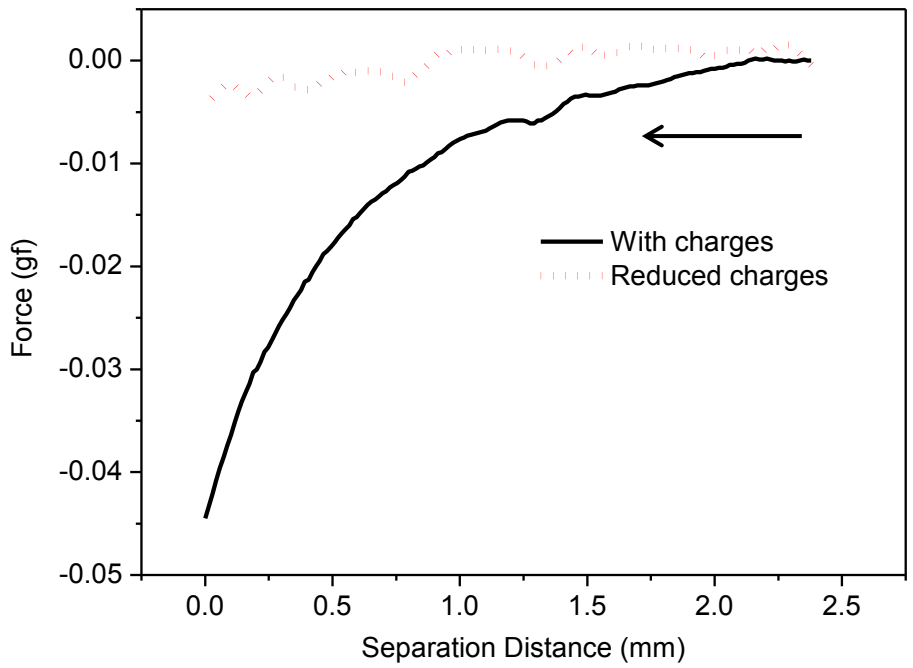

Figure 65. Force-separation distance curves for calibration, where the top substrate is a PTFE film and the bottom substrate is a single layer woven fabric made from monofilaments.

Experiments were conducted with the robustometer, where the PTFE film (top) and single layer of woven fabric (bottom) made of monofilaments acted as the two substrates, and three liquids (water, Kaydol, dodecane) with four different volumes (2, 5, 10, 20 μL) were tested. The robustometer was also calibrated first by comparing the force-separation distance curves obtained before and after the static charges were reduced with the Zerostat Antistatic gun. As shown in Figure 65, when there is no liquid between two substrates, the magnitude of the measured force (solid curve) increases as the separation distance decreases from 2.5 mm to 0 mm. After reducing the charges, It is observed that the force changes in a small range (between -0.004 and 0 gf) after the static charges has been reduced (dash curve), which is negligible for the robust tests of the hydrophobic and oleophobic fabrics. Although different hydrophobic and oleophobic fabrics are tested, their behaviors are similar and the calibration curves are alike, which are not shown for other fabrics. For this single layer woven fabric, the effects of liquid volume and surface tension are reflected in the curves and figures shown below.

Effect of Liquid Volumes

For effects of liquid volume, the results of water, Kaydol, dodecane are compared, while the force-separation distance curves of different liquids with the same volume can be found in Appendix B.

Water with different volumes

Figure 66 shows the curves for water with different volumes where top and bottom substrates are PTFE film and single layer woven fabric made from monofilaments, where the pictures are from compression of the liquid with a volume of 10 μL. The Force-Separation distance curves in Figure 66(a) displays the trend of force when a water drop is compressed as the separation distance gets smaller, to nearly zero. The forces for all four curves with different volumes increase gradually from the formation of the capillary bridge to the maximum compression of the water, and the magnitude of the force for a larger volume is higher than that of a smaller volume with the same separation distance. All forces are positive, which indicates positive forces are exerted by the PTFE film and the liquid is being squeezed on the fabric, due to the hydrophobicity of both PTFE film and fabric. At the minimum separation distance, the contact angle of water on PTFE film increases to 118° where its equilibrium contact angle is 110°, while it is 135° on FS treated fabric where its equilibrium contact angle is 111°. Comparing with the results from *Section 4.4* where the applied force decreases as the volume increases for the same structure, the conclusion for this single layer woven fabric is completely opposite. This is caused by the finite horizontal area of the parallel monofilaments to the liquid. As a drop even with a finite volume is being squeezed, it touches the border of the structure and wets along the monofilament gradually, rather than penetrating into the space between monofilaments. If there are more parallel monofilaments with the same spacing, the applied force would increase for liquids with larger volumes. The fabric has a sufficient area for the liquid to spread onto and experiments showed that the liquid prefers to span this hydrophobic surface.

The applied forces are composed of tension and Laplace forces, and the distributions of them at the minimum separation distance are shown in Figure 66(b). For liquids with different volumes, the tension forces vary slightly, but Laplace forces change dramatically. For liquid with the same volume, it is observed that Laplace force is dominant and the total force has the same trend with the Laplace force. This is partially because tension force is affected by the length of contact line between liquid and the substrates. When the liquid has been compressed to maximum, they vary only over a small range (from 1.5 mm to 3.5 mm) for all liquids. However, the Laplace force largely depends on the contact area between liquid and the substrates and the liquid curvature, which varies over a large range (from 5 to 35 mm^2), as shown in (c). In fact, for the substrates, the Laplace force is larger than tension force as long as the applied force is positive, which indicates the substrates are quite hydrophobic. In the experiments, there are two cases when the two forces are equal: a sessile drop sits on a fabric in equilibrium; the applied force is zero. When the applied force is other than zero, there is an imbalance between Laplace and tension forces, which leads to the deformation of the liquid and the change of Laplace pressure.

Figure 66. Curves for water with different volumes where top and bottom substrates are PTFE film and single layer woven fabric made from monofilaments. (a) Force-Separation distance curves for water with different volumes; (b) Force-Volume curves, including both forces caused by surface tension and Laplace pressure; (c) Radius-Volume and Contact area-Volume curves, where both radius and contact area refer to parameters of the circular contact region between liquid and fabric when the liquid has been compressed to maximum; and (d) Pressure-Volume curves. Pictures are from compression of the liquid with a volume of 10 μL.

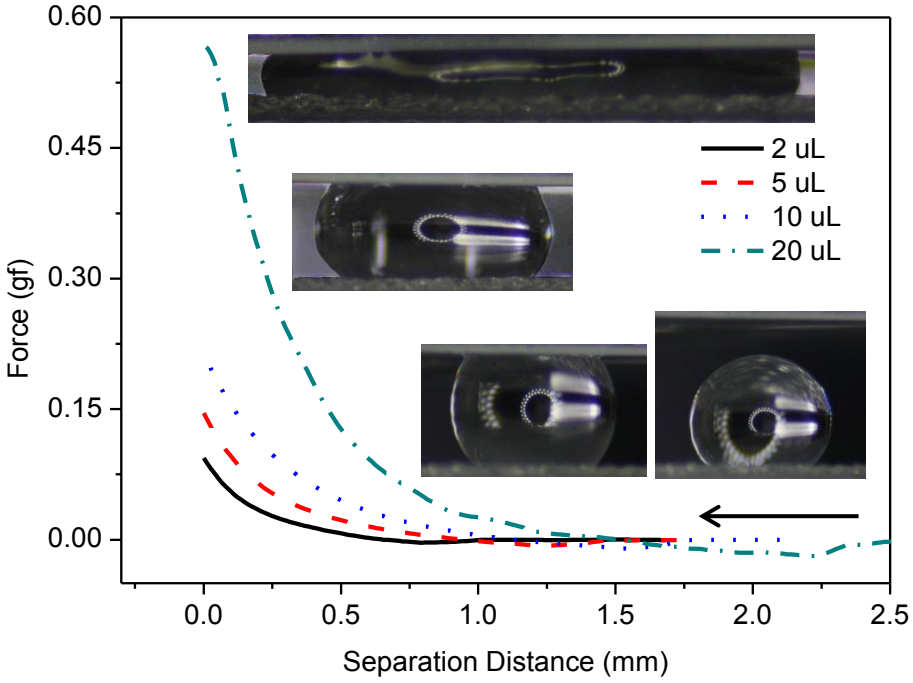
0.60
0.45
0.30
0.15
0.00
Force (gf)
0.0
0.5
1.0
1.5
2.0
2.5
Separation Distance (mm)
2 uL
5 uL
10 uL
20 uL

(a)

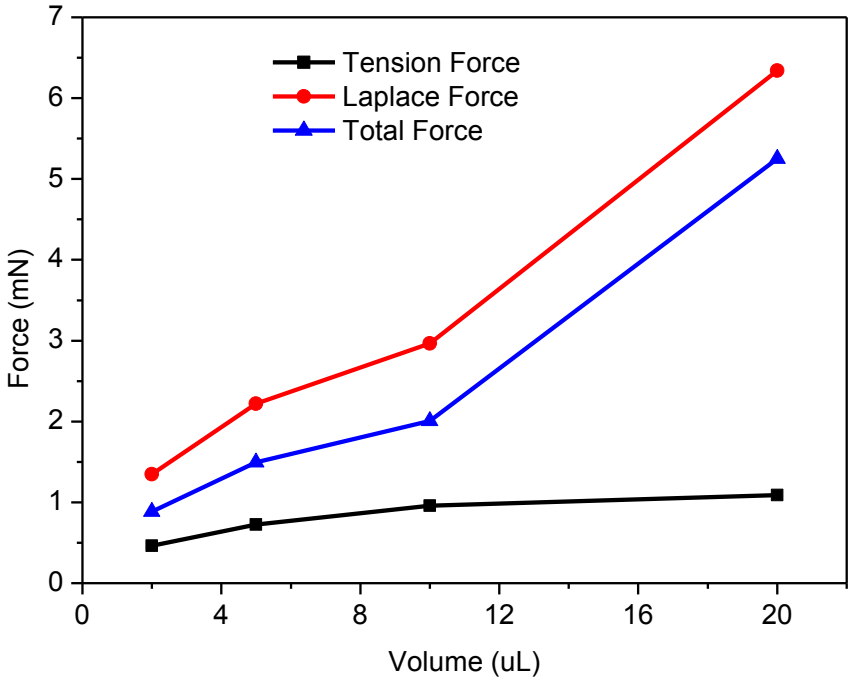
7
6
5
4
3
2
1
0
Force (mN)
0
4
8
12
16
20
Volume (uL)
Tension Force
Laplace Force
Total Force

(b)

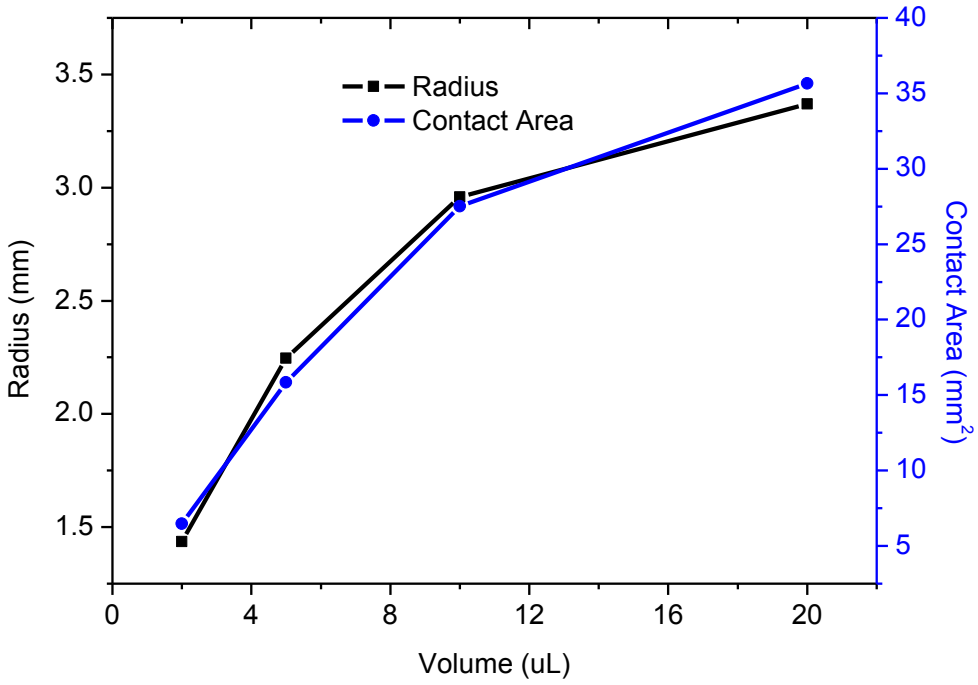
Radius
Contact Area
Radius (mm)
Contact Area (mm²)
Volume (uL)
3.5
3.0
2.5
2.0
1.5
40
35
30
25
20
15
10
5
0
4
8
12
16
20

(c)

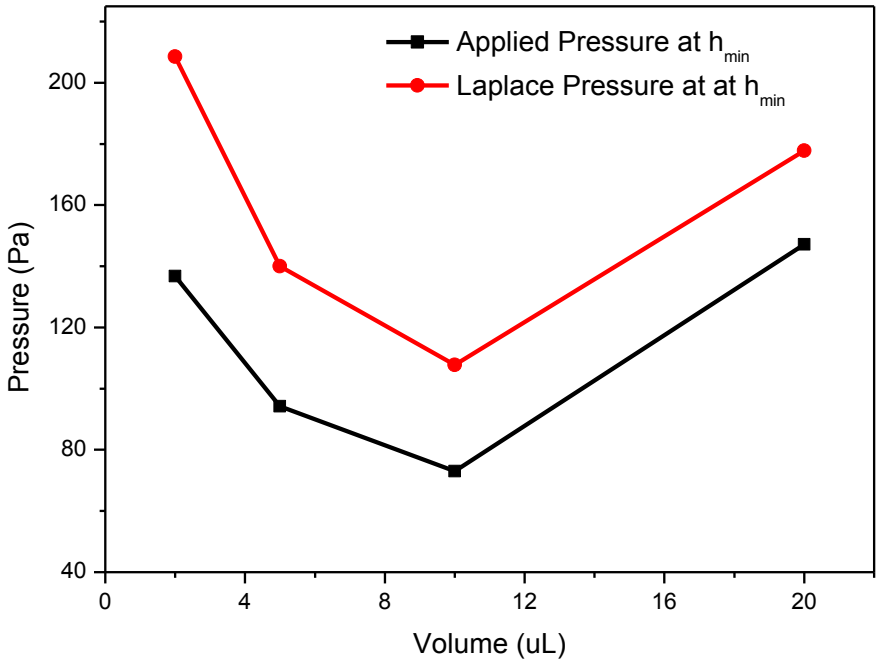
Applied Pressure at h min
Laplace Pressure at at h min
Pressure (Pa)
Volume (uL)
200
160
120
80
40
0
4
8
12
16
20

(d)

Figure 66(d), the relationship between pressures at h_{min} and volumes are displayed. The applied pressure refers to the force applied by the PTFE film divided by the contact area between liquid and fabric at the minimum separation distance or height (h_{min}), and the Laplace pressure refers to the pressure difference between the liquid and the air when the liquid has been compressed to maximum at h_{min}. The applied pressure at h_{min} is related to the applied force and contact area; liquids with larger volumes need higher forces to compress and larger contact areas form between liquids and substrates. Thus the change trend of the applied pressures at h_{min} is not necessarily the same as that of force or contact area, and to the best of our knowledge, only the capillary force rather than the applied pressure at h_{min} has been reported. From the curve, the applied pressure decreases as the volume increases from 2 to 10 μL, but increases as the volume reaches 20 μL, which shares the same trend with the Laplace pressure at h_{min}. The Laplace pressure at h_{min} is obtained from the capillary force expressions and related to the applied pressure with a difference of ($2\gamma_{LV}sin\varphi/R_D$). Therefore, the differences decrease as the radius of contact area increases since there is no significant change for the contact angle as shown in Figure 66(a).

Table 8. Comparisons of separation distances or heights, contact areas, pressures due to gravity, the Laplace pressures and the applied pressures of liquid bridges with different water volumes at h_{min} for woven fabric made of monofilaments.

Volume (μL)	2	5	10	20
Height (mm)	0.31±0.07	0.32±0.04	0.36±0.04	0.56±0.10
Contact Area (mm^2)	6.47±1.22	15.85±1.60	27.51±3.63	35.67±5.21
Pressure due to gravity (Pa)	3.04±0.69	3.14±0.69	3.53±0.39	5.49±0.98
Laplace Pressure (Pa)	208±29	140±28	108±21	178±11
Applied Pressure (Pa)	137±25	94±26	73±17	147±10

Table 8 shows the comparison of parameters as well as the variance for water with different volumes, including both the measured (height or separation distance, and contact area) and the calculated (pressure due to gravity, the Laplace pressure and applied pressure at h_{min}) ones. All the liquids have been compressed to similar heights or separation distance. If the separation distance is zero, the contact angles and contact radius of liquids on both substrates cannot be obtained. Thus, in our experiments, the liquid has been compressed to 20-25% of its original height and it has been set as zero for comparison. In the table, there is a slight increase of the height as the volume gets larger, which is due to the increase of the heights when the liquid is a sessile drop since the apparent contact angles are the same. As mentioned in the figure, the contact area between PTFE film and the fabric at the minimum height increases when the volume gets larger, and the variance is also shown in the table. Pressure due to gravity at h_{min} refers to the pressure caused by gravity when the height is smallest. When the heights for all liquids are very close, the pressure due to gravity vary in a

small range. Compared with the initial Laplace pressure (the Laplace pressure of the liquid when it is a sessile drop on the fabric), the Laplace pressure at h_{min} increases when the applied force is positive and decreases when the applied force is negative. When gravity is considered, the Laplace pressure increases gradually from the liquid in contact with PTFE film to the fabric. Meanwhile, the real robust pressure will be the combination of the pressure due to gravity and the applied pressure which is the minimum pressure to push the liquid through a fabric. In this table, the applied pressure could not force the liquid to go through the hydrophobic fabric, and thus the robust pressure is more than the sum of applied pressure and the pressure due to gravity at h_{min}. Especially, the sum of the two pressures is far less than the hydrostatic pressure (791 Pa), which makes penetration impossible.

During the experiments, as water was being compressed between substrates, it cannot penetrate through but spans between the PTFE film and the fabric, even though the thickness of the fabric is small (0.16 mm) and the spaces between the monofilaments are relatively large (between 96.57 and 225.60 μm). This indicates that the fabric is sufficiently hydrophobic to resist small water drops from penetrating into the structure even under a considerable external pressure.

Kaydol with different volumes

When the liquid changes into Kaydol, Figure 67 shows the curves for Kaydol with different volumes where top and bottom substrates are PTFE film and single layer woven fabric made from monofilaments. Similarly, Figure 67(a) displays the Force-Separation distance curves,

but the maximum applied force changes from negative (2 and 5 μL) to positive (10 and 20 μL) as the volume increases. For the curves of 2 and 5 μL liquids, the measured forces become more negative as the separation distance decreases. This implies that the liquid prefers to wet the surfaces, especially on PTFE film since it is oleophilic where the equilibrium contact angle is less than 90°. The liquid bonds the two substrates together as it is being compressed. For the curves of 10 and 20 μL liquids, there is a transition between negative and positive forces. De Souza et al[34,64] pointed out that the Laplace force is dominant when the separation distance is nearly zero, and the capillary force is attractive (repulsive) when the sum of the advancing or receding contact angles of liquids on both substrates is less (more) than 180°. However, in Figure 67(b), when the separation distance is at the maximum for all liquids, tension force plays an important role as well as the Laplace force and both are dominant terms. For all the liquids, the advancing contact angles on fabrics and PTFE films are 115°/50°for 2 μL, 130°/52° for 5 μL, 130°/57° for 10 μL, and 135°/65° for 20 μL, respectively. The capillary force for 5 μL Kaydol is negative even though the sum of contact angels are more than 180°, which is in conflict with the conclusion from De Souza et al. To further study this, the contact angles of water between PTFE film and FS treated single layer woven fabric were measured at the formation of the liquid bridge, which were 121° on fabric and 114° on PTFE film. The capillary force at this moment is less than zero and the liquid is in equilibrium. Thus, De Souza et al's conclusion cannot be applied to this study. However, from experiments, at least one of the advancing or receding contact angles should be larger (smaller) than its equilibrium contact angle on the substrate, which might lead to a positive (negative) capillary force. When both are larger than their equilibrium contact angles, the

force could be negative. When both are smaller than their equilibrium contact angles, the force must be negative. Meanwhile, the shapes of the liquid could be bi-concave or bi-convex, which is indirectly related to the capillary forces. The sign of the capillary force should be determined by Laplace pressure or the curvature of the liquids. If the Laplace pressure is positive and larger than the tension term ($2\gamma_{LV}sin\varphi/R_D$), the force will be repulsive (positive sign); if the Laplace pressure is smaller than the tension term ($2\gamma_{LV}sin\varphi/R_D$) or it is negative, the force will be attractive (negative sign). From Figure 67 and Table 9 , the Laplace pressure for 2 μL Kaydol is negative (-3.75 Pa); the Laplace pressure for 5 μL Kaydol is 11.9 Pa, but smaller than the tension term 21.6 Pa; the Laplace pressure for 10 μL Kaydol is 27.3 Pa, and larger than the tension term 16.6 Pa; the Laplace pressure for 20 μL Kaydol is 31.4 Pa, and larger than the tension term 13.9 Pa. Therefore, both signs and magnitudes of the capillary force vary as the volume changes. For a certain volume between 5 and 10 μL, at the same separation distance, the capillary force could just be zero where the Laplace pressure equals to ($2\gamma_{LV}sin\varphi/R_D$) and the Laplace force is balanced by the tension force. Beyond that volume, the Laplace force becomes larger than the tension force, and the capillary force changes to positive at the same separation distance.

Figure 67. Curves for Kaydol with different volumes where top and bottom substrates are PTFE film and single layer woven fabric made from monofilaments. (a) Force-Separation distance curves for Kaydol with different volumes; (b) Force-Volume curves, including both forces caused by surface tension and Laplace pressure; (c) Radius-Volume and Contact area-Volume curves, where both radius and contact area refer to parameters of the circular contact region between liquid and fabric when the liquid has been compressed to maximum; and (d) Pressure-Volume curves. Pictures are from compression of the liquid with a volume of 10 μL.

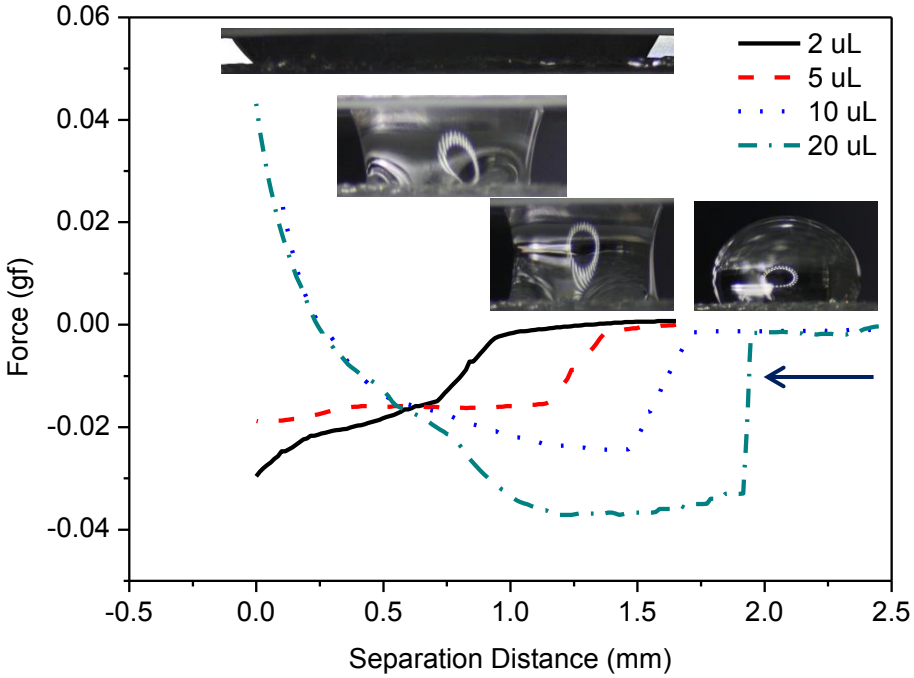
0.06
0.04
0.02
0.00
-0.02
-0.04
Force (gf)
-0.5
0.0
0.5
1.0
1.5
2.0
2.5
Separation Distance (mm)
2 uL
5 uL
10 uL
20 uL

(a)

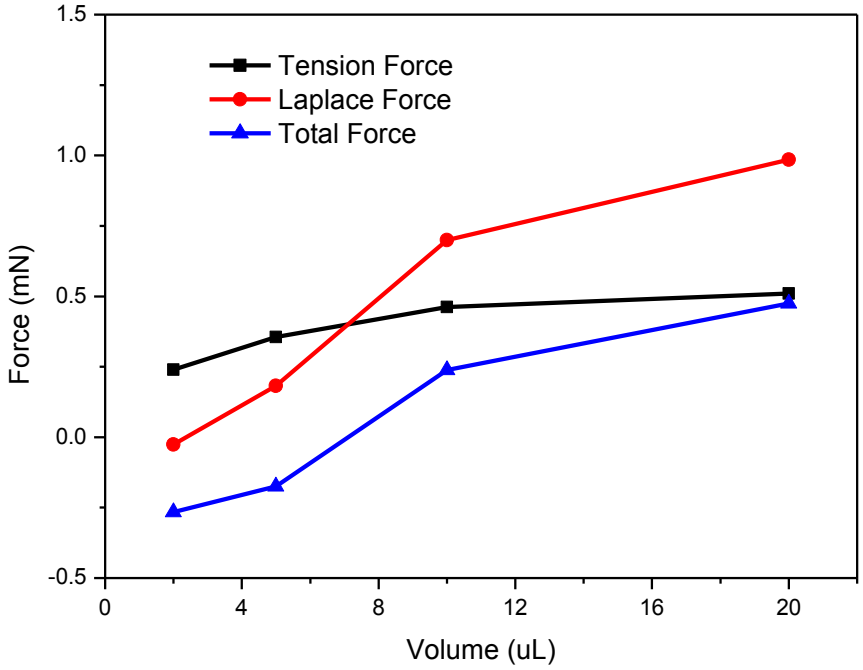
1.5
1.0
0.5
0.0
-0.5
Force (mN)
0
4
8
12
16
20
Volume (uL)
Tension Force
Laplace Force
Total Force

(b)

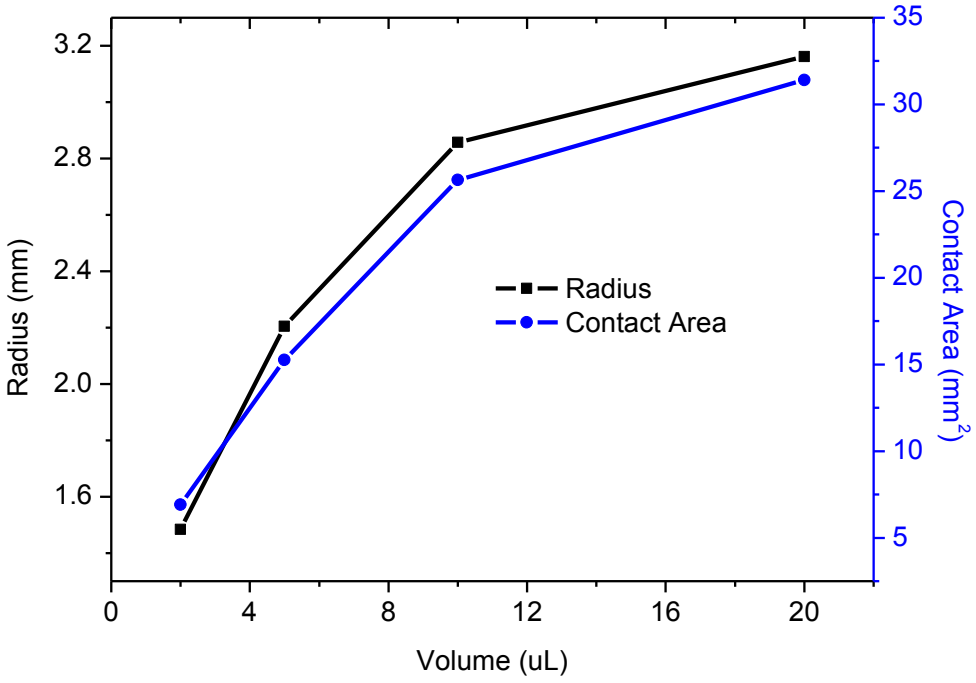
Radius (mm)
Contact Area (mm²)
Volume (uL)
Radius
Contact Area
3.2
2.8
2.4
2.0
1.6
35
30
25
20
15
10
5
0
4
8
12
16
20

(c)

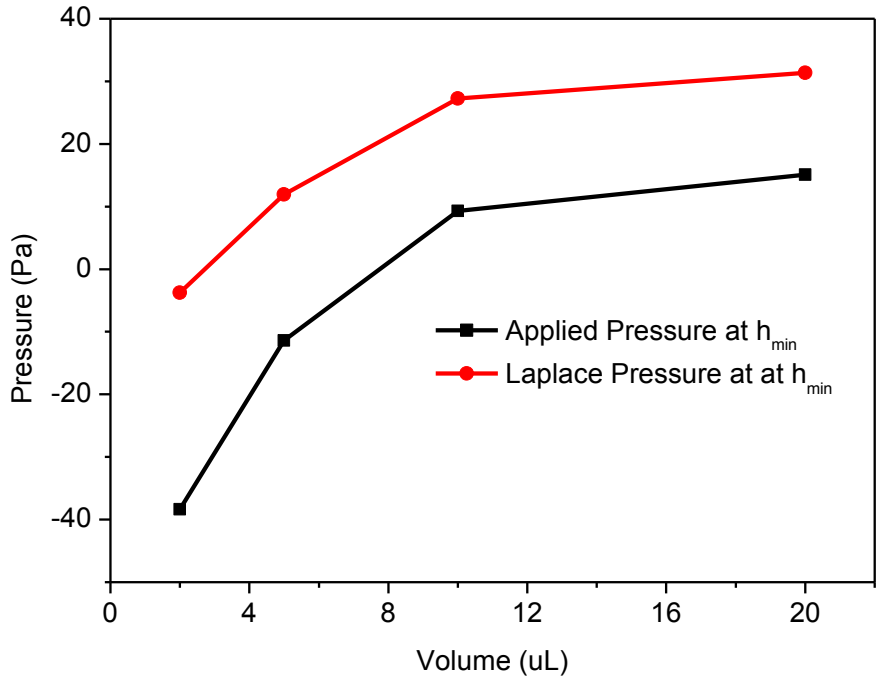
Pressure (Pa)
Volume (uL)
Applied Pressure at h min
Laplace Pressure at at h min
40
20
0
-20
-40
0
4
8
12
16
20

(d)

In Figure 67(b), when the separation distance is the smallest between substrates, the tension forces for 2 and 5 μL liquids are larger than the Laplace forces, which yield negative (attractive) total forces; the tension forces for 10 and 20 μL liquids are smaller than the Laplace forces, which yield positive (repulsive) total forces. In Figure 67(c), the radius and contact area increase as the liquid volume is getting larger at the smallest separation distance. During the push process, as the liquid spreads gradually, the contact angle on fabric decreases first and then increases slowly due to the stretch and compression of the liquid bridge by PTFE film, which can be observed from Figure 67(a) and the Appendix B**.** The change of contact angles is achieved by condensing the liquid bridge, where the waist of the liquid bridge first moves towards the fabric substrate (less than equilibrium contact angle) and then disappeared beyond the fabric (more than equilibrium contact angle). Meanwhile, the shape of the liquid bridge changes from concave to convex caused by the external force. For all liquids with different volumes, the total capillary force shares the same trend with the Laplace force since the tension forces vary in a small range. In addition, none of the Kaydol liquids penetrate through the fabric during the test. From Table 9, all the applied pressures are less than the oleostatic pressure (133 Pa) even when the pressure due to gravity is considered. It shows this FS treated single layer woven fabric is robust for Kaydol.

Table 9. Comparisons of separation distances or heights, contact areas, pressures due to gravity, the Laplace pressures and the applied pressures of liquid bridges with different Kaydol volumes at h_{min} for woven fabric made of monofilaments.

Volume (μL)	2	5	10	20
Height (mm)	0.29±0.02	0.33±0.04	0.39±0.04	0.57±0.06
Contact Area (mm^2)	6.92±0.54	15.26±1.73	25.65±2.79	31.40±2.95
Pressure due to gravity (Pa)	2.42±0.17	2.75±0.33	3.25±0.33	4.75±0.50
Laplace Pressure (Pa)	-3.8±3.3	11.9±3.1	27.3±3.8	31.4±5.0
Applied Pressure (Pa)	-38.4±3.2	-11.4±2.3	9.3±2.2	15.1±0.7

Dodecane with different volumes

When dodecane is compressed between the same pair of substrates, the wetting behavior is quite different from that of water or Kaydol. Figure 68 shows the curves for dodecane with different volumes where top and bottom substrates are PTFE film and single layer woven fabric made from monofilaments. All of the applied forces are negative, which implies the Laplace force is less than the tension force in all of them as the liquids are being compressed ($\Delta P < 2\gamma_{LV} sin\varphi / R_D$). Comparing the curve for 2 μL with other three curves, the force just decreases directly as the separation distance gets smaller. However, the forces for the other three curves decrease gradually from the formation of the capillary bridge, increase for a short period, and decrease again. This is caused by a combination of the change of advancing contact angles on the fabric and the liquid internal pressure as well as the liquid-substrate contact area. As the separation distance gets smaller, the waist of the liquid bridge in a concave shape moves downwards, and the magnitude of the total force reaches maximum as the

waist disappeared at the fabric surface where the contact angle of the liquid is around 90° and the tension force is almost vertical. Then, the shape of the liquid bridge changes from concave to convex and the capillary force becomes less negative.

Figure 68. Curves for dodecane with different volumes where top and bottom substrates are PTFE film and single layer woven fabric made from monofilaments. (a) Force-Separation distance curves for dodecane with different volumes; (b) Force-Volume curves, including both forces caused by surface tension and Laplace pressure; (c) Radius-Volume and Contact area-Volume curves, where both radius and contact area refer to parameters of the circular contact region between liquid and fabric when the liquid has been compressed to maximum; and (d) Pressure-Volume curves. Pictures are from compression of the liquid with a volume of 10 μL.

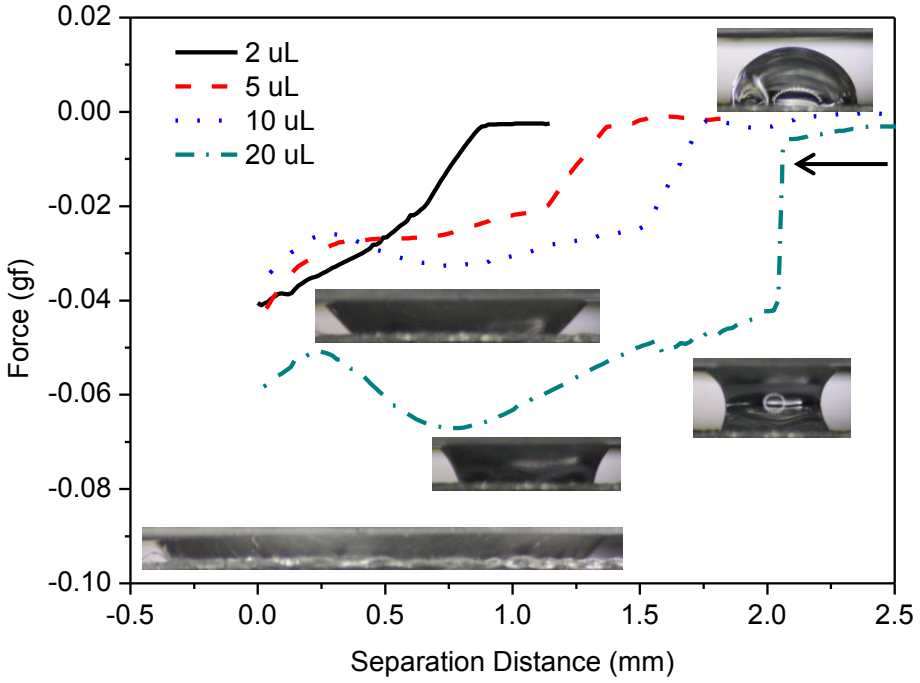
2 uL
5 uL
10 uL
20 uL
Force (gf)
Separation Distance (mm)
0.02
0.00
-0.02
-0.04
-0.06
-0.08
-0.10
-0.5
0.0
0.5
1.0
1.5
2.0
2.5

(a)

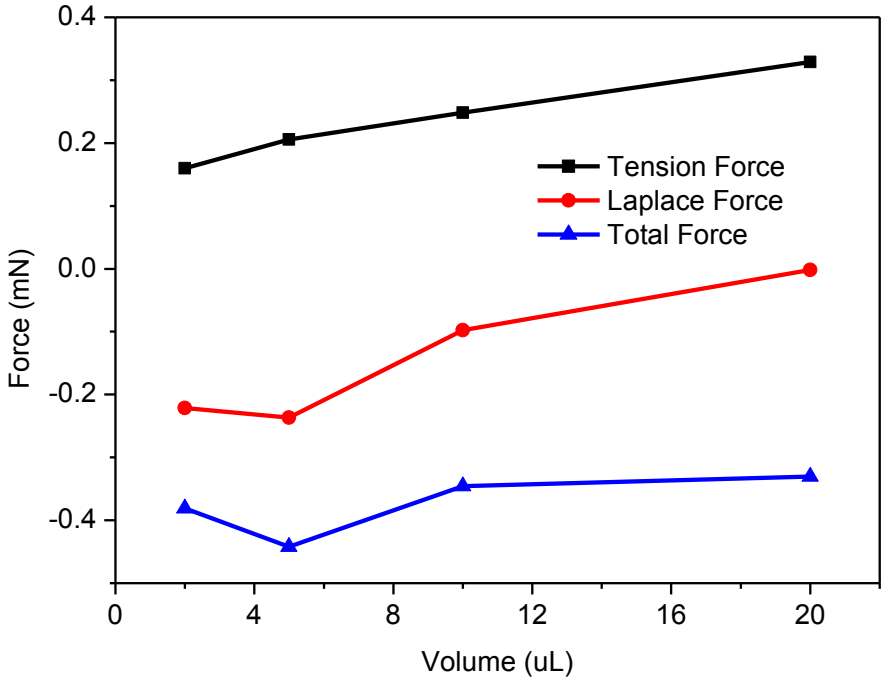
Tension Force
Laplace Force
Total Force
Force (mN)
Volume (uL)
0.4
0.2
0.0
-0.2
-0.4
0
4
8
12
16
20

(b)

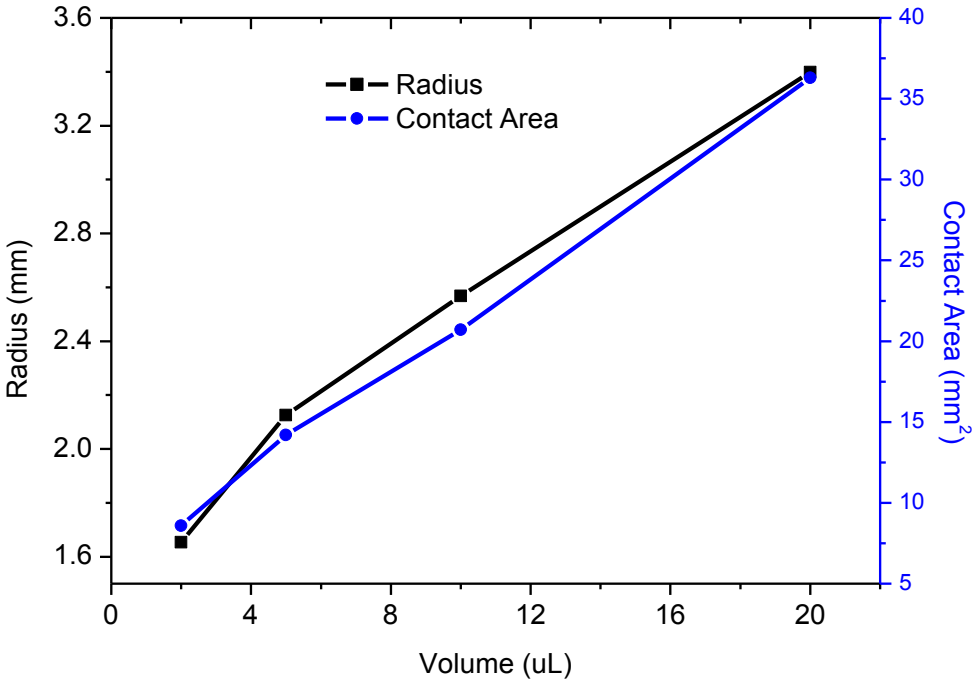
Radius
Contact Area
Radius (mm)
Contact Area (mm^2)
Volume (uL)
3.6
3.2
2.8
2.4
2.0
1.6
40
35
30
25
20
15
10
5
0
4
8
12
16
20

(c)

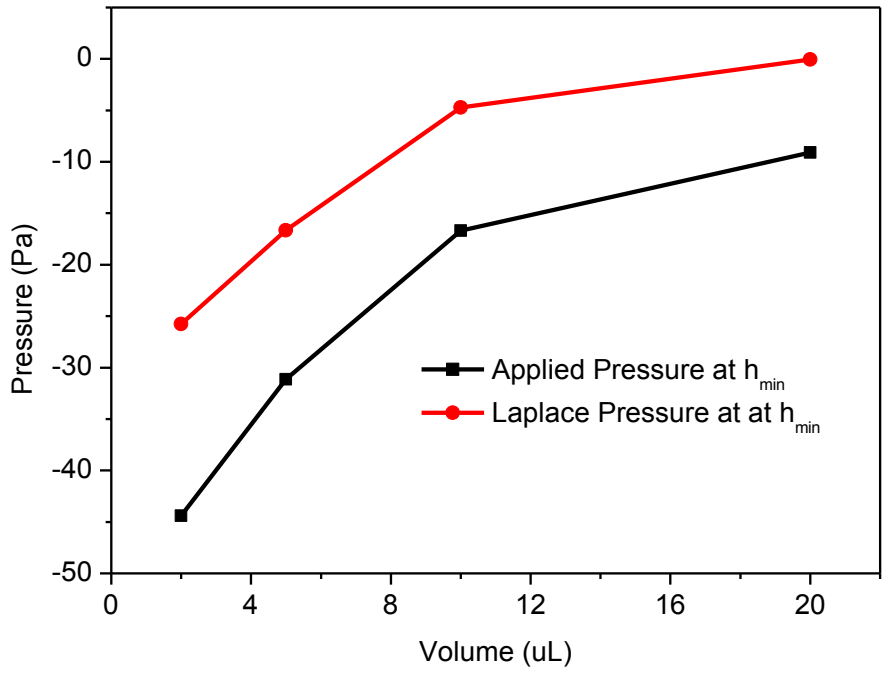
Applied Pressure at h$_{min}$
Laplace Pressure at at h$_{min}$
Pressure (Pa)
Volume (uL)
0
-10
-20
-30
-40
-50
0
4
8
12
16
20

(d)

The further decrease of the force could be due to the slight penetration of the liquid when it is metastable. This has been proved by compressing a 20 μL dodecane drop with a PTFE film attached on a glass slide (5.03 gf). The contact area of dodecane with PTFE film increases from 37.4 mm^2 when it is a sessile drop, to 80.4 mm^2 when the liquid is being squeezed under the gravity force of the glass slide with the PTFE film. The fabric was not completely wet until 5 seconds later when the contact area reached 80.4 mm^2. Thus the decrease of the capillary force could be due to the partial penetration of the dodecane, but it is not deep enough to go through the fabric. Figure 68 also shows the Force-Volume, Radius-Volume, Contact area-Volume and Pressure-Volume curves for dodecane with different volumes. For all the liquids, Laplace and total forces have the same trend in Figure 68(b). The radii and contact areas of liquid-fabric circular contact region at the smallest separation distance in Figure 68(c) increase as volumes increase. In Figure 68(d), at the minimum separation distance, the magnitude of the applied pressure decreases for larger drops; Laplace pressure changes in the same way, and all are less than the initial Laplace pressure since attraction force is applied to the drop. Since all the forces and pressures are negative, the robustness of the fabric cannot be evaluated. However, by pressing a PTFE film with a glass slide on a 20 μL dodecane drop sitting on a fabric, the drop first spread on and then penetrated though the fabric under the weight of the glass slide. This implies that this single layer woven fabric is less robust for the low-surface tension dodecane than for Kaydol and water.

Effect of Surface Tensions of Liquids

The comparisons of effects of surface tensions can be found from the previous section or Appendix B. The apparent contact angles for water, Kaydol and dodecane when in a shape of spherical cap on this fabric are 130°, 110° and 92°, respectively. As PTFE films were used to compress the liquids with the same volume but different surface tensions to the minimum separation distance, the capillary forces decrease, while the contact areas increase, when the surface tension decreases. Then, the applied pressures decrease from positive for water to negative for dodecane. The largest measured applied pressures are 147 Pa for water and 15.1 for Kaydol, which are both much less than the hydrostatic and oleostatic pressures and it is reasonable that they are not able to go through the fabric when being compressed. However, for dodecane, a negative pressure was exerted on the drop and an attractive force forms between the fabric and PTFE substrates. If an external pressure keeps on pressing on the drop, the force will be negative in a period. It changes to positive only when both fabric and liquid are compressed together. During the experiments, a 20 μL dodecane drop penetrated through this fabric when under the weight of a glass slide attached on a PTFE film, where the applied pressure is 23.8 Pa. If the same method was used to push water with a volume of 20 μL, the applied pressure could reach 3000 Pa by adding more force, but liquids still mainly spread on fabrics. For Kaydol with the same volume, it penetrates through the fabric when the applied pressure reaches 156 Pa. Therefore, the robust pressure decreases as the surface tension decreases, which agrees with the conclusion from robustness of parallel monofilaments as well as the results from hydrostatic tests. When the separation distance between two substrates is negative, it is out of the scope of our research.

4.6 Robustness of multiple layers of woven fabrics with monofilaments

From the traditional view, the robust pressure for a fabric with multiple layers would be assumed to be the sum of all the robust pressures for each single layer, which could not be true since the liquid wets the fabric layer by layer if the interactions between layers are ignored. From the study of the droplet behavior and robust analysis, if the robust pressures vary for different layers, the robustness of the fabric will be the robustness of the layer with the maximum robust pressure when the volume of the liquid is sufficient. If the robust pressures for each layer are the same, when the applied pressure reaches or exceeds the robust pressure of the first layer on the surface, the liquid will wet through the first layer and reach the next layer. When the liquid volume is sufficient, it will wet through the whole fabric, and the robust pressure of the fabric equals to the robust pressure of a single layer. When the liquid has a limited volume (no more than 20 μL), it will just wet the fabric layer by layer until the liquid volume is insufficient to reach the next layer. In this case, the robust pressure will be larger for thicker fabrics, and the liquid could never go through a fabric, when the fabric is too thick or the volume is too small or the fabric is too hydrophobic or oleophobic.

In addition, there are interactions between different layers, and it is possible that before the applied pressure reaches the robust pressure of a single layer, it could contact fibers from the following layer. This implies that the robust pressure of the fabric with multiple layers will be strongly affected by the arrangement of these single layers. The total robust pressure for the fabric will always be higher than or equal to the robust pressure of the single layer with

the minimum pressure, and lower than or equal to the robust pressure of the single layer with the maximum pressure, if the volume of the liquid is sufficient.

For this woven fabric, all three liquids cannot penetrate through it as a PTFE film is applied to squeeze the liquid to an extremely small separation distance. However, when all liquids with a volume of 20 μL were squeezed under the gravity of a glass slide with a PTFE film, only dodecane drop wets the fabric completely when the pressure is 25.5 Pa, which indicates that this fabric is less robust for this liquid and it is not necessary to test the other two liquids for the fabric made of multiple layers. Due to the high robustness of the FS treated fabrics, only two layers of the woven fabric was tested in the experiments. Experiments showed that, as the same pressure 25.5 Pa was exerted on the dodecane drop with a volume of 20 μL, the drop wets the first layer and stops on the second layer. This could be caused by the limited volume of the liquid or the oleophobicity of the fabric, which indicates that larger pressure is needed in order to force the liquid through the fabric. Therefore, the robust pressure increases as the thickness of the fabric increases, which cannot be measured due to the high robustness of the fabric.

4.7 Robustness of woven fabric with multifilament yarns

In this section, both the effects of liquid volume and surface tension have been discussed for the robustness of the woven fabric made of multifilament yarns.

Effects of Liquid Volume

Water

Figure 69(a) shows the Force-Separation distance curves for water with different volumes. As the separation distance decreases from the formation of the liquid bridge, all forces increase gradually from zero and reach their maximum as the separation distances decrease to their minimum. Comparing all four curves, the maximum force for each liquid increases as the volume gets larger. All the liquids are in a convex shape, which implies that all Laplace force haves a positive sign at the minimum separation distance as shown in Figure 69(b). The total force exhibit the same trend with the Laplace force since it is dominant compared with the tension force.

Figure 69. Curves for water with different volumes where top and bottom substrates are PTFE film and woven fabric made from multifilament yarns. (a) Force-Separation distance curves for water with different volumes; (b) Force-Volume curves, including both forces caused by surface tension and Laplace pressure; (c) Radius-Volume and Contact area-Volume curves, where both radius and contact area refer to parameters of the circular contact region between liquid and fabric when the liquid has been compressed to maximum; and (d) Pressure-Volume curves. Pictures are from compression of the liquid with a volume of 10 μL.

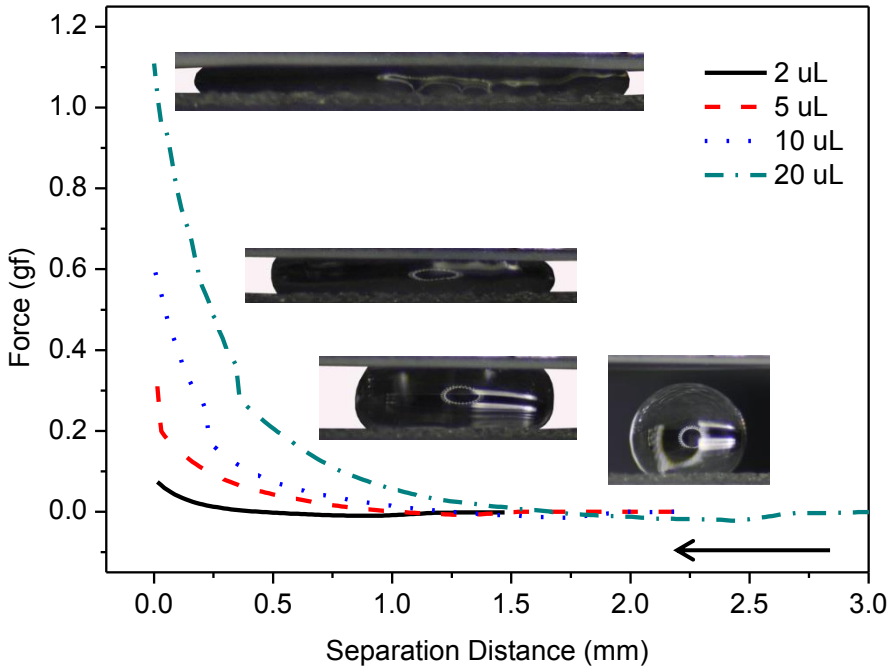
2 uL
5 uL
10 uL
20 uL
Force (gf)
Separation Distance (mm)
1.2
1.0
0.8
0.6
0.4
0.2
0.0
0.0
0.5
1.0
1.5
2.0
2.5
3.0

(a)

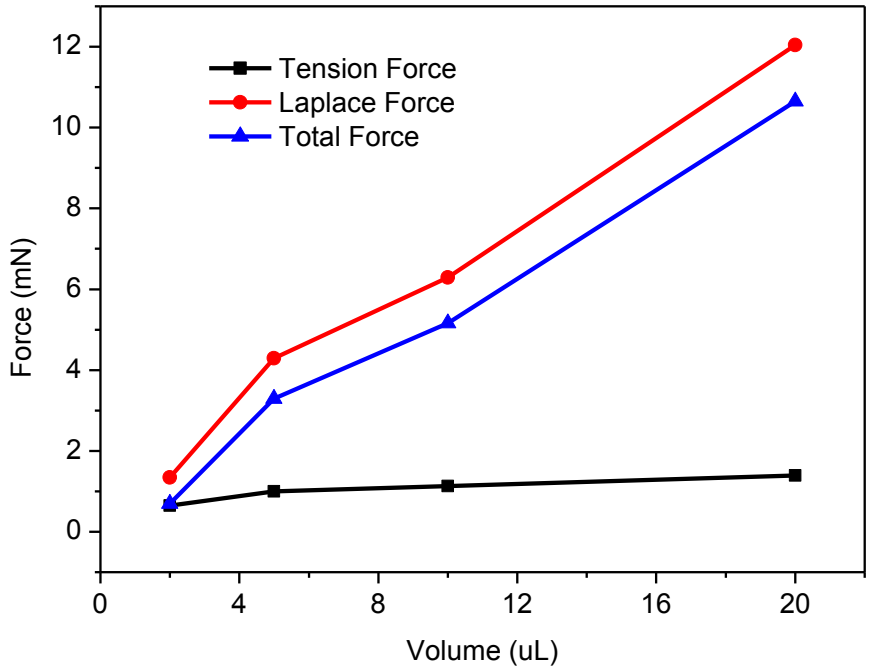
Tension Force
Laplace Force
Total Force
Force (mN)
Volume (uL)
12
10
8
6
4
2
0
0
4
8
12
16
20

(b)

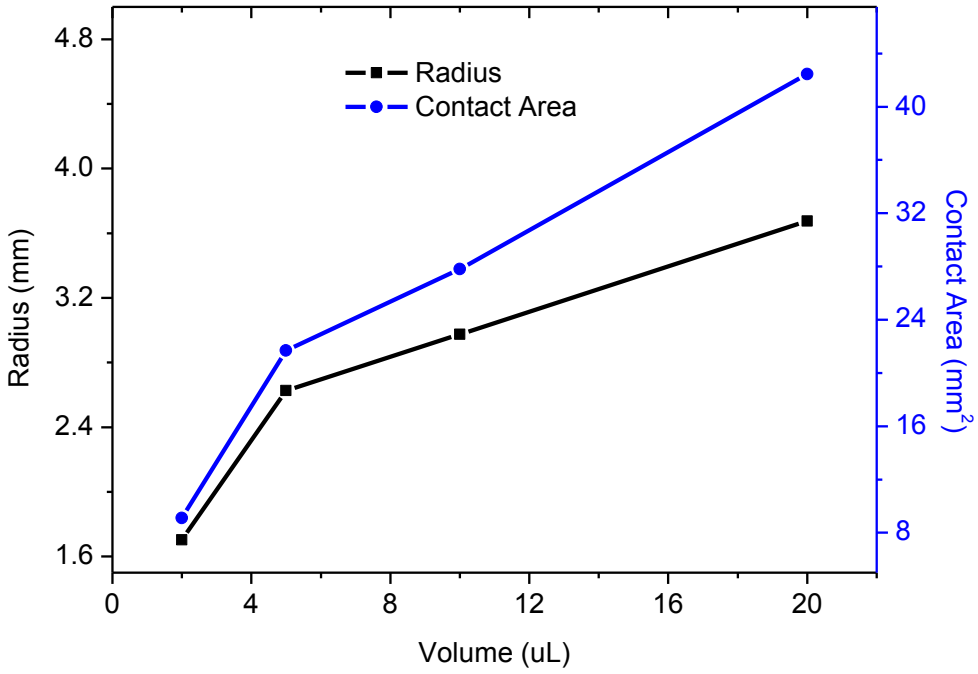
Radius
Contact Area
Radius (mm)
Contact Area (mm²)
Volume (uL)
4.8
4.0
3.2
2.4
1.6
40
32
24
16
8
0
4
8
12
16
20

(c)

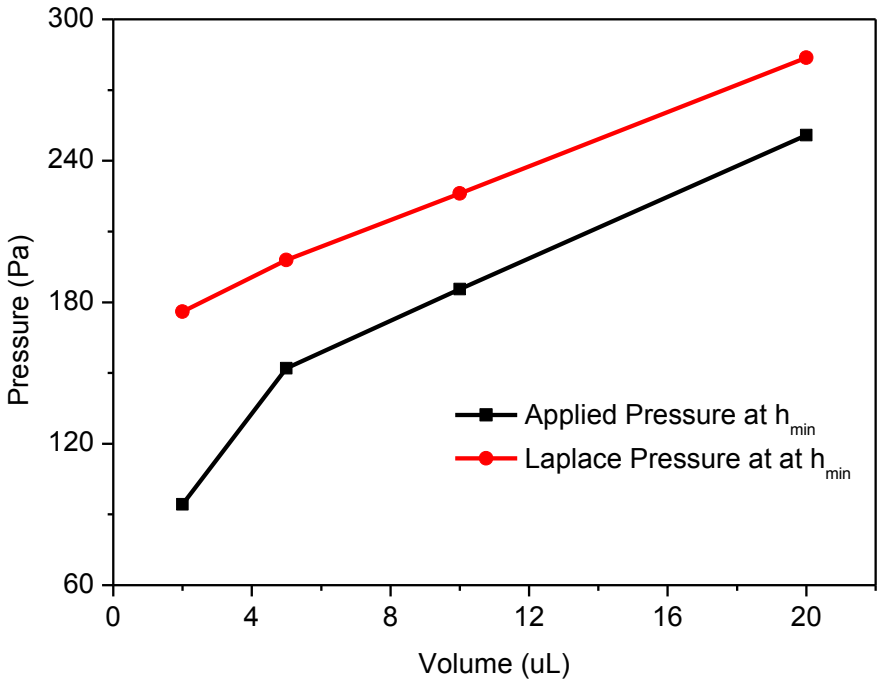
Applied Pressure at h min
Laplace Pressure at at h min
Pressure (Pa)
Volume (uL)
300
240
180
120
60
0
4
8
12
16
20

(d)

Table 10. Comparisons of separation distances or heights, contact areas, pressures due to gravity, the Laplace pressures and the applied pressures of liquid bridges at h_{min} with different water volumes for woven fabric with multifilament yarns.

Volume (μL)	2	5	10	20
Height (mm)	0.23±0.02	0.38±0.04	0.31±0.06	0.37±0.11
Contact Area (mm^2)	9.10±0.60	21.68±1.18	27.81±4.85	42.44±2.83
Pressure due to gravity (Pa)	2.25±0.20	3.72±0.39	3.04±0.59	3.63±1.08
Laplace Pressure (Pa)	176±6	200±23	226±38	284±11
Applied Pressure (Pa)	94±3	152±21	186±35	251±10

Figure 69(c) shows the Radius-Volume and Contact area-Volume curves, where both radius and contact area refer to parameters of the circular contact region between liquid and fabric when the liquid has been compressed to maximum. Both the radius and contact area are proportional to the liquid volume. From Figure 69(d) and Table 10, the Laplace pressure and applied pressure increase with a positive value as the volume of a liquid gets larger due to the application of the increasing positive force. Meanwhile the difference between the two pressures decreases, which is caused by the change of radius of the contact area between liquid and a substrate at the smallest separation distance. However, none of the liquids penetrates through the fabric, and even as the liquid has been compressed significantly, it only stays and spans on the fabric surface rather than penetrating into the structure. Therefore, this fabric is extremely robust hydrophobic for water.

Kaydol

Figure 70 shows the different curves obtained for Kaydol. As the volume increases, the force becomes more negative at the formation of the liquid bridge, while it becomes more positive at the maximum separation distance. This is all due to the change of shape of the liquids. There is a balance between the tension force and Laplace force. For the 2 μL and 5 μL Kaydol drops as they are being squeezed, the curvature of the liquid-vapor interface remains in a concave shape, which results in a Laplace force smaller than the tension force. For the 10 μL and 20 μL Kaydol drops as they are being squeezed, the curvature changes into a convex shape as the advancing contact angle increases on the fabric, which results in a Laplace force larger than the tension force. In addition, as the liquid volume increases at the minimum height between substrates, the contact radius and area increase. The applied pressure and Laplace pressure have the same trend, even when the pressure due to gravity has been included from Table 11. Although the surface tension of Kaydol is smaller than that of the water, on this fabric, Kaydol only spans between substrates and did not penetrate through the fabric. Thus, the fabric is robust for Kaydol.

Figure 70. Curves for Kaydol with different volumes where top and bottom substrates are PTFE film and woven fabric made from multifilament yarns. (a) Force-Separation distance curves for Kaydol with different volumes; (b) Force-Volume curves, including both forces caused by surface tension and Laplace pressure; (c) Radius-Volume and Contact area-Volume curves, where both radius and contact area refer to parameters of the circular contact region between liquid and fabric when the liquid has been compressed to maximum; and (d) Pressure-Volume curves. Pictures are from compression of the liquid with a volume of 10 μL.

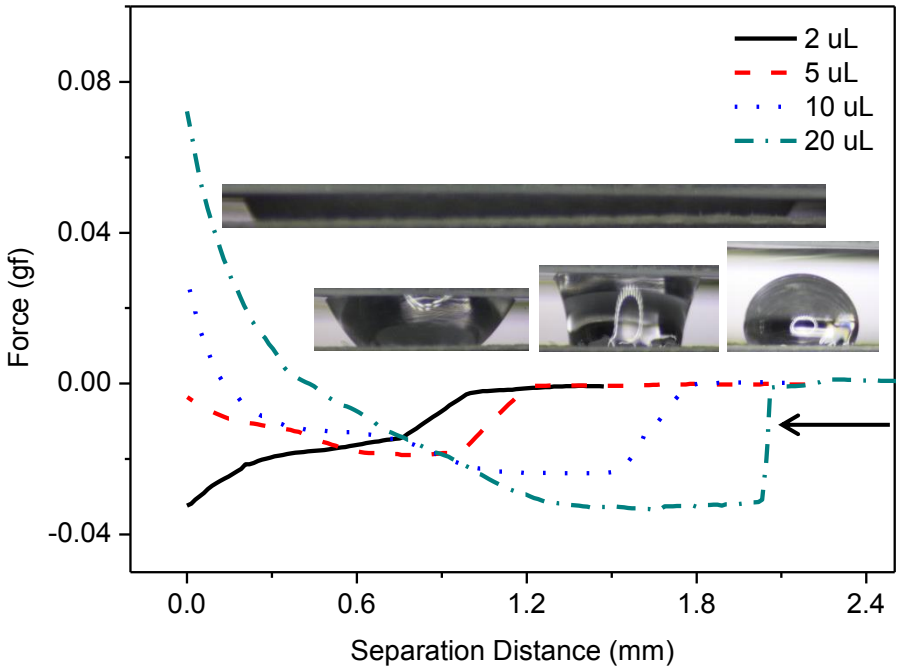
2 uL
5 uL
10 uL
20 uL
0.08
0.04
0.00
-0.04
Force (gf)
0.0
0.6
1.2
1.8
2.4
Separation Distance (mm)

(a)

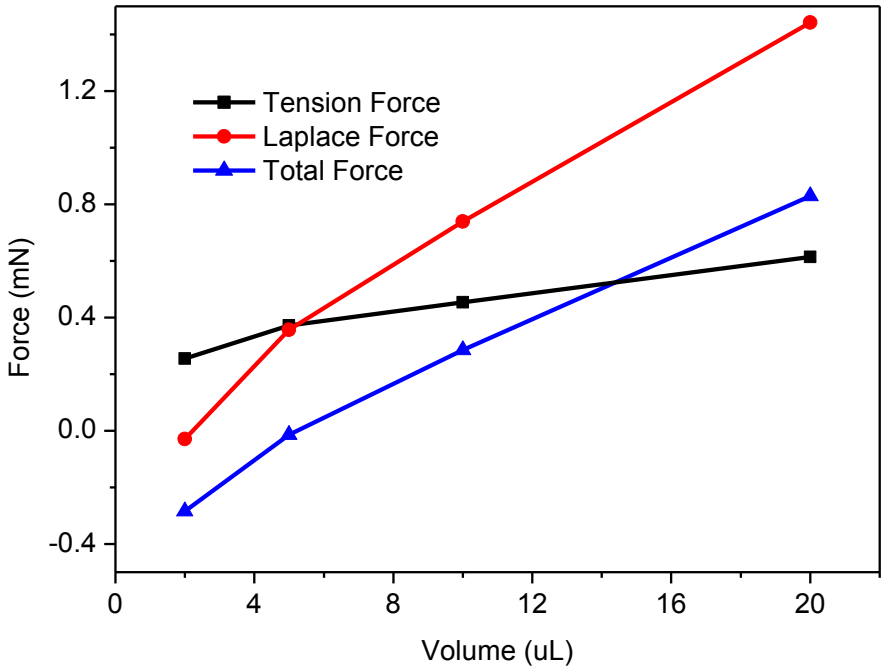
Tension Force
Laplace Force
Total Force
1.2
0.8
0.4
0.0
-0.4
Force (mN)
0
4
8
12
16
20
Volume (uL)

(b)

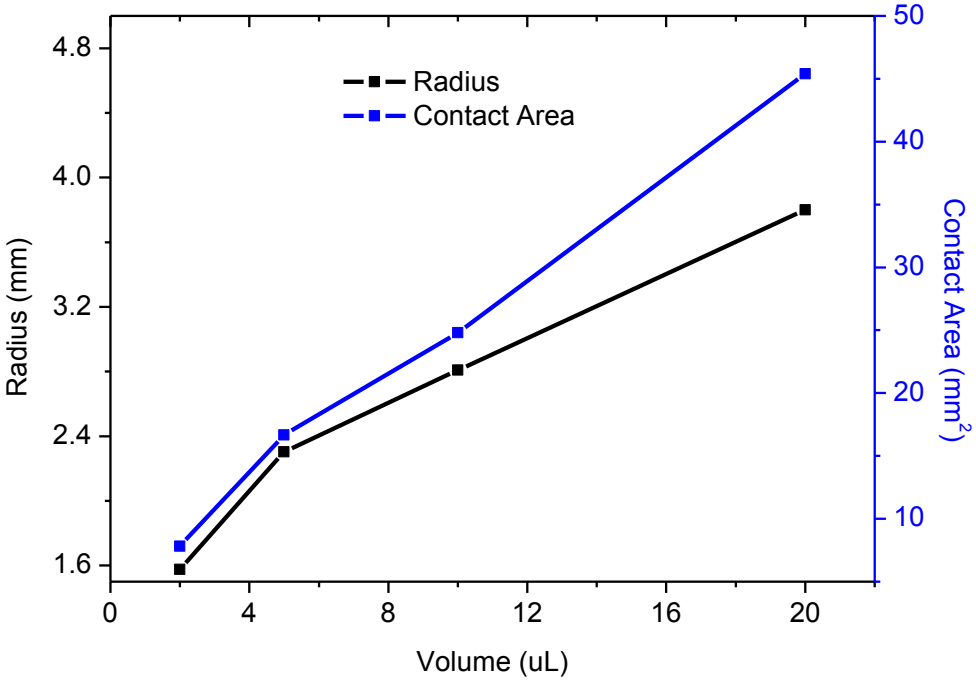
Radius
Contact Area
Radius (mm)
Contact Area (mm²)
Volume (uL)
4.8
4.0
3.2
2.4
1.6
50
40
30
20
10
0
4
8
12
16
20

(c)

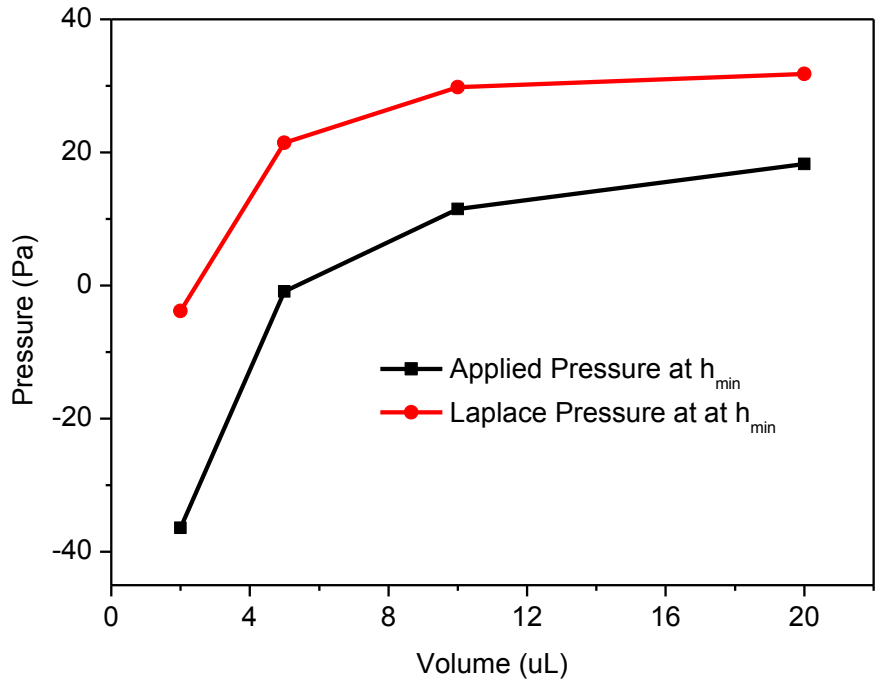
Applied Pressure at h min
Laplace Pressure at at h min
Pressure (Pa)
Volume (uL)
40
20
0
-20
-40
0
4
8
12
16
20

(d)

Table 11. Comparisons of separation distances or heights, contact areas, pressures due to gravity, the Laplace pressures and the applied pressures of liquid bridges at h_{min} with different Kaydol volumes for woven fabric with multifilament yarns.

Volume (μL)	2	5	10	20
Height (mm)	0.14±0.03	0.21±0.02	0.23±0.01	0.38±0.10
Contact Area (mm^2)	7.81±2.37	16.66±1.95	24.79±2.11	45.38±1.87
Pressure due to gravity (Pa)	1.17±0.25	1.75±0.17	1.92±0.08	3.17±0.83
Laplace Pressure (Pa)	-3.8±4.1	21.4±0.7	29.8±0.8	31.8±1.1
Applied Pressure (Pa)	-36.4±6.0	-0.9±0.1	11.5±0.5	18.3±1.2

Dodecane

Figure 69 shows comparisons of different parameters for dodecane with different volumes. Compared with water and Kaydol, the forces at the minimum height or separation distance are all negative since the liquids are all in a concave shape and the Laplace pressure is negative. As the volume increases, the total force becomes more negative, which is the sum of the Laplace force and tension force. As the contact radius and contact areas increase at the small separation distance when the volume increases, both the applied pressure and Laplace pressure decrease with negative values. This indicates that an attractive force forms and liquids prefer to span spontaneously as being compressed. Thus this fabric is also robust for dodecane for small drops.

Figure 71. Curves for dodecane with different volumes where top and bottom substrates are PTFE film and woven fabric made from multifilament yarns. (a) Force-Separation distance curves for dodecane with different volumes; (b) Force-Volume curves, including both forces caused by surface tension and Laplace pressure; (c) Radius-Volume and Contact area-Volume curves, where both radius and contact area refer to parameters of the circular contact region between liquid and fabric when the liquid has been compressed to maximum; and (d) Pressure-Volume curves. Pictures are from compression of the liquid with a volume of 10 μL.

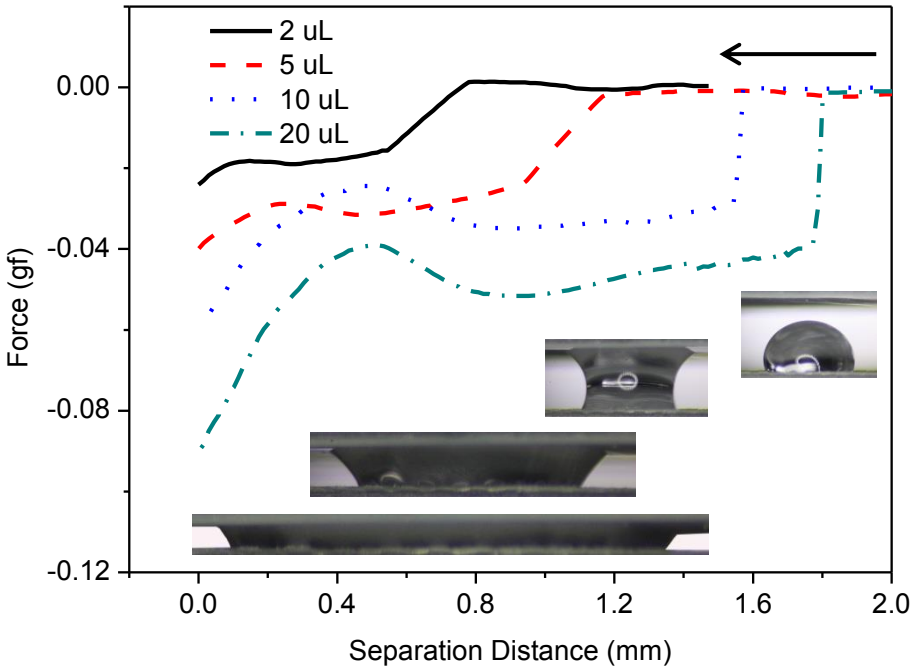
2 uL
5 uL
10 uL
20 uL
0.00
-0.04
-0.08
-0.12
Force (gf)
0.0
0.4
0.8
1.2
1.6
2.0
Separation Distance (mm)

(a)

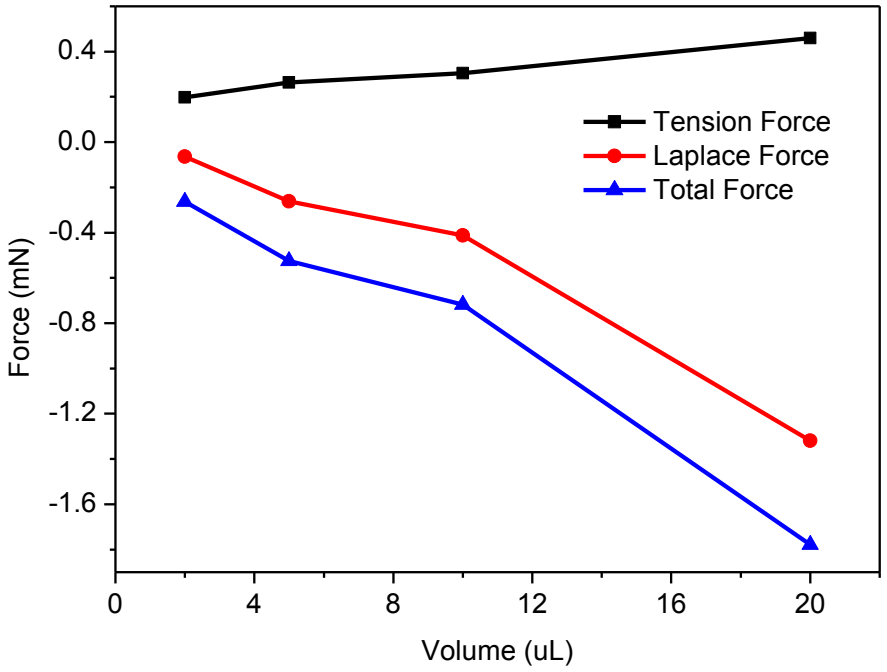
0.4
0.0
-0.4
-0.8
-1.2
-1.6
Force (mN)
Tension Force
Laplace Force
Total Force
0
4
8
12
16
20
Volume (uL)

(b)

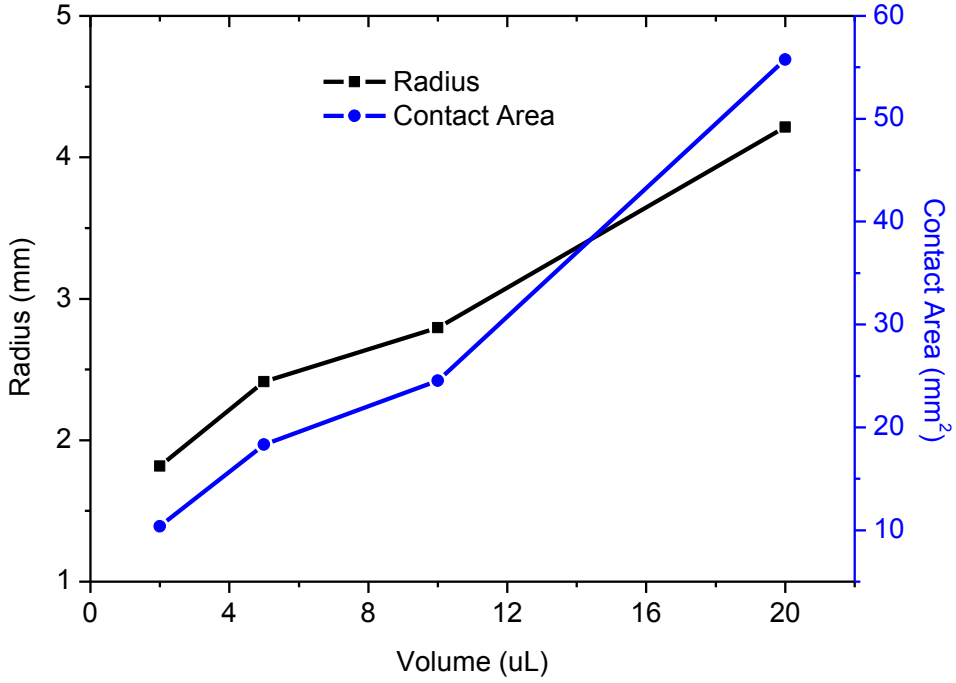
Radius
Contact Area
Radius (mm)
Contact Area (mm²)
Volume (uL)
0
4
8
12
16
20
1
2
3
4
5
10
20
30
40
50
60

(c)

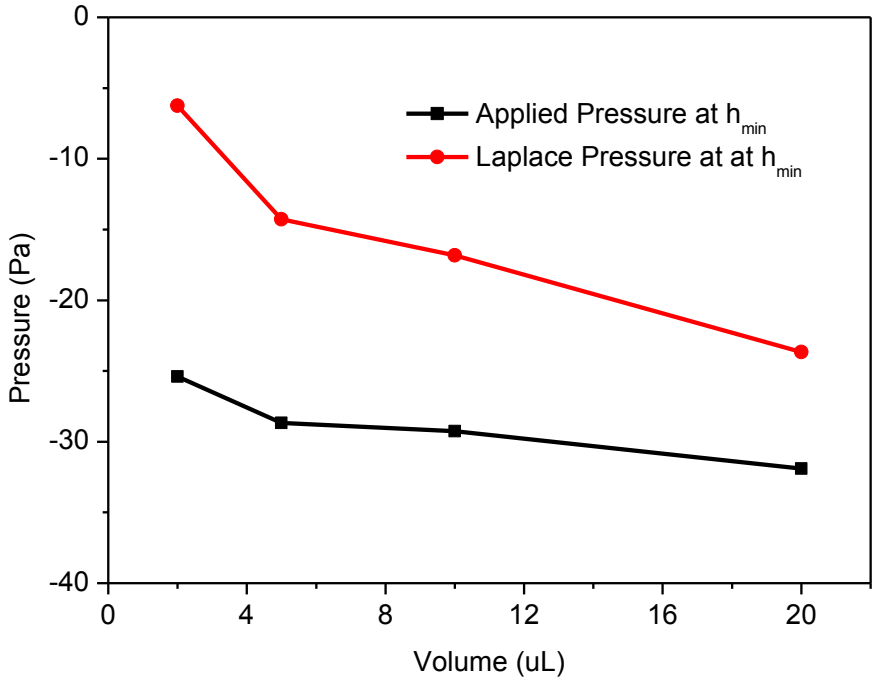
Applied Pressure at h min
Laplace Pressure at at h min
Pressure (Pa)
Volume (uL)
0
4
8
12
16
20
0
-10
-20
-30
-40

(d)

Effect of Surface Tensions of Liquids

Comparisons of effects of surface tensions can be found in the previous section or in Appendix C. For three liquids with the same volume, as they are being pressed with the PTFE film, a larger force and pressure is applied on the liquids with larger surface tensions. However, all of the liquids just spread between substrates rather than penetrating into the fabric structure. Thus the robust pressure cannot be reached or measured, but this fabric is robust for all three liquids with four different volumes when they have been compressed to almost zero.

4.8 Robustness of nonwoven fabric

For nonwoven fabrics, the robustness depends on the size of the voids in the structure, which can be seen from the structure image. Due to the non-uniformity, the robustness of nonwoven fabric will have a range, which is directly proportional to fiber diameters but inversely proportional to the edge-to-edge fiber distance. When a liquid is being squeezed between a PTFE film and the nonwoven fabric, at the moment that liquid just goes through the fabric, the profile can be analyzed as well as the force, and thus the Laplace pressure will be obtained as well as the applied pressure. The Robust pressure can be measured only if the liquid penetrates through rather than only spreading on the surface. Based on the experiments, the fabric was too robust and beyond the range of measurement. In this case, the measured pressures can be compared with the hydrostatic and oleostatic pressure which refers to the pressure caused by the gravity of the liquid when it is at rest.

Effects of Liquid Volume

From Figure 72 to Figure 74 and from Table 12to Table 14, the Force-Separation distance curves with different volumes, Force-Volume curves, Radius-Volume and Contact area-Volume curves, and (d) Pressure-Volume curves have been compared for water, Kaydol and dodecane. For all the liquids, at the minimum separation distance, the applied force with a positive value reaches its maximum. The applied force increases as well as the contact radius and contact area between liquid and a substrate. The total force changes with the same trend as the Laplace force since tension force varies in a small range for all liquids. The applied pressure and Laplace pressure at the minimum height are calculated from forces analysis, and they vary in different ways as the volume and surface tension of liquids changes. However, similar to the results from woven fabric made from multifilament yarns, all liquids just span between the nonwoven fabric and PTFE film, but they do not penetrate into or through the fabric. Therefore, this fabric is robust hydrophobic for water and oleophobic for Kaydol and dodecane.

Water

Figure 72. Curves for water with different volumes where top and bottom substrates are PTFE film and nonwoven fabric. (a) Force-Separation distance curves for water with different volumes; (b) Force-Volume curves, including both forces caused by surface tension and Laplace pressure; (c) Radius-Volume and Contact area-Volume curves, where both radius and contact area refer to parameters of the circular contact region between liquid and fabric when the liquid has been compressed to maximum; and (d) Pressure-Volume curves. Pictures are from compression of the liquid with a volume of 10 μL.

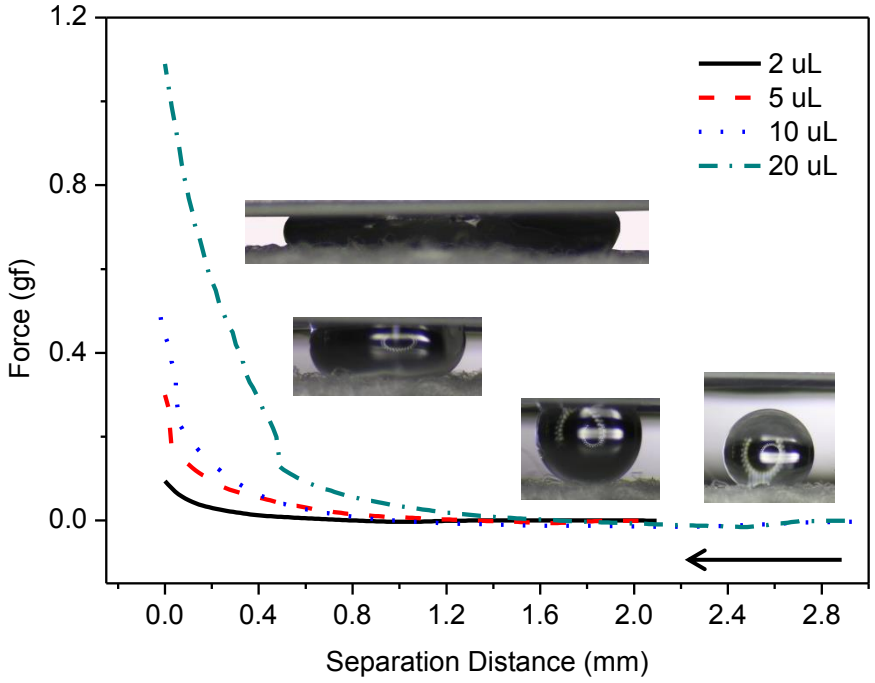
1.2
0.8
0.4
0.0
Force (gf)
2 uL
5 uL
10 uL
20 uL
0.0
0.4
0.8
1.2
1.6
2.0
2.4
2.8
Separation Distance (mm)

(a)

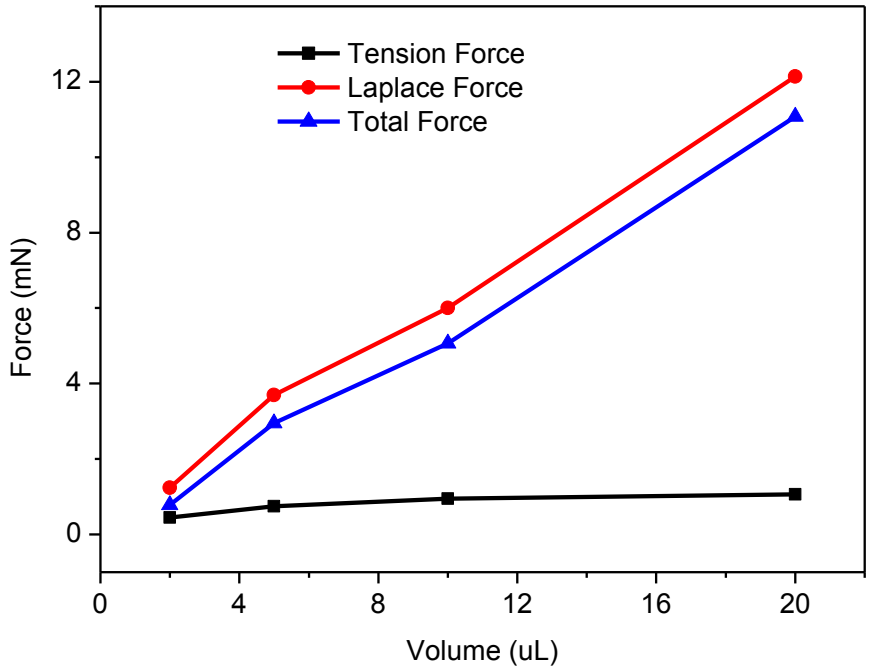
Tension Force
Laplace Force
Total Force
12
8
4
0
Force (mN)
0
4
8
12
16
20
Volume (uL)

(b)

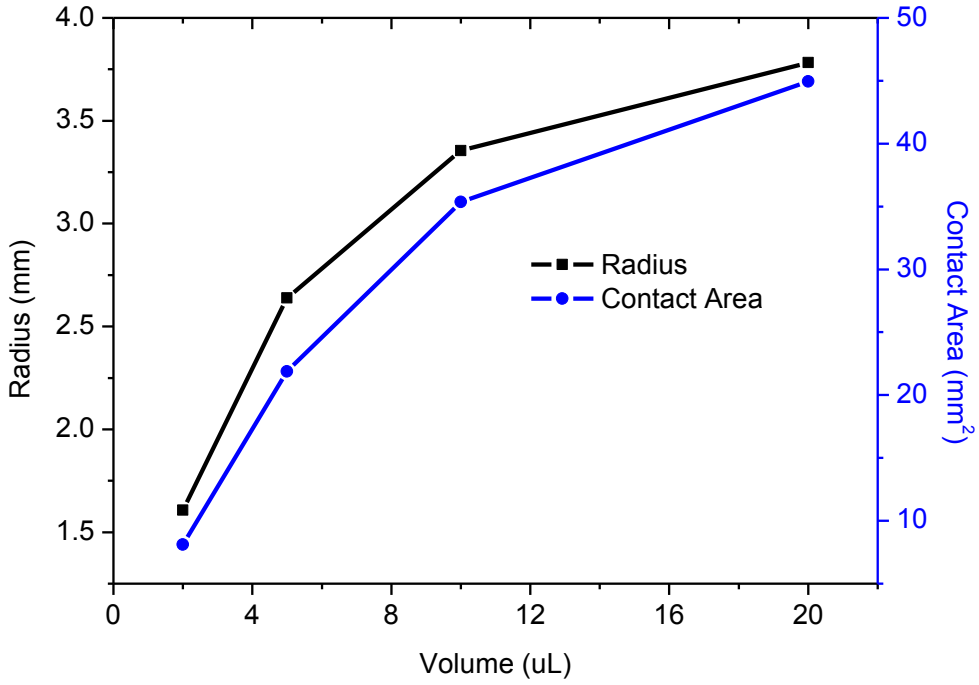
Radius (mm)
Contact Area (mm²)
Volume (uL)
Radius
Contact Area
4.0
3.5
3.0
2.5
2.0
1.5
50
40
30
20
10
0
4
8
12
16
20

(c)

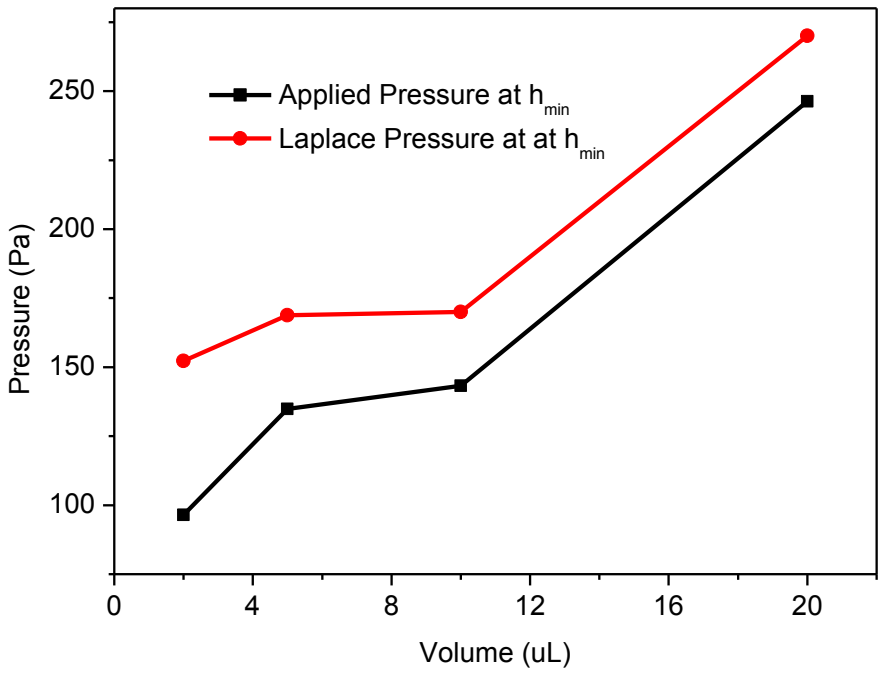
Pressure (Pa)
Volume (uL)
Applied Pressure at h min
Laplace Pressure at at h min
250
200
150
100
0
4
8
12
16
20

(d)

Table 12. Comparisons of separation distances or heights, contact areas, pressures due to gravity, the Laplace pressures and the applied pressures of liquid bridges at h_{min} with different water volumes for nonwoven fabric.

Volume (μL)	2	5	10	20
Height (mm)	0.25±0.14	0.42±0.01	0.25±0.03	0.54±0.17
Contact Area (mm^2)	8.11±0.56	21.88±0.36	35.35±4.63	44.96±3.76
Pressure due to gravity (Pa)	2.45±1.37	4.12±0.10	2.45±0.29	5.29±1.67
Laplace Pressure (Pa)	152±34	169±10	170±11	270±22
Applied Pressure (Pa)	97±14	135±10	143±10	246±23

Kaydol

Figure 73. Curves for Kaydol with different volumes where top and bottom substrates are PTFE film and nonwoven fabric. (a) Force-Separation distance curves for Kaydol with different volumes; (b) Force-Volume curves, including both forces caused by surface tension and Laplace pressure; (c) Radius-Volume and Contact area-Volume curves, where both radius and contact area refer to parameters of the circular contact region between liquid and fabric when the liquid has been compressed to maximum; and (d) Pressure-Volume curves. Pictures are from compression of the liquid with a volume of 10 μL.

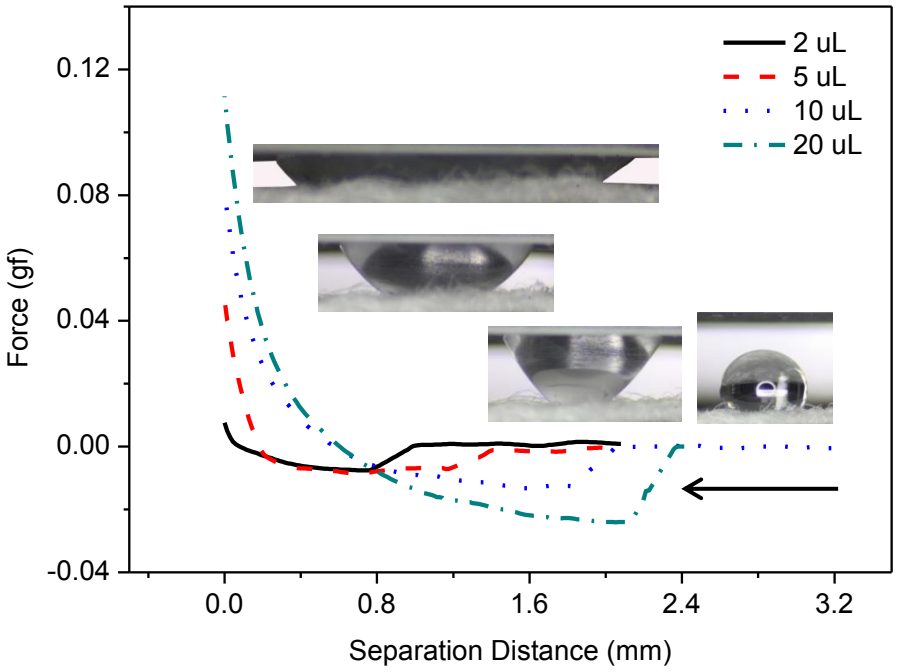
2 uL
5 uL
10 uL
20 uL
0.12
0.08
0.04
0.00
-0.04
Force (gf)
0.0
0.8
1.6
2.4
3.2
Separation Distance (mm)

(a)

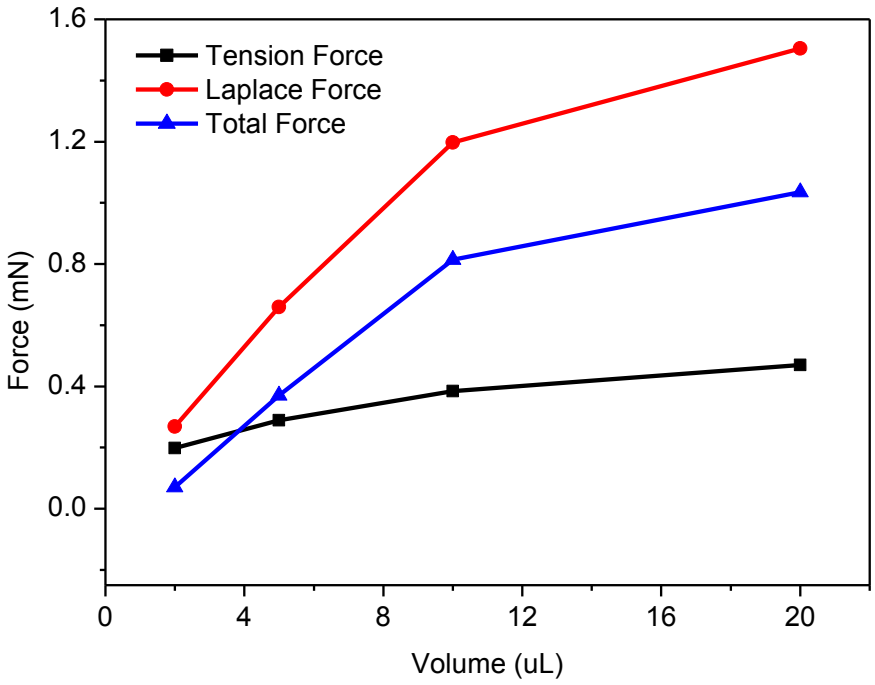
Tension Force
Laplace Force
Total Force
1.6
1.2
0.8
0.4
0.0
Force (mN)
0
4
8
12
16
20
Volume (uL)

(b)

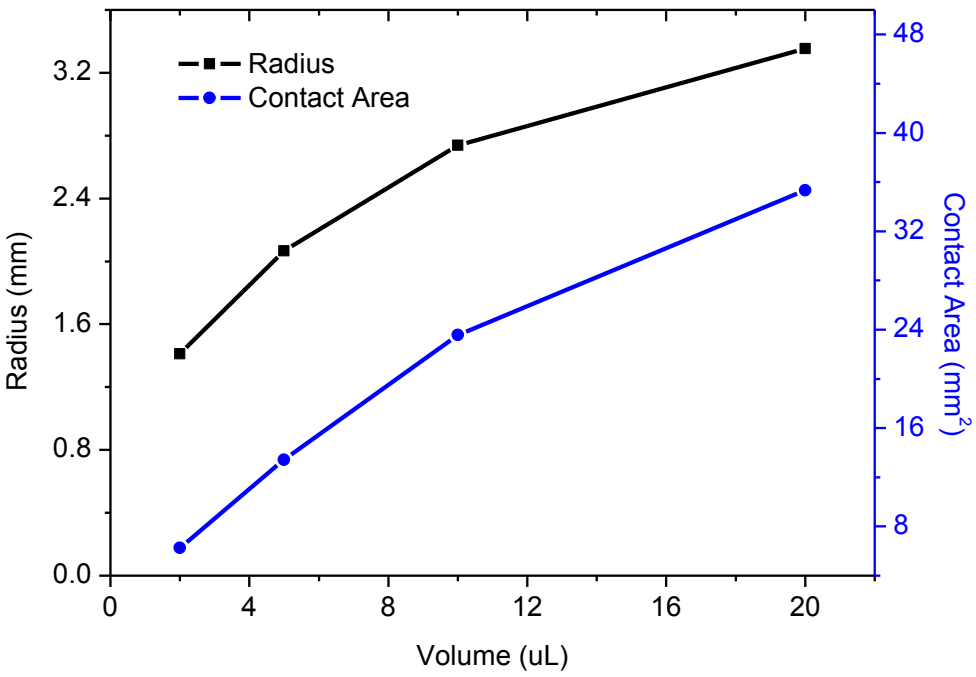
Radius
Contact Area
Radius (mm)
Contact Area (mm²)
Volume (uL)
0.0
0.8
1.6
2.4
3.2
8
16
24
32
40
48
0
4
8
12
16
20

(c)

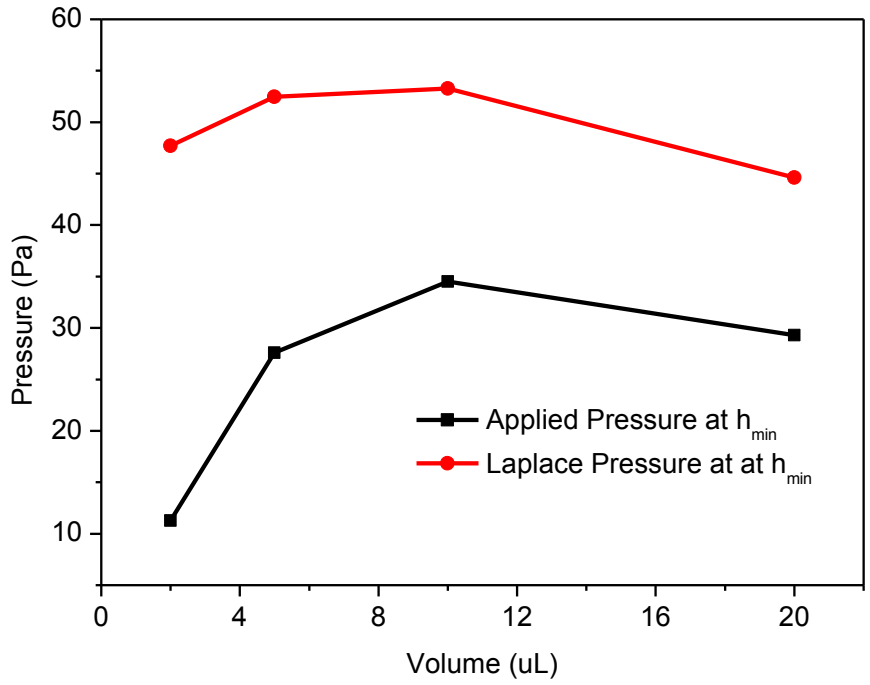
Applied Pressure at h min
Laplace Pressure at at h min
Pressure (Pa)
Volume (uL)
10
20
30
40
50
60
0
4
8
12
16
20

(d)

Table 13. Comparisons of separation distances or heights, contact areas, pressures due to gravity, the Laplace pressures and the applied pressures of liquid bridges at h_{min} with different Kaydol volumes for nonwoven fabric.

Volume (μL)	2	5	10	20
Height (mm)	0.25±0.03	0.35±0.06	0.39±0.02	0.58±0.17
Contact Area (mm^2)	6.26±0.91	13.42±2.63	23.58±1.07	35.33±2.03
Pressure due to gravity (Pa)	2.08±0.25	2.92±0.50	3.25±0.17	4.83±1.42
Laplace Pressure (Pa)	47.7±0.9	52.5±2.8	53.3±1.5	44.6±2.5
Applied Pressure (Pa)	11.3±0.4	27.6±2.2	34.5±1.8	29.3±2.7

Dodecane

Figure 74. Curves for dodecane with different volumes where top and bottom substrates are PTFE film and nonwoven fabric. (a) Force-Separation distance curves for dodecane with different volumes; (b) Force-Volume curves, including both forces caused by surface tension and Laplace pressure; (c) Radius-Volume and Contact area-Volume curves, where both radius and contact area refer to parameters of the circular contact region between liquid and fabric when the liquid has been compressed to maximum; and (d) Pressure-Volume curves. Pictures are from compression of the liquid with a volume of 10 μL.

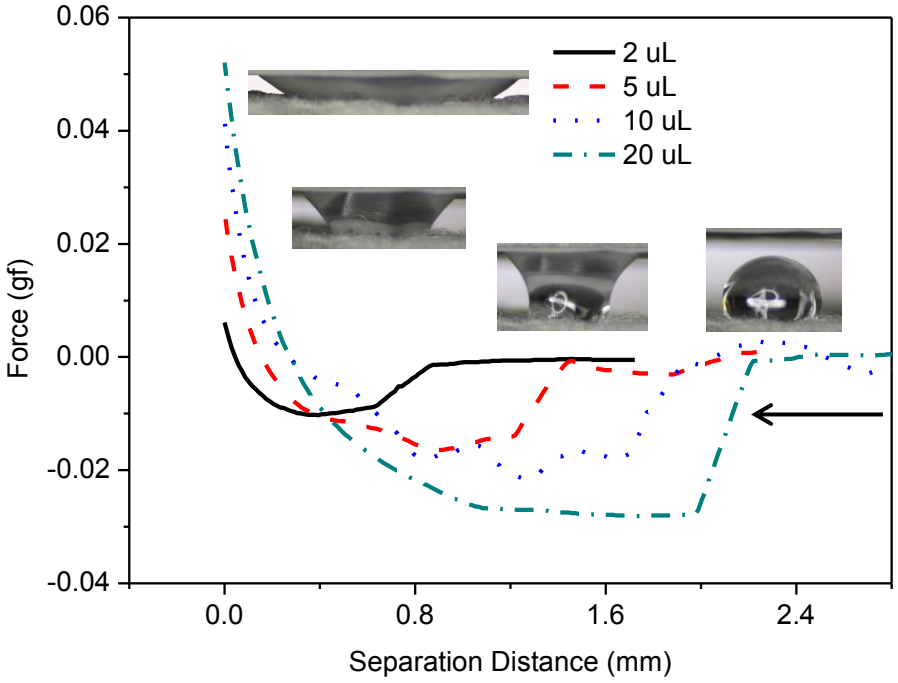
0.06
0.04
0.02
0.00
-0.02
-0.04
Force (gf)
0.0
0.8
1.6
2.4
Separation Distance (mm)
2 uL
5 uL
10 uL
20 uL

(a)

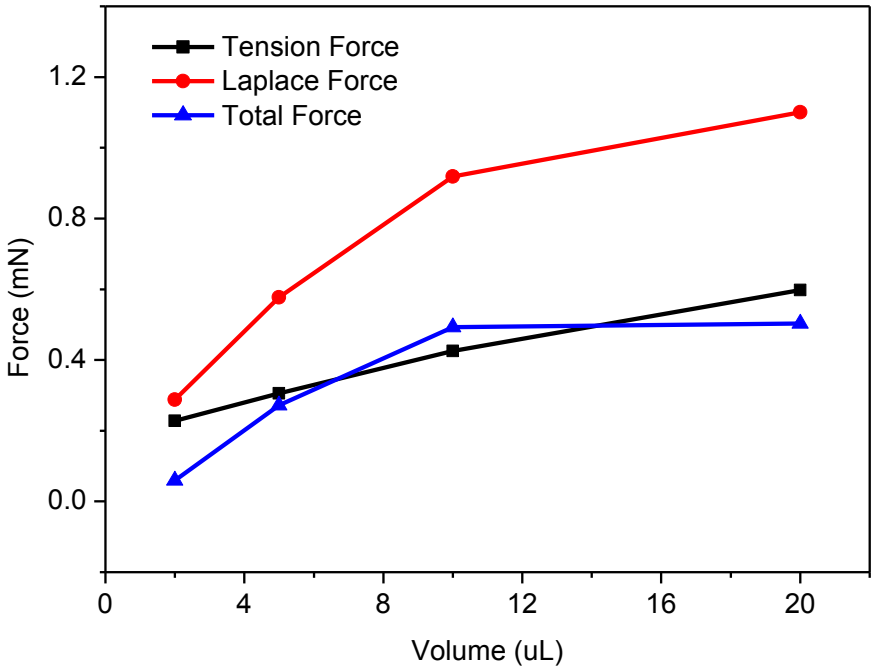
1.2
0.8
0.4
0.0
Force (mN)
0
4
8
12
16
20
Volume (uL)
Tension Force
Laplace Force
Total Force

(b)

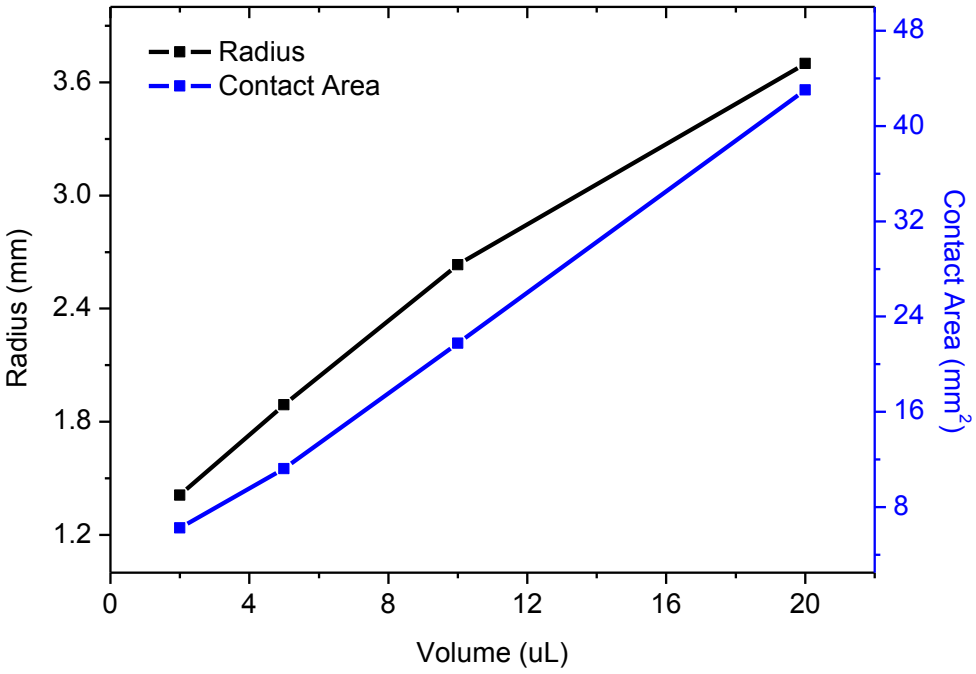
Radius
Contact Area
Radius (mm)
Contact Area (mm²)
Volume (uL)
3.6
3.0
2.4
1.8
1.2
48
40
32
24
16
8
0
4
8
12
16
20

(c)

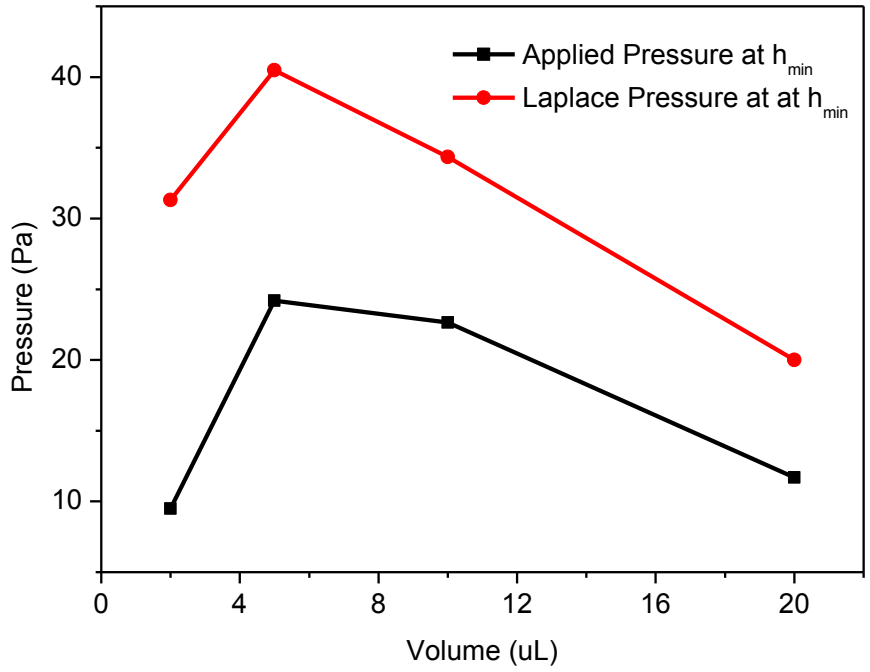
Applied Pressure at h min
Laplace Pressure at at h min
Pressure (Pa)
Volume (uL)
40
30
20
10
0
4
8
12
16
20

(d)

Table 14. Comparisons of separation distances or heights, contact areas, pressures due to gravity, the Laplace pressures and the applied pressures of liquid bridges at h_{min} with different dodecane volumes for nonwoven fabric.

Volume (μL)	2	5	10	20
Height (mm)	0.32±0.03	0.44±0.04	0.46±0.08	0.46±0.16
Contact Area (mm^2)	6.26±0.58	11.22±1.02	21.77±3.47	43.02±4.43
Pressure due to gravity (Pa)	2.35±0.22	3.23±0.29	3.38±0.59	3.38±1.18
Laplace Pressure (Pa)	31.3±2.9	40.5±4.9	34.4±2.2	20.0±2.3
Applied Pressure (Pa)	9.5±1.9	24.2±4.2	22.7±1.4	11.7±2.0

Effects of Surface Tensions of Liquids

The effects of surface tensions of liquids can be found either from the Section *Effects of Liquid Volume* or from Appendix D. The applied forces and pressures increase as the surface tension gets larger, but the robust pressure cannot be measured due to the high hydrophobicity and oleophobicity of the fabric.

CHAPTER 5. CONCLUSIONS

Understanding the robustness of a hydrophobic and oleophobic surface will provide important information to design and develop highly liquid resistance surfaces. Based on literature review, a robustometer was designed which could compress a liquid on a hydrophobic and oleophobic surface. During the push and pull process, the separation distance and applied force can be observed as well as the changing shapes of the liquid. The robustometer was calibrated by squeezing a liquid between two parallel smooth surfaces, and the capillary forces were proved to agree with previous theoretical study. In addition, the hydrophobic and oleophobic textile materials were produced by the condensation of FS on to nylon surfaces. The basic mechanism was to covert the hydrophilic and oleophilic carboxyl groups (-COOH) into hydrophobic and oleophobic carbon-fluorine groups ($-C_8F_{17}$). Robustness has been tested, by compressing the liquid from a sessile drop to a capillary bridge between a PTFE film and the FS treated fabric surface, until the separation distance is almost zero.

For the liquid bridges, an analytical solution was found for the profiles of liquid-vapor interface and it has been proved for the capillary bridges with different shapes. The profiles could be either concave or convex, and either symmetric or asymmetric, even when the surface tensions and volumes are different. Most importantly, this analytical solution also fits the liquid bridges both between smooth surfaces and between rough surfaces, which makes it possible to extend to the study of robustness of textiles. With this solution, as a PTFE film was squeezing a liquid on a hydrophobic and oleophobic fabric at a certain separation distance or

height, the Laplace pressure could be derived, which has been proved to be the same with that from the capillary force analysis. The capillary force could be either positive or negative, which depends on the competition between the Laplace force and the surface tension force. The force could be negative for both hydrophobic and oleophobic surfaces, such as between two PTFE films with a water drop; the force could be either positive or negative between a hydrophobic/oleophobic and a hydrophilic/oleophilic surface. Then, the applied or robust pressure could be obtained by dividing the applied force by the contact area and Laplace pressure can be calculated from its relationship with robust pressures, as a liquid just penetrates through a rough surface.

The robustness of parallel monofilaments was modeled both for liquid with infinite and finite volume. It was found that the liquid with a finite volume (< 20 μL) penetrates into the large spaces between adjacent monofilaments, and the liquid could wet the monofilaments from the side rather than from the gaps if the space is too small. The robust pressures for these two different phenomena are different. However, for both cases, smaller volume leads to higher robust pressure. In addition, the robust pressure decreases as the edge-to-edge distance increases. The robustness of single layer of woven fabric made of monofilaments cannot be measured since the liquids spread on the surfaces as being compressed, and it also indicates that the fabric is robust to water, Kaydol and dodecane. However, by using a PTFE film attached on a glass slide to push the liquid on the fabric, it was found that the robust pressure decreases as the volume of liquids increases or the surface tension decreases.

As the thickness of a fabric increases such as multiple layers, the robustness will also increase due to the limited volume of the liquid or the hydrophobicity and oleophobicity of the fabrics. For the woven fabric made of multifilament yarns and the nonwoven fabrics, they are too robust and the liquids could not penetrate through the structure. The woven fabric made of multifilament yarns is robust due to small space between adjacent monofilaments and yarns, while thickness of nonwoven fabric is large. This indicates that, thick fabric with high density is excellent for designing of high liquid resistance fabrics, which is inversely proportional to the air permeability.

In addition, water and oil behave differently since PTFE film is hydrophobic but oleophilic, where generally a repulsive force formed for water and an attractive force formed for oil between the film and a FS treated fabric. Only when the liquid volume is sufficiently large or the separation distance is extremely small, a repulsive force can occur for oil. Thus for oil, it is less efficient to use PTFE film to do the experiments.

CHAPTER 6. FUTURE WORK

The robustness of hydrophobic and oleophobic fabrics were discussed for small drops as they were being squeezed with a PTFE film. However, the de-wetting behavior of liquid on the fabric after the force has been released should also be studied as well as the liquid residuals on the surfaces of fabrics. In addition, as a force is applied on the liquid sitting on the fabric, the amount of liquid being pushed into the structure cannot be observed with naked eyes. Especially for the highly robust hydrophobic and oleophobic fabrics, the robustness cannot be quantified. In future, the amount of liquid within the structure should be studied. Finally, the liquid with a velocity can be impacted on the fabric to study the dynamic robustness, such as falling rain.

REFERENCES

(1) Tuteja, A.; Choi, W.; Mabry, J. M.; Mckinley, G. H.; Cohen, R. E. *PNAS: Proc Nat Acad Sci USA* **2008**, *105*, 18200–18205.

(2) Steele, A.; Bayer, I.; Loth, E. *Nano letters* **2009**, *9*, 501–5.

(3) Han, D.; Steckl, A. J. *Langmuir* **2009**, *25*, 9454–62.

(4) Aulin, C.; Yun, S. H.; Wågberg, L.; Lindström, T. *ACS Appl Mater and Interfaces* **2009**, *1*, 2443–52.

(5) Balkenende, A. R.; Boogaard, H. J. A. P. Van De; Scholten, M.; Willard, N. P. *Langmuir* **1998**, *14*, 5907–5912.

(6) Cwikel, D.; Zhao, Q.; Liu, C.; Su, X.; Marmur, A. *Langmuir* **2010**, *26*, 15289–94.

(7) He, B.; Lee, J.; Patankar, N. *Colloids and Surfaces A: Physicochem. Eng. Aspects* **2004**, *248*, 101–104.

(8) Kubiak, K. J.; Wilson, M. C. T.; Mathia, T. G.; Carval, P. *Wear* **2011**, *271*, 523–528.

(9) Lee, H. J.; Michielsen, S. *J. Polym Sci. Part B: Polym Phys.* **2006**, *45*, 253–261.

(10) Kim, S. H. *J. Adhes Sci Technol* **2008**, *22*, 235–250.

(11) Cassie, A. B. D.; Baxter, S. *Physics* **1944**, *5*, 546–551.

(12) Wenzel, R. N. *Ind Eng Chem* **1936**, *28*, 988–994.

(13) Nielsen, K.; Noordegraaf, D.; Sørensen, T.; Bjarklev, A.; Hansen, T. P. *J. Opt. A: Pure Appl. Opt.* **2005**, *7*, L13–L20.

(14) Brown, R. C. *Contemp. Phys.* **1974**, *15*, 301–327.

(15) Marchand, A.; Weijs, J. H.; Snoeijer, J. H.; Andreotti, B. *Am. J. Phys.* **2011**, *79*, 999.

(16) Choi, W.; Tuteja, A.; Chhatre, S.; Mabry, J. M.; Cohen, R. E.; McKinley, G. H. *Adv. Mater.* **2009**, *21*, 2190–2195.

(17) Deng, X.; Mammen, L.; Butt, H. J.; Vollmer, D. *Science* **2011**, *335*, 67–69.

(18) Lee, H. J.; Owens, J. R. *J. Mater. Sci.* **2010**, *45*, 3247–3253.

(19) Lee, H. J. *J. Mater. Sci.* **2009**, *44*, 4645–4652.

(20) Marmur, A. *Langmuir* **2003**, *1*, 8343–8348.

(21) Koishi, T.; Yasuoka, K.; Fujikawa, S.; Ebisuzaki, T.; Zeng, X. C. *PNAS: Proc Nat Acad Sci USA* **2009**, *106*, 8435–8440.

(22) Gao, L.; McCarthy, T. J. *Langmuir* **2009**, *25*, 7249–7255.

(23) McHale, G. *Langmuir* **2007**, *23*, 8200–5.

(24) Bhushan, B.; Jung, Y. C. *J. Phys: Condens. Matter.* **2008**, *20*, 225010.

(25) Li, X. M.; He, T.; Crego-Calama, M.; Reinhoudt, D. N. *Langmuir* **2008**, *24*, 8008–12.

(26) Wheeler, T. D.; Stroock, A. D. *Langmuir* **2009**, *25*, 7609–22.

(27) Bliznyuk, O.; Veligura, V.; Kooij, E.; Zandvliet, H.; Poelsema, B. *Phys. Rev. E* **2011**, *83*, 041607.

(28) Bratko, D.; Curtis, R. a.; Blanch, H. W.; Prausnitz, J. M. *J. Chem. Phys.* **2001**, *115*, 3873.

(29) Fedeli, L.; Turco, A.; DeSimone, A. *Continuum Mech. Thermodyn.* **2011**, *23*, 453–471.

(30) Barbieri, L.; Wagner, E.; Hoffmann, P. *Langmuir* **2007**, *23*, 1723–1734.

(31) Boreyko, J. B.; Baker, C. H.; Poley, C. R.; Chen, C.-H. *Langmuir* **2011**, *27*, 7502–9.

(32) Jung, Y. C.; Bhushan, B. *Langmuir* **2009**, *25*, 9208–18.

(33) Rabinovich, Y. I.; Esayanur, M. S.; Moudgil, B. M. *Langmuir* **2005**, *21*, 10992–7.

(34) De Souza, E. J.; Brinkmann, M.; Mohrdieck, C.; Crosby, A.; Arzt, E. *Langmuir* **2008**, *24*, 10161–10168.

(35) Butt, H. J. *Langmuir* **2008**, *24*, 4715–21.

(36) Van Honschoten, J. W.; Tas, N. R.; Elwenspoek, M. *Am. J. Phys.* **2010**, *78*, 277.

(37) Orr, F. M.; Scriven, L. E. *J. Fluid Mech.* **1975**, *67*, 723–742.

(38) Gao, L.; Mccarthy, T. J. *Langmuir* **2007**, *23*, 1999–2001.

(39) Vagharchakian, L.; Restagno, F.; Léger, L. *J. Phys. Chem. B* **2009**, *113*, 3769–75.

(40) Furmidge, C. G. L. *J. Colloid Sci.* **1962**, *17*, 309–324.

(41) Lee, H. J.; Michielsen, S. *JOTI* **2006**, *97*, 455–462.

(42) Choi, W.; Tuteja, A.; Mabry, J. M.; Cohen, R. E.; McKinley, G. H. *J. Colloid Interf Sci.* **2009**, *339*, 208–16.

(43) Bhushan, B.; Jung, Y. C.; Niemietz, A.; Koch, K. *Langmuir* **2009**, *25*, 1659–66.

(44) Bhushan, B.; Jung, C.; Nosonovsky, M. In *Springer Handbook of Nanotechnology*; 2010; pp. Part F, 1437–1524.

(45) Bhushan, B.; Nosonovsky, M.; Jung, Y. C. In *Nanotribology and Nanomechanics*; 2008; pp. 995–1072.

(46) Brewer, S. a.; Willis, C. R. *Appl Surf Sci* **2008**, *254*, 6450–6454.

(47) Blow, M. L.; Yeomans, J. M. *Langmuir* **2010**, *26*, 16071–83.

(48) Liu, Y.; Chen, X.; Xin, J. H. *Bioinsp. Biomim.* **2008**, *3*, 046007.

(49) Verho, T.; Bower, C.; Andrew, P.; Franssila, S.; Ikkala, O.; Ras, R. H. a *Adv. Mater.* **2011**, *23*, 673–8.

(50) Guo, Z.; Liu, W.; Su, B.-L. *J. Colloid Interf Sci.* **2011**, *353*, 335–55.

(51) Tuteja, A.; Choi, W.; Ma, M.; Mabry, J. M.; Mazzella, S. A.; Rutledge, G. C.; McKinley, G. H.; Cohen, R. E. *Science* **2007**, *318*, 1618–22.

(52) Fowkes, F. M. *J. Phys. Chem.* **1963**, *67*, 2538.

(53) Ostrovskaya, L.; Podesta, A.; Milani, P.; Ralchenko, V. *Europhys. Lett.* **2003**, *63*, 401–407.

(54) De Gennes, P.; BrochardWyart, F.; Quéré, D.; Widom, B. *Physics Today* **2004**, *57*, 66.

(55) Carroll, B. J. *J. Colloid Interf Sci.* **1976**, *57*, 488–495.

(56) Carroll, B. J.; Lucassen, J.; Sunlight, P. *Chem Eng Sci* **1973**, *28*, 23–30.

(57) Lorenceau, L.; Quere, D. *J. Fluid Mech* **2004**, *510*, 29–45.

(58) Michielsen, S.; Zhang, J.; Du, J.; Lee, H. J. *Langmuir* **2011**, *27*, 11867–72.

(59) Du, J.; Michielsen, S.; Lee, H. J. *Langmuir* **2012**, *28*, 722–8.

(60) Du, J.; Michielsen, S.; Lee, H. J. *Langmuir* **2010**, *26*, 16000–4.

(61) Dyba, R. V.; Miller, B. *TRJ* **1970**, *40*, 884–890.

(62) Hoit, S. Liquid Droplet Behavior on Yarns: Modeling of Filament Level Interaction, North Carolina State University, 2011.

(63) Knospe, C. R.; Nezamoddini, S. A. *J. Micro-Nano Mech.* **2009**, *5*, 57–68.

(64) De Souza, E. J.; Gao, L.; McCarthy, T. . J.; Arzt, E.; Crosby, A. J. *Langmuir* **2008**, *24*, 1391–6.

(65) Gillespie, T.; Settineri, W. J. *J. Colloid Interf Sci.* **1967**, *24*, 199–202.

(66) Alexandrou, A. N.; Bazilevskii, A. V.; Entov, V. M.; Rozhkov, A. N.; Sharaf, A. *Fluid Dynam* **2010**, *45*, 952–964.

(67) Princen, H. M. *J. Colloid Interf Sci.* **1970**, *34*, 171.

(68) Princen, H. M. *TRJ* **1970**, *40*, 1069–1072.

(69) Michielsen, S.; Lee, H. J. *Langmuir* **2007**, *23*, 6004–10.

(70) Koch, K.; Bhushan, B.; Jung, C.; Barthlott, W. *Soft Matter* **2009**, *5*, 1386–1393.

(71) Wang, C.; Wang, T.; Liao, C.; Kuo, S.; Lin, H. *Materials Science* **2011**, 16495–16500.

(72) Fabbri, P.; Messori, M.; Pilati, F. *Adv Polym Tech* **2007**, *26*, 182–190.

(73) Gao, L.; Mccarthy, T. J. *J. Am. Chem. Soc.* **2006**, *128*, 9052–9053.

(74) Lee, J. A.; Mccarthy, T. J. *Macromolecules* **2007**, *40*, 3965–3969.

(75) Lee, H. J.; Owens, J. R. *J. Mater. Sci.* **2010**, *46*, 69–76.

(76) Zhu, X.; Zhang, Z.; Men, X.; Yang, J.; Xu, X. *Appl Surf Sci* **2010**, *256*, 7619–7622.

(77) Woodward, I. S.; Schofield, W. C. E.; Roucoules, V.; Bradley, T. J.; Badyal, J. P. S. *Plasma Chem Plasma Process* **2006**, *26*, 507–516.

(78) Nättinen, K.; Nikkola, J.; Minkkinen, H.; Heikkilä, P.; Lavonen, J.; Tuominen, M. *J. Coat Technol Res* **2010**, *8*, 237–245.

(79) Kiuru, M. *Mater Lett* **2004**, *58*, 2213–2216.

(80) Balu, B.; Breedveld, V.; Hess, D. W. *Langmuir* **2008**, *24*, 4785–90.

(81) Topala, I.; Asandulesa, M.; Spridon, D.; Dumitrascu, N. *IEEE T Plasma Sci* **2009**, *37*, 946–950.

(82) Teare, D. O. H.; Spanos, C. G.; Ridley, P.; Kinmond, E. J.; Roucoules, V.; Badyal, J. P. S. *Chem. Mater* **2002**, *14*, 4566–4571.

(83) Search, H.; Journals, C.; Contact, A.; Iopscience, M.; Address, I. P. *J. Phys. D: Appl. Phys.* **2002**, *35*, 1927–1933.

(84) Ma, M.; Mao, Y.; Gupta, M.; Gleason, K. K.; Rutledge, G. C. *Macromolecules* **2005**, *38*, 9742–9748.

(85) Wang, X.; Weiss, R. a *Langmuir* **2012**, *28*, 3298–305.

(86) Teisala, H.; Tuominen, M.; Aromaa, M.; Stepien, M.; Mäkelä, J. M.; Saarinen, J. J.; Toivakka, M.; Kuusipalo, J. *Langmuir* **2012**, *28*, 3138–45.

(87) Ahuja, a; Taylor, J. a; Lifton, V.; Sidorenko, a a; Salamon, T. R.; Lobaton, E. J.; Kolodner, P.; Krupenkin, T. N. *Langmuir* **2008**, *24*, 9–14.

(88) Quéré, D.; Reyssat, M. *Phil. Trans. R. Soc. A* **2008**, *366*, 1539–56.

(89) Young, T. *Phil. Trans. R. Soc.* **1805**, *95*, 65–87.

(90) Mason, G.; Clark, W. C. *Chem Eng Sci* **1965**, *20*, 859–866.

(91) Adams, M. J.; Johnson, S. A.; Seville, J. P. K.; Willett, C. D. *Langmuir* **2002**, *18*, 6180–6184.

(92) Greenwood, J. a. *Philos Mag* **2009**, *89*, 945–965.

(93) Willett, C. D.; Adams, M. J.; Johnson, S. A.; Seville, J. P. K. *Powder Technol* **2003**, *130*, 63–69.

(94) Aris, R.; Levenspiel, O.; Petho, A. *Chem Eng Sci* **1967**, *23*, 810–812.

(95) Fortes, M. A. *J. Colloid Interf Sci.* **1982**, *88*, 338–352.

(96) McFarlane, J. S.; Tabor, D. *P ROY Soc A: Math Phy* **1950**, *202*, 224–243.

(97) O'brien, W. J.; Hermann, J. J. *J. Adhesion* **1973**, *5*, 91–103.

(98) Fisher, R. A. *J. Agr Sci* **1926**, *16*, 492–505.

(99) De Boer, P. C. T.; De Boer, M. P. *Langmuir* **2008**, *24*, 160–169.

(100) Mazzone, D. N.; Tardos, G. I.; Pfeffer, R. *J. Colloid Interf Sci.* **1986**, *113*, 544–556.

(101) Tuteja, A.; Choi, W.; Mckinley, G. H.; Cohen, R. E.; Rubner, M. F. *MRS Bull* **2008**, *33*, 752.

(102) Im, M.; Im, H.; Lee, J.-H.; Yoon, J.-B.; Choi, Y.-K. *Langmuir* **2010**, *26*, 17389–97.

(103) Im, M.; Im, H.; Lee, J.-H.; Yoon, J.-B.; Choi, Y.-K. *Soft Matter* **2010**, *6*, 1401.

(104) Tuteja, A.; Choi, W.; Mabry, J. M.; McKinley, G. H.; Cohen, R. E. *P Natl Acad Sci USA* **2008**, *105*, 18200–5.

(105) Mohan Krishnan, A. Robust Pressure of Meta-Stable Textile Fabrics, North Carolina State University, 2010.

(106) Rawal, A. *Langmuir* **2012**, *28*, 3285–9.

(107) Delaunay, C. *Journal de mathématiques pures et appliquées 1re série* **1841**, *6*, 309–314.

(108) Restagno, F.; Poulard, C.; Cohen, C.; Vagharchakian, L.; Léger, L. *Langmuir* **2009**, *25*, 11188–96.

APPENDICES

APPENDIX A. Visual Basic Code

The Visual Basic code is modified by Yongxin Wang from a package written by Dr. Stephen Michielsen.

Sheet 1

```
Option Explicit

Public continueTest As Boolean
Public Robust As Boolean

Private Sub StopButton2_Click()
    Dim yesNO As Boolean

    yesNO = MsgBox("Are you sure you want to stop the test?", _
        vbYesNo + vbCritical + vbDefaultButton2)
    If yesNO = vbYes Then
        continueTest = False
    End If
End Sub

Private Sub StartButton_Click()
    continueTest = True
    Robust = False
    Call Robust_Test
End Sub

Private Sub RobustButton_Click()
    continueTest = True
    Robust = True
    Call Robust_Test
End Sub
```

This workbook

```
Option Explicit
```

Robustness Test

```
Option Explicit

   Sub Robustness()
      Dim runTest As Boolean

      'Initialize Instruments & Test
      If Not Mettler.Init Then
         runTest = False
         MsgBox ("Error - Initializing Balance")
         Call Mettler.CloseMettler
      ElseIf Not Motor.Init Then
         runTest = False
         MsgBox ("Error - Initializing Motor")
         Call Motor.CloseMotor
         Call Mettler.CloseMettler
      ElseIf Not GetData.Init Then
         runTest = False
         MsgBox ("Error - Initializing Test")
         Call Motor.CloseMotor
         Call Mettler.CloseMettler
      Else
         runTest = True
         'Collect Data
         While runTest
            runTest = GetData.TakeData
            If Sheet1.continueTest = False Then
               runTest = False
            End If
         Wend

         Call Motor.CloseMotor
         Call Mettler.CloseMettler
         ActiveWorkbook.Save 'save file
      End If

      'clean up
      Application.StatusBar = False
      Beep
      Beep

   End Sub
```

Getting data

```
Option Explicit

    Private Sub delay(delayTime As Single)
        Dim finish As Single
        finish = Timer + delayTime
        Do While finish > Timer
        Loop
    End Sub

Public Function TakeData() As Boolean
    Dim startPosition As Long
    Dim endPosition As Long
    Dim currentBalance As Double
    Dim rowIndex As Integer
    Dim i As Integer
    TakeData = True     'Turn on TakeData mode

    Application.StatusBar = "Reading motor start position"
    'Record motor start position
    startPosition = Motor.FindPosition

    'Move motor
    'Motor.MotorSpeed (150000)
    Sheet1.Cells(1, 1) = "Balance"
    Sheet1.Cells(1, 2) = "Motor"
    Sheet1.Cells(2, 2) = startPosition
    'Start reading balance
    'Mettler.ReadBalanceContinuous

    Call MSCOM.Output(2, "V0.05 D-157000 G 1X1")
    Mettler.ReadBalanceContinuous
    rowIndex = 2
    For i = 0 To 270
    Sheet1.Cells(rowIndex, 1) = Mettler.ReadBalance
    rowIndex = rowIndex + 1
    Next

    'Stop reading balance
    Mettler.StopBalanceRead
    Application.StatusBar = "Reading motor end position"
    'Stop motor and record position
```

```
    endPosition = Motor.FindPosition
    Sheet1.Cells(rowIndex - 1, 2) = endPosition

    Call MSCOM.Output(2, "V0.05 D+165000 G 1X1")
    Mettler.ReadBalanceContinuous
    rowIndex = rowIndex
    For i = 0 To 283
    Sheet1.Cells(rowIndex, 1) = Mettler.ReadBalance
    rowIndex = rowIndex + 1
    Next

    'Stop reading balance
    Mettler.StopBalanceRead
    Application.StatusBar = "Reading motor end position"
    'Stop motor and record position
    endPosition = Motor.FindPosition
    Sheet1.Cells(rowIndex - 1, 2) = endPosition

    Sheet1.continueTest = False
    Application.StatusBar = "Test finished"

End Function

Public Function Init() As Boolean
    Dim aString As String, substrateString As String
    Dim specimenString As String, treatmentString As String
    Dim sampleFilename As String
    Dim i As Integer

   'Save information
    sampleFilename = Application.GetSaveAsFilename(sampleFilename, _
       "Excel files (*.xls), *.xls")
    Sheet1.SaveAs (sampleFilename)

    Init = True
    firstEntry = True

End Function
```

```
Private Sub ResetMinMax()
   numOfMax = 0
   numOfMin = 0
   currentMax = -100
   currentMin = 100
   lookForMax = True
   lastLookForMax = False
End Sub

Private Function SetUpHeaders(speed As Single) As Integer
   Const lowestSpeed = 0.002
   Dim rangeStr As String, commandStr As String
   Dim realSpeed As Single

   If speed = 0 Then
      currentRow = currentRow + 5
      Sheet1.Cells(currentRow, 1) = "Balance ="
      Sheet1.Cells(currentRow, 2) = balance
      If Sheet1.Robust Then
         Sheet1.Cells(currentRow, 3) = "Normal Load ="
         If Sheet1.Robust Then
            Sheet1.Cells(currentRow, 4) = forceDenom
         Else
            Sheet1.Cells(currentRow, 4) = -forceDenom
         End If
      End If
      currentRow = currentRow + 1
      Sheet1.Cells(currentRow, 1) = "Speed (cm/sec)"
      Sheet1.Cells(currentRow, 2) = "Direction"
      Sheet1.Cells(currentRow, 3) = "Fs/Fk"
      Sheet1.Cells(currentRow, 4) = "1st"
      Sheet1.Cells(currentRow, 5) = "2nd"
      Sheet1.Cells(currentRow, 6) = "3rd"
      Sheet1.Cells(currentRow, 7) = "4th"
      Sheet1.Cells(currentRow, 8) = "5th"
      Sheet1.Cells(currentRow, 9) = "6th"
      Sheet1.Cells(currentRow, 10) = "7th"
      Sheet1.Cells(currentRow, 11) = "Average"
      Sheet1.Cells(currentRow, 12) = "Standard Dev"
      currentRow = currentRow + 1
      If Sheet1.Robust Then
         Sheet1.Cells(currentRow, 2) = "Down"
      Else
```

```
            Sheet1.Cells(currentRow, 2) = "Up"
        End If
        Sheet1.Cells(currentRow, 1) = lowestSpeed * 0.0635 ' See below
    Else
        currentRow = currentRow + 3
        If Motor.direction = up Then
            Sheet1.Cells(currentRow, 2) = "Up"
            'Convert speed from rev/sec to cm/sec
            '   Screw is 40 turns/in
            '   so  turn/sec * 2.54 cm/in / 40 tpi = 0.0635
            realSpeed = speed * 0.0635
            Sheet1.Cells(currentRow, 1) = realSpeed
        Else
            Sheet1.Cells(currentRow, 2) = "Down"
            If Sheet1.Robust Then
                'Convert speed from rev/sec to cm/sec
                '   Screw is 40 turns/in
                '   so  turn/sec * 2.54 cm/in / 40 tpi = 0.0635
                realSpeed = speed * 0.0635
                Sheet1.Cells(currentRow, 1) = realSpeed
            End If
        End If
    End If
    Sheet1.Cells(currentRow, 3) = "Fs"
    Sheet1.Cells(currentRow + 1, 3) = "Fk"
    rangeStr = Format(currentRow) + ":J" + Format(currentRow) + ")"
    commandStr = "=Average(D" + rangeStr
    Sheet1.Cells(currentRow, 11).Formula = commandStr
    commandStr = "=StDev(D" + rangeStr
    Sheet1.Cells(currentRow, 12).Formula = commandStr
    rangeStr = Format(currentRow + 1) + ":J" + Format(currentRow + 1) + ")"
    commandStr = "=Average(D" + rangeStr
    Sheet1.Cells(currentRow + 1, 11).Formula = commandStr
    commandStr = "=StDev(D" + rangeStr
    Sheet1.Cells(currentRow + 1, 12).Formula = commandStr
    Sheet1.Cells(currentRow + 2, 3) = "Average Force"
    If currentRow > 20 Then
        ActiveWindow.SmallScroll down:=4
    End If
    SetUpHeaders = currentRow
End Function
```

```
Private Function CollectData() As Integer
   Const ColOffset = 3, sixPi = 18.849556
   Dim forceWeight As Single, ForceAs Single
   Dim maxTime As Single

   'Reset counters if speed or direction change due
   If (lookForMax <> lastLookForMax) And (numOfMax = 0) Then
      lastLookForMax = lookForMax
      counter = 0
      forceSum = 0
   End If

   'Read data
      forceWeight = Mettler.ReadBalance
      'Force= forceWeight
      If forceWeight > 0.9 * testWeight Then
            If Sheet1.Robust Then
             'Linber & Gralen, TRJ (1948) 18: 287, eqn 8
               Force= Log(forceWeight / testWeight) / forceDenom 'angled test?
            Else
               Force= Motor.direction * (forceWeight - testWeight) / forceDenom
            End If
        'Update counters
            counter = counter + 1
            forceSum = forceSum + force

        If lookForMax Then  'Find maximum
            If Force> currentMax Then   'Not a new max
               currentMax = force
            ElseIf Force< currentMax - 0.01 Then    'New max
            'ElseIf Force< 0.95 * (currentMax - Sheet1.Cells(7, 2)) Then
               numOfMax = numOfMax + 1     'Increment max counter
               Sheet1.Cells(currentRow, numOfMax + ColOffset) = currentMax
               lookForMax = False
               currentMax = -100
            End If
        Else              'Find minimum
            If Force< currentMin Then    'Not a new min
               currentMin = force
            ElseIf Force> currentMin + 0.01 Then    'New min
               numOfMin = numOfMin + 1     'Increment min counter
               Sheet1.Cells(currentRow + 1, numOfMin + ColOffset) = currentMin
```

```
            lookForMax = True
            currentMin = 100
          End If
        End If  'End of min/max test

        'Test for excess time without sufficient number of min/max
        maxTime = 600
        If Sheet1.Robust Then
          maxTime = maxTime * 3
        End If
        If counter > 3 * maxTime Then
          'More than 10 minutes without sufficient number of min/max
          numOfMin = 7    'Reset minimum and maximum values
          lookForMax = True
          lastLookForMax = False
        End If
        'Set current average force value
        Sheet1.Cells(currentRow + 2, ColOffset + 1) = forceSum / counter
      End If
  CollectData = numOfMin
End Function


Private Sub SetMicrometer()
  Const fiberHangerLength = 1.61
  '1.61 = Length in inches from balance to bottom of fiber hanger
  Const fiberLengthToBow = 2.36
  '2.36 = Length in inches from bottom of fiber hanger to center of bow
  Const fiberHangerWeight = 1.01
  '1.01 = Weight in grams of fiber hanger
  Dim angleCorr As Single, micrometer As Single
  Dim inString As String, ready As Integer
  Dim sleepTime As Integer

  'Alert operator
  Beep
  Beep
  Beep

End Sub
```

Mettler

```
Option Explicit

    Private Const balancePort = 1

    Private Sub delay(delayTime As Single)
       Dim finish As Single
       finish = Timer + delayTime
       Do While finish > Timer
       Loop
    End Sub

    Public Function Init() As Boolean
       Dim inString As String    ' Buffer to hold input string
       Dim Instructions As String    'Storage location for instructions
       Dim i As Integer, CRLF As String, timeOutTime As Single

       Init = True                'Set initial value
       CRLF = Chr(13) + Chr(10)    'Set Once, use many
       Call MSCOM.OpenPort(balancePort, "9600,M,7,1", 0)    'Open the Port

       Call MSCOM.Output(balancePort, "C")      ' Put Mettler under Computer Control
       i = 5
       While i >= 0               'Set up Status Bar
          delay (1) 'Sleep 1 second
          Application.StatusBar = "Please be patient ... Resetting balance" + Str(i)
          i = i - 1
       Wend
       timeOutTime = Timer + 25
       inString = ""
       Do
          If MSCOM.InBufCount(balancePort) Then
             inString = MSCOM.InputFromPort(balancePort, 0)
          End If
          Application.StatusBar = "Tare time remaining = " + Str(Int(timeOutTime - Timer))
       Loop Until Left(inString, 2) = "TA" Or Timer > timeOutTime

       'timeOutTime = 0
       If Timer > timeOutTime Then
          Application.StatusBar = "Balance Reset Failed"
          Init = False
          Application.StatusBar = "Tare Failed ... Cleanning up and Quitting"
```

```
    Else
        Application.StatusBar = "Balance Reset"
        If MSCOM.InBufCount(balancePort) Then  ' Read data.
            inString = MSCOM.InputFromPort(balancePort, 0)
        End If

    End If
End Function

Public Sub CloseMettler()
    Call MSCOM.Output(balancePort, "S")    'Stop balance output
    Call MSCOM.CloseThePort(1)
End Sub

Public Function StableReading() As Boolean
    Dim TestFlag As Boolean
    Dim Answer As Integer
    Dim DataString As String
    Dim N As Integer
    Dim timeOutTime As Single

    TestFlag = False
    N = 0
    If MSCOM.InBufCount(balancePort) Then   'Clear buffer
        DataString = MSCOM.InputFromPort(balancePort, 0)
    End If
    While Not TestFlag
        N = N + 1
        Application.StatusBar = "Waiting for Stable Reading " + Str(N)
        Call MSCOM.Output(balancePort, "S")
        timeOutTime = Timer + 5
        While MSCOM.InBufCount(balancePort) < 10 Or Timer < timeOutTime
        Wend
        DataString = MSCOM.InputFromPort(balancePort, 10)

        If Left(DataString, 2) = "S " Then
            TestFlag = True
            StableReading = True
        End If

        If N > 20 Then
            Beep
            Answer = MsgBox("Reading did not stabilize. -- Try Again?", vbYesNo)
```

```
            If Answer = vbYes Then
               N = 0
            Else
               StableReading = False
               TestFlag = True
            End If
         End If
      Wend
   End Function

   Public Sub ReadBalanceContinuous()
      'Dim aString As String

      Call MSCOM.Output(balancePort, "SIR")
      'delay (1)
      'If MSCOM.InBufCount(balancePort) Then
      '    aString = MSCOM.InputFromPort(balancePort,
MSCOM.InBufCount(balancePort))
      'End If
   End Sub


   Public Function ReadBalanceContinuous2() As String

   If MSCOM.InBufCount(balancePort) Then
      ReadBalanceContinuous2 = MSCOM.InputFromPort(balancePort, 15)
   End If

   End Function

   Public Function ReadBalance() As Single
      Dim theString As String

      theString = MSCOM.InputFromPort(balancePort, 1)
      While Left(theString, 1) <> "S"
         theString = MSCOM.InputFromPort(balancePort, 1)
      Wend
      While Not DataReady
      Wend
      theString = MSCOM.InputFromPort(balancePort, 15)
      theString = "S" + theString
      ReadBalance = Val(Mid(theString, 4, 9))
      Application.StatusBar = "Current Reading = " + theString
```

```
    End Function

    Public Sub StopBalanceRead()
       Dim aString As String
       Call MSCOM.Output(balancePort, "S")
       delay (1)
       If MSCOM.InBufCount(balancePort) Then
          aString = MSCOM.InputFromPort(balancePort,
MSCOM.InBufCount(balancePort))
       End If
    End Sub



    Public Function DataReady() As Boolean
       If MSCOM.InBufCount(balancePort) < 15 Then
          DataReady = False
       Else
          DataReady = True
       End If
    End Function
```

Motor

```
Option Explicit

    Private Const motorPort = 2
    Public direction As Integer

    Private Sub delay(delayTime As Single)
        Dim finish As Single
        finish = Timer + delayTime
        Do While finish > Timer
        Loop
    End Sub

    Public Function Init() As Boolean
        Dim inString As String
        Dim position As Long, timeOutTime As Single, timeRemaining As Integer

        Init = True     'Set initial value
        Call MSCOM.OpenPort(motorPort, "9600,N,8,1", 0)   'Open the Port

        ' Put Motor under Computer Control
        Call MSCOM.Output(motorPort, "E MN PZ X0 DA A50")
            'E = Establish computer control
            'MN = Mode = Move to set position
            'PZ = Zero relative position counter
            'X0 = Zero absolute position counter
            'DA = Zero display
            'A50 = Set acceleration to 50 rev/sec^2
        delay (1)

        If MSCOM.InBufCount(motorPort) Then     ' Read the data.
            inString = MSCOM.InputFromPort(motorPort, 0) 'Motor echoes instruction
        End If

        'Move Motor to Start Point
        If Sheet1.Robust Then
            Call MSCOM.Output(motorPort, "V1.0 D+150000 G 1X1")
        Else
            Call MSCOM.Output(motorPort, "V1.0 D-8000 G 1X1")
                'V1.0 = Maximum speed
                'D-8000 = Move to position -8000 ( = 1/40 of Lower Limit)
                'D+150000 = Move to position +150000
```

```
            'G = Go
            '1X1 = Tell me current position after move
        End If

        'Clear buffer
        If MSCOM.InBufCount(motorPort) Then
           inString = MSCOM.InputFromPort(motorPort, 0) 'Motor echoes instruction
        End If
        timeRemaining = 10
        While timeRemaining > 0
           Application.StatusBar = "Wait for Motor" + Str(timeRemaining)
           timeRemaining = timeRemaining - 1
           delay (1)
        Wend

        ' Check for data.
'       position = 0
'       If MSCOM.InBufCount(motorPort) Then
'          inString = MSCOM.InputFromPort(motorPort, 0)     ' Read data.
'          inString = Right(inString, 10)
'          position = Val(inString)
'       End If

        position = FindPosition()
        If (Not Sheet1.Robust And position > -7000) Or (Sheet1.Robust And position <
140000) Then
           Init = False
           MsgBox "Cant't initiate the motor"
        Else
           Application.StatusBar = "Motor initialized"
        End If
    End Function


    Public Sub CloseMotor()
        Dim distance As Long, inString As String
        distance = -FindPosition()
        'Move to zero at maximum speed
        Call MSCOM.Output(motorPort, "V1.0 D" + LTrim(Str(distance)) + " G 1X1")
        delay (Int(Abs(distance) / 25000))
        If MSCOM.InBufCount(motorPort) Then
           inString = MSCOM.InputFromPort(motorPort, 0)   'Clear Buffer
        End If
```

```
        Call MSCOM.Output(motorPort, "F")
        If MSCOM.InBufCount(motorPort) Then
            inString = MSCOM.InputFromPort(motorPort, 0)   'Clear Buffer
        End If
        Call MSCOM.CloseThePort(motorPort)
    End Sub

    Public Function FindPosition() As Long
        Dim inString As String

        'Clear input buffer
        If MSCOM.InBufCount(motorPort) Then
            inString = MSCOM.InputFromPort(motorPort, 0)
        End If

        Call MSCOM.Output(motorPort, "S S 1X1")  'Stop the motor
        delay (1)
        If MSCOM.InBufCount(motorPort) Then
            inString = MSCOM.InputFromPort(motorPort, 8) 'Motor echoes instruction
            inString = Left(inString, 7)
        End If

        'Read the motor position
        If MSCOM.InBufCount(motorPort) Then
            inString = Left(MSCOM.InputFromPort(motorPort, 0), 10)
            FindPosition = Val(inString)
            Application.StatusBar = "Motor position = " + inString
        End If
    End Function

Public Function ZeroSpeed() As Boolean
    Const speedZero = 0
    Dim inString As String, speed As Single

    'Stop balance output and clear buffer
    Call Mettler.StopBalanceRead

    'Check whether all angles have been run
    'If GetData.MoreAngles Then
        'Reset motor to lowest speed and start position
        'GetData.theSpeed = MotorSpeed(speedZero)
        'Restart balance output
        Call Mettler.ReadBalanceContinuous
```

```
        ZeroSpeed = True
    'Else
    '    ZeroSpeed = False
    'End If
End Function

Private Function NextSpeed(speed As Single, position As Long) As String
    Const limit& = 700000
    Const startPos002& = -8000, startPos02& = -40000, startPos2& = -300000
    Const startPos3Robust& = 150000
    Dim startPos As Long, stopAt As Long
    Dim prepositionStr As String, speedStr As String, inString As String
    Dim timeOutTime As Single

    Application.StatusBar = "Resetting motor position, please wait ..."
    If Sheet1.Robust Then
        startPos = startPos3Robust
        Select Case speed
        Case Is < 0.001
            prepositionStr = "V0.002"
            speedStr = "0.002"
        Case Is < 0.004
            prepositionStr = "V0.008"
            speedStr = "0.008"
        Case Is < 0.01
            prepositionStr = "V0.016"
            speedStr = "0.016"
        Case Else
            startPos = 0
            prepositionStr = "V0.128"
            speedStr = "1.0"
        End Select
    Else
        Select Case speed
        Case Is < 0.001
            startPos = startPos002
            prepositionStr = "V0.002"
            speedStr = "0.002"
        Case Is < 0.01
            startPos = startPos02
            prepositionStr = "V0.016"
            speedStr = "0.016"
        Case Is < 0.1
```

```
            startPos = startPos2
            prepositionStr = "V0.128"
            speedStr = "0.128"
        Case Else
            startPos = 0
            prepositionStr = "V0.128"
            speedStr = "1.0"
        End Select
    End If
    stopAt = startPos - position

    Application.StatusBar = "Changing position and speed"
    prepositionStr = prepositionStr + " D" + LTrim(Str(stopAt))
    Call MSCOM.Output(motorPort, prepositionStr)
    delay 1
    If MSCOM.InBufCount(motorPort) Then 'Motor echoes command
        inString = MSCOM.InputFromPort(motorPort, 0)
    End If
    Call MSCOM.Output(motorPort, " G 1X1")
    delay 1
    If MSCOM.InBufCount(motorPort) Then 'Motor echoes command
        inString = MSCOM.InputFromPort(motorPort, 0)
    End If
    timeOutTime = Timer + 180    'Wait for motor
    While (Not MSCOM.InBufCount(motorPort)) And (timeOutTime > Timer)
    Wend
    If MSCOM.InBufCount(motorPort) Then
        inString = MSCOM.InputFromPort(motorPort, 0)
    End If
    NextSpeed = speedStr
End Function

Private Function SetMotorSpeed(speed As Single) As Single
    Const up = 1, down = -up
    Const limit& = 700000
    Const startPos002& = -8000, startPos02& = -40000, startPos2& = -300000
    Const startPos3Robust = 150000
    Dim startPos As Long, stopAt As Long
    Dim prepositionStr As String, speedStr As String, inString As String
    Dim timeOutTime As Single
    Dim position As Long

    speedStr = Format(speed, "0.000")
```

```
'Stop motor and find current position
position = FindPosition

'Make room for data collection
If direction = down Then
   'Increase speed to next speed
   speedStr = NextSpeed(speed, position)
   speed = Val(speedStr)
   position = FindPosition

   'Was this the last speed?
   If speed > 0.5 Then
      'Move to intial point
      If Sheet1.Robust Then
         stopAt = -150000 + position
      Else
         stopAt = 8000 + position
      End If
      prepositionStr = "V0.128 D" + LTrim(Str(-stopAt))
      Call MSCOM.Output(motorPort, prepositionStr)
      If MSCOM.InBufCount(motorPort) Then 'Motor echoes command
        inString = MSCOM.InputFromPort(motorPort, 0)
      End If
      Call MSCOM.Output(motorPort, " G 1X1")
      If MSCOM.InBufCount(motorPort) Then 'Motor echoes command
        inString = MSCOM.InputFromPort(motorPort, 0)
      End If
      timeOutTime = Timer + 12    'Wait for motor
      While (Not MSCOM.InBufCount(motorPort)) And timeOutTime > Timer
      Wend
      If MSCOM.InBufCount(motorPort) Then
         inString = MSCOM.InputFromPort(motorPort, 0)
      End If

      'Stop the motor
      speed = 0
      speedStr = "0"
   End If
End If

If Sheet1.Robust Then
   direction = down
Else
```

```
        'Reverse motor direction and change limit switch
        direction = -direction
    End If
    stopAt = direction * limit& / 2& - position

    'Set motor speed
    prepositionStr = "V" + speedStr + " D" + LTrim(Str(stopAt))
    Call MSCOM.Output(motorPort, prepositionStr)
    If MSCOM.InBufCount(motorPort) Then 'Motor echoes command
      inString = MSCOM.InputFromPort(motorPort, 0)
    End If
    Call MSCOM.Output(motorPort, " G 1X1")
    If MSCOM.InBufCount(motorPort) Then 'Motor echoes command
      inString = MSCOM.InputFromPort(motorPort, 0)
    End If

    'Set return value
    SetMotorSpeed = speed
End Function

Public Function MotorSpeed(speed As Single) As Single
    Const initSpeed = 0.00011, up = 1, down = -up
    Dim sleepTime As Integer, sleepFor As Single
    Dim inString As String, sleepMessage As String

    'Initialize motor speed & position
    If speed < initSpeed Then
        direction = down
        speed = initSpeed
    End If

    'Start test at new speed
    'Suspend data collection
    Call Mettler.StopBalanceRead
    'Set motor speed, start position and stop position
    speed = SetMotorSpeed(speed)

    'Take slack out of fiber
    If speed <> 0 Then
        sleepMessage = "Taking slack out of fiber, please wait ... "
        If Sheet1.Robust Then
            sleepFor = 600 / (500 * speed) + 1
        Else
```

```
            sleepFor = 120 / (500 * speed) + 1
        End If
        While sleepFor > 0
            sleepFor = sleepFor - 1
            delay (1)
            Application.StatusBar = sleepMessage + Str(sleepFor) + " secs remaining"
        Wend
    End If

    'Clear motor input buffer
    If MSCOM.InBufCount(motorPort) Then
        inString = MSCOM.InputFromPort(motorPort, 0)
    End If

    'Resume data collection
    Call Mettler.ReadBalanceContinuous
    MotorSpeed = speed   'Set function value
End Function

Public Function AutoStop() As Boolean
    Dim aString As String

    If MSCOM.InBufCount(motorPort) Then
        aString = MSCOM.InputFromPort(motorPort, 0)
        AutoStop = True
    Else
        AutoStop = False
    End If
End Function
```

MSCOM

```
Option Explicit

    Public Sub OpenPort(thePort As Integer, theSettings As String, InputLen As Integer)
      Select Case thePort
        Case 1 ' Use COM1.
          Sheet1.MSComm1.CommPort = thePort
          'Set baud, parity, # databits, and # stopbits.
          Sheet1.MSComm1.Settings = theSettings
         ' # characters to read from buffer when Input is used.
          Sheet1.MSComm1.InputLen = InputLen
          Sheet1.MSComm1.PortOpen = True  ' Open the port.
        Case 2:  ' Use COM2.
          Sheet1.MSComm2.CommPort = thePort
          'Set baud, parity, # databits, and # stopbits.
          Sheet1.MSComm2.Settings = theSettings
         ' # characters to read from buffer when Input is used.
          Sheet1.MSComm2.InputLen = InputLen
          Sheet1.MSComm2.PortOpen = True  ' Open the port.
      End Select
    End Sub

    Public Sub CloseThePort(thePort As Integer)
      Dim dummy As String
      Select Case thePort
        Case 1
          If InBufCount(1) Then   'Clear the Buffer
            dummy = Sheet1.MSComm1.Input
          End If
          Sheet1.MSComm1.PortOpen = False 'Close ComPort 1
        Case 2
          If InBufCount(2) Then   'Clear the buffer
            dummy = Sheet1.MSComm1.Input
          End If
          Sheet1.MSComm2.PortOpen = False 'Close ComPort 2
      End Select
    End Sub

    Public Sub Output(thePort As Integer, theString As String)
      Select Case thePort
        Case 1
          Sheet1.MSComm1.Output = theString + Chr(13) + Chr(10)
```

```
            Case 2
               Sheet1.MSComm2.Output = theString + Chr(13) + Chr(10)
         End Select
      End Sub

      Public Function InBufCount(thePort As Integer) As Integer
         Select Case thePort
            Case 1
               InBufCount = Sheet1.MSComm1.InBufferCount
            Case 2
               InBufCount = Sheet1.MSComm2.InBufferCount
         End Select
      End Function

      Public Function InputFromPort(thePort As Integer, theStringLength As Integer) As
String
         Select Case thePort
            Case 1
               Sheet1.MSComm1.InputLen = theStringLength   'Set input length
               InputFromPort = Sheet1.MSComm1.Input    'Read the data
            Case 2
               Sheet1.MSComm2.InputLen = theStringLength   'Set input length
               InputFromPort = Sheet1.MSComm2.Input    'Read the data
         End Select
      End Function
```

APPENDIX B. Robustness of Single Layer of Woven Fabric with Monofilaments

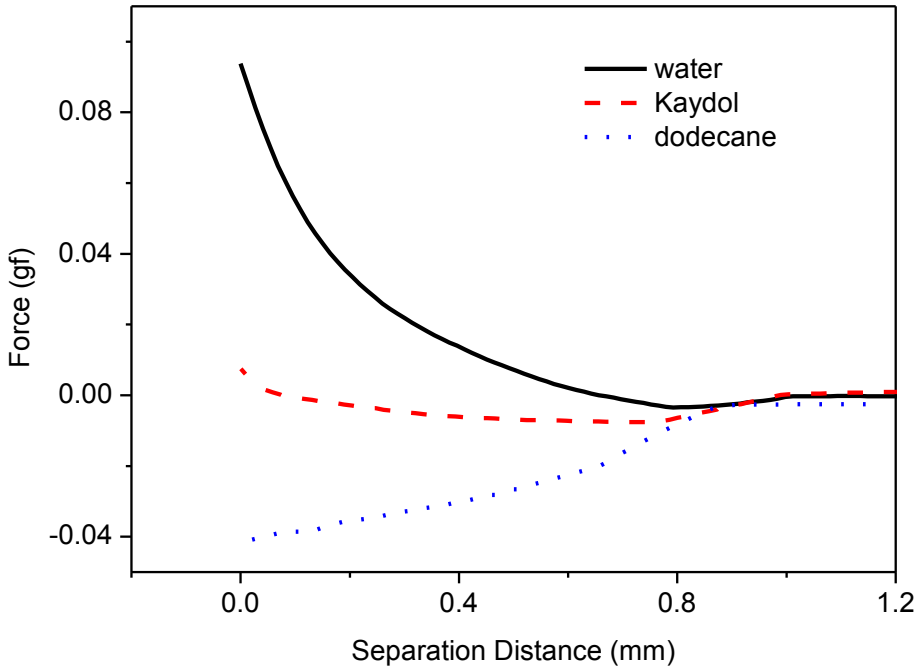

Figure B1. Effects of surface tensions of liquids when the volumes V = 2 μL.

Table B1. Comparisons of separation distances or heights, contact areas, pressure due to gravity, the Laplace pressure and the applied pressures of liquid bridges at h_{min} with different liquids when V = 2 μL on the monofilament fabric.

	Water	Kaydol	Dodecane
Height (mm)	0.31	0.29	0.23
Contact Area (mm^2)	6.47	6.92	8.59
Pressure due to gravity (Pa)	3.04	2.42	1.69
Laplace Pressure (Pa)	209	-4	-26
Applied Pressure (Pa)	137	-38	-44

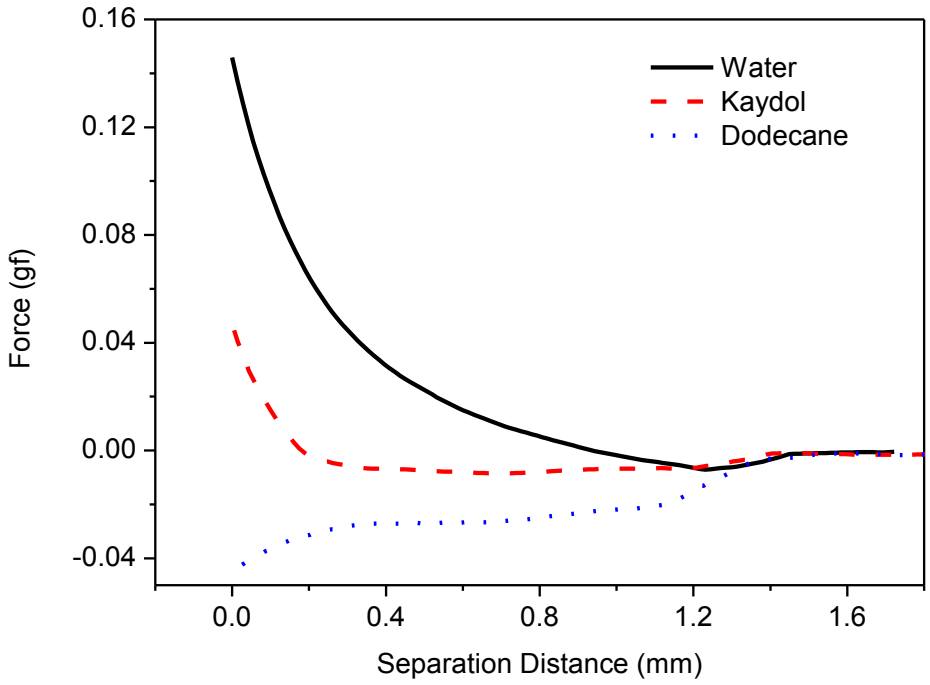

Figure B2. Effects of surface tensions of liquids when the volumes $V = 5$ μL.

Table B2. Comparisons of separation distances or heights, contact areas, pressure due to gravity, the Laplace pressure and the applied pressures of liquid bridges at h_{min} with different liquids when $V = 5$ μL on the monofilament fabric.

	Water	Kaydol	Dodecane
Height (mm)	0.32	0.33	0.35
Contact Area (mm^2)	15.85	15.26	14.19
Pressure due to gravity (Pa)	3.14	2.75	2.57
Laplace Pressure (Pa)	140	12	-17
Applied Pressure (Pa)	94	-11	-31

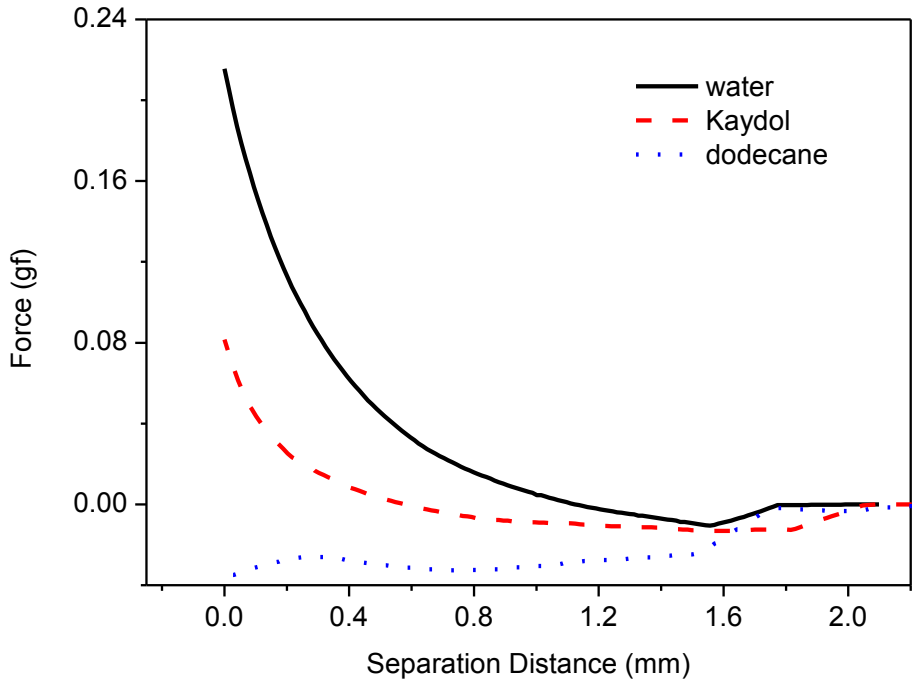

Figure B3. Effects of surface tensions of liquids when the volumes V = 10 μL.

Table B3. Comparisons of separation distances or heights, contact areas, pressure due to gravity, the Laplace pressure and the applied pressures of liquid bridges at h_{min} with different liquids when V = 10 μL on the monofilament fabric.

	Water	Kaydol	Dodecane
Height (mm)	0.36	0.39	0.48
Contact Area (mm^2)	27.51	25.65	20.71
Pressure due to gravity (Pa)	3.53	3.25	3.53
Laplace Pressure (Pa)	108	27	-5
Applied Pressure (Pa)	73	9	-17

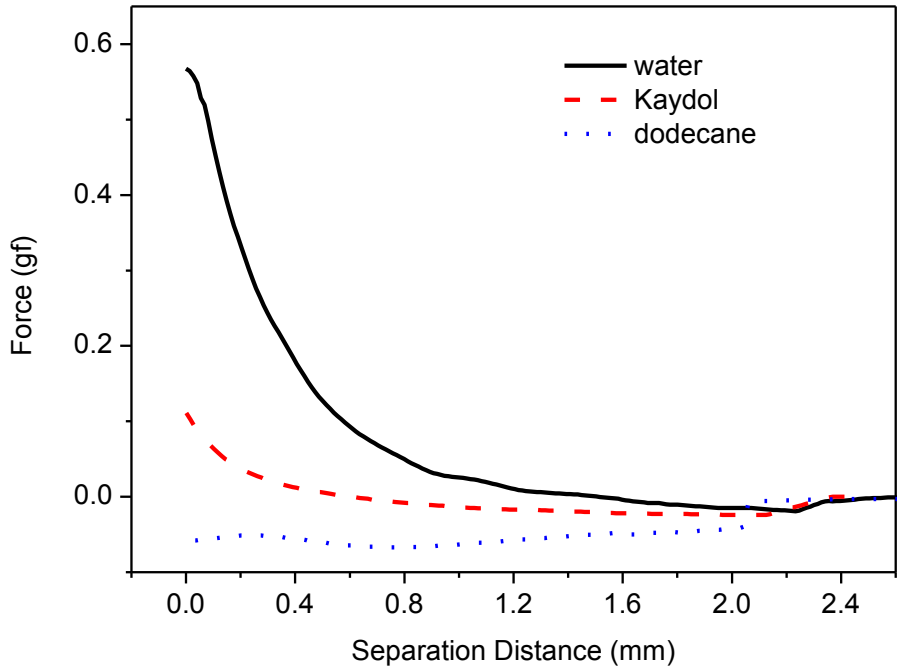

Figure B4. Effects of surface tensions of liquids when the volumes $V = 20$ μL.

Table B4. Comparisons of separation distances or heights, contact areas, pressure due to gravity, the Laplace pressure and the applied pressures of liquid bridges at h_{min} with different liquids when $V = 20$ μL on the monofilament fabric.

	Water	Kaydol	Dodecane
Height (mm)	0.56	0.57	0.55
Contact Area (mm^2)	35.67	31.40	36.29
Pressure due to gravity (Pa)	5.49	4.75	4.04
Laplace Pressure (Pa)	178	31	-7
Applied Pressure (Pa)	147	15	-16

APPENDIX C. Robustness of Woven Fabric with Multifilament Yarns

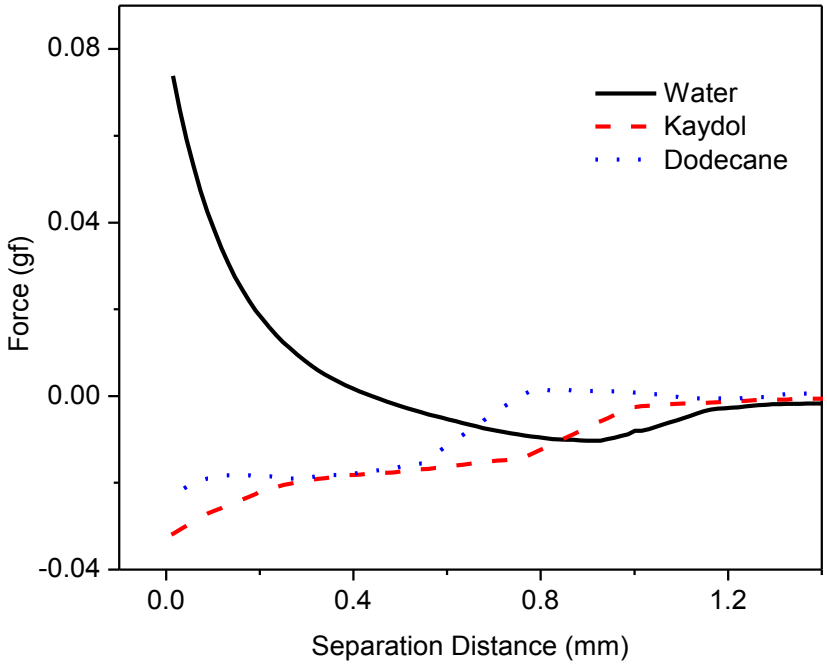

Figure C1. Effects of surface tensions of liquids when the volumes V = 2 μL.

Table C1. Comparisons of separation distances or heights, contact areas, pressure due to gravity, the Laplace pressure and the applied pressures of liquid bridges at h_{min} with different liquids when V = 2 μL on the multifilament fabric.

	Water	Kaydol	Dodecane
Height (mm)	0.23	0.14	0.15
Contact Area (mm^2)	9.10	7.81	10.36
Pressure due to gravity (Pa)	2.25	1.17	1.10
Laplace Pressure (Pa)	176	-4	-6
Applied Pressure (Pa)	94	-36	-25

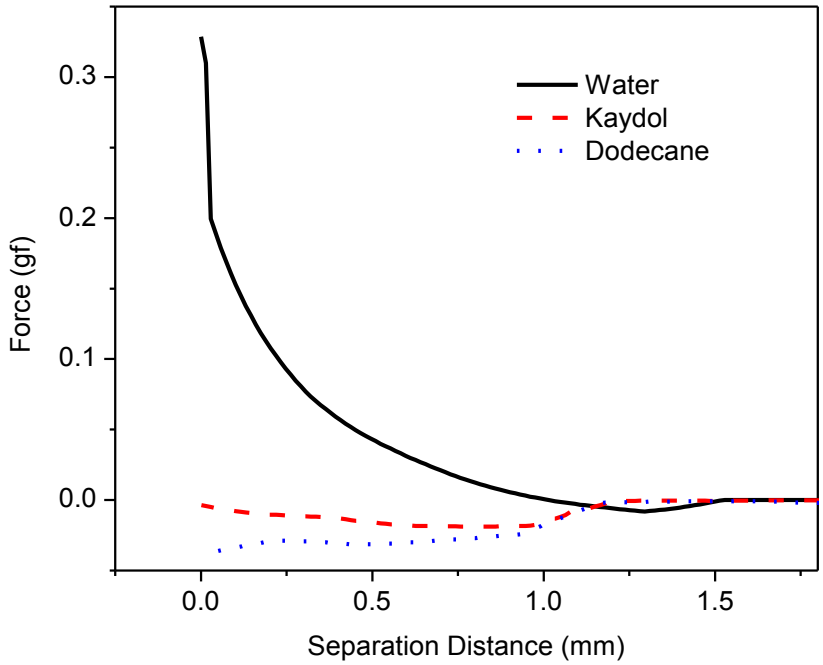

Figure C2. Effects of surface tensions of liquids when the volumes $V = 5$ μL.

Table C2. Comparisons of separation distances or heights, contact areas, pressure due to gravity, the Laplace pressure and the applied pressures of liquid bridges at h_{min} with different liquids when $V = 5$ μL on the multifilament fabric.

	Water	Kaydol	Dodecane
Height (mm)	0.38	0.21	0.22
Contact Area (mm^2)	21.68	16.66	18.31
Pressure due to gravity (Pa)	3.72	1.75	1.62
Laplace Pressure (Pa)	198	21	-14
Applied Pressure (Pa)	152	-1	-29

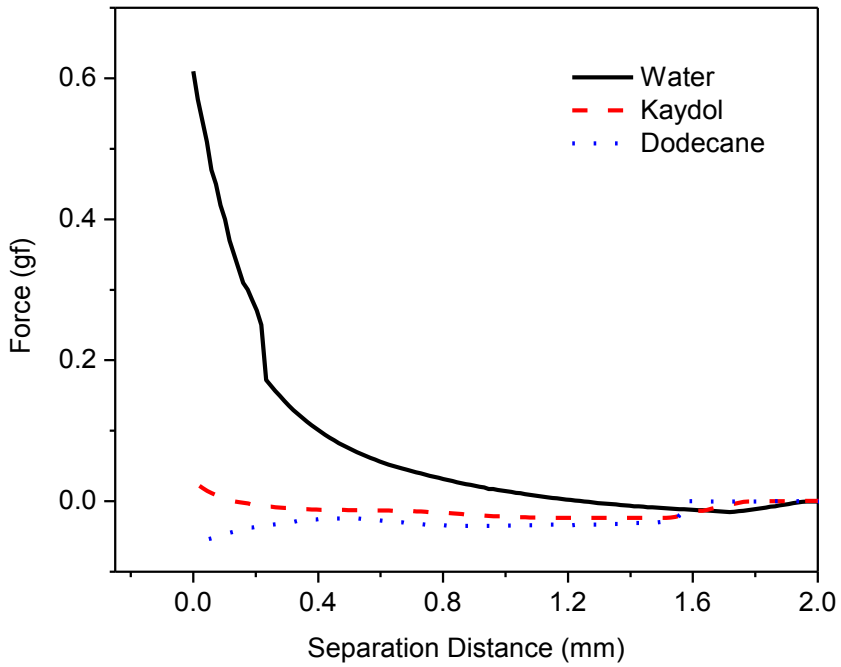

Figure C3. Effects of surface tensions of liquids when the volumes V = 10 μL.

Table C3. Comparisons of separation distances or heights, contact areas, pressure due to gravity, the Laplace pressure and the applied pressures of liquid bridges at h_{min} with different liquids when V = 10 μL on the multifilament fabric.

	Water	Kaydol	Dodecane
Height (mm)	0.31	0.23	0.18
Contact Area (mm^2)	27.81	24.79	24.55
Pressure due to gravity (Pa)	3.04	1.92	1.32
Laplace Pressure (Pa)	226	30	-17
Applied Pressure (Pa)	186	12	-29

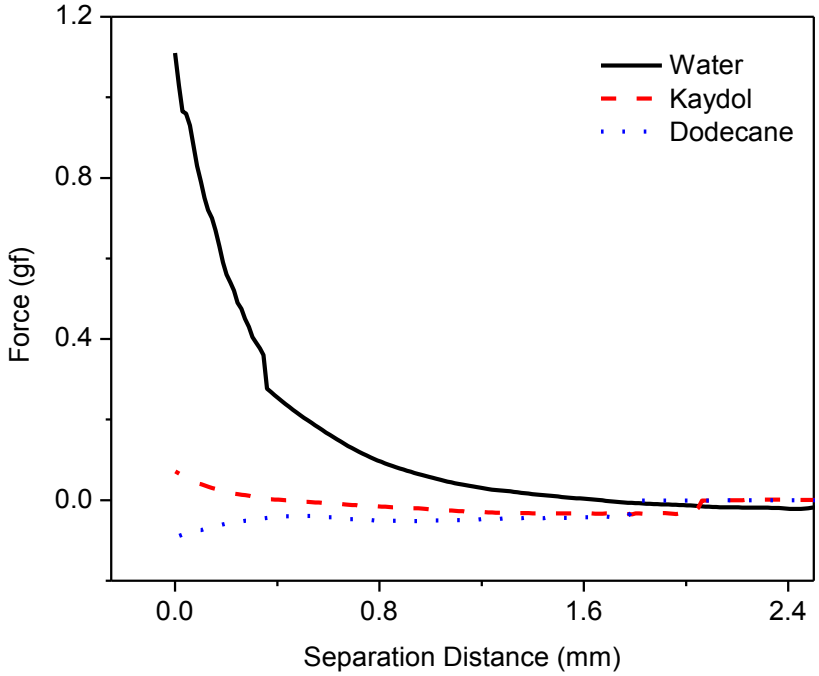

Figure C4. Effects of surface tensions of liquids when the volumes V = 20 μL.

Table C4. Comparisons of separation distances or heights, contact areas, pressure due to gravity, the Laplace pressure and the applied pressures of liquid bridges at h_{min} with different liquids when V = 20 μL on the multifilament fabric.

	Water	Kaydol	Dodecane
Height (mm)	0.37	0.38	0.48
Contact Area (mm^2)	42.44	45.38	55.75
Pressure due to gravity (Pa)	3.63	3.17	3.53
Laplace Pressure (Pa)	284	32	-24
Applied Pressure (Pa)	251	18	-32

APPENDIX D. Robustness of Nonwoven Fabrics

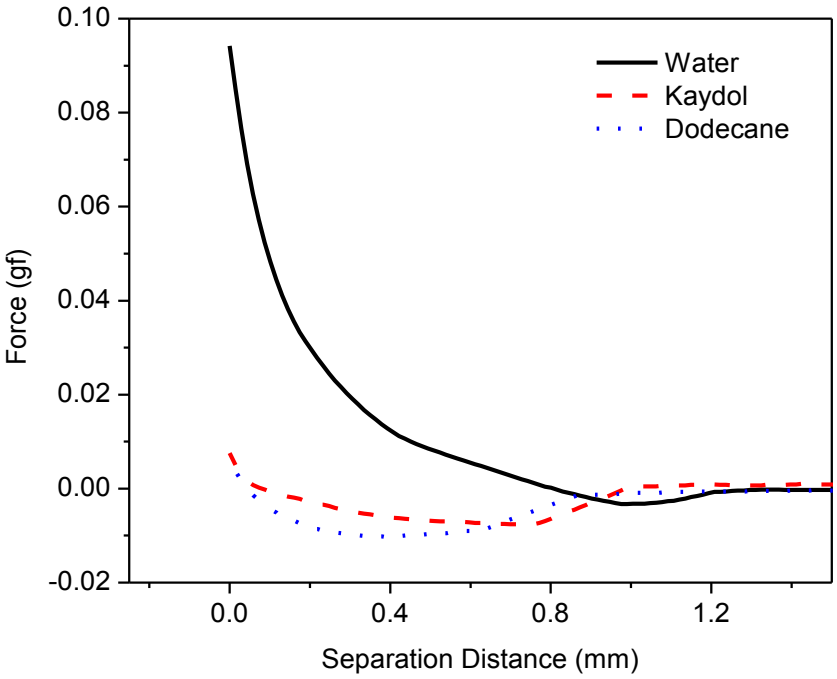

Figure D1. Effects of surface tensions of liquids when the volumes V = 2 μL.

Table D1. Comparisons of separation distances or heights, contact areas, pressure due to gravity, the Laplace pressure and the applied pressures of liquid bridges at h_{min} with different liquids when V = 2 μL on the nonwoven fabric.

	Water	Kaydol	Dodecane
Height (mm)	0.25	0.25	0.32
Contact Area (mm^2)	8.11	6.26	6.26
Pressure due to gravity (Pa)	2.45	2.08	2.35
Laplace Pressure (Pa)	152	48	31
Applied Pressure (Pa)	97	11	10

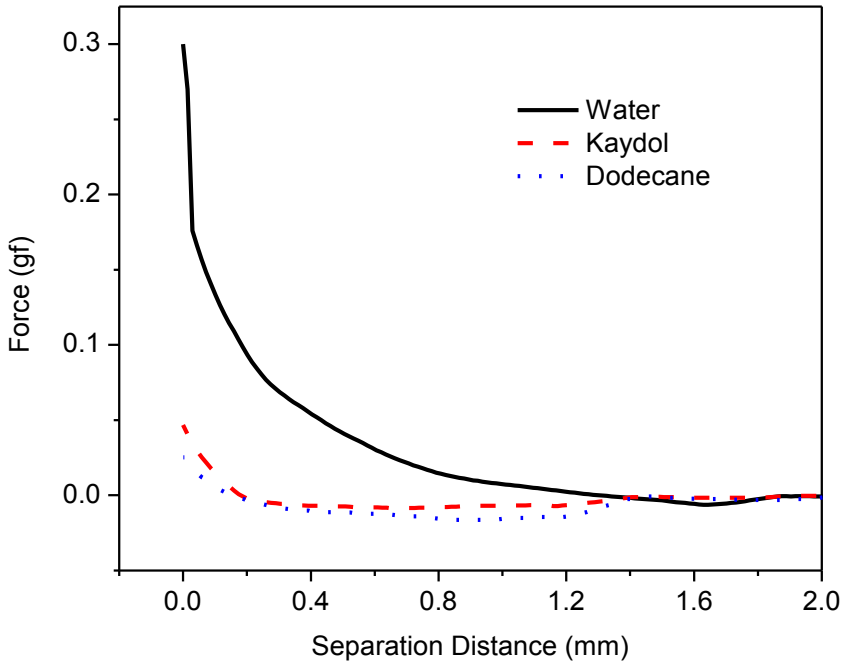

Figure D2. Effects of surface tensions of liquids when the volumes $V = 5$ μL.

Table D2. Comparisons of separation distances or heights, contact areas, pressure due to gravity, the Laplace pressure and the applied pressures of liquid bridges at h_{min} with different liquids when $V = 5$ μL on the nonwoven fabric.

	Water	Kaydol	Dodecane
Height (mm)	0.42	0.35	0.44
Contact Area (mm^2)	21.88	13.42	11.22
Pressure due to gravity (Pa)	4.12	2.92	3.23
Laplace Pressure (Pa)	169	52	40
Applied Pressure (Pa)	135	28	24

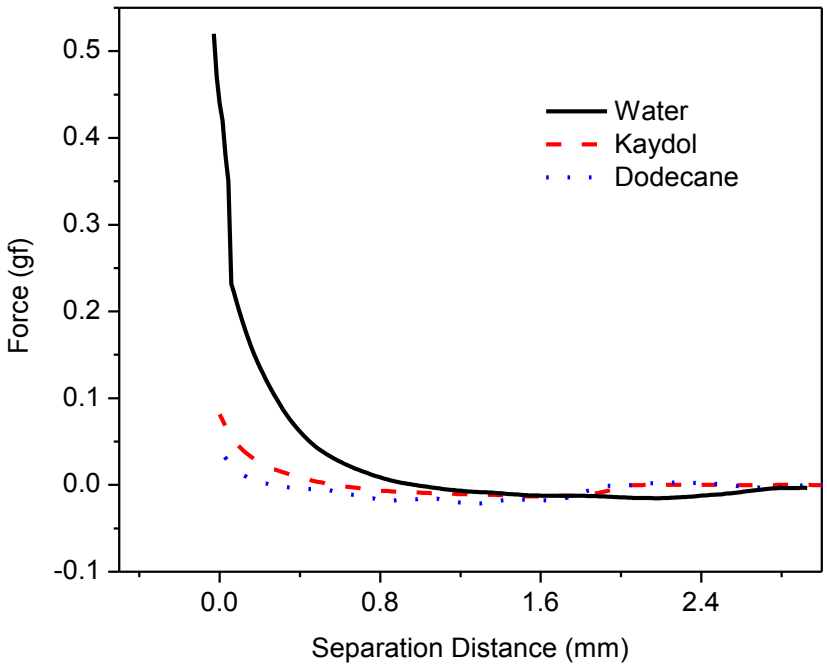

Figure D3. Effects of surface tensions of liquids when the volumes V = 10 μL.

Table D3. Comparisons of separation distances or heights, contact areas, pressure due to gravity, the Laplace pressure and the applied pressures of liquid bridges at h_{min} with different liquids when V = 10 μL on the nonwoven fabric.

	Water	Kaydol	Dodecane
Height (mm)	0.25	0.39	0.46
Contact Area (mm^2)	35.35	23.58	21.77
Pressure due to gravity (Pa)	2.45	3.25	3.38
Laplace Pressure (Pa)	170	53	34
Applied Pressure (Pa)	143	35	23

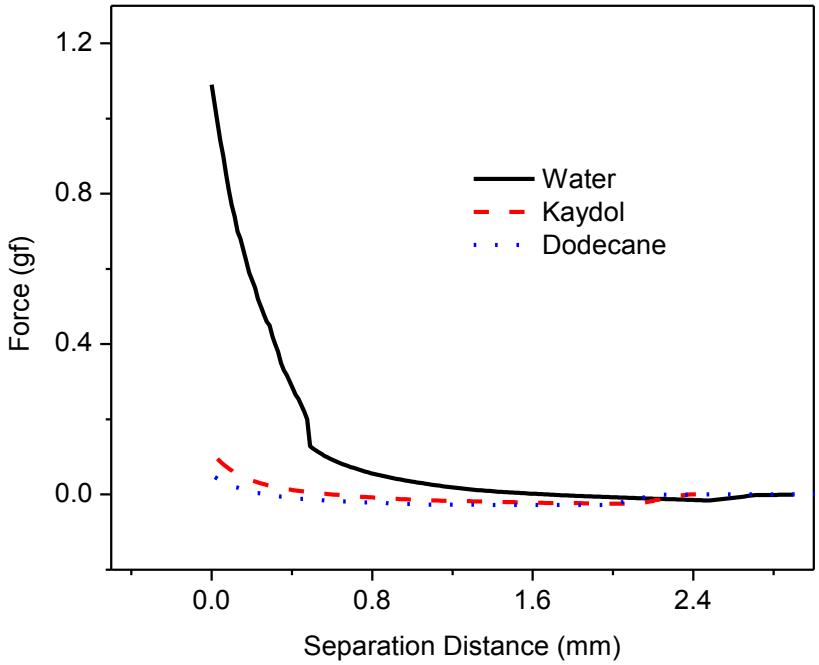

Figure D4. Effects of surface tensions of liquids when the volumes V = 20 μL.

Table D4. Comparisons of separation distances or heights, contact areas, pressure due to gravity, the Laplace pressure and the applied pressures of liquid bridges at h_{min} with different liquids when V = 20 μL on the nonwoven fabric.

	Water	Kaydol	Dodecane
Height (mm)	0.54	0.58	0.46
Contact Area (mm^2)	44.96	35.33	43.02
Pressure due to gravity (Pa)	5.29	4.83	3.38
Laplace Pressure (Pa)	270	45	20
Applied Pressure (Pa)	246	29	12